# The role of fibroblast growth factor 21 in different mouse models of mitochondrial dysfunction

## Inaugural-Dissertation

zur

Erlangung des Doktorgrades

der Mathematisch-Naturwissenschaftlichen Fakultät

der Universität zu Köln


vorgelegt von

Marijana Aradjanski

aus Kikinda, Serbien

Köln 2018

Berichterstatter: Prof. Dr. Aleksandra Trifunovic
Prof. Dr. Rudolf Wiesner

Tag der mündlichen Prüfung: 23.11.2018.

# Table of Contents

# List of Figures

# List of Tables

# Abbreviations

| | |
|---|---|
| °C | degree Celsius |
| 3’ | three prime end of DNA sequences |
| 5’ | five prime end of DNA sequences |
| A | adenosine |
| ADP | adenosine diphosphate |
| ATP | adenosine triphosphate |
| BAT | brown adipose tissue |
| bp | base pairs |
| BN | blue native |
| BSA | bovine serum albumin |
| bZIP | basic leucine zipper |
| C | cytosine |
| cDNA | complementary DNA |
| cAMP | cyclic AMP |
| CLPP | caseinolytic mitochondrial matrix peptidase proteolytic subunit |
| Cre | bacteriophage P1 derived site-specific recombinase |
| CREB1 | cyclic AMP-responsive element binding protein 1 |
| Cyt | cytochrome |
| Da | Dalton |
| DAB | diaminobenzidine tetrahydrochloride |
| DARS2 | aspartyl-tRNA synthethase, mitochondrial |
| dd$H_2O$ | double distilled water |
| DKO | double knockout |
| DNA | deoxyribonucleic acid |
| dNTP | deoxyribonucleotide-triphosphate |
| ds DNA | double strand DNA |
| ECL | enhanced chemiluminescence |
| EDTA | ethylenediaminetetraacetic acid |
| EGTA | ethylene glycol tetraacetic acid |
| eIF2α | eukaryotic translation initiation factor 2 alpha |
| ER | endoplasmatic reticulum |

| | |
|---|---|
| ERRα | steroid hormone receptor |
| ETC | electron transport chain |
| EtOH | ethanol |
| ETS | electron transfer system |
| EWAT | epididymal white adipose tissue |
| $FADH_2$ | flavin adenine dinucleotide, reduced |
| FAO | fatty acid β-oxidation |
| FCCP | carbonylcyanide p-trifluoromethoxyphenylhydrazone |
| FDR | false discovery rate |
| Fe-S | iron-sulfur |
| FFA | free fatty acid |
| FGF21 | fibroblast growth factor 21 |
| fMet-tRNA | N-formylmethionyl-tRNA |
| g | gram |
| G | guanine |
| GDF15 | growth differentiation factor 15 |
| $H_2O_2$ | hydrogen peroxide |
| HCl | hydrochloric acid |
| HEPES | N-2-hydroxyethylpiperazine-N-2-ethansulfonic acid |
| HFD | high-fat diet |
| HSP | heavy strand promoter |
| IMM | inner mitochondrial membrane |
| IMS | inter membrane space |
| IRES | internal ribosome entry sites |
| ISR | integrated stress response |
| IWAT | inguinal white adipose tissue |
| k | kilo |
| KCl | potassium chloride |
| KO | knockout |
| KOH | potassium hydroxide |
| l | liter |
| fl | loxP flanked |
| LSP | light strand promoter |

| | |
|---|---|
| m | milli |
| M | molar |
| $MgCl_2$ | magnesium chloride |
| MnSOD | manganese superoxide dismutase |
| mRNA | messenger RNA |
| mtARS | mitochondrial aminoacyl-tRNA synthethase |
| mtDNA | mitochondrial DNA |
| mtHSP70 | mitochondrial heat shock protein 70 |
| mtIF3 | mitochondrial initiation factor 3 |
| mtRF | mitocondrial reléase factor |
| mTOR | mammalian target of rapamycin |
| MTS | mitocondrial targeting sequence |
| NaCl | sodium chloride |
| NADH | nicotinamide adenine dinucleotide, reduced |
| NADP | nicotinamide adenine dinucleotide phosphate, reduced |
| NaF | sodium fluoride |
| $NAH_2PO_4$ | monosodium phosphate |
| $NaHCO_3$ | sodium bicarbonate |
| NaOH | sodium hydroxide |
| NRF1 | nuclear respiratory factor 1 |
| NRF2 | nuclear respiratory factor 2 |
| OMM | outer mitochondrial membrane |
| OXPHOS | oxidative phosphorylation |
| PAGE | polyacrylamide gel electrophoresis |
| PBS | phosphate buffered saline |
| PCR | polymerase chain reaction |
| PGC1-α | peroxisome-proliferator-activated-receptor-coactivator 1 alpha |
| Pi | Phosphates |
| POLRMT | mitochondrial RNA polymerase |
| PPARα | peroxisome proliferator activated receptor alpha |
| RNA | ribonucleic acid |
| rRNA | ribosomal RNA |
| RNase | ribonuclease |

| | |
|---|---|
| ROS | reactive oxygen species |
| rpm | revolutions per minute |
| RT | room temperature |
| rtPCR | reverse transcription polymerase chain reaction |
| SD | standard deviation |
| SDS | sodium dodecyl sulfate |
| S.E.M | standard error of the mean |
| SkM | skeletal muscle |
| ssDNA | single strand DNA |
| TBE | tris-borate-EDTA buffer |
| TE | tris-EDTA buffer |
| TFAM | mitochondrial transcription factor A |
| TFB2M | mitochondrial transcription factor B2 |
| Tris | 2-amino-2-(hydroxymethyl)-1,3-propandiole |
| tRNA | transfer RNA |
| TWEEN | polyoxethylene-sorbitan-monolaureate |
| U | units |
| uORF | upstream reading frame |
| $UPR^{mt}$ | mitochondrial unfolded protein response |
| V | volt |
| v/v | volume per volume |
| w/v | weight per volume |
| WT | wildtype |
| β-me | β-mercaptoethanol |
| µ | micro |

# Abstract

Mitochondrial dysfunction is the cause of many diseases that vary in their complexity and clinical presentation. Flawed mitochondrial protein synthesis can disrupt the homeostasis of the whole cell and activate different stress responses, which are trying to outweigh the damage. Both the depletion of mitochondrial aspartyl-tRNA synthethase (*Dars2)* in a tissue-specific manner and ATP-dependent Clp protease (*Clpp*) in whole body, leads to the activation of versatile stress responses. Remarkably, in both mouse models, we observed a significant increase in the expression of a mitokine fibroblast growth factor 21 (*Fgf21)*. This mitokine was shown to be upregulated in many different mouse models with mitochondrial dysfunction, however, its role has still not been clearly demonstrated.

In this study, we generated different double-deficient mouse models, in order to access the role of FGF21 in mitochondrial dysfunction. The results have shown that the autocrine role of FGF21 in DARS2-deficient cardiomyocytes is dispensable and the non-cell autonomous effects of the topical DARS2 depletion are independent of FGF21. Furthermore, with the depletion of FGF21 in whole body, we have shown that DARS2-deficient animals are not affected, indicating that alternative signaling pathways might be activated. Remarkably, when FGF21 was depleted in CLPP deficient animals, we observed an increase in the markers of cardiomyopathy suggesting importance of this mitokine in cardiac physiology.

In summary, these results have shown that FGF21 is not a key player mediating stress responses upon strong mitochondrial deficiency, as modeled in DARS2-deficient mice. However, this cytokine might have a more significant role in late-onset mitochondrial diseases that are modeled by the CLPP loss, which is featured by mild mitochondrial dysfunction. Moreover, the observed expression of *Fgf21* might be dose-dependent and therefore mirroring the severity of mitochondrial dysfunction. In addition, there are possibly alternative players compensating for the lack of FGF21 in mouse models with mitochondrial disease.

# Zusammenfassung

Mitochondriale Dysfunktionen sind die Ursache vieler Erkrankungen, die sich in ihrer Komplexität und klinischen Repräsentation signifikant unterscheiden können. Eine defekte mitochondriale Protein-Synthese kann die Homöostase der gesamten Zelle beeinträchtigen und so verschiedene Stress-Reaktionen zur Schadensbegrenzung aktivieren. Sowohl der gewebe-spezifische Verlust der mitochondrialen Aspartyl-tRNA-Synthethase (*Dars2*) als auch ein Defizit der ATP-abhängigen Clp-Protease (*Clpp*) im gesamten Körper führt zu vielfältigen Stress-Reaktionen. Beiden Mausmodellen gemeinsam ist jedoch ein signifikanter Anstieg in der Expression des Mitokins *Fibroblast growth factor 21* (*Fgf21).* Eine Hochregulation dieses Proteins konnte zwar in vielen verschiedenen Mausmodellen mit mitochondrialen Dysfunktionen beobachtet werden, seine funktionale Rolle war bislang jedoch unbekannt.

In der vorliegenden Studie haben wir verschiedene Doppel-Knockout-Mausmodelle generiert, um die Rolle von FGF21 in mitochondrialen Dysfunktionen näher untersuchen zu können. Die Ergebnisse zeigen, dass FGF21 eine nur unwesentliche autokrine Funktion in Dars2-defizienten Kardiomyozyten hat und nicht-zell-autonomen Effekte einer Dars2-Depletion ebenso unabhängig von FGF21 verlaufen. Eine Ganzkörper-Deletion von FGF21 beeinträchtigt zwar nicht zusätzlich den Phänotyp von Dars2-Knockout-Tieren, jedoch wurden Veränderungen im Phosphorylierungsstatus verschiedener Proteine festgestellt, was Hinweise auf alternative Signalmechanismen gibt. Interessanterweise führt einen Depletion von FGF21 in CLPP-Knockout-Tieren zu einem Anstieg von Markern, welche mit einer Kardiomyopathie in Verbindung stehen.

Zusammenfassend zeigen die vorliegenden Ergebnisse, dass FGF21 kein entscheidender Faktor bei der Vermittlung der Stress-Reaktionen in Dars2-defizienten Tieren ist. Jedoch kann nicht ausgeschlossen werden, dass dieses Zytokin eine signifikantere Rolle bei spät auftretenden mitochondrialen Erkrankungen spielt, wie sie durch den Verlust von CLPP mit milder mitochondrialer Dysfunktion veranschaulicht werden. Zudem könnte die beobachtete Expression von *Fgf21* dosis-abhängig sein und somit den Schweregrad der mitochondrialen Dysfunktion wiederspiegeln. Darüberhinaus existieren mögliche alternative Spieler, die den

Verlust von FGF21 in Musmodellen mit mitochondrialen Dysfunktionen kompensieren könnten.

# 1. Introduction

Mitochondria are organelles, which make life possible by providing energy and many other functions necessary for cells' balance and dynamic. The name of this organelle comes from the Greek language, where *mitos* means "thread" and *chondrion* represents "granules". Interestingly, mitochondria were firstly described back in 1890, by the German scientist Richard Altmann. In his book "Die Elementarorganismen und ihre Beziehungen zu den Zellen", Altmann named mitochondria bioblasts, referring to them as life germs. He believed that they were autonomous organelles important for cell metabolism and genetics, which had been proven to be true almost a century later (O'Rourke, 2010).

## 1.1. Mitochondria structure and main functions

The eukaryotic cell is a symbiotic community of two life forms, the nucleus-cytosol and the mitochondrion. Mitochondria are not self-supporting entities, since they rely for their functions on nuclear gene products which are then imported into them. (Wallace, 1992). They have a double membrane, the outer that separates them from cytosol, and the inner membrane, which form the cristae that are defining the matrix of the organelle. (Taanman, 1999). The matrix contains the mitochondrial genome, ribosomes, transfer RNAs (tRNAs) and versatile proteins and enzymes needed for the function of the organelle.

Mitochondria are thought to have originated two billion years ago from incorporated alpha-proteobacteria, introducing the oxidative respiratory system to the host cell in the times of the drastic changes in the earth's atmosphere (Gray, Burger, & Lang, 1999). During the evolution, the endosymbiont transferred many of its essential genes to the nuclear genome, by which today's mitochondria have a very efficient system of gene expression. The mitochondria still carry hallmarks of its bacterial ancestor, which are reflected on mtDNA expression machinery (Gray, 1989) .

Mitochondria perform central functions in cells, most importantly they generate the cells' main energy source – adenosine triphosphate (ATP). Moreover, they buffer cytosolic calcium levels, take part in programmed cell death, steroid synthesis, iron-sulfur cluster biosynthesis, reactive oxygen species (ROS) formation etc. (Wallace, 2009).

Mitochondrial energetics relies on the availability of reducing agents (hydrogen) that react with oxygen to generate water. Most of the usable energy comes from the breakdown of carbohydrates or fats. The outcome is the production of ATP molecules and electron donors, NADH and FADH2, through the process known as oxidative phosphorylation (OXPHOS). Electrons from the donors are then transferred to molecular oxygen and the energy released from these oxidation/reduction reactions is used to drive synthesis of ATP from ADP. This energy must be created successively, by the passage of electrons through versatile carriers, which are building up the electron transport chain (ETC). The ETC consists of four complexes which function as the carriers: complex I (CO I – NADH:ubiquinone oxidoreductase), complex II (C II – succinate dehydrogenase), complex III (C III – ubiquinol cytochrome c reductase) and complex IV (C IV – cytochrome c oxidase, COX). Complex V (C V – ATP synthase) serves to couple energy-yielding reactions of electron transport to ATP synthesis (Alberts et al., 1983). Electrons are transported from NADH to C I and from succinate through FADH2 to C II. They are further passed down to C III by coenzyme Q (CoQ/ubiquinone). The electron transport from C III to C IV is resolved by soluble cytochrome c. The free energy is produced by the passage of electrons through carriers, and the $H^+$ transport through the inner mitochondrial membrane creates the proton gradient. This energy is harvested by being coupled to ATP synthesis, which is driven by CV. This is known as chemiosmotic coupling, and it was proposed by Peter Mitchell in 1961 (Mitchell, 1961).

The organization of the OXPHOS system was modeled in different ways over time. Two main proposed models are the “fluid” and “solid” model. The ‘solid’ model was firstproposed after a successful purification of functional respiratory complexes. Here complexes unit together in a rigid structure called respirasome (Hatefi, Haavik, Fowler, & Griffiths, 1962). Later on, with the increased knowledge of the properties of the inner mitochondrial membrane (IMM), the ‘fluid’ model was proposed (Hochli & Hackenbrock, 1977). This model was later termed as the ‘random collision’ model, where it was suggested that all membrane complexes, proteins and redox components are in constant and independent diffusional motion. This model was generally accepted for a long time, until new experiments proved the existence of individual intact respiratory complexes with additional multiple comigrating respiratory complexes, known as supercomplexes. In contradiction to the ‘fluid’ model, most of the complex I appear to form associations with complex III, and some complex IV is retained in the form of I–III–IV supercomplexes. This model is a combination of both types, and represents the ‘plasticity’ model (Schagger & Pfeiffer, 2000).

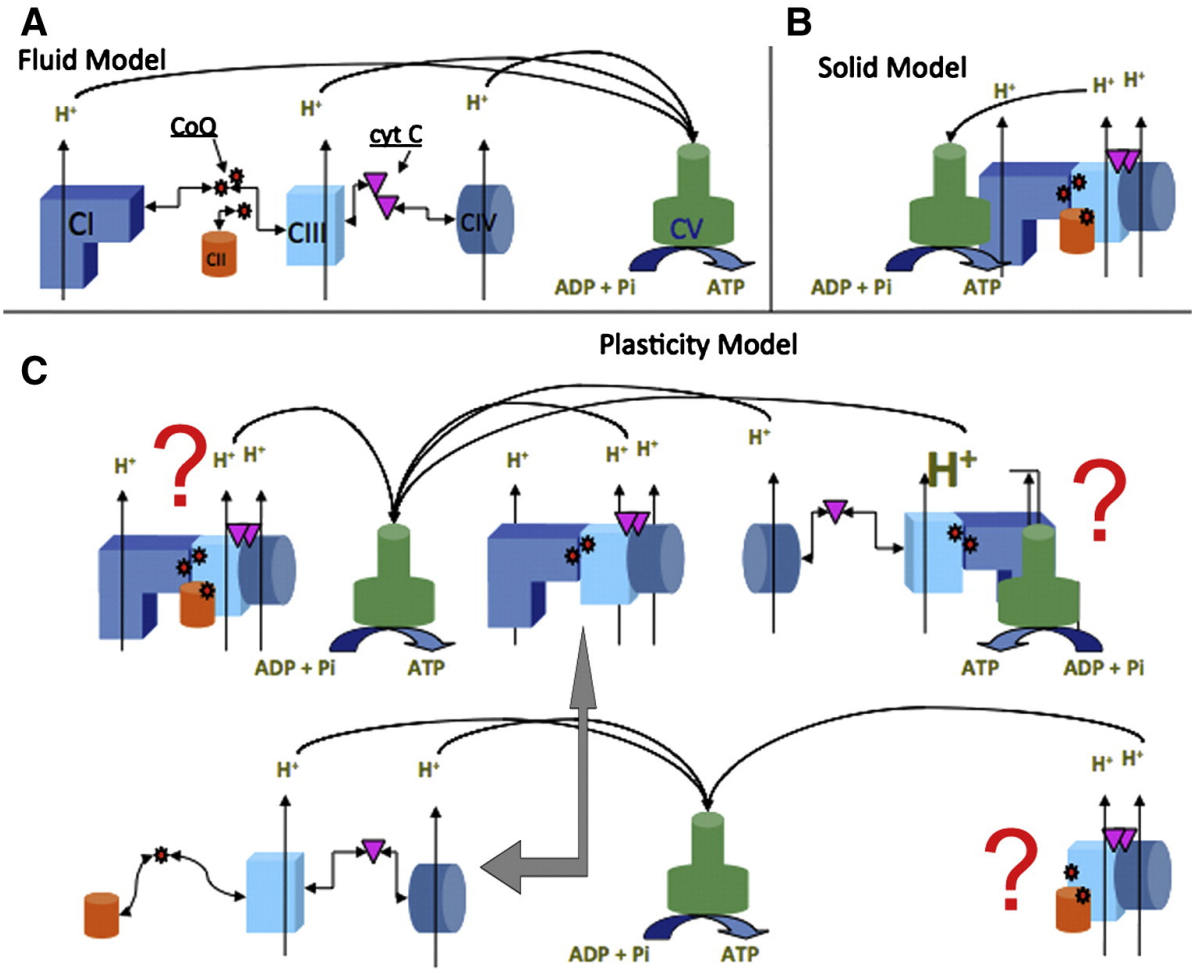


**Figure 1.1 Different models of mitochondrial respiratory chain organization.**

Schematic representation of the different models of the OXPHOS organization mentioned in the text. (A) 'random-collision' model or 'fluid model', (B) 'solid' model, and (C) the plasticity model. The question mark indicates proposed associations or supercomplexes, which are not fully confirmed. (Acin Perez R. and Enriquez JA, 2014).

It has been proposed that the benefits of supramolecular structures are enabling channeling of the substrates ubiquinone and cytochrome c or to catalytically enhance the reactions due to shorter diffusion times or stabilization of complex I (Schagger & Pfeiffer, 2000). The existence of respiratory supercomplexes have been found in different kingdoms of eukaryotes. The abundance of the supercomplexes with different compositions varies from the organism to the organism. Thus, the supercomplex with composition I + $III_2$ is the most abundant in plants, where most of the complex IV is found as monomer. I + $III_2$ + $IV_{1–4}$

supercomplex is highly present in mammals and $III_2$ + $IV_2$ in fungi (Chaban, Boekema, & Dudkina, 2014).

## 1.2. Mitochondrial gene expression

Mammalian mitochondrial DNA (mtDNA) encodes 13 proteins that are essential for OXPHOS, but the full mtDNA expression and maintenance depends on the import of a large number of nuclear-encoded proteins. MtDNA is a double stranded molecule of 16.6 kb in mammals, encodes for 13 polypeptides, 22 tRNAs and two ribosomal RNAs (rRNAs). The OXPHOS system itself has a dual genetic origin, while its subunits are encoded both by mtDNA and nuclear genes, whose products are imported into mitochondria (Cann, Stoneking, & Wilson, 1987). MtDNA has some specific features, for instance, it is transmitted almost exclusively through the female germ line. Oocytes have extremely high mtDNA copy number, whereas sperm cell mtDNA count is very low. Paternal mtDNA is usually detected only in the early pronucleus stage and the mechanism by which sperm-derived mitochondria are being eliminated is still not well understood. However, a case report of a patient with mitochondrial myopathy with a deletion in the ND2 gene showed that the change in patient's mtDNA was of paternal origin and accounted for 90% of patient's muscle mtDNA (Schwartz & Vissing, 2002). One explanation of uniparental inheritance of mtDNA could be the selective pressure in order to decrease the deleterious mutations that are present in biparental inheritance of cytoplasmic genomes (Birky, 1995; Wallace, 2007). Maternal mtDNA mutations can be transmitted to the offspring, but the phenotype severity depends on mutation load. A pathogenic mutation could be present in all copies of mtDNA or in just a few. The presence of different populations of mtDNA in a single cell is called 'heteroplasmy' in contrast to 'homoplasmy' where all the mtDNA molecules are identical (Lightowlers, Chinnery, Turnbull, & Howell, 1997). Only a mutational load above certain level can trigger a pathogenic phenotype (threshold effect). The germ line has several mechanisms to counteract maternal transmission of mtDNA mutations. A bottleneck effect is present during development, since only a small number of mtDNA molecules will populate the primordial germ cells. Moreover, there is a purifying selection mechanism that prevents specific mtDNA mutations (Poulton, 1995). Nevertheless, mothers with high mutational load in their germ line have decreased fertility (Gustafsson, Falkenberg, & Larsson, 2016; Wallace, 1993).

Mammalian mtDNA replication uses a set of different proteins in comparison to nuclear replication. At the core of the replisome is DNA polymerase-γ (POLγ), the only replicative polymerase in mitochondria. POLγ has a 3' to 5' exonuclease domain that provides a

proofreading with a low-error-frequency. This polymerase cannot use double strand DNA (dsDNA) as a template and therefore requires the DNA helicase TWINKLE. This helicase unwinds the mtDNA in 5' to 3' direction and with the help of the mitochondrial single strand DNA (ssDNA) – binding proteins (mtSSB) forms the replication fork (Clayton, 1983; Kaguni, 2004). The two strand of mtDNA differ in their guanine base composition. The one rich in guanines is therefore named 'heavy' strand (H) and the other 'light' strand (L) (Berk & Clayton, 1974). MtDNA lacks introns and has a non-coding control region, which contains promoters needed for the transcription of both the H and L strands. The central mammalian mtDNA transcription machinery includes mitochondrial RNA polymerase (POLRMT), mitochondrial transcription factor A (TFAM) and mitochondrial transcription factor B2 (TFB2M) (Peralta, Wang, & Moraes, 2012). TFAM is playing a key role in both mtDNA transcription and mtDNA maintenance, since it is helping the organization of mtDNA into nucleids (Ekstrand et al., 2004). In mammalian mitochondria, POLRMT drives transcription either from the light-strand promotor or the heavy-strand promotor. The primary polycistronic transcripts are then processed to generate individual tRNAs, rRNAs and mRNAs. 5' to 3' processing is done by RNaseP and ELAC2 (Hallberg & Larsson, 2014).

Apart from the cytoplasmic translation, mitochondria are capable of synthesizing proteins "in the house", serving their own needs. These proteins are 13 subunits of OXPHOS system and essential for its full function. The whole system enables that energy needs are met in no time. Nevertheless, it requires a coordinated synchronization of nuclear and mitochondrial gene expression. Most of the proteins involved in mitochondrial translation are encoded by the nuclear DNA and they need to be imported into mitochondria. Those proteins are the factors of initiation, elongation and termination of translation. Moreover, mitochondrial translation requires mitoribosomal proteins and the assembly factors, and last but not least, aminoacyl-tRNA synthethases and different tRNA and rRNA modifying enzymes (Smits, Smeitink, & van den Heuvel, 2010).

The mitochondrial translation machinery differs from the cytoplasmic one in many ways. The overall properties of mitochondrial ribosomes (mito-ribosomes) differ considerably from cytosolic and bacterial ones. The mammalian mito-ribosome has a low sedimentation coefficient of nearly 55S. Its body consists of a large ~39S and small ~28S subunit, which contains the mtDNA encoded 16S and 12S rRNA respectively (Taanman, 1999). Yet another difference is that mitochondrial mRNAs usually do not contain 5' untranslated nucleotides, nor 5' caps. Moreover, mitochondria have a simplified system for decoding, using only 22 tRNAs unlike 31 predicted by the "Wobble hypothesis" (Anderson et al., 1981). In addition,

mammalian mitochondria use an unique $tRNA^{Met}$ for both initiation and elongation of translation, unlike most of the lower eukaryotes (Smits et al., 2010). Mitochondrial tRNAs differ in size and shape from cytoplasmic and bacterial ones and are recognized by 19 mitochondrial aminoacyl-tRNA synthethases (ARS2-s). Two of the 19 ARS2-s are encoded by the same gene, as their corresponding cytoplasmic enzymes (Bonnefond et al., 2005).

Mitochondrial translation is divided into three phases: initiation, elongation and termination. The initiation mechanism is poorly understood, while it is not completely known how ribosome binding is facilitated due to the lack of 7-methylguanine cap which is found in cytoplasmic mRNAs (O'Brien, 2003). The first step in the initiation complex is sequence-independent binding of the small ribosomal subunit and mRNA. Mitochondrial initiation factor 3 (MtIF3) is assisting the right positioning of the start codon AUG at the peptidyl (P) site, prior to the ribosome-mRNA binding. MtIF2 is required for binding of fMet-$tRNA^{Met}$ to the small ribosomal subunit, which is followed by binding of the large ribosomal subunit to the complex and this is a GTP dependent process (Christian & Spremulli, 2009; Ma & Spremulli, 1995). The next step is elongation of translation, which requires 3 different elongation factors: mtEFTu, mtEFTs and mtEFG1. First, mtEFTu associates with an aminoacylated tRNA and GTP, carrying it to the acceptor (A) site at the small subunit where the decoding is taking place. GTP hydrolysis and releasing of mtEFTu occurs after the codon-anticondon recognition has occurred (Nagao, Suzuki, & Suzuki, 2007). As the next step, the 3' end of the aminoacyl-tRNA translocates into the P center on the large ribosomal subunit where an amino-acid is added to the growing peptide chain. This step is enabled by mtEFG1-GTP, which causes conformational changes in mitoribosome that facilitate translocation of tRNAs from A and P sites to P and exit (E) sites (Smits et al., 2010; Taanman, 1999). However, E site is actually one of the weaker tRNA-binding sites in the mammalian mitoribosome, contrasting the E site in the cytoplasmic ribosomes. Eventually, tRNAs disassociate from the mitoribosome, enabling the onset of a new cycle of elongation. The last step in mitochondrial protein synthesis is termination, which occurs when a stop codon (UAG, UAA, AGG or AGA) in the A site is recognized by a mitochondrial translation release factor (mtRF), which belongs to a larger family of mitochondrial release factors that display high conservation of a GGQ domain, which is crucial for catalyzing peptidyl-tRNA hydrolysis. In human mitochondria, mtRF1, mtRF1a, ICT1, and C12orf65 contain a GGQ domain (Wesolowska, Richter-Dennerlein, Lightowlers, & Chrzanowska-Lightowlers, 2014). The hydrolysis of the ester bond between the nascent polypeptide and tRNA is catalyzed by GTP. After this release, all the components of the machinery are available again for a new

round of translation (Bertram, Innes, Minella, Richardson, & Stansfield, 2001; Christian & Spremulli, 2012).

## 1.3. Mitochondrial stress signaling

Mitochondria are an essential part of cells for energy production and numerous processes, therefore they had to adjust to different exogenous and endogenous stresses. The ability of mitochondria to adapt to the changing conditions by activating versatile signaling pathways is known as mitochondrial stress response. The source of the stress can be diverse – oxidative damage, changes in mtDNA, OXPHOS dysfunction, accumulation of unfolded/damaged proteins etc. Mitochondria use different tools according to the type of stress they are dealing with. On the other hand, mitochondria can communicate with the nucleus and release signals, which would activate transcription of specific sets of genes that will support the survival in difficult circumstances. This is known as mitochondrial retrograde signaling.

### *Mitochondrial biogenesis*

The mitochondrial content is a highly variable feature in different tissues. For example, the heart is a muscle that is continuously being contracted and requires constant inflow of the energy, therefore cardiomyocytes are rich in mitochondria. On the other hand, in skeletal muscle, the abundance of mitochondria depends on the fibre type. Type I fibres are involved in locomotion and posture and they are known as slow-twitch muscle-fibers. They are much richer in mitochondria than type II fibers, which are used periodically for the movements that are explosive and require more strength (Hood, Tryon, Carter, Kim, & Chen, 2016). The mitochondria content is in the end a result of the organelle biogenesis and its breakdown, known as mitophagy. The biogenesis of mitochondria can be an attempt of compensation for a metabolic defect and the transcriptional regulation is mediated by specific transcriptional activators such as nuclear respiratory factors 1 and 2 (NRF1 and NRF2), cyclic AMP-responsive element binding protein 1 (CREB1), steroid hormone receptor (ERRα), peroxisome proliferator-activated receptors (PPARs). Both NRF1 and NRF2 regulate the transcription of TFAM, where ERRα promotes mitochondrial biogenesis in response to hormonal signals. However, the master regulator of mitochondria biogenesis, peroxisome-proliferator-activated receptor – coactivator – 1 alpha (PGC-1α), is the key player that is

activating transcriptional factors that are later leading to increased synthesis of key enzymes in mitochondria. Those enzymes interact with TFAM in favor to replicate more mtDNA (Arnould, Michel, & Renard, 2015). The PGC-1 family is made up of three members: PGC-1α, PGC-1β and PGC-related co-activator (PRC). Interestingly, mice lacking PGC-1α show disturbances exclusively upon stress. They have reduced exercise tolerance and a decrease in muscle mitochondria content and function. Moreover, they are failing to maintain their body temperature when exposed to cold (Spiegelman, 2007) . This suggests that PGC-1α is important for mitochondrial biogenesis on demand and its lack could be compensated with the help of the other two members of the PGC-1 family.

***mTOR***

One of the examples of retrograde signaling is the energy deprivation stress response. An increased ratio of AMP/ATP in cell triggers the activation of AMPK kinase by phosphorylation of a specific threonine (Thr 172) residue. AMPK tends to restore energy balance by activating alternative metabolic pathways that generate ATP and on the other hand, switching off anabolic processes and the ones that consume ATP (Lin & Hardie, 2017). AMPK regulates PGC-1α, which induces mitochondrial biogenesis and more ATP is produced. Moreover, AMPK regulates the serine/threonine-protein kinase mammalian target of rapamycin (mTOR). There are two different mTOR complexes in mammalas – mTORC1 and mTORC2. These two complexes are involved in different processes. While mTORC1 regulates autophagy, translation and transcription, mTORC2 is associated with cell survival and proliferation (Arnould et al., 2015). The pivotal function of mTORC1 is to promote anabolic processes through protein, lipid and nucleotide synthesis and to suppress autophagy. This is possible due to its downstream effectors, such as ribosomal S6 kinase (S6K), eukaryotic translation initiation factor 4E-binding protein (4E-BP) and unc-51-like autophagy activating kinase (ULK-1) (Rabanal-Ruiz, Otten, & Korolchuk, 2017). Under nutrient-rich conditions, mTORC1 kinase promotes growth by phosphorylation of S6K and 4EBP1.

***Autophagy***

When energy conditions are low, inhibition of mTORC1 leads toward autophagy by activation of ULK1 and different autophagy related proteins. The main role of autophagy is to reduce energy consumption when the cell is under restricted conditions. It is a highly

conserved process, which can be found in three forms: macroauotophagy, microautophagy and chaperone assisted autophagy (subsequently macroautophagy is termed as autophagy). This process involves the formation of a double-membrane autophagasome, which is fused with lysosome. Autophagy through organelle recycling is a way of saving energy. There are some types of selective autophagy such as: ER-phagy, ribophagy, pexophagy etc. Specific degradation of mitochondria is called 'mitophagy' and it recently came into focus. It has been noted that autophagy and mitophagy can be activated independently in yeast cells. Many mitophagy-specific genes were identified in yeast, among them *Atg32* which is localized around mitochondria (Kanki & Klionsky, 2009). However, mitophagy genes are not conserved in higher species, even though there are some 'functional homologs' such as PTEN-induced putative kinase 1 (PINK1) and Parkin (Narendra, Tanaka, Suen, & Youle, 2008). Autophagy and mitophagy differ in the final destination where the autophagosome will be recruited, for whose formation the inhibition of mTORC1 is required. The coordination between opposing processes such as mitophagy and mitochondrial biogenesis is essential for the cell to adjust to changing metabolic states, stresses and signals from the environment. Still, *In vivo* studies are needed to draw a clearer picture of the mitophagy process in higher organisms.

### 1.3.1 Mitochondrial unfolded protein response ($UPR^{mt}$)

Eukaryote mitochondria developed several mechanisms for quality control in order to keep mitochondrial homeostasis and prevent cell death. One of them is an internal proteolytic system, which degrades misfolded or unfolded proteins. In situations where proteins get damaged or misfolded, it is crucial that they are turned over and removed, in order to prevent deleterious consequences on the cell. Since majority of the mitochondrial proteins are coded by nuclear DNA, translated in the cytosol and imported into the mitochondria, a system that precisely monitors this translocation is needed. Mitochondrial precursor proteins are kept in an unfolded state so they can be easily translocated across the mitochondrial membranes. The main challenge here is that precursor proteins in unfolded state are more prone to make aggregates, since their hydrophobic regions are exposed and unwanted protein-protein interactions are very likely to occur. This can be overcome by the action of chaperones, which are able to guide those precursors to the mitochondrial surface. Moreover, there is a specific set of chaperones in mitochondria that takes action once the protein enters this organelle. One of them is mitochondrial heat shock protein 70 (mtHsp70), also known as GRP75, which has

been shown to help the import of proteins with mitochondrial targeting signal and later on it allows the protein to find its correct tertiary structure by keeping it in an unfolded conformation (Horwich, Weber-Ban, & Finley, 1999). Once the protein has been imported and its targeting sequence is cleaved off, it is refolded by heat shock protein 60 (HSP60) and his co-chaperonin 10 (HSP10) (Bross et al., 2007). HSP10 acts as a lid and regulates the ATP-dependent activity of HSP60. Moreover, it has been shown that GRP75 interacts with HSP10 independently of HSP60, promoting the biogenesis of its heptameric rings (Bottinger et al., 2015). Mitochondria tend to produce misfolded proteins at a low level, but in times of extensive stress those proteins might accumulate and endanger mitochondria health. Therefore, mitochondria developed a specific defense mechanism called mitochondrial unfolded protein response ($UPR^{mt}$) in order to alleviate proteotoxic stress. $UPR^{mt}$ was primarily investigated in *C. elegans (Yoneda et al., 2004)*. It has been shown that $UPR^{mt}$ can also be induced in mammalian cells by expression of truncated ornithine transcarbamoylase (ΔOTC) in the mitochondrial matrix. As the ΔOTC cannot fold properly, it forms aggregates signaling to the nucleus to transcribe genes encoding HSP60, HSP10 and additionally some proteases (Zhao et al., 2002). In *C. elegans* $UPR^{mt}$ acts through upregulation of heatshock protein 60 (*hsp-60)* and 6 (*hsp-6),* which are homologs of mammalian HSP60 and GRP75 respectively. It has been shown that treatment of worms with ethidium bromide upregulates the expression of *hsp-60* and *hsp-6.* This was due to depletion of mtDNA and therefore loss of single subunits of the multimeric complexes, which further increased the number of unassembled nuclear-coded partner subunits (Yoneda et al., 2004). In line with the previous finding, it has also been shown that disruption of mitochondrial translation leads to the activation of $UPR^{mt}$. Moreover, translation inhibitors such as doxycycline or knockdown of ribosomal proteins induce $UPR^{mt}$ (Houtkooper et al., 2013). Additionally, perturbations of ETC caused by toxins or mutations were also shown to induce $UPR^{mt}$ signaling (Durieux, Wolff, & Dillin, 2012; Feng, Bussiere, & Hekimi, 2001; Runkel, Liu, Baumeister, & Schulze, 2013). Accumulated unfolded proteins are degraded by the Clp protease proteolytic subunit (ClpP), which in worms leaves small peptides that are later transported to the outer mitochondrial membrane (OMM) with the help of HAF-1 exporter. Those peptides trigger the translocation of the transcription factor ATFS-1, which contains both a nuclear and mitochondrial localizing sequence. Under basal, physiological conditions, this factor is transported to mitochondria and degraded by the LONP1 protease. However, when there is stress, ATFS-1 is traveling to the nucleus where it activates the expression of chaperone genes, OXPHOS assembly factors and glycolysis genes (Nargund, Pellegrino, Fiorese, Baker,

& Haynes, 2012). Interestingly, the activation of UPR$^{mt}$ can occur in a cell non-autonomous manner. It has been shown that mitochondrial dysfunction in neuronal cells in *C. elegans* can activate UPR$^{mt}$ in intestinal cells (Durieux et al., 2012).

In line with both *C.elegans* and mammalian research, the ATF5 transcription factor was suggested as a mammalian homolog of ATFS-1. It has been suggested that ATF5 is necessary for the UPR$^{mt}$ activation in mammalian cells during mitochondrial stress (Fiorese & Haynes, 2017). Moreover, ATF5 was found to be transcriptionally upregulated in several mouse models of mitochondrial dysfunction. ATF5 was induced in the Deletor mouse, that carries a dominant mutation in the replicative helicase Twinkle gene. This mouse model displays mild mitochondrial myopathy with unaffected lifespan (Tyynismaa et al., 2010). Additionally, in our lab we showed recently that *Atf5* was upregulated already in a very early stage in the heart-specific DARS2-deficient mouse, with severe mitochondrial dysfunction and strongly activated mitochondrial stress response (Dogan et al., 2014a). We also have demonstrated in our lab that CLPP is dispensable for the activation of UPR$^{mt}$ in mice. Moreover, the lack of CLPP improved the OXPHOS deficiency in DARS2 deficient hearts and extended the lifespan of the mice (Seiferling et al., 2016). Apart from increased *Atf5* expression, we detected a significant *Atf4* and *Chop-10* upregulation in our DARS2-deficient mice. These transcription factors belong to another line of defense in mitochondrial stress signaling which is known as integrated stress response (ISR). The mammalian UPR$^{mt}$ is intimately associated with the integrated stress response, while UPR$^{mt}$ activation requires eIF2α phosphorylation. On the contrary, in *C. elegans* the UPR$^{mt}$ does not require eIF2α phosphorylation. The attenuation of protein synthesis possibly reduces the nascent protein load in the matrix, so that chaperones and proteases may better promote proteostasis in these mitochondria (Melber & Haynes, 2018).

### 1.3.2 Integrated stress response (ISR)

Cells deal with many different sources of stress and accordingly use different mechanisms to adapt to the current state. The integrated stress response (ISR) is a common adaptive pathway that eukaryotic cells can activate in response to different stress stimuli. The main factor in this pathway is eukaryotic translation initiation factor 2 alpha (eIF2α), which when phosphorylated impedes global translation and shifts it towards the protein synthesis of very important factors needed for cellular recovery (Pakos-Zebrucka et al., 2016). Different physiological states and pathological conditions can activate this signaling pathway. There are

four different kinases that are leading to the phosphorylation of eIF2α, which are all activated by different stimuli. PKR-like ER kinase (PERK) is activated by endoplasmatic reticulum (ER) stress, which can be due to accumulated proteins, defects in calcium homeostasis etc (Harding, Zhang, & Ron, 1999). Another kinase is general control non-derepressable 2 (GCN2) and it is activated in response to amino acid deprivation. Although, it has been shown that GCN2 is activated as a result of glucose deprivation, this is probably an indirect effect of amino acid overconsumption as a result of the low glucose level (Ye et al., 2010). The next kinase in the pathway, PKR, is activated by double-stranded-RNA (dsRNA), as a result of a viral infection (Lemaire, Anderson, Lary, & Cole, 2008). The last kinase in ISR is heme-regulated eIF2α kinase (HRI), which is mainly expressed in erythroid cells, unlike the other 3 kinases, which are broadly distributed. This kinase is activated by heme-deficiency and it protects erythroid cells from toxic globin aggregates, which are accumulated in iron deficiency (Han et al., 2001). As a response to ISR activation, those kinases lead to phosphorylation of eIF2α, which results in the global attenuation of 5'-cap-dependent protein synthesis and preferentially translation of specific mRNAs that have an upstream open reading frame (uORF) within their 5' untranslated region (5' UTR). Those mRNAs contain internal ribosome entry sites (IRES) and the 40S ribosomal subunit can be directly recruited in the vicinity of the start codon, independently of 5'-cap recognition (Komar & Hatzoglou, 2011). One of those preferentially translated mRNAs is the ATF4 transcription factor, which belongs to the family of basic leucine zippers (bZIP) activating transcription factors (ATF/CREB family) (Ameri & Harris, 2008). ATF4 is a master regulator of ISR, involved in many different functions such as energy expenditure, thermogenesis, glucose homeostasis, lipid metabolism, bone development and obesity regulation (C. Wang et al., 2010). ATF4 is upregulated upon stress and it is further activating the expression of stress-responsive genes. It can form homodimers and heterodimers with different transcription factors providing the further complexity of ISR regulation. One of those factors is CHOP, which together with ATF4 can induce autophagy upon starvation (B'Chir et al., 2013). The ISR must have its duration precisely controlled, and this is possible through the phosphatase GADD34, which dephosphorylates eIF2α (Novoa, Zeng, Harding, & Ron, 2001). The scheme of ISR is presented in Figure 1.2.

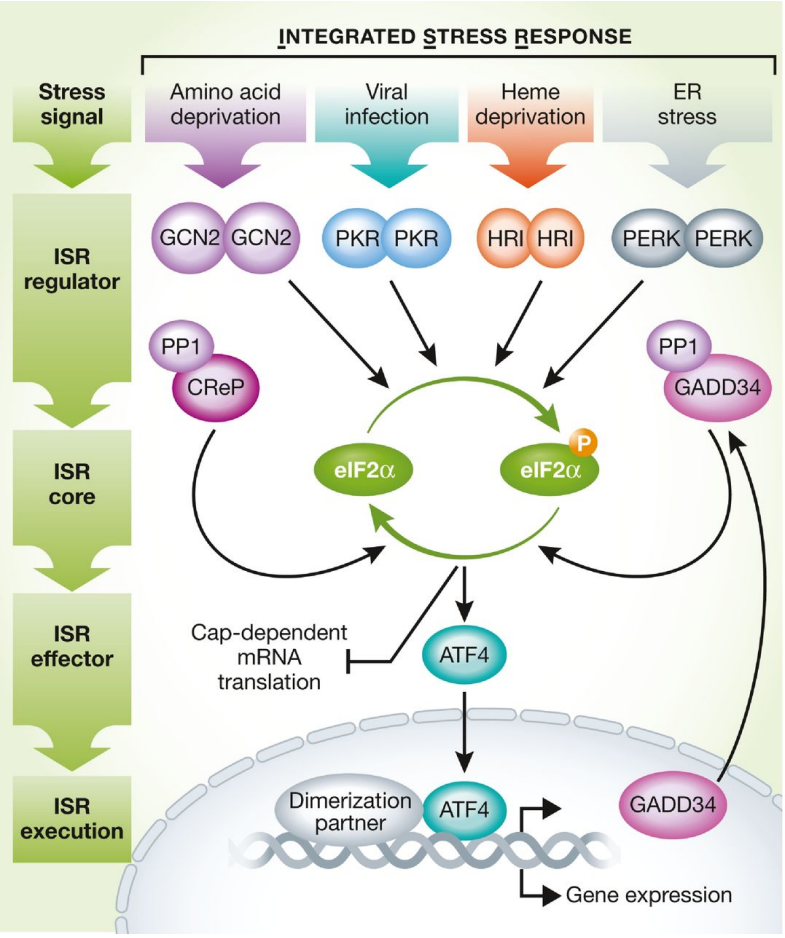


**Figure 2.2 Integrated stress response.**

Different stress stimuli are sensed through four different kinases that lead to phosphorylation of eIF2α. This leads to the repression of global protein synthesis and preferential translation of mRNA needed for the cell survival or cell apoptosis. ATF4 is the master transcription factor, which leads to the gene expression of pro-survival genes (Pakos-Zebrucka et al., 2016).

Cytosolic translation can be modulated during mitochondrial stress by the GCN2 kinase, which can be stimulated by increased ROS, amino acid reduction or ribosome stalling (B. M. Baker, Nargund, Sun, & Haynes, 2012). The phosphorylation of eIF2α will follow and subsequently activation of ATF4, ATF5 and CHOP10. The functional relationship between those three proteins in mitochondrial stress is still unclear, even though it was shown before that transcription of *Atf5* is controlled by ATF4 and CHOP10 out of the context of mitochondrial stress (Teske et al., 2013). ATF5 that is localized in the nucleus is able to activate mitochondrial-stress-response genes (Fiorese et al., 2016). A recent study demonstrated that none of the individual eIF2α –kinase knockdowns abolished *ATF4* induction in HeLa cells treated with FCCP (Quiros et al., 2017). Surprisingly, recent data from the Deletor mouse showed that mTORC1 activation stimulates ATF4 activity and

therefore it is implicated in ISR and furthermore, in $UPR^{mt}$ regulation (Khan et al., 2017). Mammalian models of mitochondrial dysfunction showed in addition that ATF4 promotes one-carbon metabolism, which is crucial for biosynthetic processes of nucleotides and amino acids (Bao et al., 2016). However, it is still not sure if the ATF4 response is adaptive or maladaptive. ATF4-dependent serine biosynthesis in respiratory chain deficiency might suggest an adaptive response by helping the cellular one-carbon availability. Also, transsulfuration represents another potential adaptive ATF4-response, since it promotes gluthathione synthesis, necessary for ROS scavenging (Bao et al., 2016; Nikkanen et al., 2016). On the contrary, a recent study showed that inhibition of ATF4 is protective in rodents with intracerebral hemorrhage, pointing out possible maladaptive aspects of this transcription factor (Karuppagounder et al., 2016).

The ISR pathway was shown to stimulate FGF21 expression. The activation of the eIF2α/ATF4 axis stimulates *FGF21* transcription as a response to amino-acid deprivation, ER stress or mitochondrial dysfunction (De Sousa-Coelho, Marrero, & Haro, 2012; Keipert et al., 2014; Schaap, Kremer, Lamers, Jansen, & Gaemers, 2013). Moreover, it was observed that the the muscle-specific overexpression of dynamin related protein 1 (DRP1) can activate the eIF2α/ATF4/FGF21 axis, which results in inhibition of muscle growth (Touvier et al., 2015). However, further studies are needed in order to decipher the precise role of FGF21 in mitochondrial dysfunction induced ISR.

### 1.3.3 Quality control of mitochondrial proteostasis

When chaperones fail to promote refolding of unfolded proteins, the proteases have the task to turn over the unfolded proteins in order to prevent the greater damage. The problem in mitochondria appears when there is an imbalance in the nuclear and mitochondrial encoded subunits of the respiratory chain (Reinecke, Smeitink, & van der Westhuizen, 2009). Furthermore, proteins can be damaged by reactive oxygen species (ROS), which can lead to loss of their function. Even though mitochondria have a specific system to alleviate ROS production by hosting a manganese superoxide dismutase (MnSOD) in their matrix, ROS can still cause protein modifications and consequently wrong folding. These proteins must be turned over by mitochondria's proteolytic machinery (Wei, Miao, Yang, & Luo, 2008) .

One of the proteases residing in the mitochondrial matrix is the LONP1 protease, which is conserved among prokaryotes and eukaryotes. It comprises three domains, an N-terminal domain, central ATPase domain, and a C-terminal protease domain. The N-terminal

domain serves for oligomerization and protein substrate binding. The AAA+ domain is in the central part and it is involved in ATP binding and hydrolysis. The C-terminal domain owns the protease domain, which contains a serine and lysine dyad in the active site (Matsushima & Kaguni, 2012). LONP1 is in charge of elimination of oxidatively damaged or denaturated proteins (C. K. Suzuki, Suda, Wang, & Schatz, 1994). Moreover, mammalian LONP1 has been shown to degrade TFAM, aconitase and Fe/S protein (Bota & Davies, 2002). The findings have shown that Lon reduces TFAM and mtDNA levels and selectively degrades TFAM in order to regulate the levels of mitochondria transcription (Matsushima, Goto, & Kaguni, 2010). In humans, LONP1 was found to be involved in the regulation of respiration, removal of the oxidized proteins and protein quality control, since it cooperates with chaperones in order to keep the proteins unfolded prior to proteolysis (Bender, Lewrenz, Franken, Baitzel, & Voos, 2011). It has been demonstrated that levels of LONP1 decline in mice skeletal muscles with age (Bota, Van Remmen, & Davies, 2002). However, constitutive expression of Lon in the fungus *Podospora anserine* results in an increased life span without affecting growth and fertility (Luce & Osiewacz, 2009).

Another protease present in the mitochondrial matrix is CLPP, which is also conserved from bacteria to higher organisms. This protease is part of larger complex together with CLPX, which is a chaperone necessary for substrate recognition. Together they form a CLPXP complex, whose homolog is absent in fermenting yeasts *S. cervisae* and *S. pombe* (Yu & Houry, 2007). In order to exert its role, CLPXP uses the energy of ATP hydrolysis. Therefore, it belongs to the special group of AAA+ proteases, which means it contains a conserved hetero-hexameric domain associated with the ATPase activity (Tatsuta & Langer, 2009). After CLPX has recognized, bound and unfolded the substrate, it translocates it to the chamber where CLPP cleaves it. The proteolytic sites of CLPP are placed inside the barrel-shaped-chamber, which is formed by two heptameric rings (Lee, Baker, & Sauer, 2010).

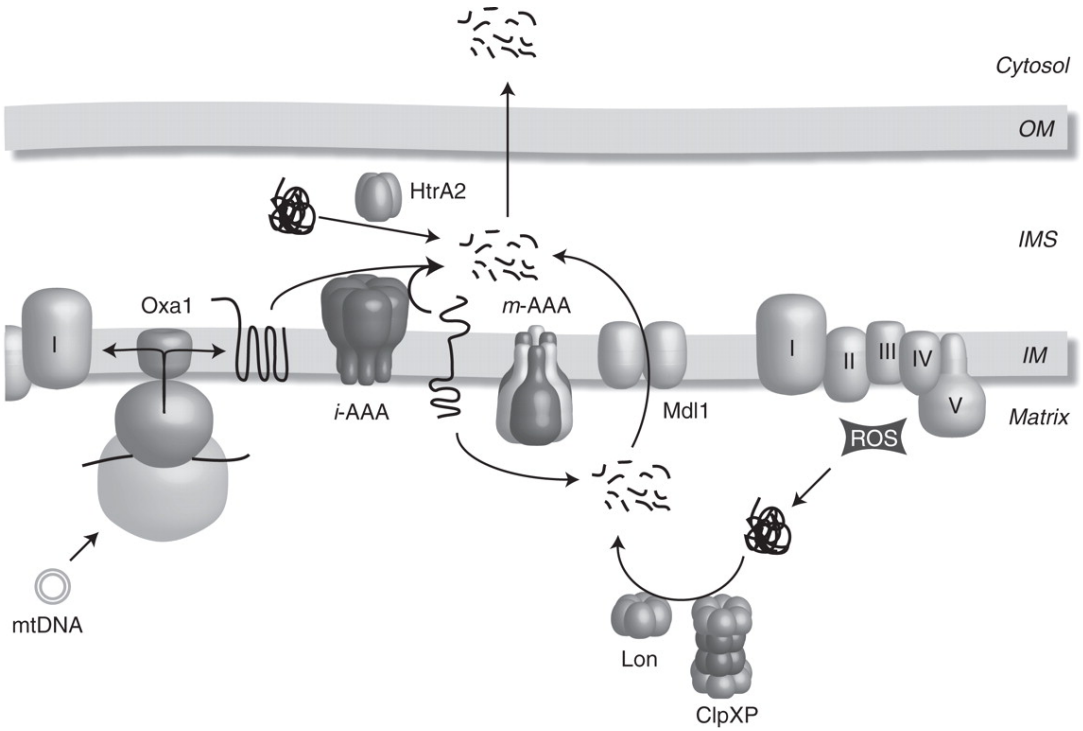


**Figure 1.3 Mitochondrial proteases.**

Unassembled subunits and unfolded or damaged proteins are turned over by either *i*- or *m*-AAA proteases. Proteins that become damaged or unfolded in the mitochondrial matrix are degraded by Lon or ClpXP. OM – outer membrane; IMS – intermembrane space; IM – inner membrane (M. J. Baker, Tatsuta, & Langer, 2011).

Apart from the soluble matrix proteases, mitochondria harbor special proteolytic machineries for membrane-integrated proteins. The inner mitochondria membrane is immensely rich in proteins and moreover, it houses the respiratory chain. Those proteins are prone to damage caused by ROS and therefore the system, which can regulate the degradation and turnover of the proteins, is highly in demand. The integrity of the inner membrane is controlled by the members of the FtsH / AAA family of proteases (filament-forming temperature-sensitive). They are building homo- or hetero-oligomeric complexes, which contain highly conserved subunits. Bacterial FtsH proteases are hexameric, barrel-like structures with an internal cavity containing proteolytic sites. Based on their topology, there are two classes of AAA complexes: *i*-AAA proteases, which are exposed to the intermembrane space, and *m*-AAA proteases, which are facing the matrix space (Tatsuta & Langer, 2009). This protease group builds homo-oligomeric structure anchored in membrane and facing the intermembrane space, comprising of Yme1 and YME1L subunits in yeast and mammalian mitochondria, repectively (Langer, Kaser, Klanner, & Leonhard, 2001). The *i*-AAA proteases have been implicated to have a role in many processes, such as: mitochondrial fusion/fission (Rainbolt, Saunders, & Wiseman, 2015), quality control and transport of

intermembrane proteins and respiratory chain (Rainey et al., 2006), and UPR$^{mt}$ (Zhao et al., 2002). The *m*-AAA protease in yeast exists as hetero-oligomeric structure comprising of Yta10 and Yta12 subunits (paraplegin and AFG3L2 in humans). Moreover, in human mitochondria, both homo-oligomeric (AFG3L2) and hetero-oligomeric (AFG3L2 and paraplegin) assemblies were found (Koppen, Metodiev, Casari, Rugarli, & Langer, 2007). AAA proteases defects are associated with different diseases. Mutations in the Spg7 gene, encoding paraplegin, cause neurodegenerative disorder – an autosomal recessive form of hereditary spastic paraplegia and mutations of Afg3l2 cause a dominant form of spinocerebellar ataxia (Casari et al., 1998; Di Bella et al., 2010). The clinical picture in the patients with Afg3l2 mutations is much more severe when compared to the patients with mutations in Spg7. This is due to the fact that Afg3l2 mutations affect both homo- and hetero-oligomeric structures. Moreover AFG3L2 is more abundant than paraplegin (Koppen et al., 2007). The *m*-AAA protease regulates mitochondrial calcium uniporter (MCU) assembly and mitochondrial calcium homeostasis (Konig et al., 2016). Additionally, it has been demonstrated that the *m*-AAA protease is responsible for the maturation of MRPL32, which is a mitochondrial ribosomal protein required for the assembly of ribosomes. A constitutive Purkinje cells *Afg3l2* KO mouse in revealed a decrease in the rate of mitochondrial translation associated with deregulated ribosomal assembly. This later led to early-onset fragmentation of the mitochondrial network, which resulted in neurodegeneration (Almajan et al., 2012).

### 1.3.4 Mitokines

In *C. elegans,* induction of UPR$^{mt}$ in the nervous system can induce the same stress response in the distal tissue, such as intestine and prolonging the lifespan in that manner. Correspondingly, it has been hypothesized that this extension of the response to the distal tissues is due to specific soluble factors, which were named “mitokines”, diffusible moleculeas released from one tissue and inducing mitochondrial pro-longevity signals in distal tissues (Durieux et al., 2012). Later on, numerous factors were described as mitokines, since they were found produced and secreted in response to mitochondrial stress. The most prominent ones are Fibroblast Growth Factor 21 (FGF21) and Growth Differentiation Factor 15 (GDF15) (Rose, Santoro, & Salvioli, 2017). The accent here is on the possibility of this proteins to function in a non-cell-autonomous manner, meaning that they could be produced in one tissue which is affected by stress and later on have an effect on another tissue, by improving its adaptive stress response.

Therefore, these factors can act in autocrine, paracrine and endocrine manner. However, it is still unknown if these soluble factors have exclusively beneficial effects or also detrimental ones. From previous data, one could hypothesize that mild mitochondrial dysfunction could have positive effects on longevity in animals as in humans, which is known as 'mitohormesis'. The main idea behind mitohormesis is that the variety of mild stresses could be beneficial for an organism by making it less susceptible to detrimental effects of larger stresses thereby leading to increased longevity. (Yun & Finkel, 2014). Moreover, it is very interesting to note that in *C.elegans* activated stress responses, such as chaperone activation, xenobiotic detoxification or oxidative stress, are all coupled to increased longevity (Shore, Carr, & Ruvkun, 2012). The main question that remains is if that mitohormetic principle can be used for finding treatments for diseases.

#### 1.3.4.1 Growth differentiation factor 15 (GFD15)

GDF15 is a member of the transforming growth factor beta (TGF β) family and recently it has been considered as a diagnostic marker for mitochondrial diseases. It is synthesized as a propeptide, which is later cleaved in ER and secreted as a mature protein. The secreted mature GDF15 is present in blood and cerebrospinal fluid, however the unprocessed forms were reported to be found in stroma (Bauskin et al., 2010). The expression of this mitokine is upregulated by different stresses and stimuli. For instance, hypoxia was shown to activate the expression of GDF15 in different types of cancer (Krieg et al., 2010). Moreover, exposure to pro-inflammatory cytokines increased the expression of GDF15 in macrophages (Bottner, Suter-Crazzolara, Schober, & Unsicker, 1999). GDF15 knockout mice have an increase in food intake and consequentially weigh more (Macia et al., 2012). On the other hand, overexpression of GDF15 leads to decreased appetite by direct action on feeding centers in the brainstem and hypothalamus (Johnen et al., 2007). Moreover, it has been shown that GDF15 has cardioprotective effects. Under pathological conditions transgenic GDF15 mice deal partially better with cardiac stress. Furthermore, recombinant GDF15 treatment has beneficial effects on apoptosis in cultured cardiomyocytes (Kempf et al., 2006). Interestingly, different mouse models with mitochondrial dysfunction in skeletal muscle were shown to be protected from diet-induced obesity and they were more insulin sensitive. This suggested the existence of specific factors, which enables dysfunctional mitochondria in a given tissue to communicate with other tissues (Kim et al., 2013). In the *Crif1* muscle-specific knockout mouse, GDF15 was found to be elevated and suggested to be

responsible for decrease of fat mass, improved insulin sensitivity and resistance to obesity (Chung et al., 2017). This suggested GDF15 as a potentially promising therapeutic agent for the obesity, caused by insulin resistance.

A couple of studies have shown that GDF15 could be a good diagnostic marker for mitochondrial diseases. In a study where enucleated cells from patients carrying MELAS mtDNA mutation fused with cultureable cells, also known as cybrid cells, were used, expression levels of *GDF15* were shown to be increased compared to control (Fujita et al., 2015). Additionally, analysis of skeletal muscle of patients carrying a mutation in the thymidine kinase 2 gene, which causes mitochondrial myopathy, showed an increase in GDF15 (Kalko et al., 2014). Mitochondrial myopathy is one of the most common manifestations of mitochondrial disease in adulthood. The Deletor mice showed a plethora of robust transcriptional and metabolic stress responses, among which is also GDF15. The upregulation of GDF15 in Deletor mouse is a result of mTORC1 activation of ATF4, which leads to the increased expression of cytokines (Khan et al., 2017).

#### 1.3.4.2 Fibroblast growth factor 21 (FGF21)

The second identified mitokine, FGF21, belongs to the family of fibroblast growth factors (FGFs), which have diverse role in signaling and development in many tissues. In mammals, there are 22 different FGFs, which can be autocrine, paracrine or endocrine. FGF21, together with FGF15/19 and FGF23 belongs to the endocrine family of FGFs, since they have a reduced affinity to heparin sulfate glycosaminoglycans (HSGAGs), which are sequestering the proteins to the extracellular matrix (BonDurant & Potthoff, 2018). FGF21 binds a tyrosine kinase receptor FGFR, which, in mammals, exists in different isoforms (1b, 1c, 2b, 2c, 3b, 3c, 4), that are tissue-specific (Kurosu et al., 2007). For the activation of FGFR by FGF21, the presence of a co-receptor β-Klotho (KLB) is necessary. KLB is a FGFR-binding single-pass transmembrane protein and essential for endocrine effects of FGF21 (M. Suzuki et al., 2008). FGF19 and FGF21 both require KLB for their action, however, FGF19 has more preferences for the FGFR4 isoform, while FGF21 preferentially binds FGFR1c and FGFR3c (X. Zhang et al., 2006). Concerning tissue specificity, FGF21 is predominantly expressed in liver, but its mRNA is also found in the other organs – thymus, pancreas, brain, white (WAT) and brown adipose tissue (BAT), skeletal muscle, testes, gastrointestinal tract and recently its expression in heart was detected (Fon Tacer et al., 2010). The expression levels in liver are impacted by many different factors, such as nutritional status, stress levels,

temperature etc. During fasting, fuel utilization is shifted from carbohydrates to ketone bodies. This involves other tissues, such as WAT, which is activating lipolysis and releasing free fatty acids (FFA) and glycerol into blood that enables ketogenesis and gluconeogenesis. On the other hand, lipid intake via suckling or consuming high-fat diet in mice, stimulates a raise of FGF21 in serum, which appears to be a result of increased blood concentrations of FFAs. Those FFAs activate PPAR α – dependent induction of FGF21 in liver (Inagaki et al., 2007). It is interesting to note that in humans the elevation of plasma FFAs has a completely opposite effect – a decrease of FGF21 levels. This discrepancy might be due to the different rates in metabolism between mice and humans (Matikainen et al., 2012). Moreover, it has been shown that exercise induces hepatic FGF21 expression through lipolysis of adipose tissue and consequently fatty acid signaling which promotes ER stress in liver (Cuevas-Ramos et al., 2012).

One of the conditions where FGF21 is induced is metabolic stress. It has been also shown that many different types of cellular stress can lead to its induction, which is why FGF21 is often referred to as a "stress hormone". Under mitochondrial stress, FGF21 production is increased in skeletal and cardiac muscle, and BAT (Dogan et al., 2014b; Keipert et al., 2015). Strikingly, the physiological relevance of this extrahepatic FGF21 is still unknown. Increased expression of FGF21 was observed in many mouse models with mitochondrial dysfunction (Dogan et al., 2014b; Trifunovic et al., 2004; Tyynismaa et al., 2010). In Deletor mouse, the expression of *Fgf21* was increased 3-fold and moreover, circulating levels of FGF21 were found to be upregulated. Serum FGF21 had systemic effects on metabolism of the mice, copying the starvation mode features, such as weight loss, high-fat diet (HD) induced obesity resistance, smaller adipocytes and lower hepatic fat content (Tyynismaa et al., 2010). Mitochondrial diseases are associated with dysregulated lipid metabolism and FGF21 has been proposed to regulate lipid usability. However, further research is needed to connect mitochondrial dysfunction and potential effects of FGF21.

It has been observed that FGF21 plays a physiological role in thermogenic activity of WAT. Adipose-derived FGF21 has been shown to have both autocrine and endocrine role and it is capable of increasing UCP1, as well as other thermogenic genes in adipose tissue during cold response. Pharmacological doses of FGF21 managed to induce thermogenic response in both BAT and WAT, by stabilizing the PGC1α protein (Fisher et al., 2012). Moreover, FGF21 increases insulin sensitivity in primary brown adipocytes by facilitating glucose uptake. This effect has been lost in mice lacking the β-Klotho co-receptor in adipose tissue (BonDurant et al., 2017). It is interesting to note that different studies showed contradictory

data on the FGF21 and lipolysis in adipose tissue. *In vivo* studies showed that there is a difference in acute and chronic FGF21 administration. A single dose of recombinant FGF21 lowers FFA concentration in blood and decreases the rate of lipolysis in WAT (Fisher et al., 2010), while the chronic states, where FGF21 is up-regulated, lead to higher levels of FFAs and increased lipolysis (Hotta et al., 2009). More than that, FGF21 was shown to mediate many more physiological roles, for instance – appetite control in brain (Markan & Potthoff, 2016), regulation of macronutrient intake (Tanaka & Kido, 2008), effects on growth and lifespan etc. (Inagaki et al., 2008).

Until recently, it has been thought that FGF21 is not expressed in heart. This is due to the fact that cardiac expression of FGF21 occurs only during stress, such as ischemic insults, fasting, obesity, mitochondrial stress etc. (Salminen, Kaarniranta, & Kauppinen, 2017). Both endogenous and exogenous FGF21, has an anti-apoptotic role and protects against isoproterenol induced cardiac insult by promoting FAO, inducing anti-oxidative signaling and reducing inflammation (Planavila, Fernandez-Sola, & Villarroya, 2017; Planavila et al., 2013). Interestingly, it has been also shown that FGF21 secreted from liver and adipose tissue can act as an endocrine protection in the ischemic myocardium (S. Q. Liu et al., 2013). As previously mentioned, FGF21 binds the FGFR1 receptor, using β-Klotho, which further activates the dimerization of the tyrosine kinase receptor. This induces autophosphorylation of the receptor and recruits and phosphorylates first adaptor protein – FRS2α. After phosphorylation of FRS2α, 4 different known pathways can be activated in cardiomyocytes (Figure 1.3). The first one is activation of the ERK1/2-CREB-Sirt1-PGC1α signaling cascade, which leads to the improved FAO by increasing the expression of MCAD (Planavila et al., 2013). The second pathway is associated with the inhibition of NFkβ, which prevents activation of pro-inflammatory cytokines such as TNFα, IL6 and MCP1. The third pathway results in a decrease in cardiac fibrotic formation, and the fourth results in the reduction of oxidative stress (Planavila et al., 2013). Very little is known about cardiac function of FGF21 in conditions of mitochondrial stress. DARS2 depletion in heart and skeletal muscle induces a 250-fold increase in *Fgf21* mRNA levels, but the function of it is still unknown (Dogan et al., 2014). In addition, a mouse model, where the mitochondrial protein p32 was depleted in heart, has shown a 40-fold increase in *Fgf21* mRNA levels. P32 is suggested to be a protein and RNA chaperone required for functional mito-ribosome formation (Saito et al., 2017). Also, *Fgf21* mRNA upregulation was detected in the hearts of mtDNA mutator mice, which are displayed with dilated cardiomyopathy and this increase was even more pronounced when the mice were additionally depleted of UCP2 (Kukat et al., 2014)

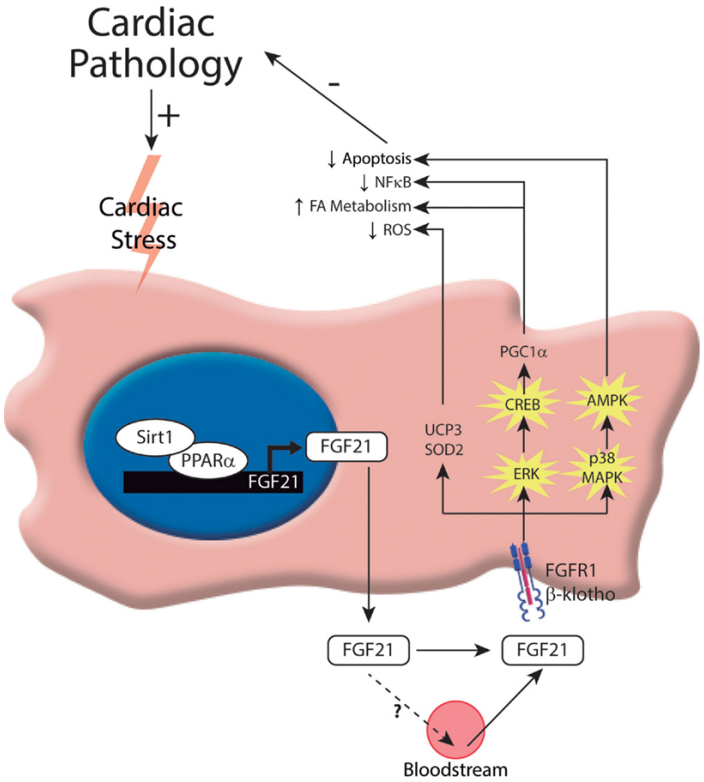


**Figure 1.4 FGF21 signaling in cardiomyocyte**

Intracellular pathways of FGF21 production and action on the heart. In response to ischeamic injury, cardiomyocytes induce the expression of FGF21. The transcriptional pathway that has been implicated in governing this process is the Sirt1–PPARα pathway. The FGF21 produced in cardiomyocites can be secreted in the bloodstream and has an action on the heart, through FGFR1- β-Klotho complex, which results in the activation of the ERK1/2 pathway. Phosphorylated CREB and p38-MAPK act through different intracellular mechanisms to exert protection against cardiac damage (Planavila et al., 2013).

## 1.4. Mouse models of mitochondrial diseases caused by defects in mitochondrial translation

Defects in mitochondrial translation cause a plethora of mitochondrial diseases, which are tissue specific and have a variety of clinical representations. These diseases are mostly featured by respiratory chain deficiency and they affect the high-energy consuming organs such as brain, heart, skeletal muscle and liver. The other tissues could be affected too, and this also contributes to the differential clinical picture of this subgroup of diseases. The mitochondrial defects in protein synthesis are caused by mutations in the genes for tRNAs, ribosomal proteins, ribosome assembly proteins, mitochondrial aminoacyl-tRNA synthetases, tRNA modifying enzymes and initiation, elongation and termination factors of translation.

### 1.4.1 Aminoacyl-tRNA synthethases in mitochondrial diseases

Aminoacyl-tRNA synthethases (aaRSs) are crucial enzymes in the initial steps of protein synthesis. They are the catalysts of a two-step reaction that charges tRNAs with their cognate amino-acid. In the first step, they activate the amino-acid with ATP, and an intermediate aminoacyl-adenylcyclate is formed. Secondly, they transfer the aminoacyl group to the 3' end of a tRNA and release adenosine monophosphate (AMP) (Diodato, Ghezzi, & Tiranti, 2014). There are cytoplasmic and mitochondrial aaRSs, and the latter are always marked with "2" after the name. Mitochondrial aaRSs are coded by nuclear DNA and imported into mitochondria due to the presence of a mitochondria targeting sequence (MTS), located at the N-terminus of the precursor. Mt-aaRSs are highly conserved enzymes and there are in total 19 of them acting in mitochondrial translation, of which two – glycine (Gly) and lysine (Lys)-RS- are coded by the same gene as nuclear homologs.

Knowing the magnitude of the translation machinery, it is not surprising that mitochondrial disorders caused by its impairment are genetically heterogeneous. All the known diseases caused by mutations in different mt-aaRSs are described in the table 1.1.

**Table 1.1. Mutations in mitochondrial aminoacyl-tRNA synthethases and their clinical manifestations.**

| gene | protein | clinical picture | onset | reference |
|---|---|---|---|---|
| DARS2 | Mt aspartyl-tRNA synthethase | Leukoencephalopathy with brain stem and spinal cord involvement and lactate elevation | Childhood/ adulthood | (van Berge et al., 2012) |
| RARS2 | Mt arginyl-tRNA synthethase | Pontocerebellar hypoplasia type 6 | Perinatal | (Edvardson et al., 2007) |
| YARS2 | Mt tyrosyl-tRNA synthethase | Myopathy, lactic acidosis and sideroblastic anemia (MLASA) | Childhood | ( Riley et al.) |
| SARS2 | Mt seryl-tRNA synthethase | Hyperuricemia, pulmonary hypertension, renal failure and alkylosis (HUPRA) | Perinatal | (Belostotsky et al., 2011) |
| AARS2 | Mt alanyl-tRNA synthethase | Cardiomyopathy, cerebellar ataxia | Childhood | (Gotz et al., 2011) |
| MARS2 | Mt methionyl-tRNA synthethase | Autosomal recessive spastic ataxia | Childhood/ adulthood | (Sasarman, Nishimura, Thiffault, & Shoubridge, 2012) |
| HARS2 | Mt histidyl-tRNA synthethase | Perrault syndrome | Childhood/ adulthood | (Pierce et al., 2011) |
| LARS2 | Mt leucyl-tRNA synthethase | Perrault syndrome | Childhood/ adulthood | (Rivera et al., 2013) |
| FARS2 | Mt phenylalanine-tRNA synthethase | Epileptic encephalopathy, lactic acidosis | Perinatal | (Elo et al., 2012) |
| EARS2 | Mt glutamyl-tRNA synthethase | Leukoencephalopathy with brain stem and thalamus involvement and high lactate | Early childhood | (Steenweg et al., 2012) |
| VARS2 | Mt valyl-tRNA synthethase | Psychomotor delay, seizures, lactic acidosis | Childhood | (Pierce et al., 2013) |
| TARS2 | Mt threonyl-tRNA synthethase | Psychomotor delay, hypotonia | Perinatal/ early childhood | (Diodato, Melchionda, et al., 2014) |
| GARS | Glycyl-tRNA synthethase | Charcot-Marie-Tooth (CMT) disease, distal motor neuropathy | Childhood/ adulthood | (Seburn, Nangle, Cox, Schimmel, & Burgess, 2006) |
| KARS | Lysyl-tRNA synthethase | Autosomal recessive CMT | Childhood/ adulthood | (Santos-Cortez et al., 2013) |

#### 1.4.1.1 DARS2 in mitochondrial diseases

The importance of undisrupted protein synthesis in mitochondria is shown through different disease phenotypes. The first mutation in mt-aaRSs was discovered in 2007 in mtAsp-RS or *Dars2* gene (Scheper et al., 2007). Mutations in *Dars2* were found in patients with affected white matter tracts, leading to motoric dysfunction and cognitive impairment. The disease is now known as leukoencephalopathy with brain stem and spinal cord involvement (LBSL) (van Berge et al., 2012). LBSL is an autosomal recessive disease with an early onset. The symptoms may vary, but the main features of the disease are learning problems, cognitive decline, spasticity and progressive cerebral ataxia. In magnetic resonance spectroscopy of the affected patients, increased lactate in the white matter can be observed. The patients are usually compound heterozygotes, with a splice mutation on one allele and a variable mutation on the other one. The splicing mutation is in intron 2, therefore affecting the splicing of the exon 3, which leads to a frameshift and premature stop codon, creating a truncated protein. The second allele usually contains a missense mutation, although deletions and nonsense mutations were found in few patients (van Berge et al., 2012). Interestingly, *Dars2* mutations affect the nervous system at the highest extent, but it is still not clear if the defect stems from the neuronal or glial cell dysfunction. It has been shown that mutations in intron 2 have more pronounced effect on neuronal cells compared to glial cells (van Berge et al., 2012; van Berge et al., 2014). We have recently shown that DARS2 depletion primarily affects forebrain neurons and it is dispensable for myelin-producing cells in mice. DARS2 deficiency in both mouse models caused appearance of COX deficient cells, but only forebrain neurons were susceptible to cell-death, followed by neuroinflammatory response (Aradjanski et al., 2017). This was in agreement with previous study where mitochondrial perturbation caused by the loss of the COX10 in Schwann cells did not induce glial cell-death (Funfschilling et al., 2012).

Another mouse model with DARS2 depletion in the heart and skeletal muscle has shown that this enzyme is essential for protein synthesis in both tissues. However, mitochondrial stress responses such as increased mitochondrial unfolded protein response ($UPR^{mt}$), increased biogenesis, decreased autophagy and upregulation of the mitokine FGF21 is only present in DARS2 depleted cardiomyocytes. The activation of these stress responses is likely induced by the perturbed proteostasis in mitochondria (Dogan et al., 2014a). The phenotype of these mice is featured with a strong clinical presentation, due to the failing heart

and robust decrease in lifespan. Interestingly, loss of CLPP in these mice extends their lifespan and improves the gross-phenotype due to slowed-down mitochondrial translation which possibly allows an augmented generation of OXPHOS subunits (Seiferling et al., 2016)

### 1.4.2 CLPP in mitochondrial diseases

Mitochondrial proteases are essential for mitochondria's health and moreover, the general cell homeostasis. CLPP, as mentioned before, is necessary for the degradation of misfolded and damaged protein. This is important for proper mitochondrial function since many potential substrates of human CLPP are involved in energy metabolism, mitochondrial translation, and amino acids and fatty acids metabolism (Bhandari et al., 2018). The phenotype of the CLPP null mice is infertility in both males and females with reduced size in male testes and female ovaries. Other prominent features of these mice are sensorineural deafness and reduction in physical growth and motor activity. Moreover, adult CLPP null mice have both a lower body weight gain and a shorter stature (Gispert et al., 2013). *Clpp* mutations in humans cause Perrault Syndrome that is featured with hearing loss, ovarian failure and growth retardation. The lifespan of the CLPP deficient mice is not affected and they have a mild mitochondrial dysfunction (Jenkinson et al., 2013). CLPP expression was found increased in some metastatic cells and research on its cellular roles has revealed that this protease is important for the pathology of several human cancers, including cell viability, proliferation, and metastasis, but it is also highly tissue-specific (Bhandari et al., 2018). In our lab, we demonstrated that in the absence of CLPP, ERAL1 degradation is attenuated and it stays attached to the small ribosomal subunit, which further leads to an impaired mitoribosomal assembly and subsequently impairs mitochondrial translation (Szczepanowska et al., 2016). CLPP deficient mice show mild respiratory chain deficiency, with complex I being the most affected and they are protected from diet-induced obesity and show a significant decrease in body weight (Becker et al., 2018).

## 1.5. Objectives

Mitochondrial dysfunction caused by impaired protein synthesis in mitochondria is featured with defective MRC. However, different stress responses are being activated even before the appearance of a respiratory chain deficiency. Heart and skeletal muscle specific *Dars2*-deficient mice show increased mitochondrial proteostasis already early in life, suggesting that there might be other mechanism than respiratory chain deficiency leading to the activation of stress responses. One of the genes expressed at the highest extent in the neonatal hearts of these mice is *Fgf21*. Its expression at 1 week of age is around 8-fold and reaching closely 250-fold upregulation at 3 weeks, persisting until the death of the mice. This implies that FGF21 might have a pivotal role in mediating mitochondrial stress responses seen in DARS2 deficient mice.

Besides, an upregulation of *Fgf21* expression is also observed in the hearts of CLPP deficient mice. CLPP deficiency leads to a milder phenotype and the lifespan of these mice is not altered. Together with that, the *Fgf21* expression in heart does not reach more than 5-fold of the increase. Furthermore, the increase in expression of this mitokine has been observed in other mouse models with mitochondrial dysfunction (Tezze et al., 2017; Tyynismaa et al., 2010)

In order to elucidate the role of FGF21, we created and analyzed different double-deficient mouse models. Heart and skeletal muscle specific *Dars2*-deficient mice were used to investigate the role of autocrine FGF21 in heart. The second model was lacking FGF21 in the whole body, with tissue-specific depletion of DARS2 and it was used to scrutinize if the endocrine role of FGF21 is dispensable. Finally, a full body knockout of CLPP and FGF21 was created in order to examine the role of FGF21 in mild mitochondrial dysfunction.

The work outlined here is a significant step for understanding the biology and role of FGF21 in mitochondrial dysfunction.

# 2. Materials and Methods

## 2.1 Mouse experiments and animal care

All mice procedures were conducted in compliance with protocols and approved by local government authorities (Bezirksregierung Köln, Cologne, Germany) and were in accordance with NIH guidelines. The mice (*Mus musculus*, C57B1/6) were housed in groups of 3 - 5 mice per cage at an ambient temperature of 22 – 24 ºC and kept at a 12-hour light / 12-hour dark cycle in the pathogen-free animal facility of the CECAD Institute. Mice were sacrificed by cervical dislocation

### 2.1.1 Mouse handling and breeding

All the handlings and breedings of mice were performed according to Silver's "Mouse genetics" (Silver, 1995).

### 2.1.2 Mice

For conducting this research, different mouse lines were used for creation of double-knockout models. Previously described (Dogan SA., 2014) mitochondrial aspartyl-tRNA synthetase (*Dars2*) gene targeting was carried out as part of the International Knockout Mouse Consortium (KOMP) (information available at http://www.knockoutmouse.org, Project ID: 41773). The mice lacking Dars2 in both heart and skeletal muscle were generated by mating Dars2$^{loxP/loxP}$ animals with transgenic mice expressing cre recombinase under the control of muscle creatine kinase promoter (*Ckmm-cre*) (Larsson et al., 1998). Conditional targeting of Fgf21 $^{loxP}$ mice was carried out in the lab of Prof. Dr. David Mangelsdorf (Potthoff et al., 2009). Fgf21 $^{loxP}$ mice were ordered from The Jackson Laboratory (strain: B6.129S6(SJL)-*Fgf21*$^{tm1.2Djm}$/J). Double-knockout mice, in heart and skeletal muscle, were generated by mating homozygous Dars2$^{loxP/loxP}$;Fgf21$^{oxP/loxP}$ mice with triple heterozygous ones - Dars2$^{loxP/wt}$;Fgf21 $^{loxP/wt}$, Ckmm-Cre$^{tg/wt}$. To generate full-body *Clpp* knockout mice, Clpp$^{fl/fl}$ were mated with transgenic mice ubiquitously expressing Cre recombinase under control of the β-actin promoter, resulting in Clpp+/-mice. Heterozygous Clpp+/- mice were further intercrossed to obtain homozygous. For the generation of double deficient *Clpp* and *Fgf21* knockout animals, Clpp$^{fl/fl}$ Fgf21$^{fl/fl}$ mice were mated with transgenic mice ubiquitously

expressing Cre recombinase (β-actin Cre).

### 2.1.3 Submandibular bleeding for blood collection

The submandibular bleeding of mice was performed without anesthesia, using a lancet and collecting a couple of drops of blood. The blood samples were stored on the room temperature for 15 minutes and subsequently centrifuged at 13.000 rpm for 20 minutes. Resulting serum was stored at -80 $^{o}$C.

### 2.1.4 Glucose levels

Glucose concentrations in fed state were measured after submandibular bleeding using glucose strips, which were read for absorbance in a reflectance meter (ACCU-CHEK AVIVA, Roche, Mannheim, Germany).

### 2.1.5 FGF21 serum levels

The levels of FGF21 in serum were measured with a Mouse/Rat FGF-21 Quantikine ELISA Kit (R&D Systems, Minneapolis, USA), using the provided instructions.

## 2.2 Molecular biology

### 2.2.1 Isolation of genomic DNA from mice ear clips

Mice ear clips were incubated overnight in the lysis buffer (100 mM Tris-HCl pH 8.5, 5 mM EDTA, 0.2% (w/v) SDS, 0.2 M NaCl, 500 mg/ml Proteinase K) in an agitating thermoshaker (Eppendorf, Hamburg, Germany) at 55 $^{o}$C. DNA was precipitated by adding an equivalent volume of isopropanol (100%) and centrifuging at maximum speed for 20 minutes. After removing the supernatant, the pellet was washed with 70% (v/v) ice-cold ethanol and centrifuged at maximum speed for 15 minutes. After complete removal of ethanol, the pellets

were left to get dry under the hood, for approximately 5 minutes. Finally, the DNA pellets were resuspended in 100 µl $dH_2O$ by shaking at 37 °C for 1 h.

### 2.2.2 Isolation of total RNA from mice tissues

Total RNA was isolated using the TRIzol reagent (Life Technologies GmbH, Darmstadt, Germany). Tissues were dissected and around 100 mg was placed into Precellys (Bertin Technologies, Versailles, France) 1.5 ml tubes with beads. The tubes were filled with 1 mL of TRIzol reagent. The tissues were further homogenized in a Precellys 24 (Bertin Technologies, Versailles, France) fast-prep machine at 5500-6000 rpm for 2x30 seconds. The homogenates were transferred to new tubes and the chloroform phase separation followed. The further RNA precipitation was done according to the manufacturer's instructions.

### 2.2.3 Quantification of nucleic acids

Both DNA and RNA concentrations were quantified by measuring the sample absorption at 260 nm and 280 nm with a NanoDrop ND-1000 UV-Vis spectrophotometer (Peqlab, Erlangen, Germany). The purity was accessed by the ratio of absorbance at 260 and 280 nm. The ratio for the pure DNA is around 1.8 and for the pure RNA – around 2.

### 2.2.4 Polymerase chain reaction (PCR)

Polymerase chain reactions (PCR) (Mullis and Faloona, 1987) were rendered using customized primers (Sigma Aldrich) listed in the Table 2.1. All amplification reactions were carried out using the Veriti Thermocycler (Applied Biosystems, Life Technologies). PCR reactions were performed in a total volume of 20 µL with approximately 50 ng DNA template, 1x DreamTaq Buffer (Thermo Scientific), 62.5 µM dNTP mix (Promega), 0.4 µM of each primer and 1U DreamTaq Polymerase (Thermo Scientific). PCR products were separated by gel electrophoresis on 2% (w/v) agarose (Sigma Aldrich) gels prepared with gel red (1:10) or ethidium bromide (1:20). PCR reactions were used to determine the genotypes of the mice.

**Table 2.1 Oligonucleotides used for genotyping of the mice**

| Gene | Company | Sequence (5' – 3') |
|---|---|---|
| ***FGF21*** | Sigma® | WT:<br>forward: GGGCTCTGATAAAGCATTCC<br>reverse: CAGCACTAAGGGAGGCAGAG<br>KO:<br>forward: CCTCCAGATTTAGGAGTGCAGA<br>reverse: AGGGAGGCAGAGGCAAGTGATT |
| ***CLPP*** | Sigma® | WT:<br>forward: GTGGATGATGGTCAGTAGAATCC<br>reverse: CCCAGACATGATTCCTAGCAC<br>KO:<br>forward: TGTGCATTCTTACCATAGTCTGC |
| ***DARS2*** | Sigma® | forward: ATGAATTCTAGGCCAGCCAC<br>reverse: TGGCAATCTCTTAGGACTAAG |
| ***CRE*** | Sigma® | Transgene forward: TAAGTCTGAACCCGGTCTGC<br>Transgene forward 3' Label:<br>GTGAAACAGCATTGCTGTCACTT<br>Internal pos. control forward: CAAATGTTGCTTGTCTGGTG<br>Internal pos. control reverse: GTCAGTCGAGTGCACAGTTT |

PCR programs for *Ckmm-cre*, *Dars2* and *Clpp* PCR started with 5 minutes of denaturation at 95 $^{o}$C, followed by 35 cycles consisting of denaturation at 95 $^{o}$C for 30 seconds, annealing (at 53 $^{o}$C for *Ckmm Cre*, 61 $^{o}$C for *Clpp*, 56 $^{o}$C for *Fgf21* KO and 60 $^{o}$C for *Dars2* ) for 30 sec and elongation at 72 $^{o}$C for 30 sec, and a final elongation step at 72 $^{o}$C for 5 min. For *Fgf21* WT the annealing temperature was decreased by 0.5 $^{o}$C for each cycle.

### 2.2.5 Reverse transcriptase PCR and quantitative real-time PCR

The total RNA that was previously isolated was treated with DNAse. 10 µg RNA in 1x DNase buffer and 2U DNaseI (NEB) at 37 °C for 10 min. This was further followed with the addition of 10 mM EDTA and heat inactivation of the DNase at 75 °C for 10 min. Digested RNA (100 ng µL-1 per sample) was reverse transcribed using the High capacity reverse transcription kit (Applied Biosystems, Life Technologies). So generated cDNA was amplified with Brilliant III Ultra-Fast SYBR QPCR Master Mix (Agilent Technologies, see Table 2.2).

Real-time PCR was performed on QuantStudio K FlexSystem (Applied Biosystems, Life Technologies). Samples were adjusted for total RNA content by Hypoxanthine-guanine phosphoribosyltransferase (HPRT). Relative expression of mRNAs was determined using a comparative method ($2^{-\delta\delta CT}$) according to the ABI Relative Quantification Method.

**Table 2.2 Oligonucleotides used for SYBR real-time PCR.**

| gene | forward primer | reverse primer |
|---|---|---|
| *Hprt* | GCCCCAAAATGGTTAAGGTT | TTGCGCTCATCTTAGGCTTT |
| *Ndufa9* | GGCCAGCTTACCTTTCTGGAA | GCCCAATAAGATTGATGACCACG |
| *Ndufb6* | TGGAAGAACATGGTCTTTAAGGC | TTCGAGCTAACAATGGTGTATGG |
| *Ndufs2* | TCGTGCTGGAACTGAGTGGA | GGCCTGTTCATTACACATCATGG |
| *Ndufv2* | GGCTACCTATCTCCGCTATGA | TCCCAACTGGCTTTCGATTATAC |
| *Sdha* | GAACACTCCAAAAACAGACCTGC | TCCACCACTGGGTATTGAGTAG |
| *Uqcrc1* | AGACCCAGGTCAGCATCTTG | GCCGATTCTTTGTTCCCTTGA |
| *Ucp1* | AGCCATCTGCATGGGATCAAA | GGGTCGTCCCTTTCCAAAGTG |
| *Cidea* | TGACATTCATGGGATTGCAGAC | GGCCAGTTGTGATGACTAAGAC |
| *Dio2* | CAGCTTCCTCCTAGATGCCTA | CTGATTCAGGATTGGAGACGTG |
| *Cdsn* | TTGCTGATGGCCGGTCTTATT | GCCAGTCTTTCCAATGAGACAAG |
| *Scd3* | GTTGCCACTTTACTGAGATACGC | GAAGCCCTCGCCCATACTT |
| *Pparα* | AACATCGAGTGTCGAATATGTGG | CCGAATAGTTCGCCGAAAGAA |
| *Pparγ* | CCTGAAGCTCCAAGAATACCA | GCCTGATGCTTTATCCCCACA |
| *Pgc1α* | TATGGAGTGACATAGAGTGTGCT | CCACTTCAATCCACCCAGAAAG |
| *Fgf21* | GTGTCAAAGCCTCTAGGTTTCTT | GGTACACATTGTAACCGTCCTC |
| *Atf4* | GCAAGGAGGATGCCTTTTC | GTTTCCAGGTCATCCATTCG |
| *Chop* | CTGGAAGCCTGGTATGAGGAT | CAGGGTCAAGAGTAGTGAAGGT |
| *mtHsp70* | TGGTGAGCGACTTGTTGGAAT | ATTGGAGGCACGGACAATTTT |
| *Lonp1* | ATGACCGTCCCGGATGTGT | CCTCCACGATCTTGATAAAGCG |
| *Afg3l2* | GTTGATGGGCAATACGTCTGG | GACCCGGTTCTCCCCTTCT |

| | | |
|---|---|---|
| *Psat1* | AGTGGAGCGCCAGAATAGAA | CTTCGGTTGTGACAGCGTTA |
| *Phghd* | GACCCCATCATCTCTCCTGA | GCACACCTTTCTTGCACTGA |
| *Fgf21* | GTGTCAAAGCCTCTAGGTTTCTT | GGTACACATTGTAACCGTCCTC |
| *Fgfr1* | TATGTCCAGATCCTGAAGAC | GAGAGTCCGATAGAGTTACC |
| *Fgf19* | CCAGAGAACAGCTCCAGGAC | TCCATGCTGTCACTCTCCAG |
| *Fgf23* | TGGGCACTGCTAGAGCCTAT | CTTCGAGTCATGGCTCCTGT |
| *Klb* | CTAAACCAGGTTCTTCAAGC | GATCTGCTTGTAGTAATGAGC |
| *Sirt1* | GCAGGTTGCAGGAATCCAA | GGCAAGATGCTGTTGCAAA |
| *Nppa* | ATGGGCTCCTTCTCCATCA | CCTGCTTCCTCAGTCTGCTC |
| *Nppb* | GGATCTCCTGAAGGTGCTGT | TTCTTTTGTGAGGCCTTGGT |
| *Tfam* | AACCTTTGACACTCAGTTCATTTTTCT | CAAGGCTCAAAAGGTCAACAGA |
| *Tnfα* | GGAACTGGCAGAAGAGGCACTC | GCAGGAATGAGAAGAGGCTGAGAC |
| *Il6* | CTCTGGGAAATCGTGGAAA | CCAGTTTGGTAGCATCCATC |
| *Ilb* | GCACTACAGGCTCCGAGATGAAC | TTGTCGTTGCTTGGTTCTCCTTGT |
| *Glut4* | GAGCCTGAATGCTAATGGAG | GAGAGAGAGCGTCCAATGTC |
| *Cd36* | AGATGACGTGGCAAAGAACAG | CCTTGGCTAGATAACGAACTCTG |
| *Igf1* | AAATCAGCAGCCTTCCAACTC | GCACTTCCTCTACTTGTGTTCTT |
| *Pdk4* | AGGGAGGTCGAGCTGTTCTC | GGAGTGTTCACTAAGCGGTCA |

## 2.3 Biochemistry

### 2.3.1 Protein extraction from tissues

Approximately 3 $mm^3$ of tissues were used as the starting point. The dissected piece was placed into Precellys (Bertin Technologies, Versailles, France) 1.5 ml tubes with beads containing 500 µl of organ lysis buffer (50 mM HEPES, pH 7.4, 50 mM NaCl, 1% (v/v) Triton X-100, 0.1 M NaF, 10 mM EDTA, 0.1% (w/v) SDS, 10 mM Na-orthovanadat, 2 mM PMSF, 1x protease inhibitor cocktail (Sigma Aldrich) and if necessary 1x PhosSTOP phosphatase inhibitor (Roche)). The tissues were homogenized in a Precellys 24 (Bertin Technologies, Versailles, France) fast-prep machine at 5500 rpm for 2x30 seconds. After incubation on ice for 10 minutes, the samples were centrifuged at 13000 rpm for 45 minutes at 4 °C. The supernatant was transferred into a new tube and the protein concentrations were measured by Bradford reagent (Sigma Aldrich, Seelze, Germany), according to the manufacturer's instructions. The adipose tissue required one extra centrifugation step in order to remove the fat layer which was forming on the top of the samples. Proteins were stored at -80 °C until used.

### 2.3.2 Mitochondria isolation from heart

The freshly dissected tissues for mitochondria isolation were transferred into a 50 ml falcon tube which includes 20 ml of mitochondria isolation buffer (MIB: 100 mM sucrose, 50 mM KCl, 1 mM EDTA, 20 mM TES, 0,2% BSA free from fatty acids, pH 7.2). After the blood removal, the tissues were grinded using a razor blade. Furthermore, the pieces were transferred into a glass homogenizer tube and further processed with a Potter S homogenizer (Sartorius) at 1200 rpm with 10-15 strokes (1 mg/ml of Subtilisin A was added). The homogenate was transferred into 50 ml Falcon tube and centrifuged at 8500 g for 5 minutes at 4 °C. The supernatant, with floating fat, was discarded and the pellet was resuspended by shaking in 30 ml MIB. Another centrifugation step (at 800 g for 5 minutes at 4 °C) was performed and this time the supernatant, comprising of mitochondria, was transferred into a new 50 ml tube. The supernatant was then centrifuged at 8500 g for 5 minutes at 4 °C to pellet mitochondria. The supernatant was decanted and the remaining pellet in resuspended in 50 µl MIB without BSA. The concentrations were measured by Bradford reagent (Sigma Aldrich, Seelze, Germany) according to the manufacturer's instructions.

### 2.3.3 Blue Native polyacrylamide gel electrophoresis (BN-PAGE)

BN-PAGE was conducted using the Novex Bis-Tris system (Life Technologies GmbH, Darmstadt, Germany) following the manufacturer's instructions. For the mitochondrial complexes analysis, approximately 20-40 μg were lysed using 1% DDM. The lysed mitochondria were run on 4-16% Bis-Tris gradient gels. The transfer onto PDVF membranes was followed by immunodetection using antibodies for mitochondrial complexes.

### 2.3.4 Western blot analysis

Protein extracts were boiled for 5 min at 95 °C in Laemmli loading buffer (50 mM Tris-HCl, pH 6.8, 2% SDS, 10% Glycerol, 1% β-mercaptoethanol, 12.5 mM EDTA, 0.02% Bromophenol Blue). Proteins were resolved on SDS polyacrylamide gels, which were in the range between 8% and 15%, depending on the size of protein. Protein marker (PageRuler™ Prestained Protein Ladder) was loaded in the first well of the gel. Wet transfer (Bio-Rad) for 3 hours at 400mA was used for the proteins to pass to the nitrocellulose membrane. The membrane was later on stained with Ponceau solution in order to access the efficiency of the transfer. For the blocking, 5% non-fat dried milk in PBST or 5% BSA in TBST according to the antibodies was used. Membranes were further incubated in the primary antibodies at 4 °C overnight (Table 2.3). After washing the membranes three times in PBST or TBST for 5 min each, membranes were incubated for 1 h at RT with the respective secondary antibody (diluted 1:2000, Sigma Aldrich). Again membranes were washed three times in PBS-T or TBS-T and signals were visualized using ECL solution (GE Healthcare) and exposition to X-ray films (Fujifilms). Films were developed in an automatic developer (Kodak). Western blots were quantified using the ImageJ software

**Table 2.3 Primary antibodies used for immunodetection.**

| Antigen | Company | Dilution |
|---|---|---|
| GLUT-4 | Millipore | 1:1000 |
| HSP60 | BD Biosciences | 1:1000 |
| ClpP | Sigma Aldrich | 1:1000 |
| HSC 70 | Santa Cruz | 1:10000 |
| Grp75 | Abcam | 1:1000 |
| LONP1 | Abcam | 1:1000 |
| ATF5 | Abcam | 1:1000 |
| ATF4 | Santa Cruz | 1:1000 |
| TRAP-1 | BD Biosciences | 1:1000 |
| ERAL-1 | Abcam | 1:1000 |
| NDUFA9 | Molecular Probes | 1:1000 |
| NDUFB6 | Invitrogen | 1:5000 |
| NDUFS2 | Abcam | 1:2000 |
| NDUFS3 | Mitosceinces | 1:1000 |
| NDUFV2 | Proteintech | 1:2000 |
| SDHA | Invitrogen | 1:10000 |
| UQCRC1 | Invitrogen | 1:5000 |
| UQCRFS1 | Mitosceinces | 1:1000 |
| COX1 | Invitrogen | 1:2000 |
| COX4I1 | Invitrogen | 1:2000 |
| ATP5A1 | Mitosceinces | 1:1000 |
| MnSOD2 | Millipore | 1:1000 |
| PGC-1alpha | Santa Cruz | 1:1000 |
| Akt | Cell Signaling | 1:1000 |
| Phospho-Akt | Cell Signaling | 1:1000 |
| LC-3 | Cell Signaling | 1:1000 |
| TOM20 | Santa Cruz | 1:1000 |
| UCP2 (C-20) | Santa Cruz | 1:1000 |

| Antigen | Company | Dilution |
|---|---|---|
| OAT | Abcam | 1:1000 |
| EIF2S1 | Abcam | 1:1000 |
| EIF2S1-Phospho S51 | Abcam | 1:1000 |
| ACADS | Santa Cruz | 1:1000 |
| ACADVL | Santa Cruz | 1:1000 |
| MCAD | Santa Cruz | 1:1000 |
| GDF-15 | Santa Cruz | 1:1000 |
| MTHFD-2 | Abcam | 1:1000 |
| OXPHOS cocktail | Abcam | 1:1000 |
| Klotho ß | R&D Systems | 1:500 |
| TFAM | Courtesy of N.Larsson's Lab | 1:1000 |
| AFG3L2 | Courtesy of E. Rugarli's Lab | 1:1000 |
| VDAC | Cell Signaling | 1:1000 |
| AMPK | Cell Signaling | 1:1000 |
| Phospho-AMPK | Cell Signaling | 1:1000 |
| Beclin | Cell Signaling | 1:1000 |
| Sirt-1 | Cell Signaling | 1:1000 |
| UCP1 | Courtesy of N.Larsson's Lab | 1:1000 |
| Calnexin | Calbiochem | 1:2000 |
| Ubiquitin | BD Biosciences | 1:1000 |
| PRAS-40 | Cell Signaling | 1:1000 |
| Phospho-PRAS-40 | Cell Signaling | 1:10000 |
| 4EB-P1 | Cell Signaling | 1:1000 |
| Phospho- 4EB-P1 | Cell Signaling | 1:1000 |
| CPT-1 | Santa Cruz | 1:1000 |
| MRPS35 | Proteintech | 1:1000 |
| Phospho-ERK1/2 | Cell Signaling | 1:1000 |
| Tubulin | Sigma Aldrich | 1:5000 |

## 2.4 Histological Analyses

### 2.4.1 Cryostat sections

For fresh-frozen sections, tissues were directly isolated after sacrificing the animals, directly embedded in Tissue-Tek (Sakura, Alphen aan den Rijn, The Netherlands) and placed onto dry ice until they froze. Frozen tissues were cut on a Leica CM1850 cryostat with a thickness of 7 µm. Sections were directly mounted onto microscope slides and stored at -20 °C.

### 2.4.2 COX-SDH staining

COX-SDH staining was performed on fresh-frozen sections, which were air-dried for half an hour after removal from the -80 °C. Firstly, COX staining solution (0.8 ml 3,3 diaminobenzidine tetrahydrochloride, 0.2 ml 500 µM cytochrome c, a few grains of catalase) was applied in amount to cover the sectioned tissue and incubated in a humid chamber at 37 °C for 40 minutes. After the washings step with PBS, sections were further incubated in SDH staining solution (0.8 ml 1.875 mM Nitroblue tetrazolium, 0.1 ml 1.3 M sodium succinate, 0.1 ml 2 mM Phenazine methosulphate, 0.01 ml 100 mM Sodium azide) for half an hour at 37 °C and consequentially washed in PBS, dehydrated with increasing ethanol concentration (75% for 2 minutes, 95% for 2 minutes, 100% for 10 minutes), air dried, and mounted in D.P.X. (VWR, Darmstadt, Germany).

### 2.4.3 Hemotoxylin and Eosin staining (H&E Staining)

H&E staining, used for a morphology overview, was applied on paraffin sections of adipose tissue. The adipose tissues were fixed in 4 % PFA in PBS overnight at 4 °C. The following day, the tissues were transferred into fresh PBS and dehydrated (Leica ASP200S) using increasing concentrations of ethanol (30 %, 2 h; 50 %, 2 h; 96 %, 1 h; 100 %, 4 h). After 4-hour-incubation in Xylol, the samples were incubated in paraffin for 4 h at 62 °C, followed by embedding (Leica EG1150H). Furthermore, embedded tissues were cut with the thickness of 5 micrometers using microtome (Leica RM2255) and transferred onto Polysine microscope glass slides (VWR). After an overnight incubation at 37 °C, the samples were

deparaffinized (20 min Xylol, 2 min 100 % EtOH, 2 min 96 % EtOH, 2 min 75 % EtOH, 1 min tap water) and stained
in hematoxylin for 4 minutes, followed by a short wash in tap water. Additionally, the sections were incubated in tap water for 15 minutes, short washed in deionized water and stained in Eosin for 1 minute. Next, the tissues were transferred into deionized water and drained in an increasing ethanol row (75 % EtOH, 1 min; 96 % EtOH, 1 min; 100 % EtOH, 1 min; Xylol, 1 min). Eventually, the samples were mounted with Entellan and glass coverslips. Finally, the stained sections were visualized in 20 x magnification (Leica SCN400 slide scanner & Client software).

### 2.4.4 Oil red O staining

Oil red O (ORO) staining is used for the visualization of fat content and it was performed on adipose tissue cryosections. The sections were air dried for 10 min and surrounded with a PAP pen (Sigma-Aldrich). The staining involved sections being covered with ORO solution for 5 min and counterstained with Mayer's Hematoxylin for 30 sec. The slides were then rinsed under running tap water before they were mounted with FluorSave Reagent (Calbiochem).

## 2.5 Proteomics analyses

### 2.5.1 In-solution digest

Heart and liver tissues were both used for label-free quantification of the proteome. First of all, the tissues were disrupted using liquid nitrogen and dissolved in 8M Urea buffer, with the addition of 1x proteinase inhibitor. After acetone-precipitation, 50 μg of proteins was used for the digestion. The heart samples that were used for phospho-proteomics analyses were additionally containing phosphatase inhibitor and 500 μg was used for the digestion. Proteins were reduced by one-hour incubation with 5mM dithiothreitol at 37 °C and thiols were carboxymethylated with 10 mM iodoacetamide for 30 minutes. The digestion with Lys-C at 37 °C for 4 hours followed and, in the end, samples were left overnight with trypsin at 37 °C. The digestion was stopped with 1% formic acid the next day. StageTip purification of the samples was performed according to the CECAD proteomics facility instructions.

### 2.5.2 Serum proteomics

7 µL of serum that was collected as previously described in 2.1.3, was handed to the CECAD proteomics facility and further used for analyses.

### 2.5.3 Mass-spectrometry

The label-free proteomic profiling of heart and liver tissues was performed in the CECAD proteomics facility according to the provided protocols. The mass spectrometry (LC-MS/MS) device was made up of an EASY n-LC1000 (Thermo Scientific) linked via a nano-electrospray ionization source (Thermo Scientific) to an ion-trap based bench top Q-Executive Plus (Thermo Scientific). The experiment and data analysis were performed by the CECAD proteomics facility.

## 2.6 Computer analyses

### 2.6.1 Statistical analyses

Statistical significance of data sets with two independent groups were analyzed for using two-tailed unpaired Student's t-test. Data sets with more than two groups were analyzed using one-way analysis of variance (ANOVA) followed by Tukey's post hoc test. All p-values below 0.05 were considered statistically significant; *p <0.05, ** p< 0.01, ***p< 0.001, ****p< 0.0001. All data are presented as mean ± SD.

### 2.6.2 Software

Statistical analysis and data visualization were managed using Microsoft Excel and Graphpad Prism 6 (Graphpad Software). Figures and Illustrations were prepared with Adobe Illustrator CS4 (Adobe Systems). For the enrichment of proteomics data, Bioconductor, Enrichr and Reactome software were used.

## 2.7 Chemicals and biological material

**Table 2.5 Chemicals**

| Chemical | Supplier |
|---|---|
| β-mercaptoethanol | Sigma Aldrich |
| Acetic acid | AppliChem |
| Catalase, bovine liver | Sigma Aldrich |
| Acryamide-Bisacrylamide 40 | Carl Roth |
| Agarose LE | Ambion |
| Albumin from bovine serum fatty acid free (BSA) | Sigma Aldrich |
| Ammonium bicarbonate | Sigma Aldrich |
| Ammonium persulfate (APS) | Sigma Aldrich |
| Bromophenol blue | Merck |
| Coomassie Brilliant Blue R-250 | Merck |
| Cytochrome C, bovine heart | Sigma Aldrich |
| Diaminobenzidine tetrahydrochloride (DAB) | Sigma Aldrich |
| Dithiothreitol (DTT) | Sigma Aldrich |
| Ethanol | AppliChem |
| Ethylenediaminetetraacetic acid (EDTA) | Sigma Aldrich |
| Glucose | Merck |
| Glycerol | Sigma Aldrich |
| Glycine | AppliChem |
| HEPES | AppliChem |
| Hydrochloric acid (HCl) | VWR |
| Isopropanol | AppliChem |
| Magnesium sulfate ($MgSO_4$) | Merck |
| Methanol | AppliChem |
| Milk powder | AppliChem |
| Monopotassium phosphate ($KH_2PO_4$) | Sigma Aldrich |
| Nitrotetrazolium blue (NTB) | Sigma Aldrich |
| Paraformaldehyde | Sigma Aldrich |
| Phenazine methosulphate (PMS) | Sigma Aldrich |
| Polyethylenglycol | Sigma Aldrich |
| PonceauS | Sigma Aldrich |
| Potassium chloride (KCl) | Sigma Aldrich |
| Potassoium hydroxide (KOH) | Sigma Aldrich |

| | |
|---|---|
| Sodium azide | Sigma Aldrich |
| Sodium chloride (NaCl) | Sigma Aldrich |
| Sodium dodecyl sulfate (SDS) | AppliChem |
| Sodium fluoride (NaF) | AppliChem |
| Sodium hydroxide (NaOH) | AppliChem |
| Sodium orthovanadat | AppliChem |
| Sucrose | Sigma Aldrich |
| Tetramethylethylenediamine (TEMED) | Sigma Aldrich |
| Tris | Sigma Aldrich |
| Triton X-100 | Sigma Aldrich |
| Trizma Base | Sigma Aldrich |
| Tween-20 | VWR |

# 3. Results

## 3.1. Tissue-specific depletion of FGF21 under Ckmm-Cre promoter does not influence the overall phenotype of the DARS2-deficient mice.

To decipher the *in vivo* role of FGF21 in DARS2-deficient hearts, where the immense mRNA upregulation of this cytokine was shown (Dogan et al., 2014), FGF21 was selectively deleted in a tissue-specific manner. Using *Ckmm*-promoter driven Cre recombinase, both *Dars2* and *Fgf21* were deleted in heart and skeletal muscle. *Dars2* conditional gene targeting was conducted in the context of the International Knockout Mouse Consortium (KOMP) as previously reported (Dogan et al., 2014). The fibroblast growth factor 21 (*Fgf21*) gene targeting was carried out in the lab of Prof. David Mangelsdorf that was described earlier (Potthoff et al., 2009).

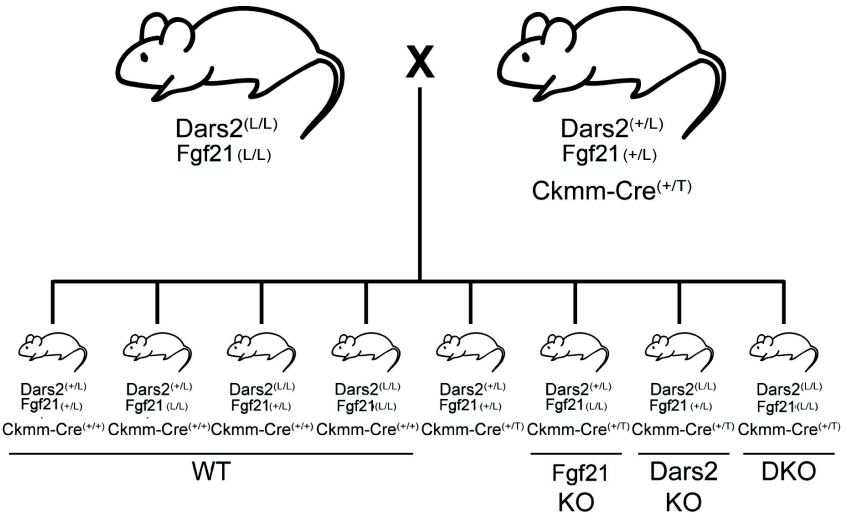


**Figure 3.1 Breeding scheme for generation of double-knockout mice.**

Heterozygous mice Dars2 loxP/wt; Fgf21 loxP/wt; Ckmm-Cre tg/wt were mated with the homozygous mice Dars2 loxP/loxP; Fgf21 loxP/loxP.

Double-knockout mice (DKO_fl), in heart and skeletal muscle, were generated by mating homozygous Dars2$^{loxP/loxP}$;Fgf21$^{oxP/loxP}$ mice with triple heterozygous ones - Dars2$^{loxP/wt}$;Fgf21 $^{loxP/wt}$, Ckmm-Cre$^{tg/wt}$ (Figure 3.1). Finally, 4 different genotypes were obtained and used for the next experiments. As a Wt, we used all the mice without Ckmm-Cre transgene; Dars2$^{loxP/wt}$;Fgf21 $^{loxP/loxP}$, Ckmm-Cre$^{tg/wt}$ is further reffered as fgf21_fl;

Dars2$^{loxP/loxP}$;Fgf21 $^{loxP/wt}$, Ckmm-Cre$^{tg/wt}$ is further reffered as dars2_fl and Dars2$^{loxP/loxP}$;Fgf21 $^{loxP/loxt}$, Ckmm-Cre$^{tg/wt}$ is referred in the text as dko_fl.

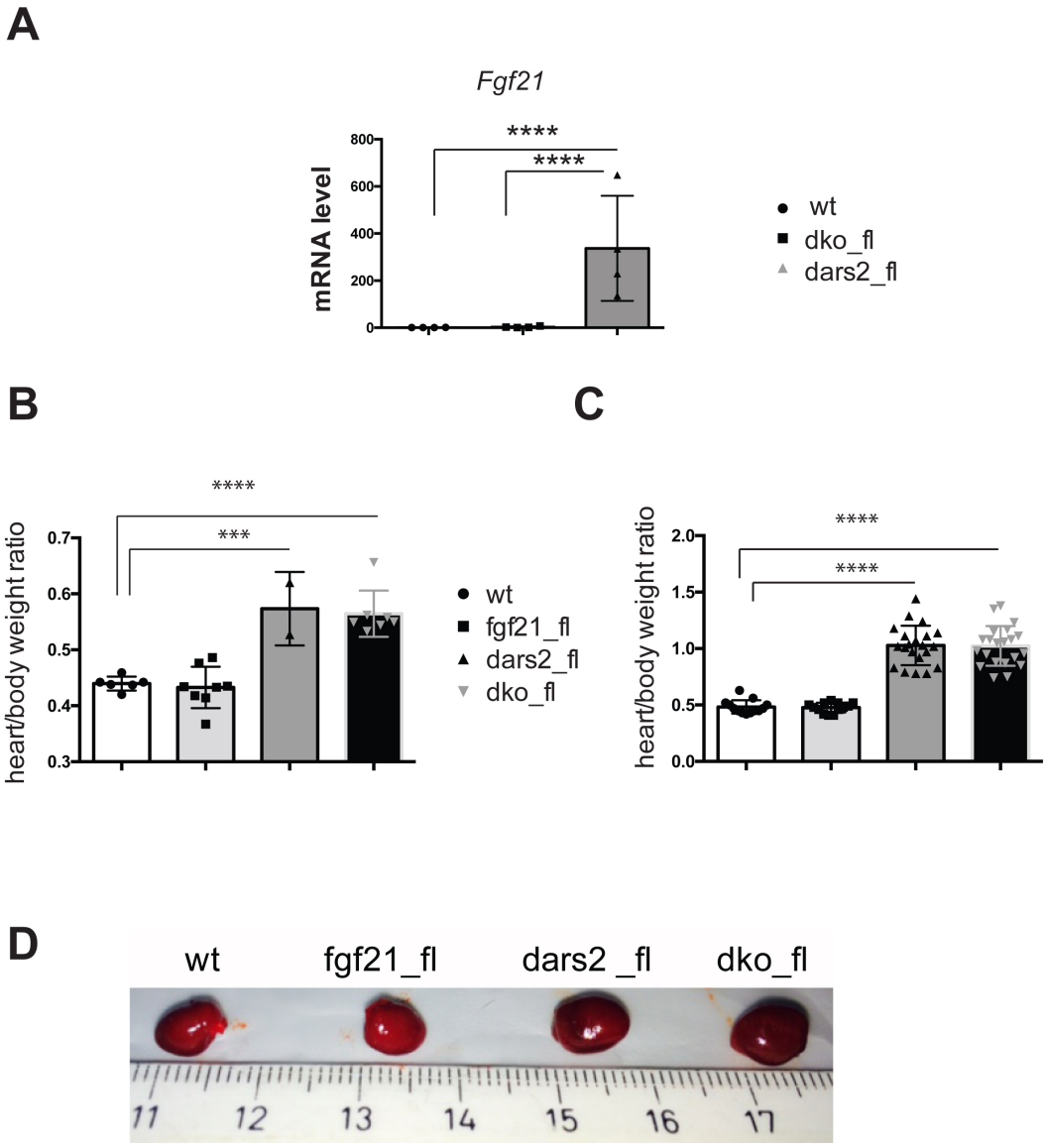


**Figure 3.2 Heart to body weight ratio stays unchanged with the depletion of FGF21 in cardiac and skeletal muscle of DARS2 deficient mice.**

**(A)** Relative expression levels of *Fgf21* in hearts of the 6-week-old mice (n=5) **(B)** Heart to body weight ratio in mice at 3-4 weeks of age (n=6). **(C)** Heart to body weight ratio in mice at 6 weeks of age (n=20). **(D)** Photos representing the size of hearts at 6 weeks of age in designated genotypes. Data are presented as mean ± SD (***P<0.001; **** P<0,0001; one-way ANOVA, Tukey's post hoc test).

We showed earlier that *Dars2* deletion in heart leads to a severe cardiomyopathy, which causes death at 7-8 weeks of age (Dogan et al., 2014). As a primary stress response, an immense *Fgf21* mRNA upregulation was observed, starting at 1 week of age. The increase was further intensified at 3 and 6 weeks of age. This suggested that FGF21 might have a

pivotal role in mediating stress responses in DARS2-deficient hearts. In the double knockout model, both *Fgf21* and *Dars2* deletion in heart and skeletal muscle was mediated by the *Ckmm* promoter that triggers activation of Cre after embryonic day 15.5 (E15.5) (Lyons et al., 1991). Interestingly, these double knockout mice were not different from the *Dars2* KO animals concerning the lifespan and gross phenotype. *Fgf21* expression levels were strongly upregulated in DARS2-deficient hearts, and its expression was absent in DKO_fl (Figure 3.2A). Heart to body weight ratio both at 3 and 6 weeks of age was not significantly different between DARS2-deficient mice and the DKO_fl mice (Figure 3.2B-C). The heart size was not affected by the depletion of FGF21 (Figure 3.2D).

## 3.2. The severity of cardiomyopathy is not affected by additional depletion of FGF21 in DARS2-deficient hearts.

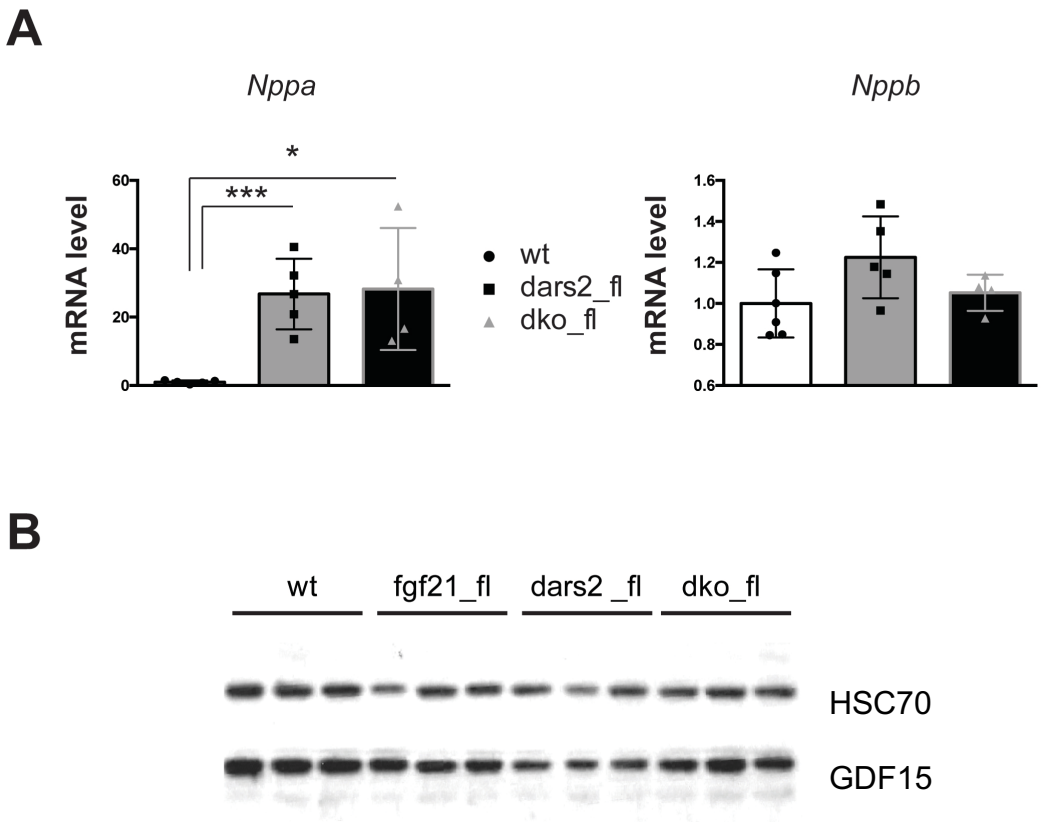


**Figure 3.3 Cardiomyopathy levels are not affected by the depletion of FGF21.**

**(A)** Relative expression levels of cardiomyopathy markers (*Nppa, Nppb)* in 6-week-old mice (n=5). **(B)** Western Blot analysis of GDF15 levels in total protein extracts from heart (n=3).
Data are presented as mean ± SD (*P<0.05, ***P<0.001; one-way ANOVA, Tukey's post hoc test).

In order to access the molecular phenotype of the cardiomyopathy, the expression levels of hypertrophy markers were measured in the hearts of mice. Natriuretic peptides A (*Nppa*) and B (*Nppb)* were measured using real-time PCR and while *Nppa* levels were increased in both DARS2- and FGF21-deficient hearts, *Nppb* levels have not showed the same trend. However, there was no difference in *Nppa* levels between *Dars2* KO and DKO_fl mice (Figure 3.3A). This further suggested that there might be some compensation from different cardiomyokines, therefore the protein levels of GDF15 were measured by Western Blot. GDF15 has been given the role of cardiomyokine, which could also improve the metabolic state of an organism and affect the stress response pathways Interestingly, protein levels were not affected in any of the knockout mice (Figure 3.3B). Even though the overall

phenotype of the DARS2-deficient mice was not affected by FGF21 depletion, further analyses of DKO_fl mice were performed due to the possibility that this cytokine could affect metabolic and stress response pathways.

### 3.3. Strong respiratory chain deficiency in DARS2-deficient hearts is not further aggravated, nor improved by additional FGF21 depletion.

It has been shown earlier that CI and CIV of mitochondrial respiratory chain were severely affected in DARS2-deficient hearts (Dogan et al., 2014). To investigate if the OXPHOS was affected with the additional topical depletion of FGF21, complexes were separated by Blue-native polyacrilamide-gel electrophoresis (BN-PAGE). Interestingly, the levels of CI and CIV were decreased to the same level in DARS2-deficient and DKO_fl mice (Figure 3.4A). Furthermore, the *steady-state* levels of different OXPHOS subunits were measured by Western Blot analyses and led to the same result, confirming once more that FGF21 depletion does not affect the functionality of mitochondrial respiratory chain (Figure 3.4B) . As an additional outlook, an enzymatic COX/SDH staining was performed on the heart cryosections. This staining has shown a decrease in cytochrome c oxidase (COX) activity in both DARS2-deficient and DKO_fl hearts, which is represented by the blue colour coming from succinate dehydroganese activity (SDH) which can penetrate when COX activity is decreased (Figure 3.4C).

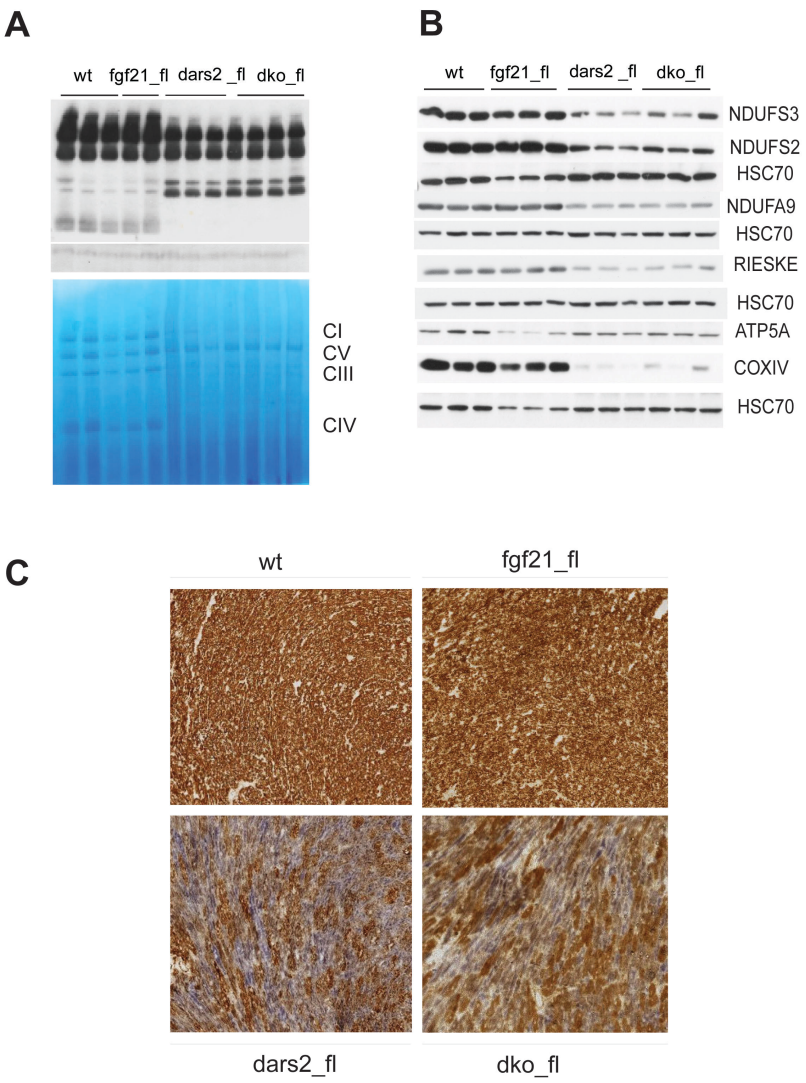


**Figure 3.4 Characterization of mitochondrial respiratory chain deficiency by different methods shows no effect of FGF21 depletion.**

**(A)** Blue-native PAGE (BN-PAGE) analysis of respiratory chain complexes in the heart mitochondria from 6-week-old mice. **(B)** Western Blot analysis MRC steady state levels from total heart extracts (n=3). **(C)** COX-SDH enzymatic histochemical double staining of fresh-frozen hearts (size: 7 µm).

It is interesting to note that in previous work on DARS2-deficient hearts it was shown that respiratory chain subunits were not overall decreased at 3 weeks of age. Moreover, DARS2-deficient mice show no drastic changes in phenotype compared to WT mice at 3 weeks of age (Dogan et al., 2014). In this study, additional subunits of CI were checked, and they showed the decrease in their levels already at 3 weeks of age (Figure 3.5). However, every change observed is due to the DARS2 depletion exclusively. NDUFA9, a subunit of CI, show no changes at the 3 weeks of age, in contrast to NDUFS4, which is already severely decreased at this point (Figure 3.5A). On the other hand, steady-state levels of other

complexes show DARS2-dependent changes. CIII subunit RIESKE show much more drastic decrease in DARS2 and DKO hearts than Core1 CIII subunit (UQCRC1). Both COXI and COXIV, which are subunits of CIV, show decrease when DARS2 is absent in the heart at the 3 weeks of age (Figure 3.5B). Moreover, TFAM levels, which could suggest the equivalent of mitochondrial biogenesis, stay unchanged at 3 weeks of age (Figure 3.5C). Taken together, these data clearly show that FGF21 depletion does not influence the MRC levels regardless of the age and overall state of the animals. On the other hand, DARS2 depletion in the heart affects the steady-state levels of some OXPHOS subunits already at 3 weeks of age.

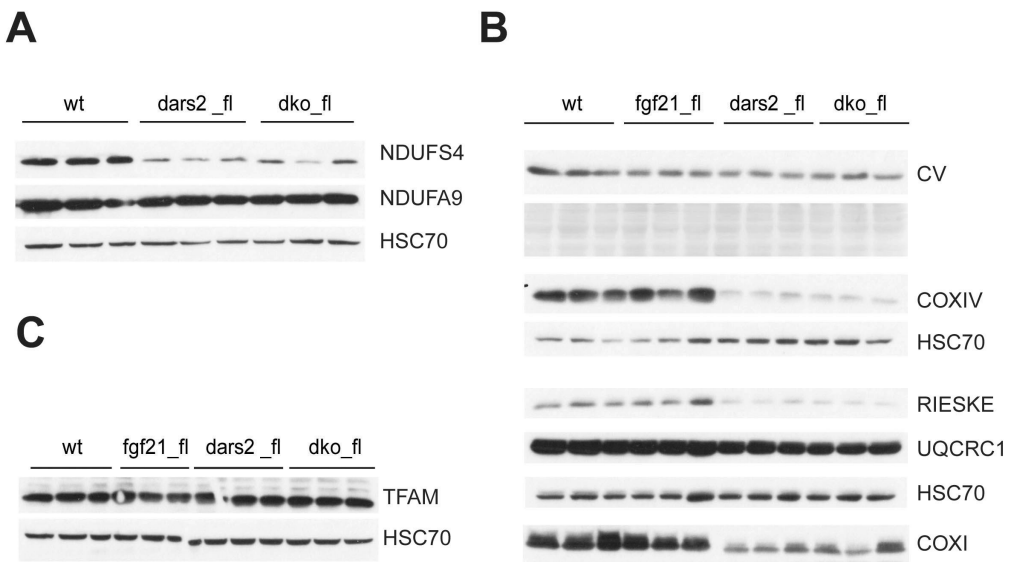


**Figure 3.5 Steady-state levels of MRC subunits in hearts of 3-week-old mice show no changes upon FGF21 depletion.**

**(A)** Western Blot analysis of indicated complex I subunits from total heart extracts (n=3). **(B)** Western Blot analysis of MRC steady state levels from total heart extracts (n=3). **(C)** Western Blot analysis TFAM levels from total heart extracts (n=3).

## 3.4. Mitochondrial and cellular stress responses seen in DARS2-deficient hearts do not depend on the presence of FGF21.

Increased mitochondrial biogenesis is often a compensatory mechanism for the respiratory chain deficiency, when cell will try to produce more mitochondria in order to increase its energetic capacity. To investigate if the mitochondrial biogenesis is occurring, multiple methods are necessary for an end confirmation. In the previous study of DARS2 deficient hearts, citrate-synthase activity assay, mtDNA levels, PGC1α and TFAM expression were measured to confirm the increased biogenesis (Dogan et al., 2014). In this study, the PGC1α and TFAM protein and expression levels were analyzed (Figure 3.6A-B). Interestingly, both PGC1α and TFAM are mildly increased at the protein level in both DARS2 deficient and DKO_fl hearts (Figure 3.6A), but decreased at mRNA level (Figure 3.6B). *Pgc1α* expression is significantly decreased in DKO_fl hearts, when compared to the WT.

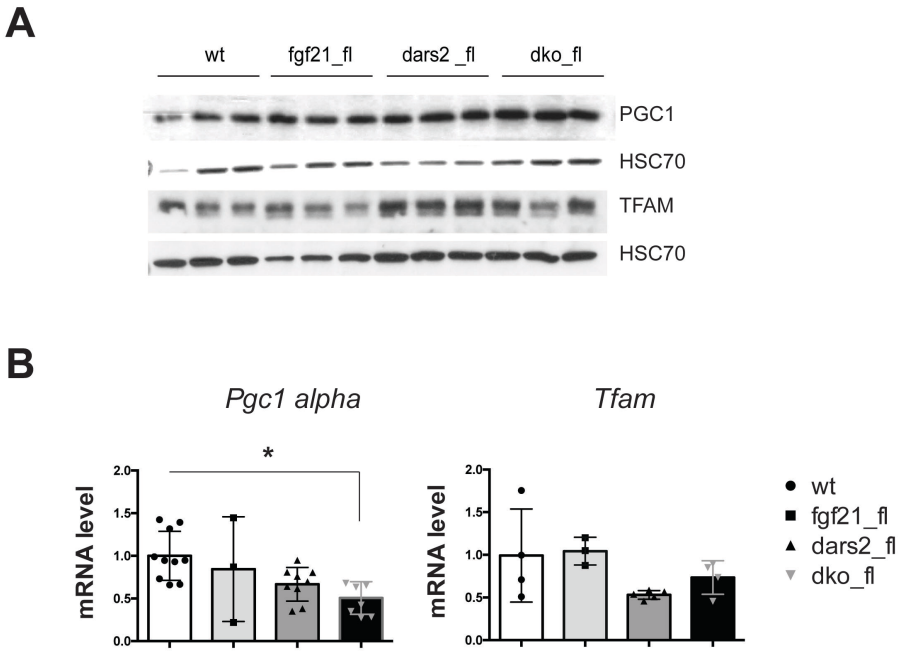


**Figure 3.6 Protein and expression levels of PGC1α and TFAM, which are involved in mitochondrial biogenesis.**

**(A)** Western Blot analysis of PGC1α and TFAM from total heart extracts of 6-week-old mice (n=3). **(B)** Relative expression levels of *Pgc1α* and *Tfam* in heart extracts (n=5). Data are presented as mean ± SD (*P<0.05, **P<0.01, ***P<0.001; one-way ANOVA, Tukey's post hoc test).

Taken together, further analyses would be necessary to conclude if mitochondrial biogenesis is affected by the FGF21 depletion.

Furthermore, the translational defect in DARS2-deficient hearts was shown to affect mitochondrial proteostasis. This leads to the activation of $UPR^{mt}$. As shown before, DARS2 depletion in heart leads to the upregulation of proteases LONP1 and AFG3L2 and increased levels of mitochondrial chaperones HSP60 and GRP75. Seeing that proteostasis response is activated already at 3 weeks of age has led to the clue that there is something other than MRC deficiency mediating all the stress responses (Dogan et al., 2014). As FGF21 was one of the primarily upregulated parameters, it was necessary to check if this protein might have influence on the proteostatic response. Expression levels of *Lonp1 and Afg3l2* were increased in a DARS2-dependent manner (Figure 3.7A), since FGF21 depletion has not induced any changes. Moreover, *Hsp60* levels were not even affected by the DARS2 depletion (Figure 3.7A). On the protein level, proteases LONP1 and AFG3L2 (not shown) were upregulated in both DARS2 deficient and DKO_fl hearts, followed by increase in GRP75 protein levels. HSP60 levels were not increased significantly, which is also in agreement with its mRNA levels (figure 3.7B). In conclusion, FGF21 has no influence on proteostasis, which is unbalanced in DARS2 deficient hearts.

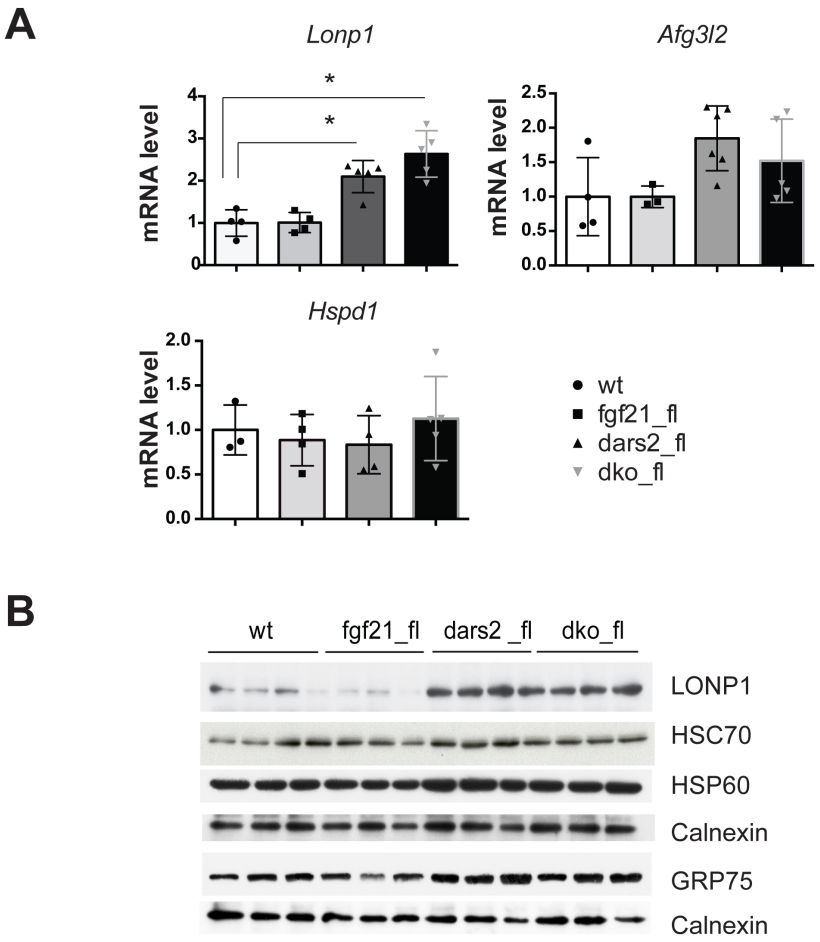


**Figure 3.7 Protein and expression levels of mitochondrial proteases.**

**(A)** Relative expression levels of *Lonp1* and *Afg3l2* in heart extracts (n=5). **(B)** Western Blot analysis of LONP1 from total heart extracts of 6-week-old mice (n=3). Data are presented as mean ± SD (*P<0.05; one-way ANOVA, Tukey's post hoc test).

From the previous data shown here, it could be hypothesized that mitochondrial stresses are over-activated in DARS2-deficient hearts and the effects of FGF21 are not visible due to the possible stress overload. This could point out that some higher levels of regulation still could be affected and therefore cellular stresses needed an examination. Integrated stress response (ISR) is regulated through the phosphorylation of translational initiation factor alpha (eIF2α). When phosphorylated, the global translation is attenuated and internal ribosome entry sites (IRES) - containing mRNA are preferentially translated, which means that only proteins needed for cell survival are produced. A master regulator of ISR is the transcription factor ATF4, which activates transcription of cell-survival genes, among, which is also CHOP10. We showed that phosphorylation of eIF2α was increased in mice lacking DARS2

in heart, and FGF21 depletion has not additionally affected its levels. It is puzzling that non-phosphorylated form of eIF2α showed decrease in the hearts lacking DARS2 (Figure 3.8A). This creates even more increased ratio of phosphorylated and non-phosphorylated form and emphasize the severity of the stress caused by DARS2 depletion.

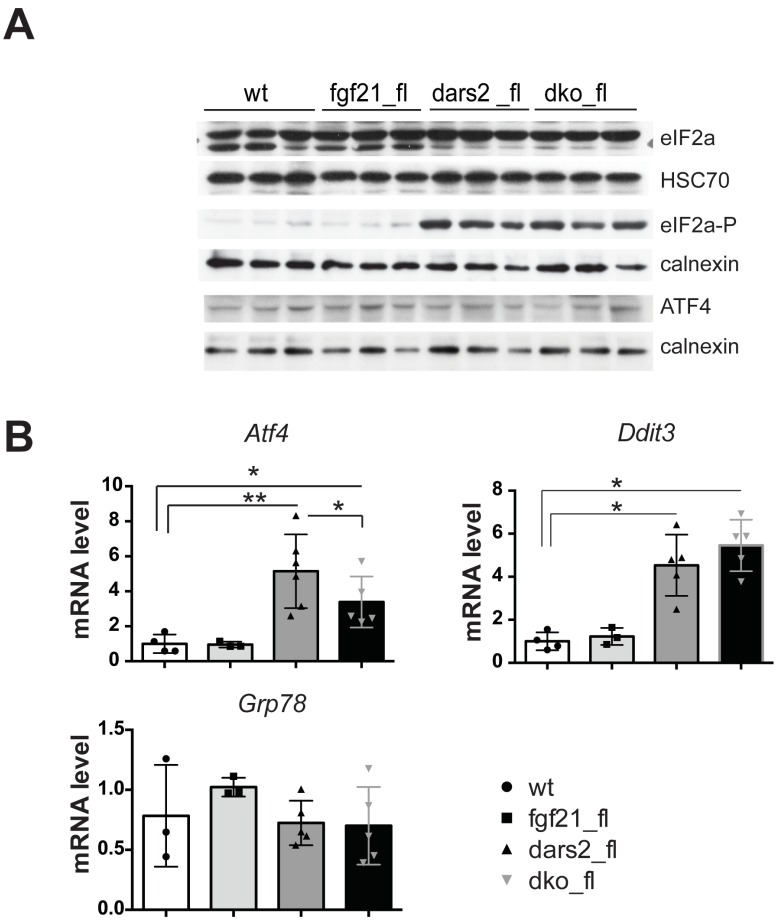


**Figure 3.8 Protein and expression levels of integrated stress response keyplayers.**

**(A)** Western Blot analysis of phosphorylated and non-phosphorylated eIF2α protein from total heart extracts of 6-week-old mice (n=3). **(B)** Relative expression levels of *Atf4* and *Chop10* in heart extracts (n=5). Data are presented as mean ± SD (*P<0.05, **P<0.01; one-way ANOVA, Tukey's post hoc test).

ATF4 protein levels were not changed at all (Figure 3.8A), but the expression levels were significantly upregulated in *Dars2* knockout mice (Figure 3.8B). Remarkably, the depletion of FGF21 in DARS2-deficient heart did have an effect and it decreased the expression levels of the *Atf4*. Still, the *Atf4* expression in DKO_fl was significantly increased when compared to the WT. Notwithstanding, *Chop10* expression was increased in both DARS2-deficient and DKO_fl hearts. Considering that ISR is also activated by endoplasmatic reticulum (ER) stress,

the mRNA levels of ER chaperone *Grp78* were measured, but no difference was observed (Figure 3.8B).

Another cells' survival mechanism activated in the times of elevated stress is autophagy. In DARS2-deficient hearts, the suppression of LC3B-I to LC3B-II conversion and accumulation of p62 and BECLIN-1 was detected, suggesting a reduction in autophagy. Polyubiquitinated proteins were not observed, but this could be due to the high background of the immuno-detection (Figure 3.9). Collectively these data suggest that FGF21 depletion in heart does not affect the level of autophagy.

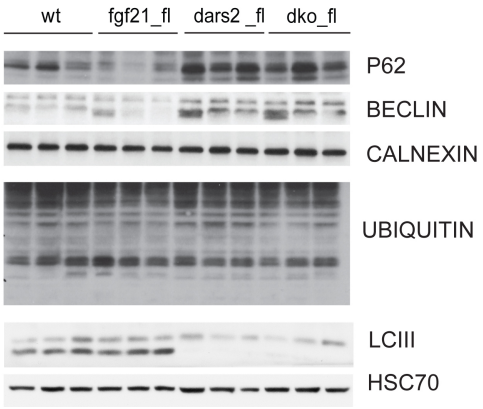


**Figure 3.9 Protein levels of autophagy markers in 6-week-old hearts.**

Western Blot analysis of p62, Beclin, LCIII and Ubiquitin in total heart extracts of 6-week-old mice (n=3).

The evident lack of changes caused by FGF21 depletion in heart, prompted us to look further for possible roles of this mitokine. One study suggested that FGF21 might have protective effects, by helping stressed heart to withstand oxidative stress (Planavila et al., 2015). Therefore, we measured UCP3 and MnSOD2 proteins levels, but no changes were observed (Figure 3.10). This might be due to the fact that different triggers of stress in heart activate different coping mechanisms.

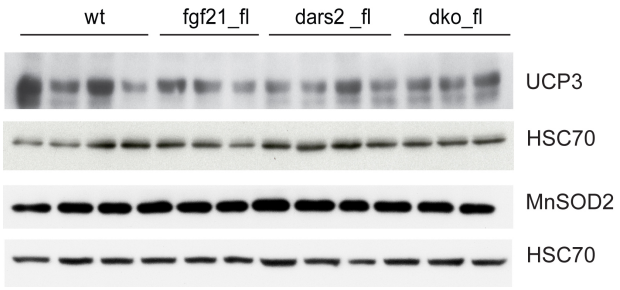


**Figure 3.10 The levels of proteins involved in oxidative stress in 6-week-old hearts.**

Western Blot analysis of UCP3 and MnSOD2 in total heart extracts of 6-week-old mice (n=3).

Cellular metabolism can be affected by mitochondrial dysfunction. Recently, it has been shown that in mitochondrial diseases *de novo* serine biosynthesis drives gluthatione production and moreover the cellular folate driven one-carbon cycle is disturbed. The one-carbon cycle produces formyl-methionine for mitochondrial translation, nicotinamide adenine dinucleotide phosphate (NADPH) for membrane synthesis, and format - the leading 1C donor for cytoplasmic purine synthesis (Nikkanen et al., 2016). Here we have showed that the rate-limiting enzyme of the folate cycle – methyltetrahydrofolate dehydroganese 2 (MTHFD2) was markedly upregulated both at 3 and 6 weeks of age, again, in DARS2-deficient hearts and independently of FGF21 depletion (Figure 3.11A). Both *Mthfd2* and *Fgf21* gene expression is induced by the ATF4 binding their promoters.

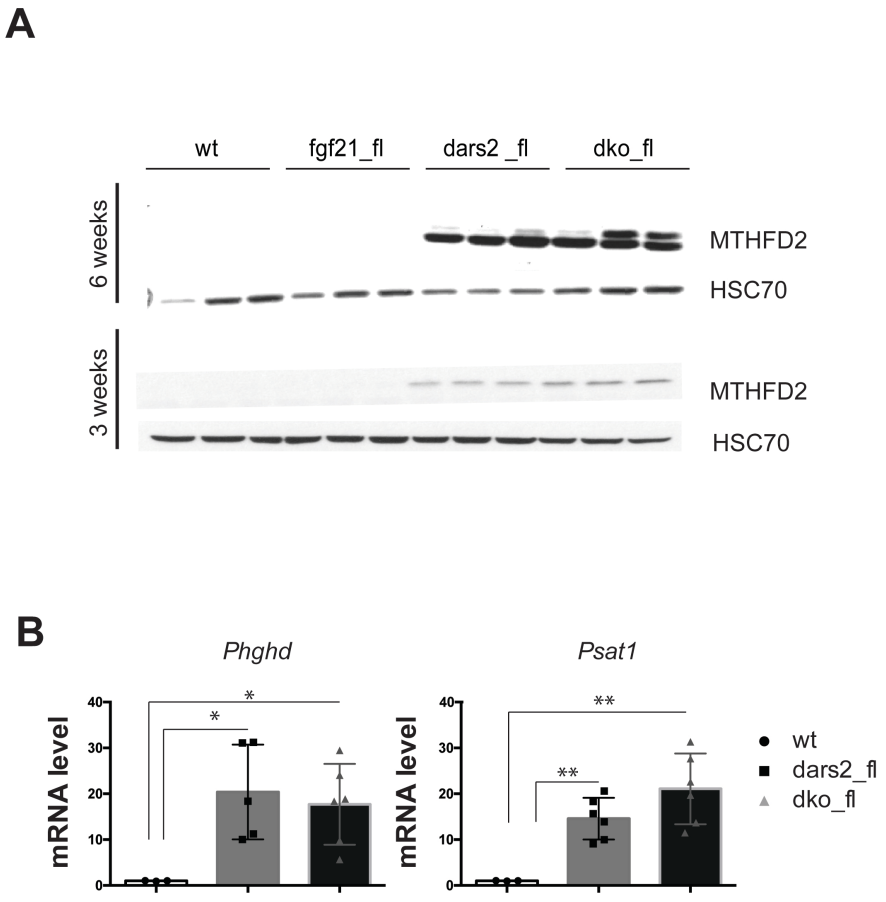


**Figure 3.11 The protein and expression levels of 1-carbon-metabolism enzymes in the total heart extracts.**

**(A)** Western Blot analysis of MTHFD2 protein from total heart extracts of 3 and 6-week-old mice (n=3). **(B)** Relative expression levels of *Phghd* and *Psat1* in heart extracts of 6-week-old mice (n=5).
Data are presented as mean ± SD (*P<0.05, **P<0.01, one-way ANOVA, Tukey's post hoc test).

The rate-limiting enzymes in de novo serine biosynthesis (*Phghd, Psat1)* were upregulated at mRNA level and this increase was not attenuated by the FGF21 depletion (Figure 3.11B). These results show that disrupted one-carbon metabolism is one of the early changes in DARS2-deficient hearts and FGF21 depletion does not affect it.

Mechanistic (mammalian) target of rapamycin (mTOR) complex I (mTORC1) is a major regulator of metabolic signaling (Khan et al., 2017). The function of mTORC1 in mitochondrial dysfunction is poorly understood *in vivo*. The next question was if mTORC1 had a role in the induction of the various stress responses seen in DARS2-deficient hearts and if this is affected by FGF21 loss. Different proteins serve as a read-out for mTORC1 activation. Here, phosphorylated forms of 4EBP1 and PRAS40 were increased in DARS2-deficient hearts and not affected by further depletion of FGF21 (Figure 3.12).

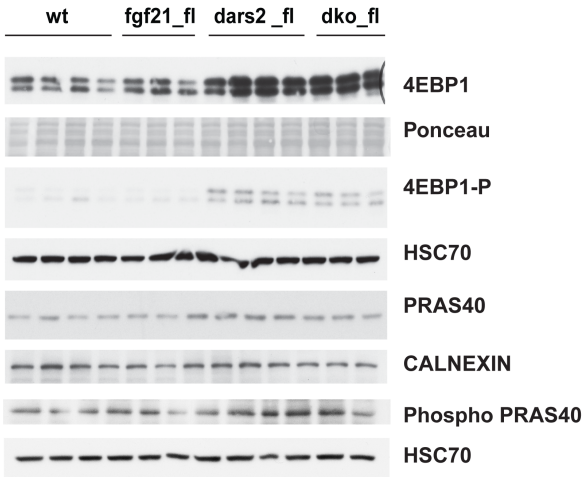


**Figure 3.12 mTORC1 activation is increased in DARS2-deficient hearts and it is not affected by the loss of FGF21.**

Western Blot analysis of phosphorylated and non-phosphorylated mTORC1 proteins from total heart extracts of 6-week-old mice (n=3).

In conclusion, FGF21 depletion in heart does not influence cellular metabolism and ISR. The ATF4, which has been shown to bind directly the promoter of *Fgf21* (Tyynismaa et al., 2010), is decreased in its absence, but this does not affect the overall stress caused by DARS2 depletion.

## 3.5. The loss of DARS2 in heart affects glucose and fatty-acid metabolism, independently of FGF21.

The heart metabolism relies mostly on the usage of fatty-acids and partly on energy yielded by glycolysis (Grynberg & Demaison, 1996). In order to investigate the overall metabolism in hearts of DARS2-deficient and DKO mice, glucose levels were measured. These mice, due to their poor health, could not get through the starvation process, therefore the glucose levels were measured in fed state. However, there was still a significant drop in the levels in both *Dars2* KO and DKO_fl (Figure 3.13A). Moreover, the GLUT4, an insulin-dependent glucose transporter found in heart, skeletal muscle and adipose tissue, was decreased at the protein level in DARS2-deficient hearts, additionally indicating the decrease in glucose metabolism. Insulin-induced translocation of GLUT4 to the plasma membrane requires phosphorylation of Akt kinase at $Ser^{473}$ (Zhu et al., 2013). The results of this study showed the increase in phosphorylation of Akt regardless of decreased GLUT4 protein levels, which could be due to the insulin resistance (Figure 3.13B). *Glut4* expression was decreased, following the trend of the protein levels (Figure 3.13C). Moreover, insulin-growth-factor 1 (IGF-1), which is an activator of Akt-pathway and it has insulin-like effects (Rotwein, 2017), showed upregulated expression in both DARS2-deficient and DKO_fl hearts. The upregulation is more pronounced in DKO_fl hearts and this might be due to the fact that FGF21 is a known inhibitor of IGF-1 (Figure 3.13C).

Mitochondrial pyruvate dehydrogenase kinases (PDKs) catalyze the oxidative decarboxylation of pyruvate, and link glycolysis to the tricarboxylic acid cycle and ATP production. There are 4 different PDKs, where PDK4 is expressed in most of the tissues. Expression levels of *Pdk4* were significantly upregulated in DARS2-deficient hearts when compared to the DKO_fl. It is known that upregulation of *Pdk4* occurs in insulin-resistant state, but how the FGF21 loss influence it in cardiac tissue, is still not clear. Lastly, *Pparg*, which is implicated in cardiac health, showed no changes in its expression levels (Figure 3.13C). These results show that glucose metabolism is impaired in DARS2-deficient hearts, independently of FGF21. The impaired glucose metabolism in failing heart could be due to the increased availability of non-esterified free-fatty acids (NEFA) in blood. The increased serum NEFA in *Dars2* KO mice was previously reported in our lab (Dogan et al., 2014).

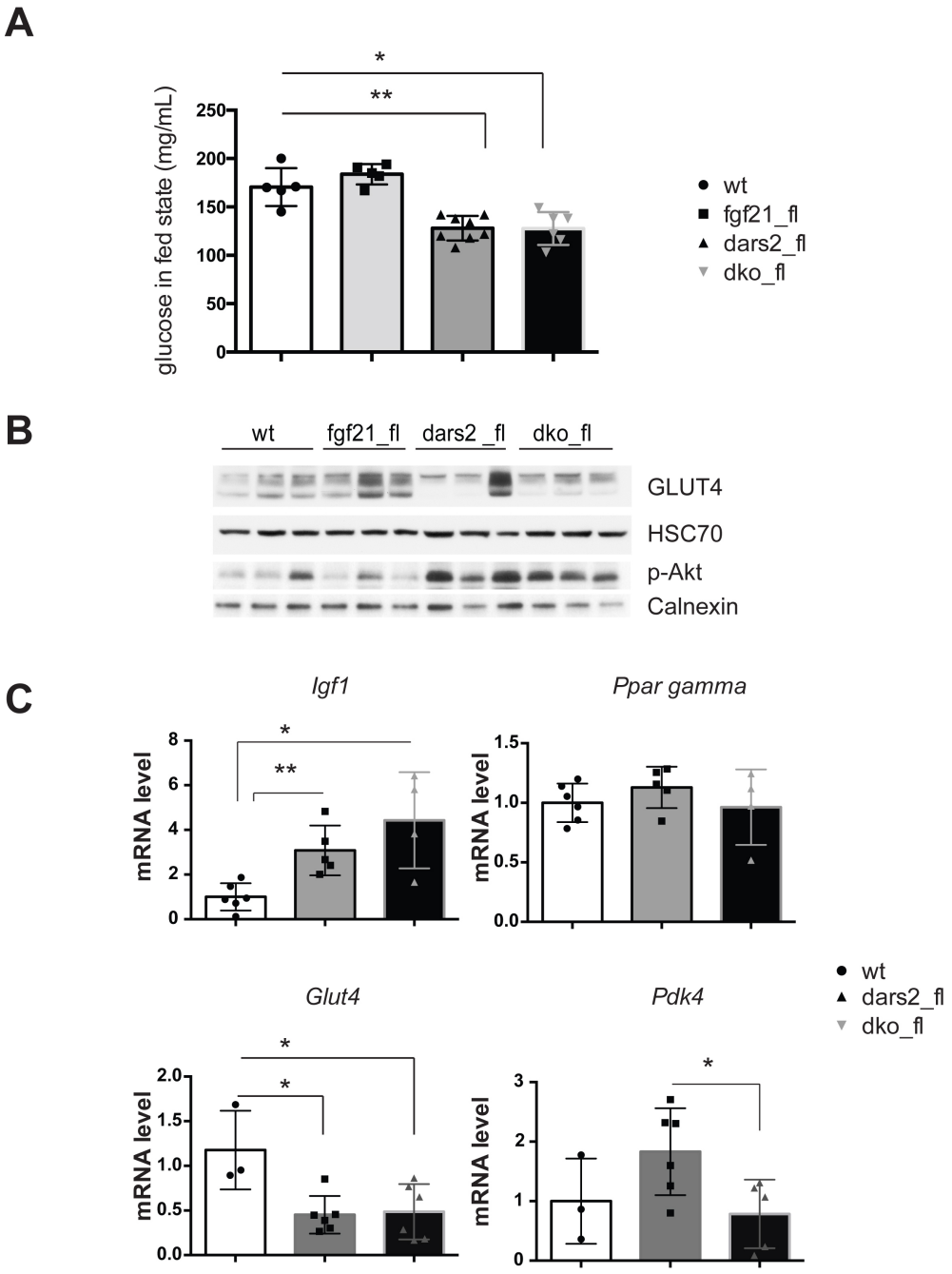


**Figure 3.13 Glucose metabolism is affected upon loss of DARS2 in heart, but not affected with the further depletion of FGF21 in the same tissue.**

**(A)** Glucose levels (mg/mL) measured in non-fasted mice at 6 weeks of age (n=5). **(B)** Western Blot analyses of GLUT4 protein in 6-week-old hearts (n=3). **(C)** Relative expression levels of *Igf1, Pparg, Glut4* and *Pdk4* in heart extracts of 6-week-old mice (n=5).

Data are presented as mean ± SD (*P<0.05, **P<0.01; one-way ANOVA, Tukey's post hoc test).

Mitochondria are crucial for fatty-acid oxidation (FAO). In order to gain more insight in cardiac FAO of DARS2-deficient mice and how FGF21 influences it, acyl-CoA dehydroganese enzymes were analyzed. These enzymes differ in their specificity for short (ACADS), medium (MCAD), long (ACADL) and very long (ACADVL) chain acyl-CoAs. The Western Blot analyses showed no changes in ACADS and MCAD levels (Figure 3.14A), in contrary to ACADVL, which was increased in DARS2-dependent manner (Figure 3.14B). This result might imply that the increased NEFA detected in blood serum of DARS2-deficient mice are comprised of very long chain fatty-acids.

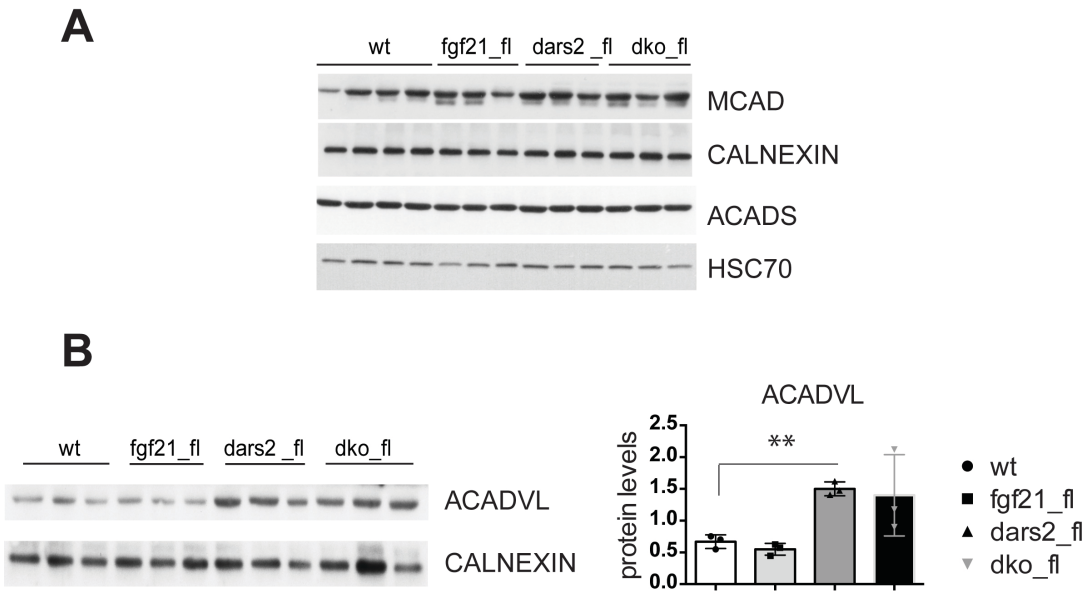


**Figure 3.14 Protein levels of fatty-acid oxidation (FAO) enzymes.**

**(A)** Western Blot analyses of FAO enzymes – MCAD and ACADS protein levels in 6-week-old hearts (n=3).
**(B)** Western Blot analysis and protein quantification of ACADVL protein in 6-week-old hearts (n=3).
Data are presented as mean ± SD (*P<0.05, **P<0.01, ***P<0.001; one-way ANOVA, Tukey's post hoc test).

Cytokines have been reported to have a role on the cardiovascular health. Different cytokines are divided into several classes, according to their function. TNF-α belongs to the family of tumor necrosis factors and it is mostly expressed in macrophages, but it has been shown that cardiomyocytes produce it too (Y. Chen et al., 2010). The expression level measurements gave a surprising result – a decrease in both DARS2 and DKO_fl compared to

WT. Additionally, the expression in DKO_fl hearts was significantly reduced compared to DARS2-deficient heart. *Il1-β* mRNA levels stayed unaffected and *Il-6* expression was increased in a DARS2-dependent manner (Figure 3.15). This inconsistency in results could be due to a few reasons. One cause could be of technical nature, since the immune cells are mainly present in blood and this could interfere with the expression levels seen only in cardiomyocytes. Another cause could be the fact that these three cytokines belong to different groups, and it has been shown before, that IL-1 interleukins are more involved in the pathogenesis of ischemia/reperfusion cardiac injury, where IL-6 is more involved in different cardiomyopathies (Bartekova, Radosinska, Jelemensky, & Dhalla, 2018). According to these results, increase in *Il-6* might indicate that there is a DARS2-dependent increase in inflammation, however this is independent of FGF21.

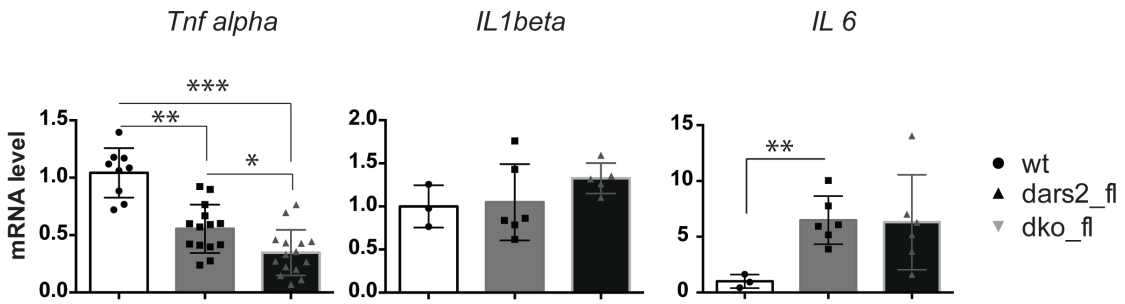


**Figure 3.15 Inflammation response in 6-week-old hearts of WT, DARS2 and double knockout hearts.**

Relative expression levels of different cytokines (TNFα, IL-1β and IL-6) involved in inflammatory response. Data are presented as mean ± SD (*P<0.05, **P<0.01, ***P<0.001; one-way ANOVA, Tukey's post hoc test).

## 3.6. Liver phenotype is not affected by mitochondrial dysfunction in heart.

The previous data in cardiac tissue were consistent in showing that FGF21 has no evident autocrine effects on the heart. This was the reason to have a further look on possible cell-non-autonomous effects of both DARS2 and FGF21 deficiency in heart. Liver is the main metabolic tissue and FGF21 has a relevant role in many metabolic processes, therefore this was the next organ of choice for further experiments. Overall liver phenotype was not affected by depletion of neither DARS2 nor FGF21, as H&E staining revealed (Figure 3.16).

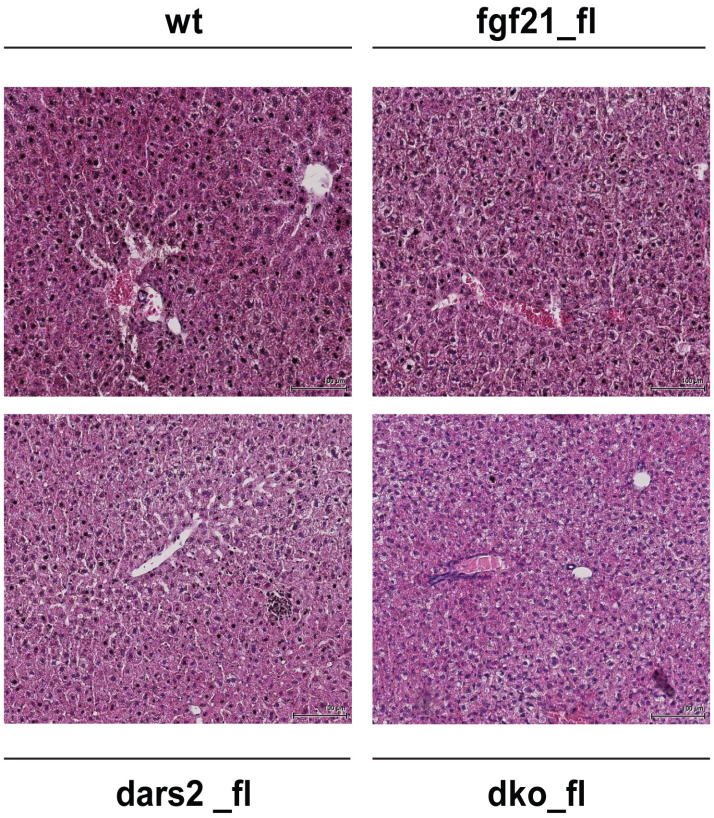


**Figure 3.16 The overal liver phenotype is not affected by mitochondrial dysfunction in**

**(**H&E staining on cryosections (7µm) from liver of the 6-week-old mice (scale bar: 100 µm).

Furthermore, OXPHOS deficiency was not observed in liver. Both protein (Figure 3.17A) and mRNA levels (Figure 3.17B) of different MRC subunits stayed unchanged in all genotypes.

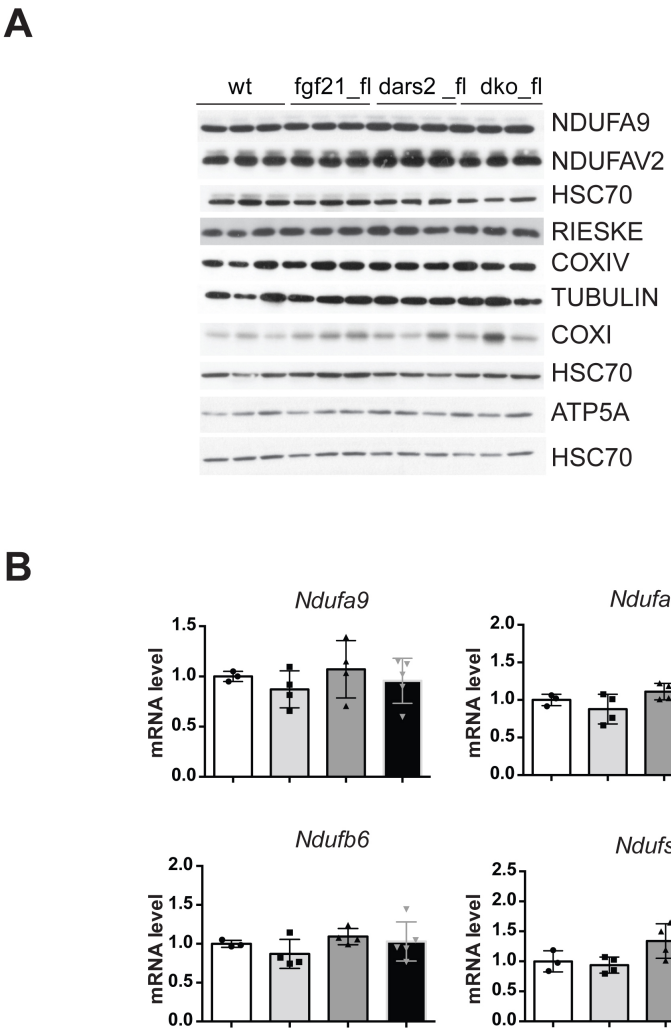


**Figure 3.17 Liver OXPHOS is not affected by the depletion of DARS2 or FGF21 in heart and skeletal muscle.**

Western Blot from total liver extracts **(A)** and relative expression levels **(B)** of indicated MRC subunits. Data are presented as mean ± SD (one-way ANOVA, Tukey's post hoc test).

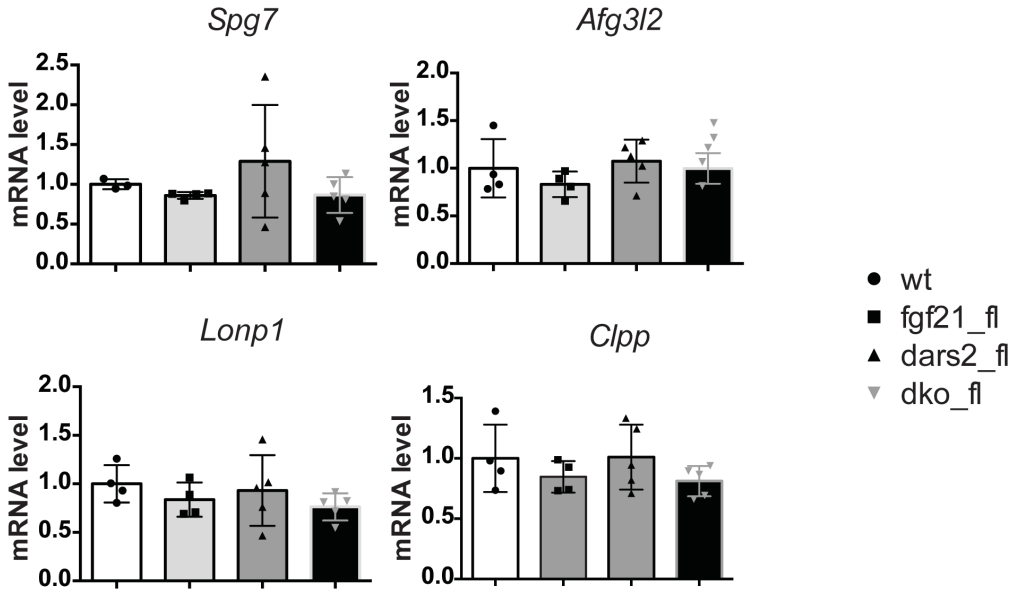


**Figure 3.18 Mitochondrial proteases expression levels stay unchanged in liver the livers of DARS2 deficient mice.**

Relative expression levels of indicated mitochondrial proteases in liver (n=4-5).
Data are presented as mean ± SD (*P<0.05, **P<0.01, ***P<0.001; one-way ANOVA, Tukey's post hoc test).

Liver mitochondrial proteostasis was not affected by the proteostatic stress observed in heart of DARS2-deficient mice. Here, mRNA levels of *Spg7, Afg3l2, Lonp1 and Clpp* were not changed with the DARS2 and FGF21 depletion in the heart (Figure 3.18). Interestingly, markers of mitochondrial biogenesis – TFAM, TOMM20 and PGC1α were not changed when analyzed at the protein level (Figure 3.19A), however *Pgc1α* mRNA was substantially upregulated (~5-fold) (Figure 3.19B) in the liver of heart-specific *Dars2* KO mice. Additionally, the master regulator of integrated stress response – ATF4, was not affected at the protein level, but its mRNA levels were 2-fold upregulated in *Dars2* heart-specific knockout mice. This could suggest that liver is also accommodating to some cellular stress caused by the overall pathological state of the DARS2-deficiency in heart (Figure 3.19A-B). MTHFD2 and GDF15, which are known to be involved in cellular metabolism, were not affected in the liver of *Dars2* KO mice (Figure 3.19A). Furthermore, *Fgf21* expression was comparable between genotypes, but *Klb* was upregulated in *Dars2* KO and DKO_fl mice (Figure 3.19C).

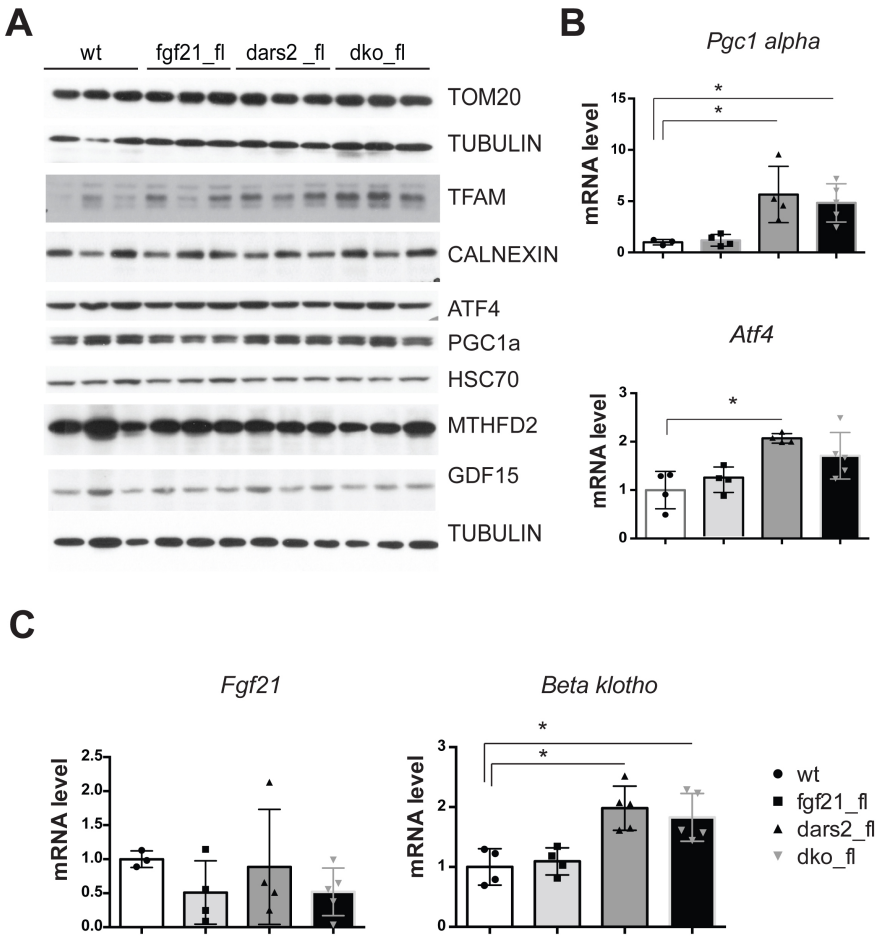


**Figure 3.19 Non-cell-autonomous mitochondrial stress response is not activated in the liver of DARS2 deficient mice.**

**(A)** Western Blot analyses of TOM20, TFAM, ATF4 and PGC1α in total protein extracts from the livers of 6-week-old mice (n=3). **(B)** Relative expression levels of *Pgc1α* and *Atf4* in liver (n=4-5). **(C)** Relative expression levels of *Fgf21* and *Beta klotho (Klb)* in liver (n=4-5). Data are presented as mean ± SD (*P<0.05; one-way ANOVA, Tukey's post hoc test).

In summary, these data obtained from the liver, show that there are some significant changes, but it is still not clear if these mild changes could be assigned to cell non-autonomous effects of the failing heart. The increased expression of *Pgc1α* and *Atf4* could suggest that there is an activation of cellular stress response, which might be due to the metabolic changes caused by cardiac failure.

## 3.7. Loss of DARS2 in heart and skeletal muscle leads to whitening of BAT and increased lipolysis in WAT.

Brown adipose tissue (BAT) influences the whole body energy expenditure. Together with the beige adipose tissue, BAT has capacity to burn glucose and fat to produce heat. This thermogenic capacity is mediated in large part by uncoupling protein 1 (UCP1), which is located in the inner mitochondrial membrane and can dissipate the proton gradient (Ricquier, 2017). One of the aims in this study was to see how mitochondrial dysfunction in heart can influence distant metabolic tissues, and therefore, BAT and white adipose tissue (WAT) were analysed. In BAT, complex I subunits remained unchanged (Figure 3.20A), as well as the subunits of CIII, CIV and CV (published in the master thesis of Christoph Brandsheid). The morphology analyses of BAT showed the features of whitening when DARS2 was absent in heart. Moreover, DKO_fl mice showed even more pronounced phenotype of whitening (Figure 3.20 B).

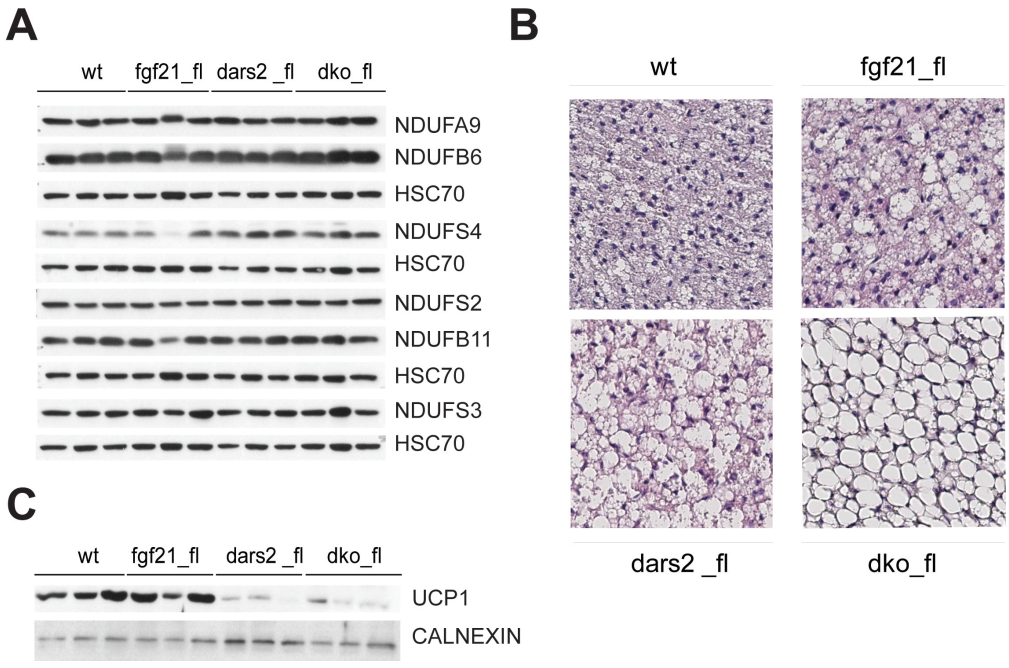


**Figure 3.20 BAT is going through the process of whitening in DARS2-dependent manner.**

**(A)** Western Blot analyses of indicated mitochondrial complex I subunits in total protein extracts from BAT of 6-week-old mice (n=3). **(B)** H&E staining on cryosections from BAT of 6-week-old mice (n=3). **(C)** Western Blot analyses of UCP1 protein in total extract from BAT of 6-week-old mice (n=3).

It was surprising to see that UCP1 protein was almost absent in BATs of DARS2-deficient mice and this was not affected in any way by the loss of FGF21 (Figure 3.20C). These results show that failing heart due to the DARS2 depletion leads to the whitening of BAT, independently of FGF21.

WAT is another important metabolic tissue, which can function as energy storage. What makes it so metabolically important is its capability of "browning", which can increase overall energy expenditure (Carobbio, Guenantin, Samuelson, Bahri, & Vidal-Puig, 2018). Browning of WAT is displayed as appearance of multilocular lipid droplets and large number of mitochondria. That type of adipocytes is referred as "beige" or "brite". They also show increased expression in thermogenic genes such as *Dio2, Cidea and Ucp1*. There are different types of WAT – subcutaneous inguinal WAT (iWAT) and epididymal WAT (eWAT). Here, the morphology of both iWAT and eWAT was changed in mice with DARS2-deficient hearts. In both *Dars2* KO and DKO_fl mice, WAT showed the brown-like phenotype. On the other hand, the observed smaller adipocytes could be the result of the increased lipolysis in WAT (Figure 3.21).

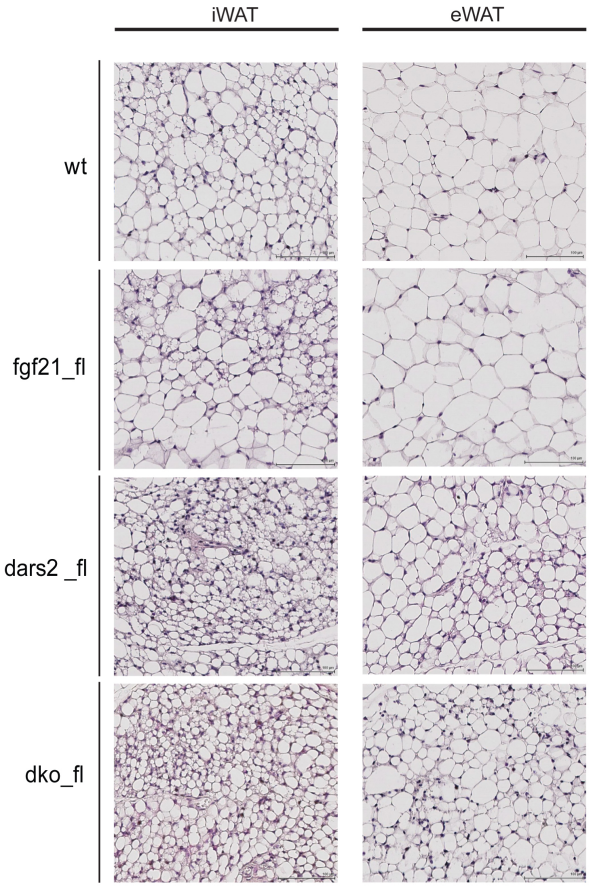


**Figure 3.21 iWAT and eWAT show brown-like phenotype in DARS2 and DKO mice.**

H&E staining on cryosections from iWAT and eWAT of 6-week-old mice (n=3).

To access the browning status, the expression levels of brown adipocytes markers were measured in both types of WAT. The results are contradicting, since they show major decrease in *Ucp1, Cidea and Dio2* levels in iWAT of DARS2-deficient and DKO_fl mice. (Figure 3.22A). This result is not in line with the morphological phenotype of the browning WAT showed previously (Figure 3.22). In eWAT, expression levels of *Ucp1, Cidea and Dio2* show inconclusive result, suggesting that those might be not the only markers of the browning status (Figure 3.22B).

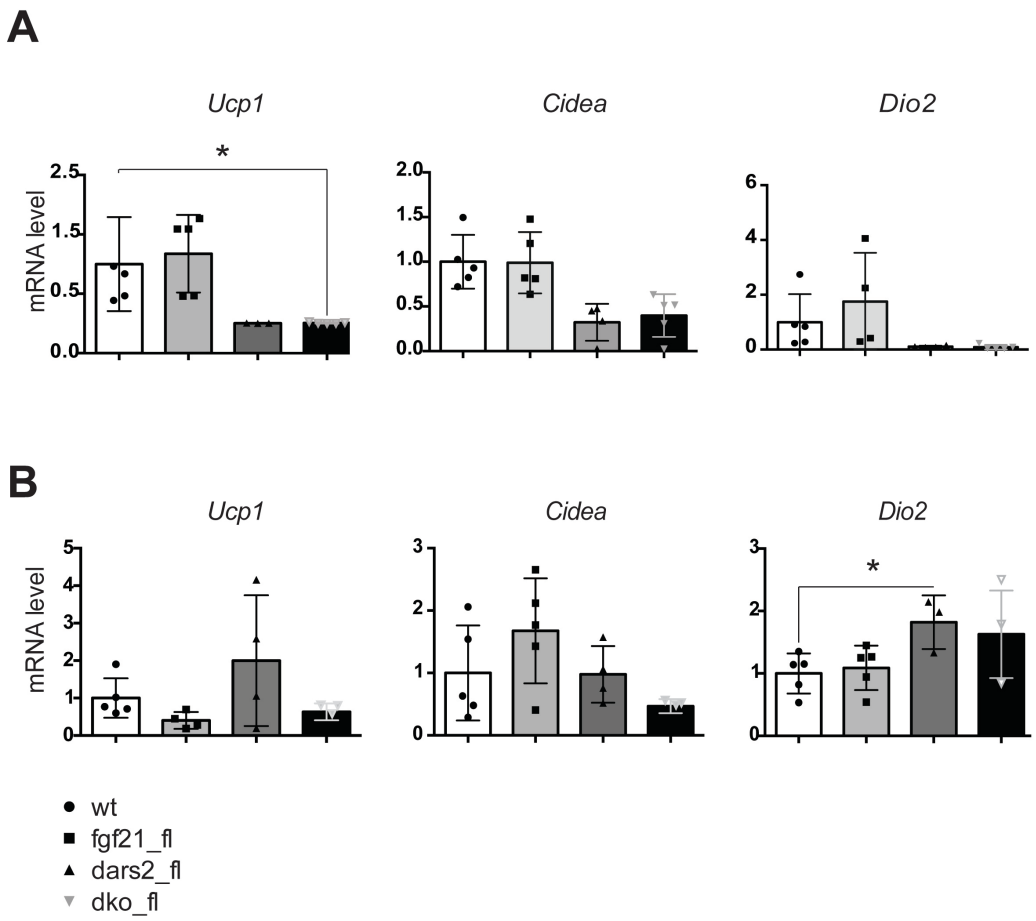


**Figure 3.22 Browning markers in iWAT and eWAT.**

Relative expression levels of browning markers *Ucp1, Cidea and Dio2* in iWAT **(A)** and eWAT **(B)** from extracts of 6-week-old mice (n=5). Data are presented as mean ± SD (*P<0.05; one-way ANOVA, Tukey's post hoc test).

In summary, the BAT and WAT analyses show that there are changes in overall metabolism associated with the failing heart caused by mitochondrial dysfunction. Further

analyses are necessary to confirm the metabolic signaling pathways leading to the whitening of BAT, considering that UCP1 might be not the only factor that is involved in browning.

## 3.8. Label-free quantitative profiling of hearts show no significant differences between *Dars2* KO and DKO_fl mice.

In order to verify previous evidence on the missing autocrine role of FGF21 in heart, the label-free quantitative profiling by mass-spectrometry was performed on heart lysates of the 6-week-old mice. Whole proteome was analyzed and this included a detection of 5890 proteins of which 736 were annotated in mitocarta. Four different replicates for each of four different genotypes were used and significance in differential expression was calculeted using p-values <0,05, which was adjusted to a false discovery rate (FDR) of 5%. In the end, this provided a q-value which was accounted for a final significance factor, when lower than 0,05. This reduces the number of false positive findings among the significant p-values. The fold change was represented in log2 scale, which means that a unit change of 1 corresponds to a 2-fold difference. The whole proteome data of 6-week-old hearts show no significant changes between DARS2-deficient and DKO_fl mice. Gluthathione- S transferase (GST) enzyme, was detected in 2 samples out of 4 in both DARS2 and DKO_fl, and absent in controls. However, this enzyme was increased in DKO _fl hearts in comparison to *Dars2* KO. The best known role of GST is its engagement in xenobiotics detoxification. But more interestingly, recently it has been shown that different isoforms of GST can modulate signaling pathways controling cell proliferation and apoptosis. Moreover, mitogen-activated protein kinases (MAPKs) were showed to induce the expression of xenobiotic enzymes. MAPK1 and MAPK3 were specifically showed to be important in FGF21 signaling pathway (Tanajak, Chattipakorn, & Chattipakorn, 2015). The volcano plots of WT vs. *Dars*2 KO and WT vs. DKO_fl show slightly different patterns, even though DKO_fl vs. *Dars2* KO show no significant changes (Figure 3.23).

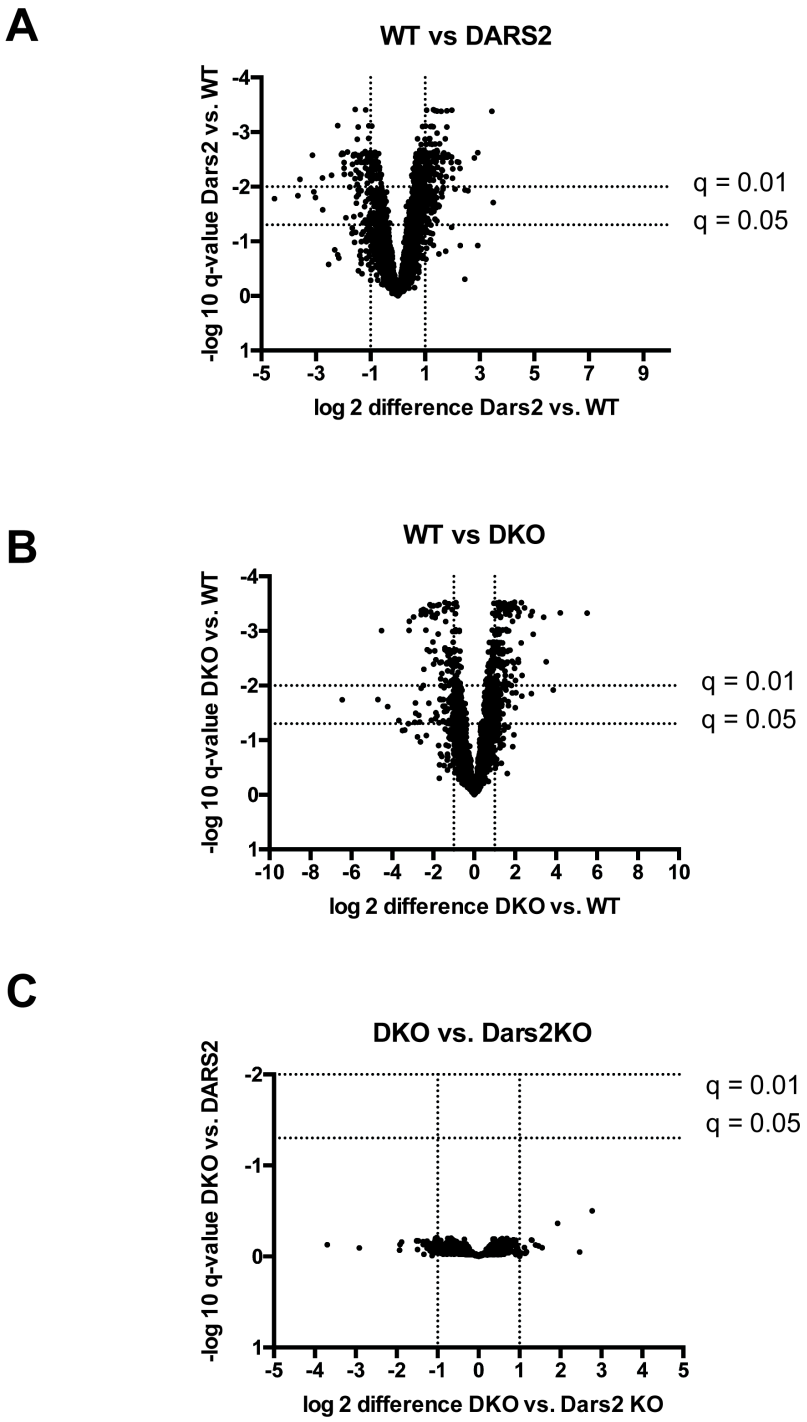


**Figure 3.23 Quantitative assessment of heart proteomics in 6-week-old mice.**

Proteins were quantified by label-free mass-spectrometry analysis. Volcano plots of differential abundance of heart proteins between WT and DARS2 KO **(A)** WT and DKO **(B)** and DARS2 KO and DKO_fl mice **(C).** Proteins are plotted according to statistical significance (−log10 *p*-value) and relative abundance (log2 fold change) (FDR<0.1).

In order to access those differences shown in the volcano plots, some filtering of data was performed. The proteins that were detected only in DARS2-deficient heart and were not present in DKO_fl hearts (marked in black), and vice versa (marked in red), are shown below (Table 3.8).

**Table 3.1 Proteomics data of differentially expressed proteins in DARS2 deficient and DKO hearts.**

The proteins expressed in DARS2-deficient hearts and absent in DKO_fl are marked in black, while proteins marked in red represent the ones detected in DKO_fl, but absent in DARS2-deficient hearts.

| | |
|---|---|
| Histamine N-methyltransferase | **Hnmt** |
| Synaptopodin-2 | **Synpo2** |
| Extracellular matrix protein 1 | **Ecm1** |
| Niemann-Pick C1 protein | **Npc1** |
| Phospholipid-transporting ATPase;Probable phospholipid-transporting ATPase IIA | **Atp9a** |
| Ras-related protein Rab-33B | **Rab33b** |
| Complement component C9 | **C9** |
| Serum amyloid A-4 protein | **Saa4** |
| Ubiquitin-conjugating enzyme E2 H | **Ube2h** |
| Desmoglein-4 | **Dsg4** |
| Arginase-1 | **Arg1** |
| Protein archease | **Zbtb8os** |
| Ubiquitin thioesterase OTUB2 | **Otub2** |
| Conserved oligomeric Golgi complex subunit 3 | **Cog3** |
| N-acetylgalactosamine-6-sulfatase | **Galns** |
| Phosducin-like protein | **Pdcl** |
| Target of rapamycin complex subunit LST8 | **Mlst8** |
| Methionine-R-sulfoxide reductase B1 | **Msrb1** |

The proteins absent in DKO_fl hearts were analyzed using KEGG pathways library. The enriched pathways include histidine metabolism, coagulation cascade, lysosome and ubiquitin-mediated proteolysis pathway. The proteins that are present only in DKO_fl hearts, when enriched and analyzed using KEGG pathways, were shown to be part of arginine biosynthesis pathway, arginine and proline metabolism and mTOR signaling (Table 3.8).

The overall difference in whole proteome between DARS2-deficient and DKO_fl hearts are subtle and there is so no significant difference in any of the detected proteins. Conversely, DARS2-deficient heart shows many significant changes when compared to the WT hearts. Those are the first whole proteome data achieved from this mouse model. The protein that is strikingly upregulated in DARS2-deficient hearts is ALDH18A1. This enzyme catalyzes a critical step in biosynthesis of proline, ornithine and arginine. The log2 difference is 8,77, which is nearly 400-fold change. The MTHFD1L, the enzyme involved in tetrahydrofolate synthesis in mitochondria, is ~30-fold increased In DARS2-deficient hearts. In the scale of ~20-fold increase are: PHDGH – an enzyme involved in serine biosynthesis, ERO1L – oxidoreductase in ER, PCK2 – phosphoenolpyruvate carboxykinase 2, PYCR2 – mitochondrial enzyme involved in the last step of proline synthesis and PSAT1 – involved in serine biosynthesis (Figure 3.24A). Enrichment of the proteins increased in DARS2-deficient hearts showed that one-carbon metabolism and amino-acid biosynthesis pathways are the most upregulated ones (Figure 3.24B). Moreover, mitochondrial ribosomal proteins of both small and large subunits are significantly upregulated, as well as some of the amino-acid transporters. Interestingly, none of the fibroblast growth factors was detected in the analyzed hearts.

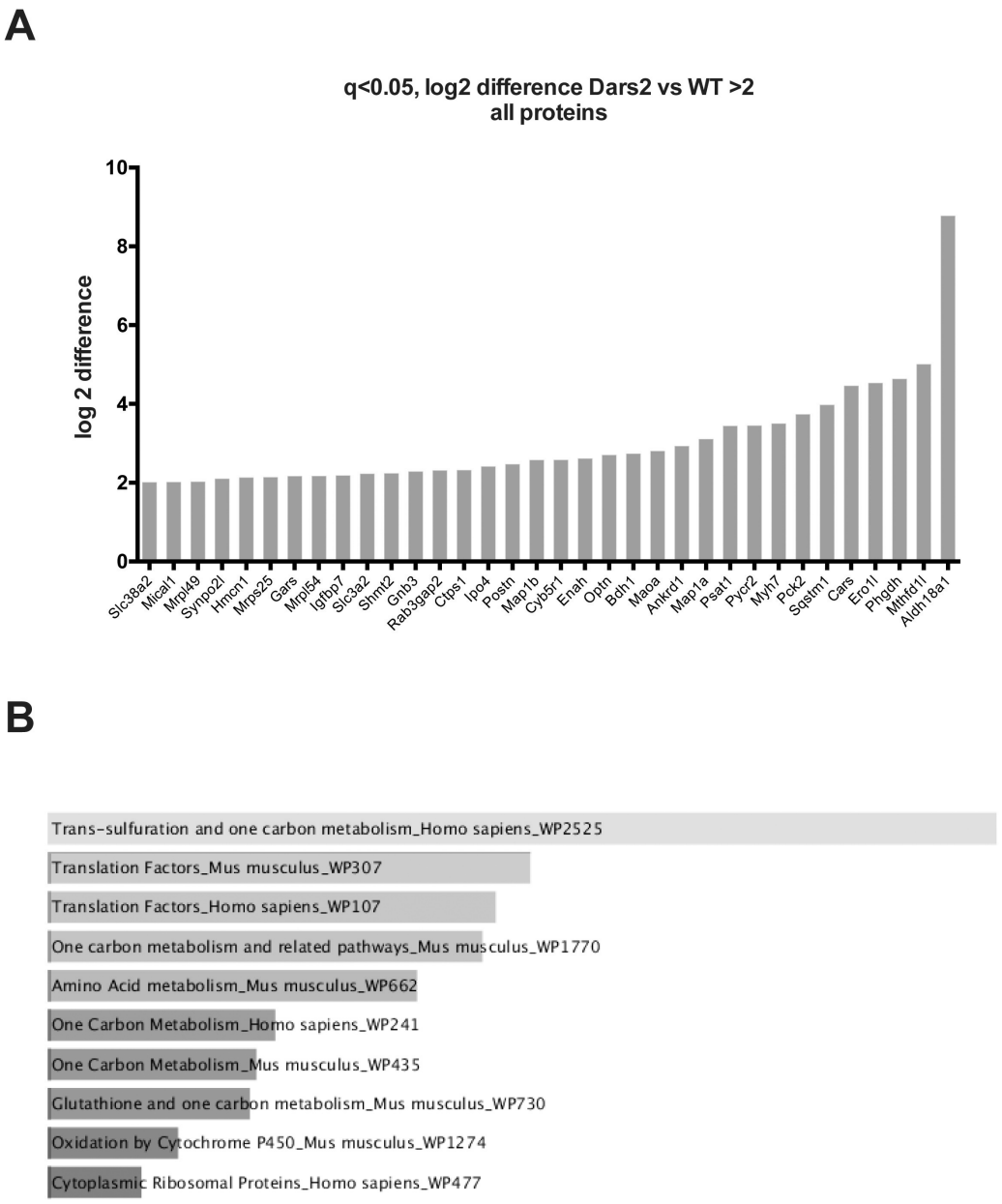


**Figure 3.24 Quantitative assessment of the most up-regulated proteins in *Dars2* knockout compared to wild type mice.**

**(A)** Significantly increased proteins in DARS2-deficient hearts compared to WT; Log2 difference DARS2 vs WT >2, q<0,05. **(B)** Enrichment analysis of the upregulated pathways in DARS2-deficient hearts (Wiki Pathways).

Analysis of the proteins decreased in DARS2-deficient hearts compared to WT showed that CPS1 – a protein involved in urea cycle, is most prominently downregulated. Right after it comes BHMT – an enzyme involved in homocysteine metabolism. CI and CIV subunits also show a strong downregulation in DARS2-deficient hearts, as well as some of the CIII subunits, but to a lower extent (Figure 3.25A). In summary, the proteins that are significantly downregulated in DARS2-deficient hearts belong to the OXPHOS system and amino-acid metabolism pathways (Figure 3.25B).

**A**

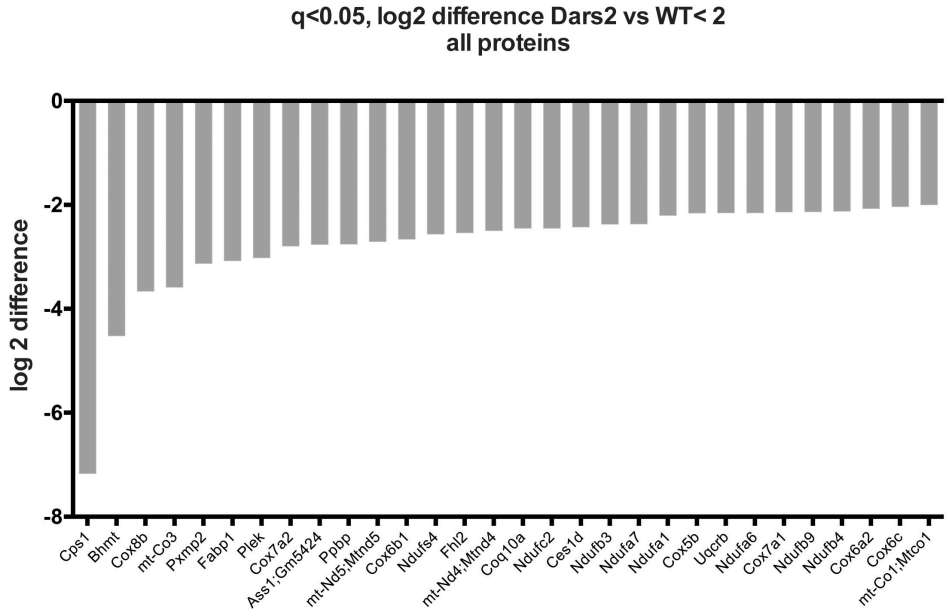


**B**

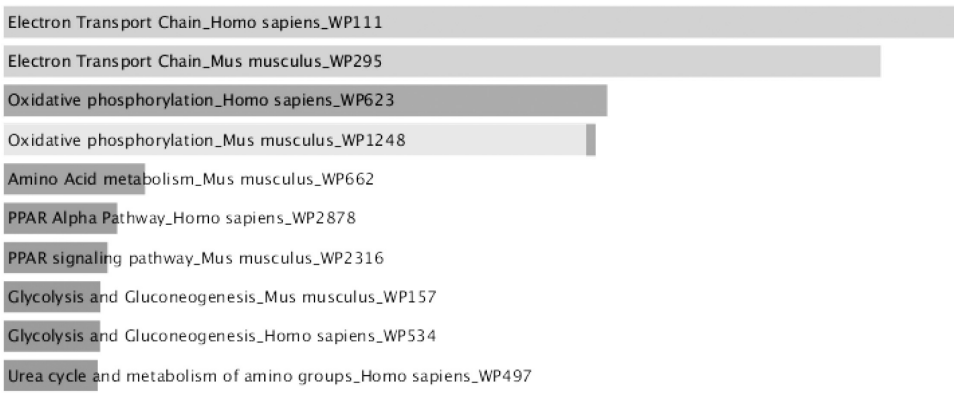

**Figure 3.25 Quantitative assessment of the most down-regulated proteins in *Dars2* knockout compared to wild type mice.**

**(A)** Significantly decreased proteins in DARS2-deficient hearts compared to WT; Log2 difference DARS2 vs WT >2, q<0,05. **(B)** Enrichment analysis of the down-regulated pathways in DARS2-deficient hearts (Wiki Pathways). Log2 difference DARS2 vs WT <2, q<0,05.

Coupled with the previous data, the whole proteome analysis at early stage (between 3 and 4 weeks) was performed in the same manner in order to observe the first changes in DARS2-deficient mice, when animals were still in good health. Moreover, the analysis of the early changes in proteome could exclude the possibility of strong *Dars2* KO phenotype masking the effects of FGF21 loss. 5735 proteins were detected in total heart lysates. There were no significant differences between DARS2-deficient and DKO_fl hearts and the volcano plots of *Dars2* KO proteome compared to WT showed less changes than at 6 weeks of age, which is in line with the age-related phenotype of the mice (Figure 3.26A). Complex I and IV subunits were already significantly downregulated at 3 weeks of age (Figure 3.26B). Strikingly, ALDH18A1, PHGHD, PCK2 and SLC3A2 are strongly increased already at the early stage, which might suggest that the primary stress responses are related to the unbalanced amino-acid metabolism (Figure 3.26C). Additionally, the whole proteome data showed that already at 2 weeks of age, PHGHD, PSAT1 and ALDH18A1 are the most upregulated proteins in DARS2-deficient hearts (Kaspar S., unpublished data). These data demonstrate that autocrine FGF21 is dispensable for the pathology of DARS2 deficiency in heart and there are possibly some other key players causing the primary stress responses. The amino-acid biosynthetic pathways disbalance could be one of the earliest pathological changes in DARS2 - deficient hearts.

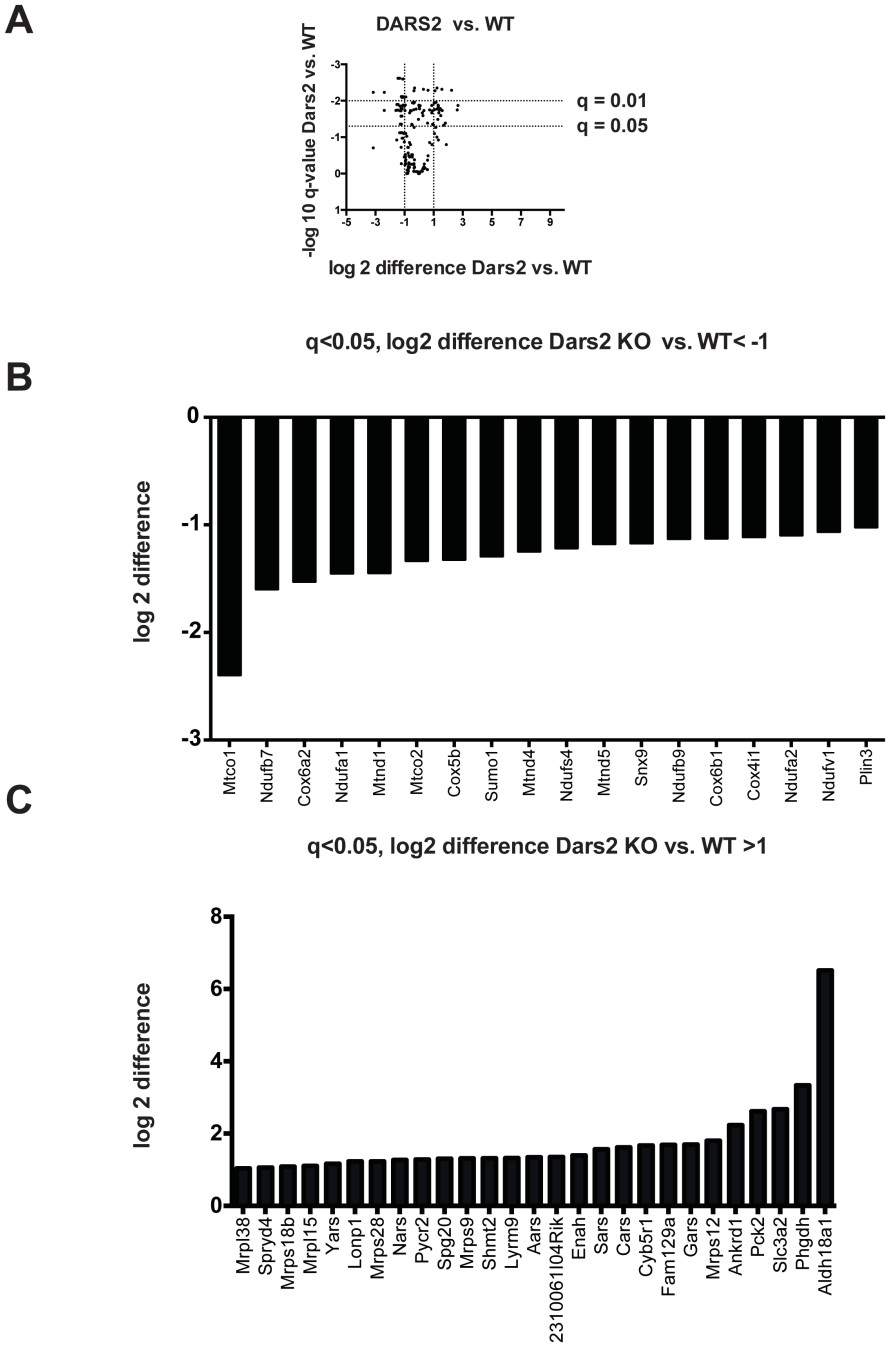


**Figure 3.26 Quantitative assessment of heart proteomics in 3-week-old mice.**

**(A)** Proteins were quantified by label-free proteomic analysis. Volcano plots of differential abundance of heart proteins between *Dars2* KO and WT. **(B)** Down-regulated proteins in *Dars2* KO vs WT from mitocarta. **(C)** Up-regulated proteins from mitocarta in *Dars*2 KO vs WT. Proteins are plotted according to statistical significance (−log10 *p*-value) and relative abundance (log2 fold change) (FDR<0.1).

## 3.9. Downstream ERK1/2 signaling in the heart is still activated in the absence of FGF21.

Next, downstream signaling pathways of FGF21 were analysed in 6-week-old hearts. It is known that FGF21 next to FGFR1 receptor requieres β-KLOTHO (KLB) co-receptor in order to activate downstream signaling pathways. ERK1/2, also known as MAPK3/MAPK1, is one of the kinases known to be activated by FGF21. Here, protein levels of both KLB and ERK1/2 were analysed and surprisingly we detected the upregulation in both DARS2-deficient and DKO_fl mice (Figure 3.27A). This result once more confirmed that the absence of autocrine FGF21 does not influence the stress signaling in DARS2-deficient hearts. Moreover, expression levels of *Klb* were significantly increased in DKO_fl when compared to the WT hearts (Figure 3.27B). This might imply that there is some compensatory effect due to the lack of FGF21. Two more endocrine fibroblast growth factors, FGF19 and FGF23, have the preference for the same receptor, but they have not shown increase in their expression levels (Figure 3.27B). PPARα and SIRT1 were shown to induce Fgf21 expression in cardiomyocytes, by binding to its promoter (Planavila et al., 2013). *Pparα* expression levels were significantly decreased in both DARS2-deficient and DKO_fl hearts. On the other hand, *Sirt1* was mildly upregulated in DKO_fl when compared to the WT hearts (Figure 3.27B).

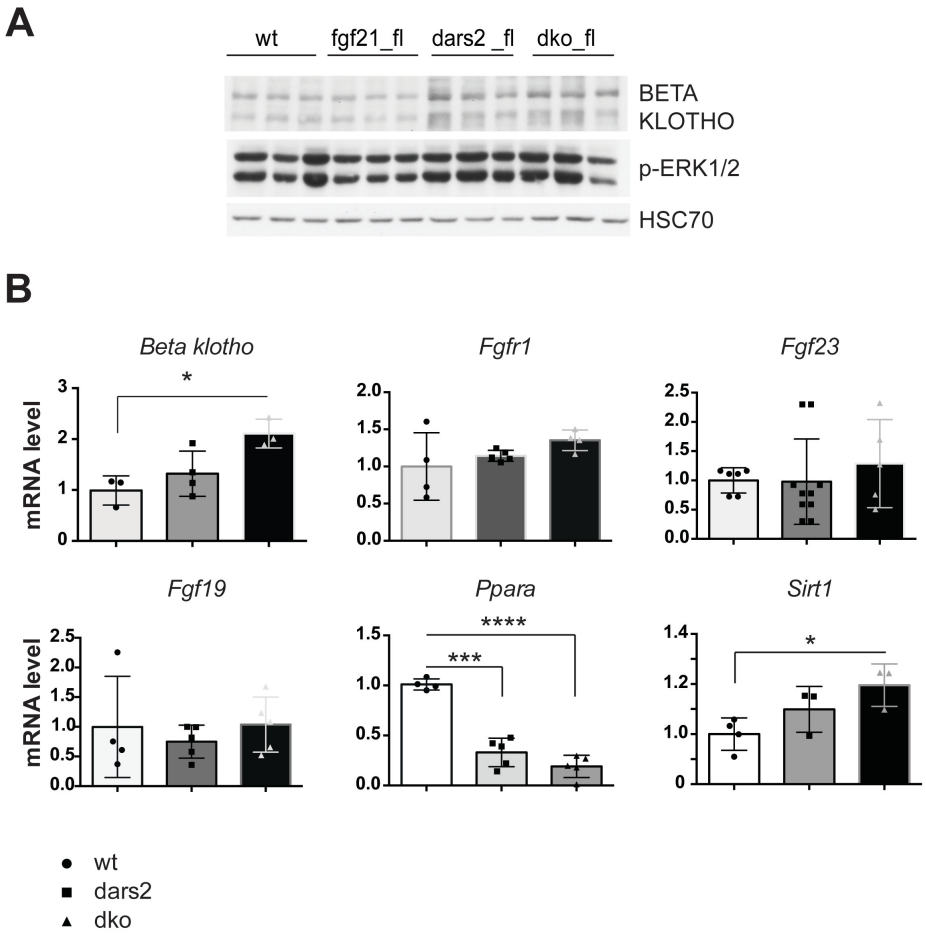


**Figure 3.27 FGF21 signaling cascade is activated even with its absence in the heart.**

**(A)** Western Blot analysis of β-Klotho (KLB) and phosphorylated ERK1/2 protein from total heart extracts of 6-week-old mice (n=3). **(B)** Relative expression levels of *Klb, Fgfr1, Fgf19* and *Fgf23* in heart extracts of 6-week-old mice (n=5). Data are presented as mean ± SD (*P<0.05, ***P<0.001, ****P<0.0001; one-way ANOVA, Tukey's post hoc test).

This unexpected upregulation of ERK1/2 and KLB despite the absence of FGF21 suggested that endocrine FGF21 from bloodstream could still activate the signaling cascade in the heart. Endocrine FGF21 indeed requires KLB for its action. Therefore, serum levels of FGF21 were measured by an immunoassay. The increased FGF21 serum levels were detected in DARS2-deficient mice, which is in line with previous findings (Dogan et al., 2014). Moreover, the levels of this cytokine were significantly downregulated in DKO mice, but still present at low level (Figure 3.28). It is not clear if those low levels could still activate the signaling pathways in an endocrine way. In order to answer this question, a new mouse model was created.

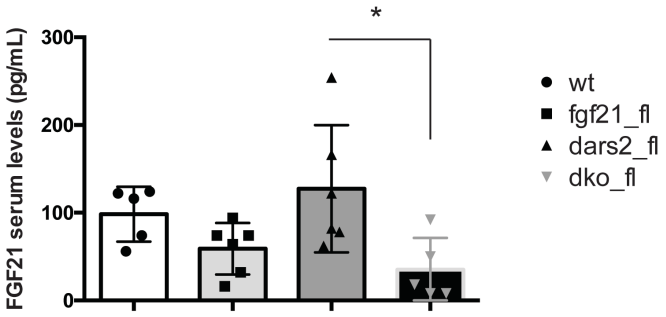


**Figure 3.28 FGF21 serum levels are decreased, but still present with the loss of FGF21 in heart.**

FGF21 levels in serum of 6-week-old mice measured by using ELISA FGF21kit (n=6-10). Data are presented as mean ± SD (*P<0.05; one-way ANOVA, Tukey's post hoc test).

## 3.10. Full body depletion of FGF21 in mice lacking DARS2 in heart and skeletal muscle does not affect the overall phenotype of the knockout.

To investigate if the endocrine FGF21 secreted from other tissues is compensating for its absence in heart, a new mouse model was created. This time, heart and skeletal muscle specific *Dars2* KO mice were lacking FGF21 in whole body. Surprisingly, these new double-deficient (DKO) mice were also indistinguishable from *Dars2* KO mice. They did not differ in lifespan nor body weight. The heart to body weight ratio was not significantly changed (Figure 3.29A). Moreover, cardiac label-free quantitative profiling of 6-week-old mice showed no significant changes in the whole proteome (Figure 3.29B). Additionally, the proteins shown to have a role in amino-acid biosynthesis and one-carbon metabolism were checked by Western Blot. In previous model, whole proteome data showed strong upregulation of those proteins (Figure 3.24). Here, MTHFD2, PYCR2 and SHMT2 showed strong increase in *Dars2* KO hearts, but again, full-body depletion of FGF21 did not have any further effects (Figure 3.29C). In previously described model, LONP1 was also shown to be one of the most prominent changes among the mitochondrial proteases. Here, the protein levels of LONP1 measured by Western Blot were upregulated in DARS2-dependent manner (Figure 3.29C) and this was also confirmed by proteomics data. The decrease in steady state levels of different OXPHOS subunits in *Dars2* KO was not changed in DKO (Figure 3.29D). Curiously, even when FGF21 is missing in BAT, the morphology of the tissues remains the same like in *Dars2* KO mice (Figure 3.29E). This is peculiarly interesting because it has been shown that FGF21 induces UCP1 expression. Taken together, these results show that even full-body depletion of FGF21 does not influence the phenotype of the *Dars2* KO mice.

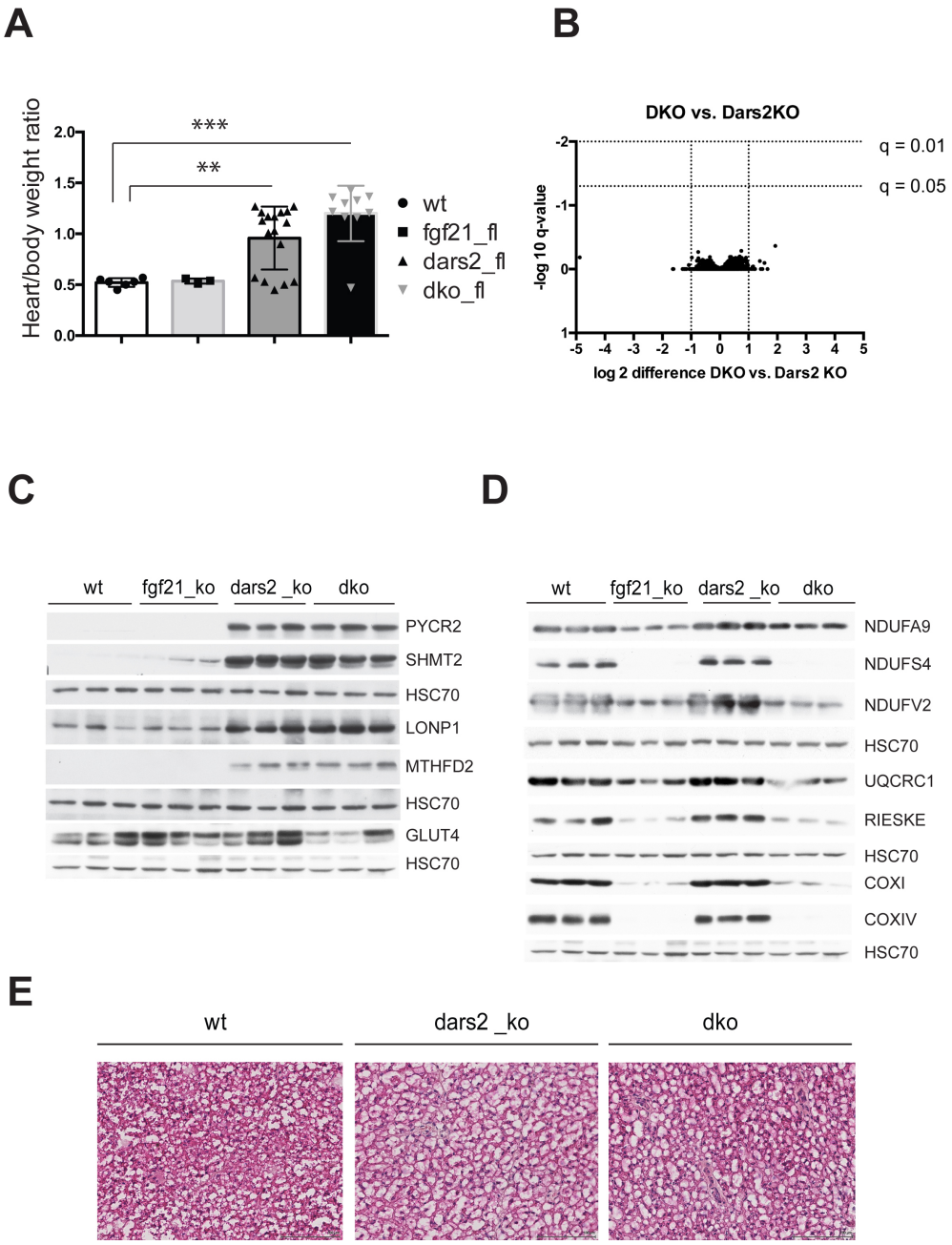


**Figure 3.29 Full-body depletion of FGF21 in DARS2 tissue-specific KO does not affect heart phenotype.**

**(A)** Heart to body weight ratio in indicated genotypes. **(B)** Western Blot analyses of the proteins involved in 1-carbon metabolism and LONP1 protease from total heart lysates of 6-week-old mice (n=3). **(C)** Volcano plots of differential abundance of heart proteins between DKO and DARS2 KO. **(D)** Western Blot analyses of the mitochondrial complex I subunits and GLUT4 from total heart lysates of 6-week-old mice (n=3).

Since full-body depletion of FGF21 showed no difference in *Dars2* KO phenotype, next thing to access were the signaling pathways that are known to be involved in FGF21 signaling. mTOR pathway was shown to be activated in *Dars2* KO heart, but neither the heart-specific (Figure 3.12) nor full-body FGF21 depletion (Figure 3.30A) leads to any change in its activation. The major regulator of the ISR, phosphorylated eIF2α, was shown to be upregulated in DARS2-deficient hearts. It is also known that FGF21 is a downstream target of ATF4, whose expression is induced by phosphorylated eIF2α. However, full-body (Figure 3.30B) as well as the heart-specific FGF21 depletion (Figure 3.8) does not change the level of phosphorylation of this factor.

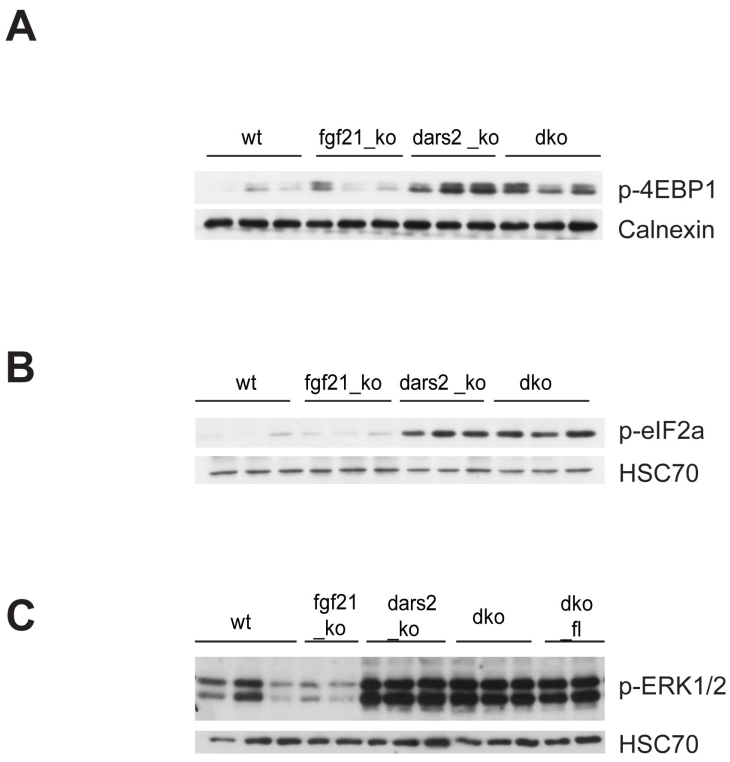


**Figure 3.30 Full-body depletion of FGF21 in *Dars2* tissue-specific KO does not influence the phosphorylation status of different proteins.**

Western Blot analyses of phosphorylated 4EBP1 **(A)** eIF2 alpha **(B)** and ERK1/2 **(C)** from total heart lysates of 6-week-old mice (n=3).

The ultimate question is if the known cascade through ERK1/2 can be activated also in the absence of FGF21. Here, phosphorylated ERK1/2 levels were analysed in both full-body (DKO) and heart-specific (DKO_fl) double-deficient mice. Interestingly, ERK1/2 was activated at the same level in *Dars2* KO, DKO_fl and DKO mice, independently of autocrine or endocrine FGF21 (Figure 3.30C). This suggests that there might be some compensatory pathways in the absence of this cytokine. Since FGF21 binds a receptor which is a tyrosin kinase, phosphorylation status in heart was accessed. In order to find alternative pathways which could be activated with the loss of FGF21, phospho-proteomics analyses were performed on heart tissue lysates from all five genotypes. The enrichment analyses using KEGG pathways showed that there are differences between tissue-specific DKO_fl and DKO hearts. The common pathways that were upregulated in both double-deficient mouse models when compared to DARS2-deficient mice were involving ribosome, splicosome and PPAR signaling (Figure 3.31A). The downregulated patways in both double-deficient mouse models are shown in Figure 3.31B. The proteins which were downregulated to the highest extent in DKO compared to DARS2-deficient hearts are listed in Table 3.9. Interestingly, we did not observe changes in ERK1/2 kinases (MAPK3/MAPK1), which is in line with the Western Blot data shown in Figure 3.30.

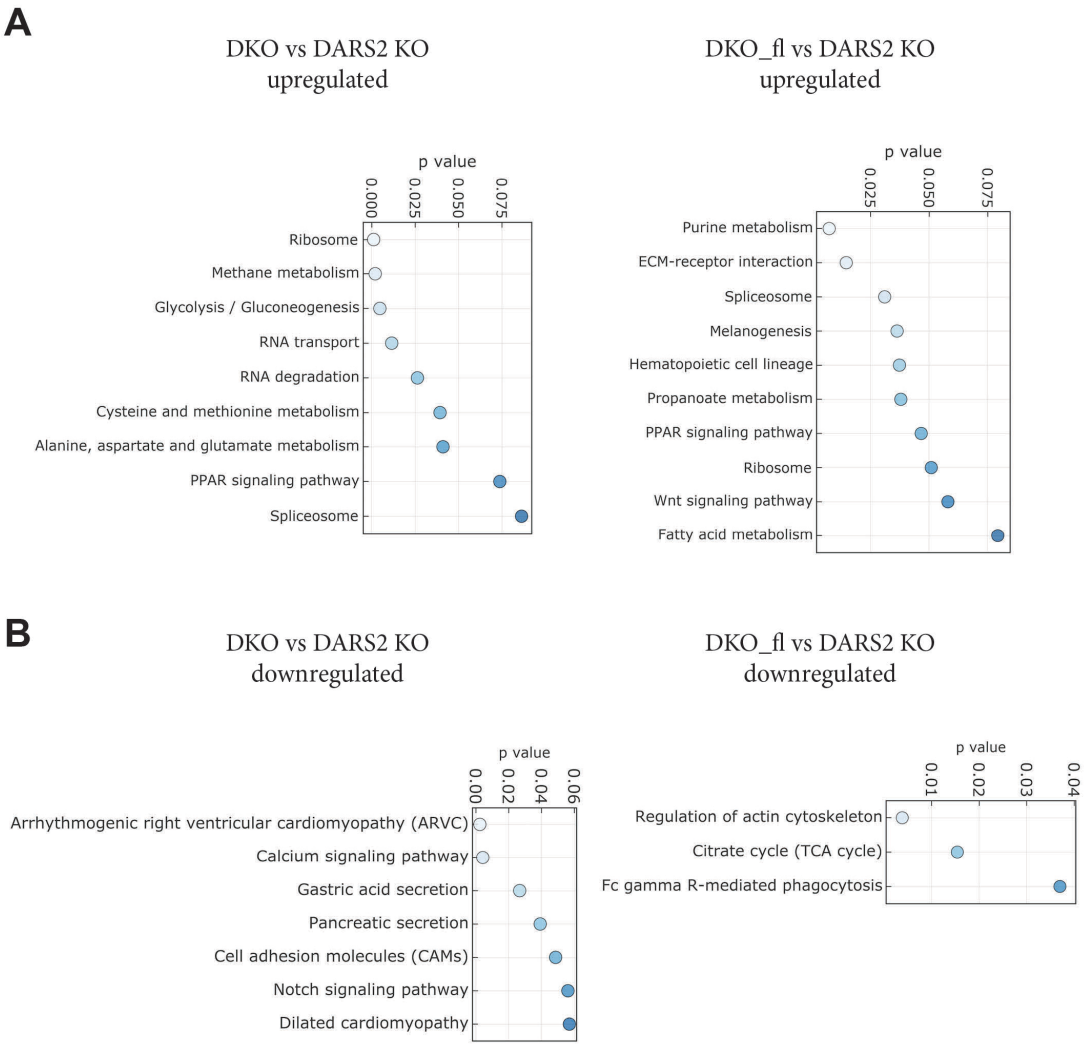


**Figure 3.31 Phospho-proteomics analyses; KEGG pathways enrichment.**

KEGG pathways enrichment of phospho-proteome in DKO compared to DARS2 KO and DKO_fl compared to DARS2 KO (DKO_fl: tissue-specific double-deficient mice; DKO: double-deficient mice lacking FGF21 in whole body, and DARS2 in heart and skeletal muscle). Pathways which are upregulated (A) and downregulated (B) in DKO and DKO_fl compared to DARS2 KO.

Moreover, we compared pathways which were differentially regulated in DKO_fl and DKO (Figure 3.32).

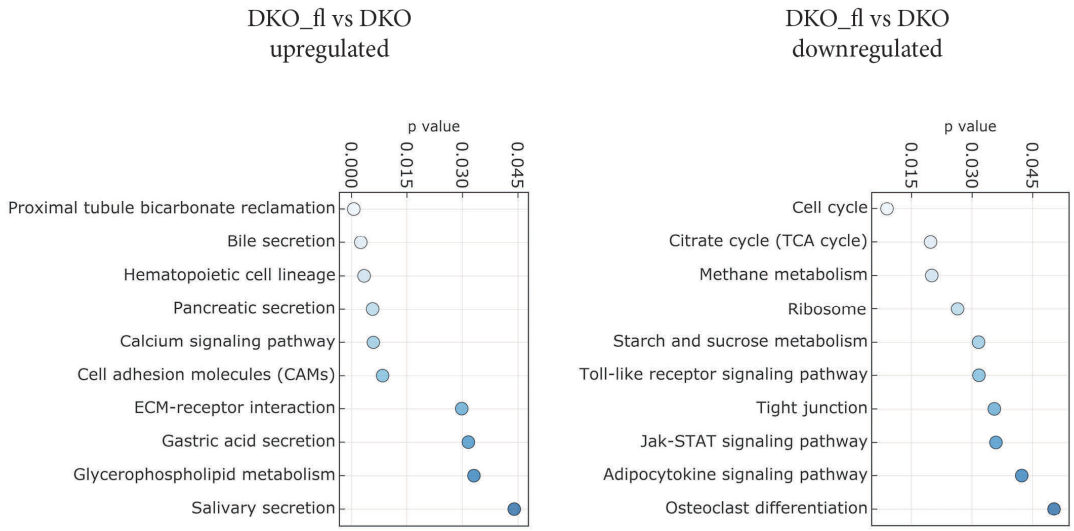


**Figure 3.32 Phospho-proteomics analyses; KEGG pathways enrichment.**

Enrichment of the upregulated and downregulated in DKO_fl compared to DKO using KEGG pathways

**Table 3.2 Phosphorylated proteins which are decreased in DKO vs DARS2-deficient hearts.**

Proteins are selected according to significance q<0,05 and log2 fold change <-1.

| protein | function | Log2 change |
|---|---|---|
| Bnip3 | Apoptosis | -3,3 |
| Arpp19;Ensa | Insulin secretion stimulation | -3,1 |
| Fam126a | Not known | -2,4 |
| Ppp1r12a | Phosphatase | -2,1 |
| Araf | Mitogenic signaling | -1,8 |
| Map1a | Cytoskeletal organization | -1,7 |
| Pak2 | Cytoskeleton; stimulation of cell proliferation | -1,7 |
| Tomm70a | Mitochondrial import | -1,5 |
| Slc8a1 | Calcium transmembrane transport | -1,5 |
| Slc25a4 | Mitochondrial ADP/ATP transport | -1,5 |

Furthermore, we analyzed serum proteome in order to check if there are possible candidates that might be compensatory to the lack of FGF21. Unfortunately, we did not detect any other protein belonging to the fibroblast gorwth factor family. The only changes we observed are decreased epidermal growth factor receptor – EGFR and elongation factor 1 alpha-1 – EEF1A1 in DKO when compared to DARS2-deficient mice. Increased apolipoprotein D, as well as the fructose bisphosphatasealdolase, were observed in *Dars2* KO when compared to control. Apolipoprotein D was shown to have cardioprotective effects and its plasma levels are increased during myocardial infarction (Tsukamoto et al., 2013).

## 3.11. FGF21 is not responsible for the induction of stress responses in CLPP KO mice.

The severity of stress caused by DARS2 deficiency is possibly masking the effects of FGF21 depletion. In order to exclude this option, a new double-deficient mouse model was created, lacking FGF21 and CLPP in whole body (DKO_wb). CLPP deficiency induces mild phenotype and lifespan stays unaffected. The main features of *Clpp* KO mice is moderate complex I deficiency, accompanied by decreased body weight and hearing loss (Jenkinson et al., 2013). Despite the loss of FGF21, phenotype of DKO_wb mice at 16-18 weeks of age was almost identical to *Clpp* KO mice. *Fgf21* expression is approximately 5-fold increased in *Clpp* KO hearts (Figure 3.33A). The body fat was decreased at the same extent in both *Clpp* KO and DKO_wb mice (Figure 3.33B). Concerning the glucose metabolism, both glucose and insulin tolerance test od DKO_wb followed the trend of *Clpp* KO mice (Figure 3.33C).

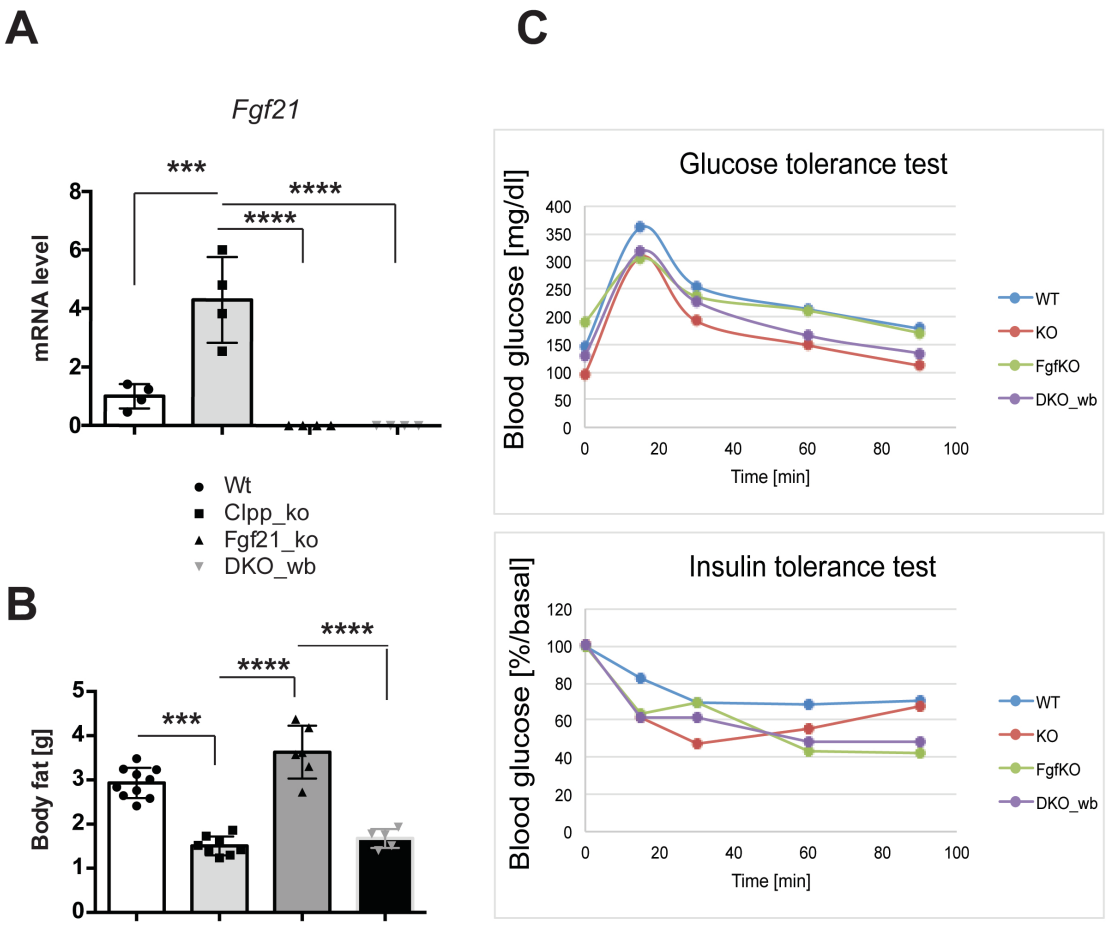


**Figure 3.33 Body weight and insulin/glucose tolerance in *Clpp* KO mice is not affected with the loss of FGF21.**

**(A)** Relative expression levels of *Fgf21* in total RNA from heart in 16-week-old mice (n=5) **(B)** Body fat in grams measured by NMR (n=6-8). **(C)** Glucose and insulin tolerance test in fasted mice.
Data are presented as mean ± SD (*P<0.05, **P<0.01, ***P<0.001; one-way ANOVA, Tukey's post hoc test).

Along with the previous analyses in *Dars2* KO hearts, versatile stress response markers were analyzed also in *Clpp* KO mice, where the depletion of FGF21 did not induce any change. LONP1 protease levels stayed unchanged, while mitochondrial chaperone GRP75 and CLPP substrate -TRAP1, were induced at the same level in both *Clpp* KO and DKO_wb. Moreover, ATF4 was not differentially upregulated when FGF21 was absent in *Clpp* KO. The PGC1α levels were increased in both *Clpp* KO and DKO_wb hearts and MnSOD2 was not changed in any of the genotypes (Figure 3.34A).

In our lab, we have recently identified some of the CLPP substrates - ornithine aminotransferase (OAT) and elongation factor G1 (EFG1) (Szczepanowska et al., 2016). Both substrates were accumulated in *Clpp* KO and DKO_wb hearts (Figure 3.34B). Cardiomyokine GDF15 protein levels were accessed, hence its similar functions with FGF21. The levels of GDF15 were not changed in any genotype (Figure 3.34C). Given the previous findings in DARS2 and FGF21 double-deficient mice, it was surprising to observe that ERK1/2 activation in *Clpp* KO mice is absent with the loss of FGF21 in full body (Figure 3.34C). This result may be an indication that different cardiac stress load activates divergent signaling pathways.

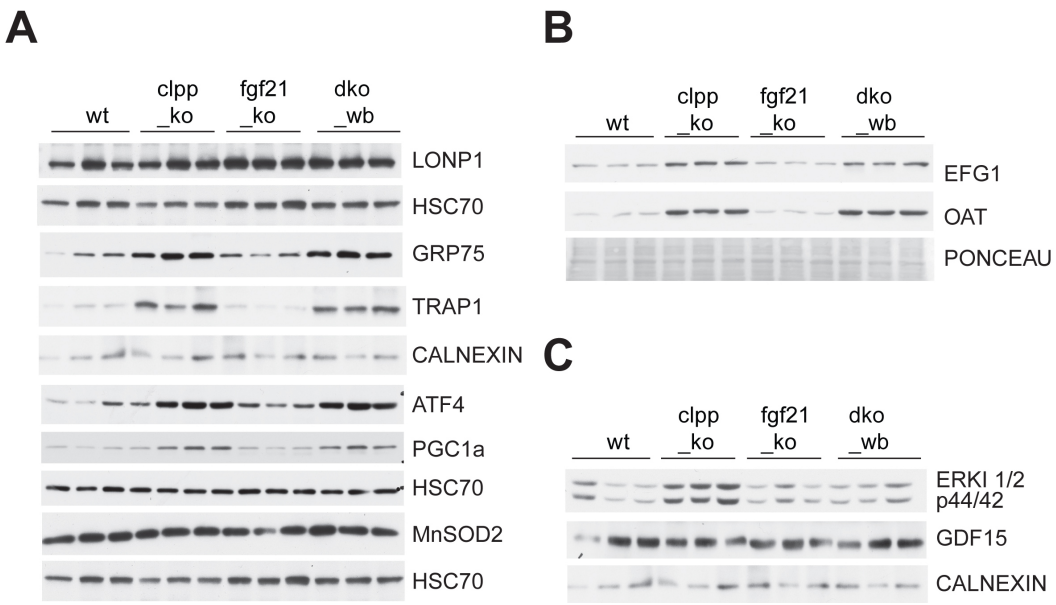


**Figure 3.34 Stress responses in the heart of *Clpp* KO mice are not affected by the additional depletion of FGF21.**

Heart lysates Western Blot analyses of mitochondrial stress response markers **(A),** CLPP known substrates **(B),** phosphorylated ERK1/2 and cardiomyokine GDF15 **(C)** in 16-week-old mice.

## 3.12. Label-free quantitative profiling of heart reveals upregulation in cytoplasmic ribosomal proteins, histones and cytoskeleton proteins in mice lacking both CLPP and FGF21.

Previous data showed that most of the changes observed stem from CLPP depletion, however, ERK1/2 activation was ablated with the loss of FGF21. To analyze it in more unbiased way and check for other possible changes, the label-free quantitative profiling of whole cardiac proteome was performed, in pursuence for new possible effectors. For the analysis we used whole heart lysates from the mice between 16 and 18 weeks of age, including 4 biological replicates per genotype. The data showed 38 significantly upregulated (Figure 3.35A) and 13 downregulated proteins in DKO_wb compared to *Clpp* KO hearts (Figure 3.35A). KEGG and GO enrichment analyses of DKO_wb differences compared to *Clpp* KO were perfomed and revealed that most of the upregulated proteins in DKO_wb belong to the splicesome machinery, cytoplasmic ribosome and cytoskeletal proteins involved in cardiac-contraction (Figure 3.35B). When the list of these proteins was analyzed by Enrichr platform, the results associated the increase in cytoskeletal proteins to hypertrophic and dilated cardiomyopathy, impliying that loss of FGF21 can possibly influence the cardiac muscle contraction. Moreover, RAB8B is a GTPase that has been shown to react with cytoskeletal proteins and it was also upregulated in DKO_wb hearts. When analysing these proteins in *Clpp* KO compared to WT, it is interesting to observe that 19 out of 51 proteins are significantly changed in *Clpp* KO compared to WT. Those are the proteins belonging to cytoplasmic ribosome and splicesome and interestingly, they are downregulated in *Clpp* KO. The cytoskeletal proteins related to cardiomyopathy were specifically seen upregulated in DKO_wb hearts.

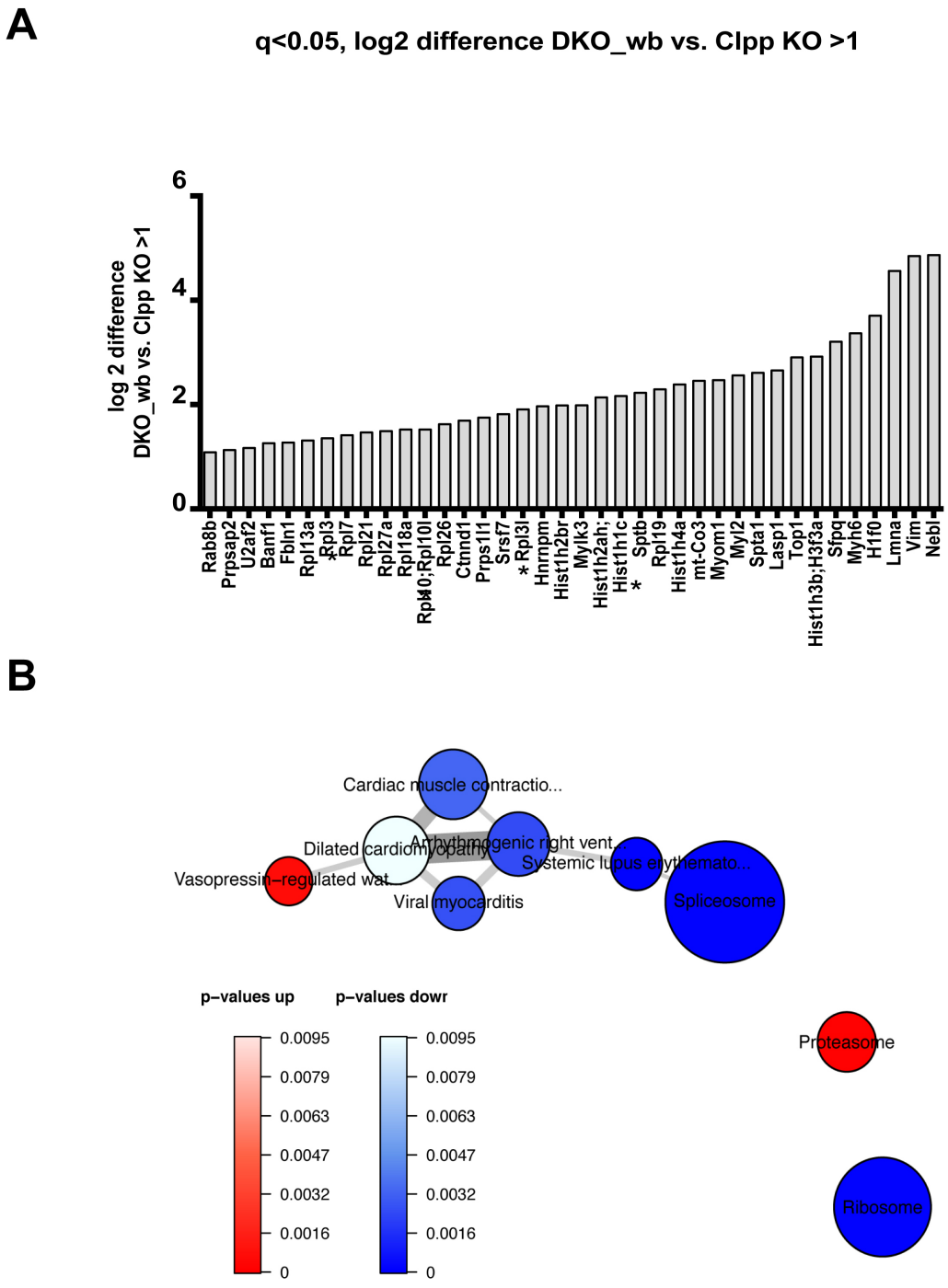


**Figure 3.35 Quantitative assessment and enrichment of upregulated proteins in the hearts of DKO_wb compared to *Clpp* KO.**

**(A)** Label-free quantification of heart proteomes showing proteins, which are up-regulated in the DKO_wb when compared to the *Clpp* KO mice. **(B)** The panel representing KEGG enrichment analysis using Wilcoxon statistical test.

On the other hand, 13 proteins were shown to be downregulated in DKO_wb compared to *Clpp* KO hearts (Figure 3.36A). Those are mostly involved in different metabolic pathways (Figure 3.36B), but it is difficult to claim the significance of certain pathways obtained from Enrichr analysis, since the number of differentially regulated proteins was very low. Further analysis using Reactome Pathway Database showed the involvement of those downregulated proteins in fructose metabolism, fatty acyl- CoA biosynthesis, negative regulation of MAPK pathway and tRNA modification in nucleus and cytosol, among many others.

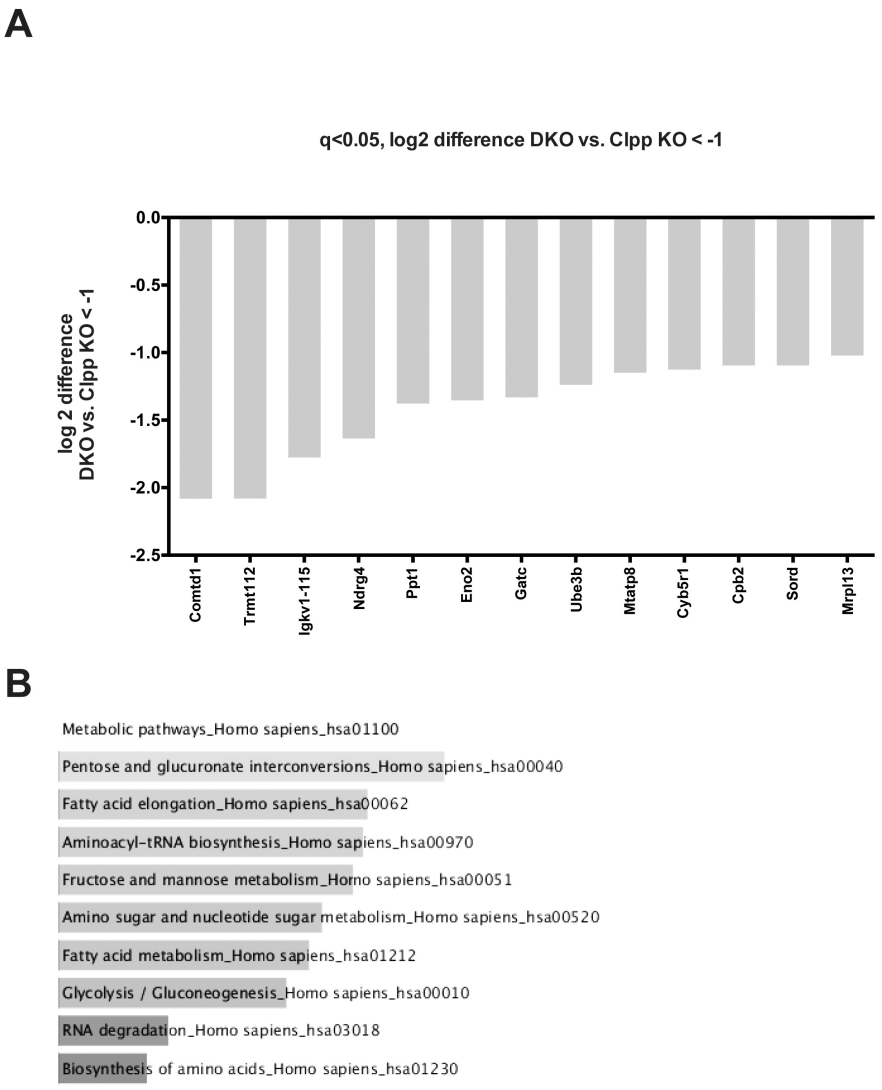


**Figure 3.36 Quantitative assessment of proteins downregulated in hearts of DKO_wb compared to *Clpp* KO.**

**(A)** Label-free quantification of heart proteomes showing proteins, which are down-regulated in the DKO_wb when compared to the *Clpp* KO mice. **(B)** Most upregulated pathways in Wiki Pathways Database.

In the end, the changes seen in a single full-body *Fgf21* KO were compared to control mice (Figure 3.37A-B).


**Figure 3.37 Quantitative assessment of KEGG enrichment pathways changed in *Fgf21* KO hearts.**

Most upregulated **(A)** and downregulated **(B)** pathways in FGF21 KO hearts using KEGG Pathways Database.

Most of the significantly changed proteins in *Fgf21* KO are downregulated. 5 mitochondrial proteins are strongly downregulated in the absence of FGF21. NNT or mitochondrial NAD(P) transhydroganese is the most severely affected enzyme and it is involved in transhydrogenation of NAD and NADP. Also, it functions as a proton pump and it may play a role in ROS detoxification (Murphy, 2015). Another 2 severely downregulated proteins are aminotrasferases, ABAT and GPT2. The former is 4-aminobutyrate and the latter is alanine aminotransferase. Also, mitochondrial 5(3)-deoxyribonucleotidase was shown to be

downregulated, followed by mitochondrial 39S ribosomal protein (Figure 3.37). These data show that FGF21 loss in *Clpp* KO mice does have an effect and possibly worsens the cardiac health, even though the changes are still not visible. On the other hand, the lack of FGF21 alone induces changes in mitochondria. Further analyses of the older mice would be necessary to see if the heart of these mice is getting impaired.

### 3.13. FGF21 loss in *Clpp* KO mice leads to the whitening phenotype.

Morphological analysis of BAT showed that the loss of FGF21 leads to the whitening phenotype, increasing the size and number of white unilocular adipocytes. This is even more evident in DKO_wb when compared to single *Fgf21* KO mice. *Clpp* KO mice were more abundant in paucilocular adipocytes (Figure 3.38A).

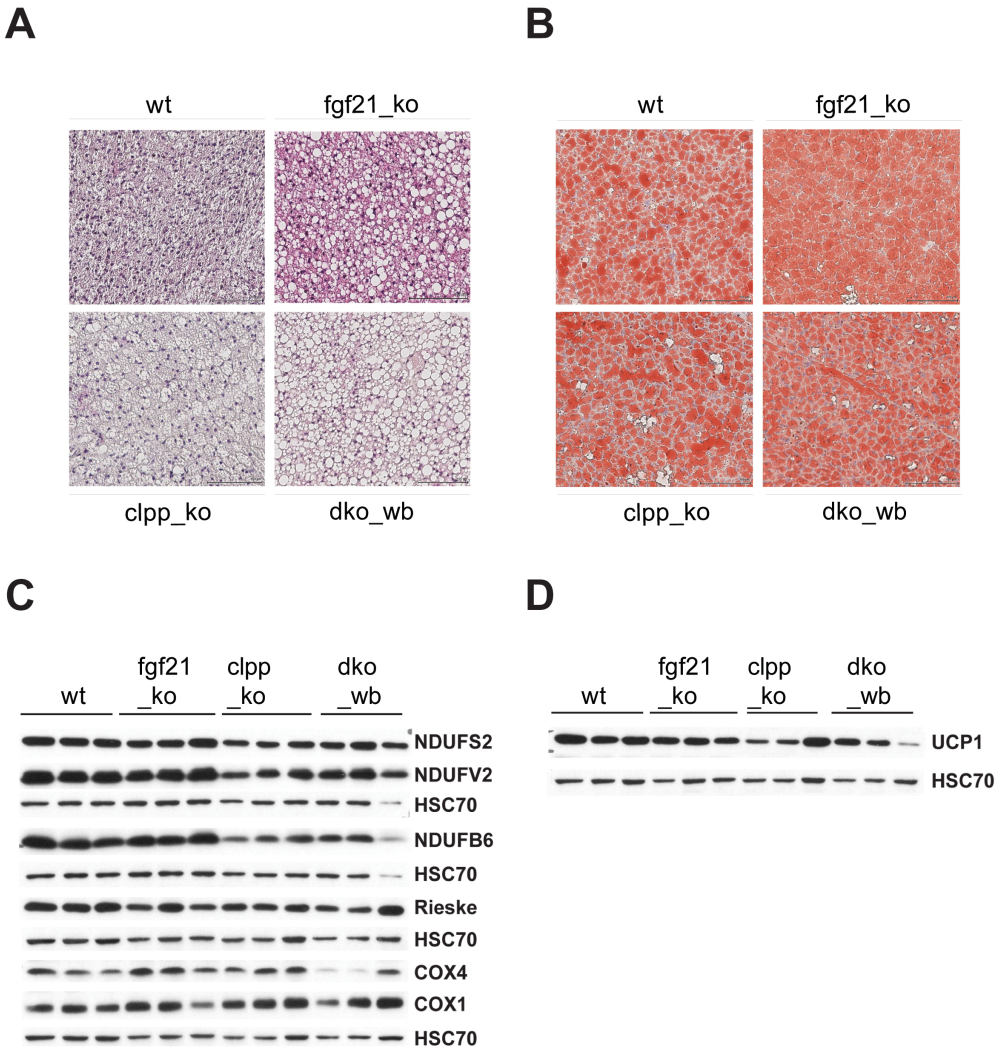


**Figure 3.38 The loss of FGF21 in *Clpp* KO BAT leads to the loss of UCP1 protein and whitening phenotype.**

**(A)** H&E staining on cryosections from BAT of 16-week-old mice (n=3). **(B)** Oil-red O staining on BAT cryosections (n=3); (Scale bar=100 μm). **(C)** Western blot analyses of indicated mitochondrial complex I subunits and **(D)** UCP1 protein.

Oil-Red staining was used to detect lipid content in BAT and *Fgf21* KO showed apparent lipid increase, but surprisingly DKO_wb lipid content seemed lower (Figure 3.38B) when compared to the morphology of adipocytes (Figure 3.38A). To further access the role of

FGF21, OXPHOS analysis in BAT was performed. Steady-state levels of NDUFS2, NDUFV2 and NDUFB6 showed visible decrease in their levels in the CLPP-dependent manner, while on the other hand, CIII and CIV subunits remain unchanged (Figure 3.38C). Apart from the mitochondrial respiration, BAT is engaged in producing heat with the help of UCP1, which uncouples respiratory chain and ATP production. Therefore, UCP1 levels were measured and interestingly, no significant changes were observed (Figure 3.38D). It has been shown in our group that UCP1 levels are mildly downregulated in *Clpp* KO female mice, and not affected in males. When exposed to cold, both male and female mice were affected and showed deranged thermogenesis capacity. Moreover, it was claimed that FGF21 induces thermogenic capacity of BAT (Wall et al., 2015). Together, these data show that loss of FGF21 worsens browning phenotype by increasing the lipid content, but it does not affect mitochondrial dysfunction seen in *Clpp* KO mice.

Upon histological analyses of different fat depots, it has been observed that both iWAT (subcutaneous) and eWAT (visceral) are not going through the browning process when FGF21 is absent (Figure 3.39A-B). The browning is taking place only in *Clpp* KO white depots, and more extensively in iWAT (Figure 3.39B). This result was not foreseen, since the previous data showed more intensive browning phenotype in eWAT (Becker et al., 2018).

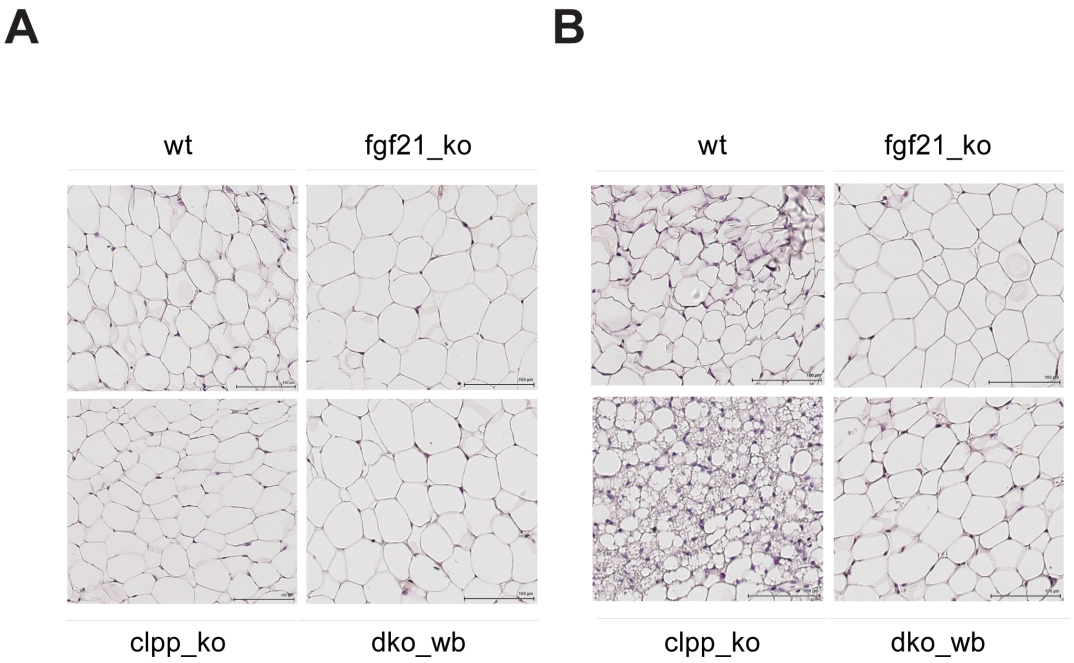


**Figure 3.39 The loss of FGF21 induces whitening of both eWAT and iWAT.**

H&E staining on cryosections from eWAT **(A)** and iWAT **(B)** of 16-week-old mice (n=3) ; (Scale bar=100 μm).

In summary, browning observed in *Clpp* KO mice is inhibited when FGF21 is absent and this is not relient on UCP1 levels.

# 4. Discussion

The multifaceted mitochondria have always been of a great interest for different research areas. The knowledge of mitochondrial physiology has dramatically increased in the last decade and many new aspects of this organelle are being investigated. Mitochondria are prone to damage, that could come from mtDNA defects, oxidative stress or different functional or morphological alternations. Mitochondria dysfunction leads to many different types of diseases, such as neurodegenerative disorders, metabolic diseases, cancer etc. An interesting question left unanswered is how mitochondria dealwith different sources of stress and which mechanisms are activated in different tissues.

In recent years, FGF21 got a lot of attention in metabolism research and not so much later, its relation to mitochondrial diseases and ageing has been observed. FGF21 can function in an endocrine manner and it has been shown to elicit diverse aspects of the adaptive starvation response. The main functions asigned to this cytokine are improvement of insulin sensitivity, increases in hepatic fatty acid oxidation, blocking of somatic growth, increasing glucose uptake in adipocytes etc. (Fisher & Maratos-Flier, 2016) However, its upregulated expression was observed recently in different mouse models with mitochondrial dysfunction (Dogan et al., 2014b; Tyynismaa et al., 2010). Correspondingly, in DARS2 heart and skeletal muscle deficient mice, which are featured with the activated mitochondrial stress responses due to impaired OXPHOS, we observed an immense 250- fold *Fgf21* upregulation in heart (Dogan et al., 2014a). Besides, in CLPP deficient mice, which are mirroring the mild mitochondrial dysfunction phenotype, we observed around 20-fold increase in cardiac *Fgf21* expression (Becker et al., 2018)

We created different double-deficent mouse models in order to investigate the role of FGF21 in mild and severe mitochondrial dysfunction, as well as its cell-autonomous and non-cell-autonomous effects on different tissues. The mouse model lacking DARS2 and FGF21 only in heart and skeletal muscle aimed to investigate the autocrine effects of FGF21 in cardiomyocytes, whereas another model, which in oppposite lacks FGF21 in the whole body, was created to answer the question if endocrine FGF21 serves the role in failing heart. The *Dars2* KO model is displayed with severe mitochondrial dysfunction and the lifespan of these mice is strikingly shortened. Finally, we wanted to investigate the role of FGF21 in mild mitochondrial dysfunction and therefore we created the full-body deficient CLPP mice, lacking FGF21 in the same manner.

## 4.1 Autocrine role of FGF21 in DARS2-deficient cardiomyocytes is expendable.

The cardiac *Fgf21* expression upregulation was observed already at 1 week of age in DARS2 KO mice and raised up to 250 fold, prior to death at 7-8 weeks of age. Moreover, its upregulation was present even before the other stress responses were activated in this mouse model. Increased proteostatic response and $UPR^{mt}$ were observed at 3 weeks of age, which was prior to OXPHOS deficiency (Dogan et al., 2014a). Together, those results led to the conclusion that something different than OXPHOS impairment that causes the activation of all those stress responses in DARS2-deficient cardiomyocytes and FGF21 appeared as a plausible candidate to investigate. Additionally, *Fgf21* expression levels were not increased in other tissues. However, we detected an increase in serum and speculated that this increase reflects the upregulation of *Fgf21* in heart (Dogan et al., 2014a).

In this study, first we generated a mouse model which lacks both DARS2 and FGF21 in heart and skeletal muscle. Surprisingly, there were no differences in gross phenotype nor lifespan of the DKO mice, compared to Dars2 KO. Heart to body weight ratio stayed unchanged with the loss of FGF21, as well as cardiomyopathy markers (Section 3.1). Those first results suggested that there might be some compensatory mechanism taking over in the absence of FGF21. Therefore the levels of another well known cardiomyokine –GDF15, were accesed. GDF15 was shown to be induced during heart failure and it may influence different processes in cardiac remodeling (Wollert & Kempf, 2012). Moreover, the blood levels of GDF15 might reflect mitochondrial dysfunction, and thus it could be used as a biomarker for mitochondrial diseases (Fujita, Taniguchi, Shinkai, Tanaka, & Ito, 2016). Interestingly, its expression upregulation is very often following the increase in *Fgf21* expression (Khan et al., 2017; Tezze et al., 2017). Furthermore, GDF15 was detected as a cell-non-autonomous myomitokine which regulates systemic energy homeostasis in a mouse model lacking a protein of the large mitoribosomal subunit in skeletal muscle (Chung et al., 2017). This is in line with the results from the Deletor mouse, where FGF21 was assigned a role of a myomitokine that is capable of improving the overall metabolic state (Tyynismaa et al., 2010). However, the heart protein levels of GDF15 were not changed in any of the genotypes in our tissue-specific knockouts. On the other hand, its expression level was immensly upregulated at a very early stage (2 weeks), but not the protein levels (unpublished data from S. Kaspar).

In DARS2-deficient hearts we observed the activation of mitochondrial stress responses, such as increased mito-biogenesis, activation of $UPR^{mt}$, increased mitochondrial proteases and decrease in autophagy (Dogan et al., 2014b). Remarkably, primary changes reflected in the levels of proteases and the other stress responses followed at the later stage. When FGF21 is absent, none of these stress responses is additionally affected. Even though its expression is already increased at 1 week of age, autocrine FGF21 seems not to be a mediator of previously mentioned stress responses seen in DARS2 –deficient hearts (Section 3.4). In conjunction with the increased *Fgf21* expression, transcription factors *Atf4* and *Atf5* were also increased in DARS2-deficient hearts. Those transcriptions factor were shown to be involved in an evolutionary conserved stress response pathway known as integrated stress response (ISR). There is a compelling evidence that *Fgf21* expression can be stimulated by ISR through the eIF2α/ATF4 axis. Several studies detected AARE – amino acid response elements – in the promoter of the *FGF21* gene (De Sousa-Coelho et al., 2012). This ISR induction of *Fgf21* helps in combating different cellular stresses, such as mitochondrial stress, ER stress, amino-acid deprivation stress etc. (Salminen et al., 2017). In our study, we observed increased eIF2α phosphorylation in both DARS2-deficient and DKO hearts. Interestingly, the non-phosphorylated form of eIF2α was decreased in DARS2-dependent manner, which was not reported before. Additionally, ATF4 protein levels were not affected by DARS2 nor FGF21 depletion, in spite of the increase in its mRNA levels in DARS2-deficient heart. This increase was significantly alleviated in DKO, confirming that ATF4 can induce FGF21, but obviously this did not influence the phenotype of already severely affected *Dars2* KO mice. Furthermore, it has been shown that ISR induces several survivial mechanisms, such as autophagy (B'Chir et al., 2013). In our study, we observed a decrease in autophagy in DARS2-deficient hearts, by following markers such as BECLIN-1, conversion of LC3-I to LC3-II and p62. The loss of FGF21 did not affect the status of autophagy. Curiously, it has been demonstrated that loss of *Atg7* in skeletal muscle, which is an important constituent of autophagy machinery, induced mitochondrial dysfunction and concomitant *Fgf21* expression through the eIF2α/ATF4 axis (Keipert et al., 2014). As mentioned before, eIF2α reduces the cytoplasmic translation and preferentially induces mRNA which contains short upstream open reading frames (uORF). In *Dars2* KO mice, CHOP-10 is one of the first transcription factors which is upregulated at a very early stage (Dogan et al., 2014). It has been shown that in the case when ATF4 is not able to restore proteostatic control, CHOP10 is induced, which switches the cell to a terminal outcome (Teske et al., 2013). This is in line with our findings in DARS2 KO hearts, where *Chop-10* expression levels are exceeding *Atf4*

with time and this immense upregulation is in agreement with the severity of the phenotype observed in DARS2-deficient mice. However, FGF21 depletion did not affect the levels of CHOP10 in *Dars2* KO hearts.

The AARE response also induces the expression of methylene tetrahydrofolate dehydrogenase 2 (MTHFD2), which is important for the mitochondrial folate cycle, as a rate-limiting enzyme. It has been reported in Deletor mice that induction of MTHFD2 is associated with abberant nucleotide synthesis, imbalanced dNTP pools and the induction of serine and gluthathione synthesis. The one-carbon (1C) metabolism is a metabolic pathway, which is essential to most cell types and organisms. It provides 1C-units to major anabolic cellular pathways: nucleotide synthesis, methylation reactions and mitochondrial translation initiation. (Nikkanen et al., 2016). The mitochondrial folate metabolism is of great importance for mitochondrial translation. It uses THF and 1C-donors serine, glycine or sarcosine as inputs and produces fMet for mitochondrial translation initiation, NADPH and formate (Fan et al., 2014). In recent studies it was reported that mitochondrial DNA depletion triggers, via the transcription factor ATF4, expression of serine synthesis genes – *PHGHD*, *PSAT1*, and *PSPH* - thereby increasing 1C-metabolism (Bao et al., 2016). In our study, we observed a robust upregulation in protein levels of MTHFD2 in DARS2-deficient and DKO hearts, already at 3 weeks of age and persisting till 6 weeks of age, when the animals were dying. Moreover, expression levels of *Psat1* and *Phghd* were around 20-fold increased in DARS2-dependent manner, while the FGF21 depletion did not have any influence on folate and serine metabolism, even though *Atf4* expression was alleviated in DKO hearts. In a recent follow-up of the Deletor mouse study, it has been observed that the main manifestations of mitochondrial myopathy, such as induction of GDF15 and FGF21, $UPR^{mt}$ and imbalances in 1-C metabolism, are all part of skeletal muscle ISR which is controlled by mTORC1 (Khan et al., 2017). It is interesting to note that in this case mTORC1 is an upstream regulator of FGF21, however, there are many studies showing tissue-specific effects of FGF21 being upstream of mTORC1. It has been reported that FGF21 activates mTORC1 in adipocytes through MAPK signaling and it led to surprisingly beneficial metabolic effects, such as increased glucose uptake and improved insulin sensitivity, increased adiponectin secretion and induction of UCP1 (Minard et al., 2016). Nevertheless, administration of FGF21 in mice inhibits mTORC1 in the liver, and improves insulin sensitivity of hepatocytes (Gong et al., 2016). In an earlier study, it has been shown that mice overexpressing FGF21 have extended lifespan up to 40%. Remarkably, this was due to the blunting of GH/IGF-1 signaling, which FGF21 is exerting through the control of STAT5, independently of mTORC1 (Y. Zhang et al.,

2012). In our study, we observed a strong upregulation of *Igf-1* expression in DARS2-deficient hearts, which was intensified in DKO. Binding of insulin-growth-factor 1 to its receptor leads to phosphorylation of Akt1, which further phosphorylates PRAS40 that relieves inhibition of mTORC1 (H. Wang et al., 2012). mTORC1 boosts protein synthesis by phosphorylating the eukaryotic initiation factor 4E (eIF4E)-binding protein 1 (4E-BP1) and the p70 ribosomal S6 kinase 1 (S6K1). Those proteins are also used as read-outs for mTORC1 activation. Our results showed that both phosphorylation of PRAS40 and 4E-BP1 are increased in DARS2-deficient hearts and not affected by the loss of autocrine FGF21. These data suggest that FGF21 in cardiomyocytes is not implicated in the control of mTORC1.

Taken together, the presented data indicate that all mitochondrial and cellular stress responses seen activated in DARS2-deficient hearts are not affected by the endogenous loss of FGF21. On one hand, increased mitochondrial biogenesis, proteostasis, $UPR^{mt}$, decreased autophagy and on the other hand, imbalanced one-carbon metabolism, serine synthesis, FAO and glucose metabolism, are all disrupted to the same extent in DARS2-deficient and DKO hearts (Sections 3.4 and 3.5). The loss of FGF21 alone does not differ from the WT phenotype. Overall, these data show that autocrine FGF21 is dispensable in *Dars2* KO heart pathology. However, we wanted to further look into non-cell-autonomous effects of cardiac FGF21 loss in DARS2 deficient animals.

## 4.2 Cell non-autonomous effects of DARS2 depletion in cardiomyocytes are not dependent on FGF21.

The endocrine action of FGF21 is not a typical hormonal response, since its induction was confirmed in many different tissues. Moreover, it can be secreted from one organ, and have effects on distant others. One demonstration of this communication between distal tissues was done in *C. elegans,* where $UPR^{mt}$ that was induced in the nervous system generated the same stress response in intestine (Durieux et al., 2012). Another example comes from *Drosphila* study where the AMPK-induced autophagy in brain promoted intestinal autophagy in a cell non-autonomous manner (Ulgherait, Rana, Rera, Graniel, & Walker, 2014). FGF21 has some of the properties needed for a cell non-autonomous mediator. It is secreted during stress and can improve metabolic homeostasis of the whole organism by communicating with the other tissues. It has been shown that during heart ischemia FGF21 is secreted from liver and adipose tissue with the aim to alleviate myocardial injury and help the recovery of the heart (S. Q. Liu et al., 2013). There is currently a lot of evidence on how skeletal muscle FGF21 secretion improves whole body metabolism by influencing adipose tissue (Kim et al., 2013; Miyake et al., 2016). In the case of the Deletor mouse, FGF21 secreted from skeletal muscles leads to widespread changes in lipid metabolism, such as low fat content in the liver, with resistance to high-fat diet and smaller adipocyte size (Tyynismaa et al., 2010). However, Deletor mice lack TWINKLE in the whole-body and therefore it is not clear if these changes in metabolism come from an underlying mitochondrial dysfunction in all tissues. In our study, we analyzed the cell non-autonomous effects on the liver and adipose tissue. The overall liver phenotype was not changed – OXPHOS was not affected by the loss of DARS2 in heart, nor by the additional depletion of FGF21. Proteases AFG3L2, SPG7, CLPP, LONP1 stayed unchanged as well as ATF4 and MTHFD2 protein levels. Generally, liver morphology looked unchanged when all of the mouse models were compared to WT. Label-free proteome profiling showed no significant differences when different genotypes were compared to WT livers. Interestingly, liver *Pgc1α* expression levels were approximately 5-fold increased in both DARS2 and DKO mice. This could be assigned to a metabolic stress response, since liver is the main metabolic tissue and it is probably trying to compensate for the general energy deprivation observed in DARS2 KO mice. Moreover, *Atf4* expression was slightly increased in DARS2 KO, but both PGC1α and ATF4 protein levels were unchanged (Section 3.6). It is important to highlight that liver is the major tissue for FGF21 expression and in order to prevent a feedback effect of the autocrine FGF21, it does not express FGFR1. However, KLB – the co-receptor is still expressed, because other endocrine FGFs can use it

for its effects. Interestingly, we observed increased expression of *Klb* in the liver, while *Fgf21* was not significantly changed. Furthermore, expression of fatty-acid translocators - *Pparγ* and *Cd36,* were increased in DARS2 KO and DKO mice. This suggests that the demand for transferring FFAs from the blood into the liver is increased, which is consistent with the previously observed increase in serum FFA in DARS2 KO mice.

Autophagy deficiency in skeletal muscle induces mitochondrial dysfunction, which results in expression of *Fgf21* through ATF4. FGF21 is secreted from the skeletal muscle and has beneficial effects such as increasing insulin sensitivity and protecting from diet-induced obesity, with increased FAO and browning of WAT (Kim et al., 2013). The mouse model lacking tuberous sclerosis complex 1 (TSC1) in skeletal muscle, which causes constitutive activation of mTORC1 and enhances protein synthesis, also induces FGF21 secretion from skeletal muscle and improves overall systemic metabolism. This again shows that FGF21 is a stress-induced mitokine, in this case induced by endoplasmatic reticulum (ER) stress, through the PERK/eIF2α/ATF4 axis (Guridi et al., 2015). On the other hand, TFAM deletion has tissue-specific consequences. Its deletion in pancreas leads to impaired mitochondria and glucose intolerance (Silva et al., 2000), while a skeletal-muscle-specific TFAM depletion leads to improved glucose tolerance (Wredenberg et al., 2006). Moreover, TFAM deletion in adipose tissue leads to increased mitochondrial oxidation in fat and positive metabolic effects, despite an increased oxidative stress. These mice are protected from age- and diet- induced obesity, they have improved glucose and insulin function and higher energy expenditure (Vernochet et al., 2012).

In our heart and skeletal muscle specific DARS2 KO model we observed changes in both white and brown adipose tissue. BAT contains many mitochondria involved in FAO and it can express UCP1, which allows mitochondrial proton leak that leads to thermogenesis through energy expenditure (Ricquier, 2005). In previously mentioned models, where mitochondrial dysfunction was caused in skeletal muscle, BAT was featured with increased thermogenic capacity and upregulated *Ucp1* expression. However, we observed something different. First of all, the morphology of BAT showed increased lipid content in DARS2 KO mice and this was even more pronounced in DKO mice. Apart from that, UCP1 protein levels were barely detectable in both DARS2 KO and DKO mouse. These results confirmed the "whitening" of BAT, which is contrary to what has been shown before in relation to cardiomyopathy. Nevertheless, BAT "whitening" related to mitochondrial dysfunction has been reported. A Costeff syndrome model has a mutation in the mitochondrial membrane protein *Opa3* gene, which leads to mitochondrial fragmentation. These mice show a failure to

thrive and have a reduced body weight, due to disturbances in lipid metabolism. They observed enlargement of BAT, increased lipid content and decreased UCP1 levels (90%). This phenotype presentation resembles the one we saw in DARS2 KO mice. Intrinsically, in these mice lipid uptake is unimpeded, but there is impaired lipid utilization. Moreover, the browning of eWAT and decrease in its weight was observed, which was explained through subsided availability of FFA, that are now taken by BAT. Interestingly, UCP1 changes were not detected, despite the appearance of multilocular beige adipocytes (Wells et al., 2012). When we analyzed WAT, we observed the decrease in adipocyte size in *Dars2* KO and DKO mice, in both eWAT and iWAT. Moreover, *Ucp1* expression levels were downregulated in iWAT and stayed unchanged in eWAT (Section 3.7). It is important to emphasize that loss of FGF21 in heart and skeletal muscle does not influence the adipose tissue phenotype observed in DARS2 KO mice. Moreover, we checked the steady-state levels of OXPHOS subunits in BAT and they were not affected in any of the KOs. Besides, we investigated the levels of FAO enzymes, glucose transporters 1 and 4, mitochondrial stress markers in BAT and none of them was affected. These results are perplexing since we did not observe obvious signs of mitochondrial dysfunction in BAT, besides downregulation of UCP1. Interesting question here is what is causing this impairment in lipid usage and decrease in UCP1? Is it the immense increase of FFA observed in serum of the DARS2 KO mice? Is BAT trying to hamper the heat production and prevents energy waste in the mice that are already suffering energy deficiency? Those questions still have to be addressed.

### 4.3 What is happening downstream of FGF21 signaling and is there a compensation from exogenous factors?

In previously presented data, we have showed that endogenous FGF21 does not affect stress responses observed in DARS2 KO. Moreover, FGF21 in heart does not have cell non-autonomous effects on liver and adipose tissue. This led us to inspect what is happening downstream of FGF21 in heart. Until recently, it has been believed that FGF21 was not induced in heart. This was mainly because FGF21 is not detectable in heart under physiological conditions, but only under conditions of increased stress. This was demonstrated in a study where isproterenol was applied to induce cardiac injury in mice, and they observed how mice lacking FGF21 are withstanding the stress compared to WT animals. This study demonstrated that $FGF21^{-/-}$ mice have decreased FAO, increased inflammatory response and worsened cardiac hypertrophy, followed by apoptosis (Planavila et al., 2013). It

has been demonstrated that FGF21 can both be induced and target cardiac cells. The induction was shown to occur through PPARα/SIRT1 binding directly to the *Fgf21* promoter. The targeting of cardiac cells was taking effect through the FGFR1/KLB complex and concomitant ERK1/2 phosphorylation (Planavila et al., 2013). Interestingly, in our study induction of *Fgf21* under PPARα/SIRT1 control was not shown. On the contrary, we observed a downregulation of *Pparα* expression in both DARS2-deficient and DKO hearts, while *Sirt1* levels were mildly increased in DKO. Curiously, we saw an upregulation of KLB co-receptor protein levels in both *Dars2* KO and DKO hearts. This result suggests that there might be some compensation through exogenous factors (Section 3.9). KLB is expressed at low levels in heart, when compared to the other tissues. Nevertheless, skeletal muscle does not express KLB and therefore it is an organ that only contributes to the systemic FGF21 pool but cannot be targeted by it (Kilkenny & Rocheleau, 2016). What we showed earlier in *Dars2* KO mice is that immense upregulation of *Fgf21* expression is detected only in cardiomyocytes. Liver, skeletal muscle, pancreas, brown and white adipose tissue did not show any increase in this mitokine, therefore we concluded that the FGF21 serum level increase originates from a cardiac secretion (Dogan et al., 2014). This is a bit puzzling bearing in mind that in our DKO mice, we observed the KLB upregulation at the same extent as in the *Dars2* KO mice. How do we explain the FGF21 serum levels? When we measured serum levels of FGF21 in DKO mice, we saw a decrease in comparison to the *Dars2* KO mice, however it was not completely absent. Does even a small amount of FGF21 in blood can compensate for the absence of the endogenous one? Is it exogenous FGF21 or something else that is compensating for the absence of the autocrine one? In order to answer this question in a well-grounded manner, we created a new mouse model, DARS2-heart-and-skeletal muscle -specific KO, which is this time lacking FGF21 in whole body. The DKO mice showed no difference in phenotype compared to the DKO_fl. We checked activation of ERK1/2 through phosphorylation, which is a well-established signaling pathway of the FGF21/FGFR1/KLB axis and to our surprise, we saw that ERK1/2 activation occurred to the same extent in *Dars2* KO, DKO and DKO_fl hearts (section 3.10).

There are multiple possible hypotheses rising from the presented data. First of all, different kind of stresses might probably use different signaling pathways for their activation. Ischemia/reperfusion injury and severe mitochondrial dysfunction in heart might not both necessarily use only the ERK1/2 pathway for FGF21 induction. Secondly, the severe phenotype of DARS2-deficient mice might be overpowering any possible effect of FGF21 depletion, or more precisely, the saturation with stress responses is diminishing the role of

FGF21 in severe mitochondrial dysfunction. Thirdly, other endocrine fibroblast growth factors might be compensating for the lack of FGF21 and activating the same signaling pathways. Lastly, there might be some unknown factors, which are substituting FGF21. However, serum proteomics data did not yield enough comprehension on this possibility, since none of the growth factors nor other cardiomyokines were detected in the samples.

### 4.4 Loss of FGF21 in CLPP deficient mice leads to increased cardiomyopathy markers and cytoplasmic ribosomal proteins.

Next, we created a new mouse model to study the role of FGF21, with the idea that DARS2 depletion might be too severe for detecting changes caused by loss of FGF21. We used CLPP-deficient mice, which are featured with mild mitochondrial dysfunction, without any impact on longevity (Becker et al., 2018). CLPP deficient mice reproduce the Perrault syndrome clinical picture, seen in humans with mutations in this gene, which is displayed with reduced body weight and growth retardation, deafness and sterility (Jenkinson et al., 2013). Moreover, we detected around 20-fold upregulation of *Fgf21* expression in heart of *Clpp* KO mice. Therefore, we depleted FGF21 in the whole body in *Clpp* KO mice to study its role in mild mitochondrial dysfunction.

Recently, it has been shown that different kind of mitochondrial perturbations can induce FGF21 secretion from different tissues to serum (Dogan et al., 2014b; Tyynismaa et al., 2010; Vandanmagsar et al., 2016). In *Clpp* KO mice, serum levels of FGF21 are increased as well, and elevated *Fgf21* expression was observed in different tissues, correlating with the degree of mitochondrial dysfunction (Doctoral dissertation of C. Becker). In our study, we analyzed heart, liver, BAT and WAT of the CLPP/FGF21-double-deficient mice (DKO_wb), due to the previously observed *Fgf21* expression upregulation in those tissues in CLPP-deficient mice. No systemic metabolic adaptation of *Clpp* KO mice, such as reduced body weight and increased insulin sensitivity, were due to FGF21 (Section 3.13). In our DKO_wb mice, glucose and insulin tolerance test results followed the trend of CLPP-deficient mice.

Liver, as the main site of FGF21 production, showed no difference in mitochondrial complex and supercomplex levels between CLPP-deficient and DKO mice (Doctoral dissertation of C. Becker).

Next, we wanted to investigate the role of FGF21 in heart with mild mitochondrial dysfunction and compare it to the previously described models. From all the tissues tested in CLPP-deficient mice, the most immense upregulation of the *Fgf21* expression was detected in

heart, which correlates with the level of mitochondrial dysfunction (Doctoral dissertation of C. Becker). This could already suggest a tissue-specific importance of this mitokine. However, mitochondrial stress response markers were upregulated in CLPP-deficient mice and FGF21 depletion had no impact on it. Additionally, GDF15 levels were not changed in any of the genotypes, excluding a possible compensation of this cardiomyokine. Surprisingly, activation of ERK1/2 by phosphorylation was observed only in CLPP-deficient mice. FGF21 depletion completely ablated this activation, which is in contrary to the previously described results in DKO and DKO_fl mice. This result might point out that the FGF21-ERK1/2 signaling axis is the pathway of choice in mild mitochondrial dysfunction. There is not much data on the role of FGF21 in heart in association with mitochondrial disease. However, it has been shown previously that FGF21 protects heart from apoptosis in diabetic mouse models via the ERK1/2 signaling pathway (C. Zhang et al., 2015). ERK1/2 belongs to the family of mitogen-activated protein kinases (MAPKs) and it is able to phosphorylate a great number of different kinases and transcription factors to regulate cellular development, cell survival and death. Activation of ERK1/2 controls the regulation of meiosis, mitosis, and post-mitotic function, which are closely related to cell growth, cell proliferation, differentiation, migration, and survival and therefore this pathway is crucial in understanding cancer biology. The canonical MAPK pathway is activated by a process in which the growth factors, such as fibroblast growth factors (FGFs) and epidermal growth factors (EGFs), bind to the cell-surface receptors, mainly tyrosine kinase receptors (RTK), resulting in the dimerization and trans-phosphorylation of RTK (F. Liu, Yang, Geng, & Huang, 2018). Well-known intracellular targets of ERK1/2 include Elk-1, c-Fos, MSK-1, c-Myc, GATA4, Ets1/2, Mcl-1, Bcl-XL, IEX-1 etc. (Xu et al., 2016).

Our result suggests that severe mitochondrial dysfunction as seen in DARS2-deficient mice, might use alternative signaling pathways and skip the FGF21-ERK1/2 axis. On the other hand, in moderate mitochondrial deficiency, ERK1/2 might be the pathway of choice for FGF21. But the question still remains – what are the effects of this FGF21-ERK1/2 activation?

Label-free quantification of the whole proteome in heart showed significant upregulation of sarcomeric proteins in DKO. Cardiac muscle as well as skeletal muscle consists of sarcomeres, which are built of thick and thin filaments, comprised of myosin and actin respectively. Those proteins and the ones spanning between filaments, such as vimentin, myomiosin and nebulin, are very important for cardiac contractility (Martonosi, 2000). This increase in contractile proteins in cardiac pathology is in the line with previous research on

skeletal musle myopathies, where the accumulation of those proteins was also observed on proteomics data (Maerkens et al., 2016). Interestingly, we also detected a large number of histone proteins being upregulated in DKO, which might suggest changes in chromatin structure. Changes in chromatin structure are known to alter transcriptional programs of cells and this was already shown to be the case in adult-onset cardiomyopathies, where the transcriptional reprogramming led to hyper-contractility followed by heart failure (Mahmoud & Poizat, 2013). However, we could not observe other signs of failing heart in our DKO mice, which were analyzed at 16 weeks. Therefore, analysis of older animals might reveal if the cardiomyopathy is in development. Another puzzling result obtained from the whole proteome data is a confident upregulation of the cytoplasmic 60S ribosomal proteins in DKO mice. The ribosome has historically been considered to have no cell-specific functions, but rather serving a "housekeeping" role. Yet, there are novel data in literature pointing out on non-canonical roles of ribosomal proteins. In one study, it has been shown that the 60S ribosomal protein L13a is a molecular switch for translational silencing of a gene that might be involved in oxidative damage and is a risk for cardiovascular diseases. Moreover, they have demonstrated that L13a protein can bind 3'UTR element and act as a regulatory protein of translation (Mazumder et al., 2003). For instance, RPL26, that we detected in our proteomics data, was shown to trigger cell-death by binding the 5'UTR of *p53* gene (Takagi, Absalon, McLure, & Kastan, 2005). Furthermore, RPL3L, also seen in our data, was shown to be a negative regulator of striated muscle growth (Chaillou, Zhang, & McCarthy, 2016). The roles of individual RPs are difficult to predict, and the question is if the increase in 60S ribosomal proteins specifically represent a new stress response. Not so much is known about this, but there are some data showing a consistent dysregulation of individual RPs in different diseases (Guimaraes & Zavolan, 2016). Moreover, our phospho-proteomics data show upregulation of ribosomal proteins in DKO compared to DARS2-deficient mice. Further studies are needed to investigate if there is a functional connection between FGF21 and changes observed in the proteomics data.

One of the first identified actions of FGF21 was its ability to increase thermogenesis via UCP1 induction and expression of other thermogenesis genes in BAT. Moreover, it has been shown that cold exposure induced BAT *Fgf21* expression through beta-adrenergic signaling that further induced activating transcription factor 2 (ATF2) (Hondares et al., 2011). This regulation of non-shivering thermogenesis by FGF21 was not limited only to BAT, but it also involved iWAT and eWAT, where appearance of Ucp1-expressing multilocular brown-like adipocytes was detected (Fisher et al., 2012). Interestingly, in CLPP-deficient mice we

observed increased fat depots in BAT, which was exacerbated with the loss of FGF21. However, we have not observed changes in UCP1 levels, despite the dissociation of lipid storage from lipid use, contrary to the DARS2/FGF21 model. Previously reported data from our lab showed decreased UCP1 levels in female *Clpp* KO mice upon cold exposure (Becker et al., 2018). Furthermore, we observed a browning phenotype in iWAT and eWAT of CLPP-deficient mice. eWAT was presented with a decrease in adipocyte size in CLPP-deficient mice, which was abrogated by the FGF21 loss. On the other hand, iWAT was featured with the appearance of brown-like adipocytes, but this effect was also diminished with the loss of FGF21. This cytokine is also required for physiological adaptations during cold exposure, where it has been shown to stabilize protein levels of PGC-1α in order to exert its effects (Fisher et al., 2012). However, a very recent work has demonstrated that cold-induced browning of iWAT was not dependent on FGF21. RNA sequencing revealed major changes in UCP1 - deficient BAT and iWAT, but the loss of FGF21 had no effects at all (Keipert et al., 2017). In conclusion, FGF21 release from BAT of UCP1 - deficient mice is probably a compensatory mechanism. Additionally, transcriptional profiling in *Ucp1* KO iWAT showed a selective increase in the *Pm20d1* gene, which codes for an enzyme that has been suggested to be involved in n-acyl amino acids generation, which were earlier proposed to be endogenous uncouplers (Keipert et al., 2017; Long et al., 2016). However, these alternative thermogenic mechanisms require more in-depth investigations using mouse models.

In our mouse models, the loss of FGF21 exacerbates the whitening phenotype, but this is not in relation with UCP1 levels. Further analyses of the transcriptome and proteome are needed in order to look for potential alternative mechanisms of the whitening.

### 4.5 Integrated whole proteome data show FGF21-dependent changes.

All three mouse models showed that FGF21 has no effect on the gross phenotype of the mice. However, some changes on the molecular level were detected. Starting with the DKO_wb mice, whole proteome data revealed significant influence of FGF21 on cardiomyopathy markers, ribosomal stress and structural components of chromatin. This does imply that FGF21 might have a role in cardiac stress, but the mechanisms are still up to be elucidated. Interestingly, the most prominent change in the whole proteome data from heart related to FGF21 loss is a severe decrease of the mitochondrial NAD(P)-transhydrogenase, (NNT) in both FGF21 and DKO_wb. In comparison, data from DKO mice showed the NNT downregulation in single *Fgf21* KO, but to lesser extent. This might be due to the age difference, since the mice lacking DARS2 were analyzed at 6 weeks and *Clpp* KO mice at 16 weeks. Curiously, we have not observed this change in tissue-specific *Fgf21* KO. NNT is an inner mitochondrial membrane integral protein and it uses the proton motive force generated by the ETC to catalyze the transfer of hydride ($H^-$) between NAD(H) and NADP(+) . Under physiological conditions, NNT uses energy from the mitochondrial proton gradient to produce NADPH, which is used for the TCA intermediates replenishment and in free radical detoxification (Ciccarese & Ciminale, 2017). Silencing of this enzyme in cells showed increased sensitivity to oxidative stress (Yin, Sancheti, & Cadenas, 2012). Reduced NNT activity is responsible for diminished insulin secretion and impairment in glucose metabolism in C57BL/6J mice that have a naturally occurring in-frame five-exon deletion in Nnt that removes exons 7-11 (Freeman, Hugill, Dear, Ashcroft, & Cox, 2006). However, we used C57BL/6N strain in our study, which has a wild-type version of *Nnt*. Curiously, it has been reported that in situations of pathological cardiac workload, NNT can reverse its function and oxidize NADPH to regenerate NADH for ATP, at the cost of an antioxidative capacity. This reverse mode of NNT increases ROS emission and leads to maladaptive heart remodeling (Nickel et al., 2015).

*Gpt2* codes for a mitochondrial alanine aminotransferase, that catalyzes the transamination reaction in the glucose-alanine cycle, which exports amino acid catabolites from muscle to the urea cycle. We detected downregulation of this enzyme in our 16-week-old *Fgf21* KO, but not the 6-week-old mice. Interestingly, elevated plasma alanine was reported to be a biomarker of pediatric mitochondrial diseases (Shatla et al., 2014). On the other hand, GPT2 was more than 4-fold-increased in CLPP-deficient hearts, which was balanced out in DKO_wb. Another mitochondrial enzyme decreased in *Fgf21* KO is pyruvate dehydrogenase kinase isoform 4 (PDK4), which is phosphorylating and inhibiting pyruvate

dehydrogenase and thereby reduces the capacity for glucose oxidation (Chambers et al., 2011). It is known from literature that both *Fgf21* and *Pdk4* are targets of hepatic PPARα (Vernia et al., 2014) and that administration of FGF21 in hepatocytes induces PDK4 levels, which is in line with previous findings that FGF21 improves FAO (Samms et al., 2015). A mitochondrial protein affected by FGF21 depletion in CLPP-deficient mice is NADH-cytochrome b5 reductase 1 (CYB5R1). This enzyme is involved in desaturation and elongation of fatty acids, cholesterol biosynthesis, and, in erythrocytes, methemoglobin reduction (Plitzko et al., 2016). Moreover, *Cyb5r1* was shown to be a target of ATF4 and MYC in mouse hearts with mitochondrial dysfunction (Kuhl et al., 2017). In this interesting study, they compared several mouse models with mitochondrial dysfunction in heart, differing in severity and onset of the phenotype. Strikingly, ALDH18A1 - the first enzyme in glutamate to proline conversion pathway, was among the most upregulated proteins in almost all the knockouts (Kuhl et al., 2017). Our study has shown that this enzyme was immensely upregulated in DARS2-deficient hearts, but the loss of FGF21 did not have any effect on it. Moreover, ALDH18A1 was increased in CLPP-deficient hearts to a much lesser extent, and also not influenced by the FGF21 depletion. Moreover, enzymes of one-carbon metabolism were shown to be among the most upregulated proteins in all of our models, but FGF21 also has no influence on their levels. However, phospho-proteomics data from DARS2 and DKO_fl mice showed that purine metabolism pathways, which are tightly regulated by one-carbon metabolism, were enriched in the latter. Furthermore, the enrichment of the phospho-proteome also showed upregulation of PPARα signaling in both whole-body and tissue-specific DKO. In DARS2-deficient mice lacking FGF21 in whole body, alanine, aspartate and glutamate metabolism pathways were upregulated. Notably, the importance of glutamate got a lot of attention lately and it was demonstrated that glutamine-glutamate influx into mitochondria delivers α-ketoglutarate to the TCA cycle for the generation of high-energy molecules such as NADH and $FADH_2$. The oxidation of α-ketoglutarate is an OXPHOS-independent energy-generating pathway offering a potentially significant source of ATP in mtDNA mutant cells (Q. Chen et al., 2018).

It is very challenging to draw a conclusion about the role of FGF21 from the integrated proteomics data obtained from different mouse models representing mild and severe mitochondrial dysfunction. It might be that FGF21 is associated with modulation of how energy is being used in the time of stress, but it is not a crucial mediator of these stress responses seen in mitochondrial dysfunction. Potentially, FGF21 might be important for ROS regulation and its function in signaling through NNT. Further functional analyses of NNT,

PDK4 and different aminotransferases are needed to answer if those changes were specifically FGF21-dependent. Metabolomics data would yield additional clues on whole-body metabolism, especially the amino-acid content and preferentially used energy sources in the time of mitochondrial stress of different severity.

## 4.6 Summary

Our results demonstrate that FGF21 depletion in mouse models with either mild or severe mitochondrial dysfunction does not change the gross phenotype of the mice. However, our proteomics data showed changes in cardiomyopathy markers with FGF21 depletion in CLPP-deficient mice, which are featured with mild complex I deficiency and a leaner phenotype. Moreover, the enzymes involved in glucose/fatty-acid/amino-acids metabolism, such as NNT, PDK4 and GPT2 showed immense decrease in 16-week-old whole-body *Fgf21* KO mice. Furthermore, the ERK1/2 signaling axis is abrogated with the loss of FGF21 in *Clpp* KO mice, while in the model of severe cardiomyopathy induced by DARS2 depletion, ERK1/2 cascade is active even in the absence of FGF21, suggesting alternative compensatory pathways. This result proposes a more relevant role of this cytokine in late-onset mitochondrial diseases and its expression might be dose-dependent, mirroring the level of stress.

This research is contributing to the general knowledge of FGF21 in mitochondrial disease and cardiomyopathy, and to our knowledge, it is the first study where FGF21 was depleted in different mouse models of mitochondrial dysfunction to access its cardiac role.

# Bibliography


Alberts, B., Bray, D., Lewis, J., Raff, M., Roberts, K., & Watson, J.D. (1983). *Molecular biology of the cell*. New York & London: Garland Publishing Inc.

Almajan, E. R., Richter, R., Paeger, L., Martinelli, P., Barth, E., Decker, T., . . . Rugarli, E. I. (2012). AFG3L2 supports mitochondrial protein synthesis and Purkinje cell survival. *J Clin Invest, 122*(11), 4048-4058. doi: 10.1172/JCI64604

Ameri, K., & Harris, A. L. (2008). Activating transcription factor 4. *Int J Biochem Cell Biol, 40*(1), 14-21. doi: 10.1016/j.biocel.2007.01.020

Anderson, S., Bankier, A. T., Barrell, B. G., de Bruijn, M. H., Coulson, A. R., Drouin, J., . . . Young, I. G. (1981). Sequence and organization of the human mitochondrial genome. *Nature, 290*(5806), 457-465.

Aradjanski, M., Dogan, S. A., Lotter, S., Wang, S., Hermans, S., Wibom, R., . . . Trifunovic, A. (2017). DARS2 protects against neuroinflammation and apoptotic neuronal loss, but is dispensable for myelin producing cells. *Hum Mol Genet, 26*(21), 4181-4189. doi: 10.1093/hmg/ddx307

Arnould, T., Michel, S., & Renard, P. (2015). Mitochondria Retrograde Signaling and the UPR mt: Where Are We in Mammals? *Int J Mol Sci, 16*(8), 18224-18251. doi: 10.3390/ijms160818224

B'Chir, W., Maurin, A. C., Carraro, V., Averous, J., Jousse, C., Muranishi, Y., . . . Bruhat, A. (2013). The eIF2alpha/ATF4 pathway is essential for stress-induced autophagy gene expression. *Nucleic Acids Res, 41*(16), 7683-7699. doi: 10.1093/nar/gkt563

Baker, B. M., Nargund, A. M., Sun, T., & Haynes, C. M. (2012). Protective coupling of mitochondrial function and protein synthesis via the eIF2alpha kinase GCN-2. *PLoS Genet, 8*(6), e1002760. doi: 10.1371/journal.pgen.1002760

Baker, M. J., Tatsuta, T., & Langer, T. (2011). Quality control of mitochondrial proteostasis. *Cold Spring Harb Perspect Biol, 3*(7). doi: 10.1101/cshperspect.a007559

Bao, X. R., Ong, S. E., Goldberger, O., Peng, J., Sharma, R., Thompson, D. A., . . . Mootha, V. K. (2016). Mitochondrial dysfunction remodels one-carbon metabolism in human cells. *Elife, 5*. doi: 10.7554/eLife.10575

Bartekova, M., Radosinska, J., Jelemensky, M., & Dhalla, N. S. (2018). Role of cytokines and inflammation in heart function during health and disease. *Heart Fail Rev, 23*(5), 733-758. doi: 10.1007/s10741-018-9716-x

Bauskin, A. R., Jiang, L., Luo, X. W., Wu, L., Brown, D. A., & Breit, S. N. (2010). The TGF-beta superfamily cytokine MIC-1/GDF15: secretory mechanisms facilitate creation of latent stromal stores. *J Interferon Cytokine Res, 30*(6), 389-397. doi: 10.1089/jir.2009.0052

Becker, C., Kukat, A., Szczepanowska, K., Hermans, S., Senft, K., Brandscheid, C. P., . . . Trifunovic, A. (2018). CLPP deficiency protects against metabolic syndrome but hinders adaptive thermogenesis. *EMBO Rep, 19*(5). doi: 10.15252/embr.201745126

Belostotsky, R., Ben-Shalom, E., Rinat, C., Becker-Cohen, R., Feinstein, S., Zeligson, S., . . . Frishberg, Y. (2011). Mutations in the mitochondrial seryl-tRNA synthetase cause hyperuricemia, pulmonary hypertension, renal failure in infancy and alkalosis, HUPRA syndrome. *Am J Hum Genet, 88*(2), 193-200. doi: S0002-9297(10)00646-4 [pii]
10.1016/j.ajhg.2010.12.010

Bender, T., Lewrenz, I., Franken, S., Baitzel, C., & Voos, W. (2011). Mitochondrial enzymes are protected from stress-induced aggregation by mitochondrial chaperones and the Pim1/LON protease. *Mol Biol Cell, 22*(5), 541-554. doi: 10.1091/mbc.E10-08-0718

Berk, A.J., & Clayton, D.A. (1974). Mechanism of mitochondrial DNA replication in mouse L-cells: Asynchronous replication of strands, segregation of circular daughter molecules, aspects of topology and turnover of an initiation sequence. *J. Mol. Biol., 86*(Number), 801-824.

Bertram, G., Innes, S., Minella, O., Richardson, J., & Stansfield, I. (2001). Endless possibilities: translation termination and stop codon recognition. *Microbiology, 147*(Pt 2), 255-269. doi: 10.1099/00221287-147-2-255

Bhandari, V., Wong, K. S., Zhou, J. L., Mabanglo, M. F., Batey, R. A., & Houry, W. A. (2018). The Role of ClpP Protease in Bacterial Pathogenesis and Human Diseases. *ACS Chem Biol, 13*(6), 1413-1425. doi: 10.1021/acschembio.8b00124

Birky, C.W. (1995). Uniparental inheritance of mitochondrial and chloroplast genes: Mechanisms and evolution. *Proc Natl Acad Sci USA, 92*(25Number), 11331-11338.

BonDurant, L. D., Ameka, M., Naber, M. C., Markan, K. R., Idiga, S. O., Acevedo, M. R., . . . Potthoff, M. J. (2017). FGF21 Regulates Metabolism Through Adipose-Dependent and -Independent Mechanisms. *Cell Metab, 25*(4), 935-944 e934. doi: 10.1016/j.cmet.2017.03.005

BonDurant, L. D., & Potthoff, M. J. (2018). Fibroblast Growth Factor 21: A Versatile Regulator of Metabolic Homeostasis. *Annu Rev Nutr*. doi: 10.1146/annurev-nutr-071816-064800

Bonnefond, L., Fender, A., Rudinger-Thirion, J., Giege, R., Florentz, C., & Sissler, M. (2005). Toward the full set of human mitochondrial aminoacyl-tRNA synthetases: characterization of AspRS and TyrRS. *Biochemistry, 44*(12), 4805-4816. doi: 10.1021/bi047527z

Bota, D. A., & Davies, K. J. (2002). Lon protease preferentially degrades oxidized mitochondrial aconitase by an ATP-stimulated mechanism. *Nat Cell Biol, 4*(9), 674-680.

Bota, D. A., Van Remmen, H., & Davies, K. J. (2002). Modulation of Lon protease activity and aconitase turnover during aging and oxidative stress. *FEBS Lett, 532*(1-2), 103-106. doi: S0014579302036384 [pii]

Bottinger, L., Oeljeklaus, S., Guiard, B., Rospert, S., Warscheid, B., & Becker, T. (2015). Mitochondrial heat shock protein (Hsp) 70 and Hsp10 cooperate in the formation of Hsp60 complexes. *J Biol Chem, 290*(18), 11611-11622. doi: 10.1074/jbc.M115.642017

Bottner, M., Suter-Crazzolara, C., Schober, A., & Unsicker, K. (1999). Expression of a novel member of the TGF-beta superfamily, growth/differentiation factor-15/macrophage-inhibiting cytokine-1 (GDF-15/MIC-1) in adult rat tissues. *Cell Tissue Res, 297*(1), 103-110.

Bross, P., Li, Z., Hansen, J., Hansen, J. J., Nielsen, M. N., Corydon, T. J., . . . Gregersen, N. (2007). Single-nucleotide variations in the genes encoding the mitochondrial Hsp60/Hsp10 chaperone system and their disease-causing potential. *J Hum Genet, 52*(1), 56-65. doi: 10.1007/s10038-006-0080-7

Cann, R.L., Stoneking, M., & Wilson, A.C. (1987). Mitochondrial DNA and human evolution. *Nature, 325*(Number), 31-36.

Carobbio, S., Guenantin, A. C., Samuelson, I., Bahri, M., & Vidal-Puig, A. (2018). Brown and beige fat: From molecules to physiology and pathophysiology. *Biochim Biophys Acta*. doi: 10.1016/j.bbalip.2018.05.013

Casari, G., De Fusco, M., Ciarmatori, S., Zeviani, M., Mora, M., Fernandez, P., . . . Ballabio, A. (1998). Spastic paraplegia and OXPHOS impairment caused by mutations in

paraplegin, a nuclear-encoded mitochondrial metalloprotease. *Cell, 93*(6Number), 973-983.

Chaban, Y., Boekema, E. J., & Dudkina, N. V. (2014). Structures of mitochondrial oxidative phosphorylation supercomplexes and mechanisms for their stabilisation. *Biochim Biophys Acta, 1837*(4), 418-426. doi: 10.1016/j.bbabio.2013.10.004

Chaillou, T., Zhang, X., & McCarthy, J. J. (2016). Expression of Muscle-Specific Ribosomal Protein L3-Like Impairs Myotube Growth. *J Cell Physiol, 231*(9), 1894-1902. doi: 10.1002/jcp.25294

Chambers, K. T., Leone, T. C., Sambandam, N., Kovacs, A., Wagg, C. S., Lopaschuk, G. D., . . . Kelly, D. P. (2011). Chronic inhibition of pyruvate dehydrogenase in heart triggers an adaptive metabolic response. *J Biol Chem, 286*(13), 11155-11162. doi: 10.1074/jbc.M110.217349

Chen, Q., Kirk, K., Shurubor, Y. I., Zhao, D., Arreguin, A. J., Shahi, I., . . . D'Aurelio, M. (2018). Rewiring of Glutamine Metabolism Is a Bioenergetic Adaptation of Human Cells with Mitochondrial DNA Mutations. *Cell Metab, 27*(5), 1007-1025 e1005. doi: 10.1016/j.cmet.2018.03.002

Chen, Y., Pat, B., Zheng, J., Cain, L., Powell, P., Shi, K., . . . Dell'italia, L. J. (2010). Tumor necrosis factor-alpha produced in cardiomyocytes mediates a predominant myocardial inflammatory response to stretch in early volume overload. *J Mol Cell Cardiol, 49*(1), 70-78. doi: 10.1016/j.yjmcc.2009.12.013

Christian, B. E., & Spremulli, L. L. (2009). Evidence for an active role of IF3mt in the initiation of translation in mammalian mitochondria. *Biochemistry, 48*(15), 3269-3278. doi: 10.1021/bi8023493

Christian, B. E., & Spremulli, L. L. (2012). Mechanism of protein biosynthesis in mammalian mitochondria. *Biochim Biophys Acta, 1819*(9-10), 1035-1054. doi: 10.1016/j.bbagrm.2011.11.009

Chung, H. K., Ryu, D., Kim, K. S., Chang, J. Y., Kim, Y. K., Yi, H. S., . . . Shong, M. (2017). Growth differentiation factor 15 is a myomitokine governing systemic energy homeostasis. *J Cell Biol, 216*(1), 149-165. doi: 10.1083/jcb.201607110

Ciccarese, F., & Ciminale, V. (2017). Escaping Death: Mitochondrial Redox Homeostasis in Cancer Cells. *Front Oncol, 7*, 117. doi: 10.3389/fonc.2017.00117

Clayton, D.A. (Ed.). (1983). *Replication of mammalian mitochondrial DNA*. Boston: Martinus Nijhoff Publishing.

Cuevas-Ramos, D., Almeda-Valdes, P., Meza-Arana, C. E., Brito-Cordova, G., Gomez-Perez, F. J., Mehta, R., . . . Aguilar-Salinas, C. A. (2012). Exercise increases serum fibroblast growth factor 21 (FGF21) levels. *PLoS One, 7*(5), e38022. doi: 10.1371/journal.pone.0038022

De Sousa-Coelho, A. L., Marrero, P. F., & Haro, D. (2012). Activating transcription factor 4-dependent induction of FGF21 during amino acid deprivation. *Biochem J, 443*(1), 165-171. doi: 10.1042/BJ20111748

Di Bella, D., Lazzaro, F., Brusco, A., Plumari, M., Battaglia, G., Pastore, A., . . . Taroni, F. (2010). Mutations in the mitochondrial protease gene AFG3L2 cause dominant hereditary ataxia SCA28. *Nat Genet, 42*(4), 313-321. doi: 10.1038/ng.544

Diodato, D., Ghezzi, D., & Tiranti, V. (2014). The Mitochondrial Aminoacyl tRNA Synthetases: Genes and Syndromes. *Int J Cell Biol, 2014*, 787956. doi: 10.1155/2014/787956

Diodato, D., Melchionda, L., Haack, T. B., Dallabona, C., Baruffini, E., Donnini, C., . . . Ghezzi, D. (2014). VARS2 and TARS2 mutations in patients with mitochondrial encephalomyopathies. *Hum Mutat, 35*(8), 983-989. doi: 10.1002/humu.22590

Dogan, S. A., Pujol, C., Maiti, P., Kukat, A., Wang, S., Hermans, S., . . . Trifunovic, A. (2014a). Tissue-specific loss of DARS2 activates stress responses independently of

respiratory chain deficiency in the heart. *Cell Metab, 19*(3), 458-469. doi: 10.1016/j.cmet.2014.02.004

Dogan, S. A., Pujol, C., Maiti, P., Kukat, A., Wang, S. Y., Hermans, S., . . . Trifunovic, A. (2014b). Tissue-Specific Loss of DARS2 Activates Stress Responses Independently of Respiratory Chain Deficiency in the Heart. *Cell Metab, 19*(3), 458-469. doi: 10.1016/j.cmet.2014.02.004

Durieux, J., Wolff, S., & Dillin, A. (2012). The cell-non-autonomous nature of electron transport chain-mediated longevity. *Cell, 144*(1), 79-91. doi: S0092-8674(10)01434-0 [pii]

10.1016/j.cell.2010.12.016

Edvardson, S., Shaag, A., Kolesnikova, O., Gomori, J. M., Tarassov, I., Einbinder, T., . . . Elpeleg, O. (2007). Deleterious mutation in the mitochondrial arginyl-transfer RNA synthetase gene is associated with pontocerebellar hypoplasia. *Am J Hum Genet, 81*(4), 857-862. doi: 10.1086/521227

Ekstrand, M.I., Falkenberg, M., Rantanen, A., Park, C.B., Gaspari, M., Hultenby, K., . . . Larsson, N. G. (2004). Mitochondrial transcription factor A regulates mtDNA copy number in mammals. *Hum. Mol. Genet., 13*(9), 935-944.

Elo, J. M., Yadavalli, S. S., Euro, L., Isohanni, P., Gotz, A., Carroll, C. J., . . . Suomalainen, A. (2012). Mitochondrial phenylalanyl-tRNA synthetase mutations underlie fatal infantile Alpers encephalopathy. *Hum Mol Genet, 21*(20), 4521-4529. doi: 10.1093/hmg/dds294

Fan, J., Ye, J., Kamphorst, J. J., Shlomi, T., Thompson, C. B., & Rabinowitz, J. D. (2014). Quantitative flux analysis reveals folate-dependent NADPH production. *Nature, 510*(7504), 298-302. doi: 10.1038/nature13236

Feng, J., Bussiere, F., & Hekimi, S. (2001). Mitochondrial electron transport is a key determinant of life span in Caenorhabditis elegans. *Dev Cell, 1*(5Number), 633-644.

Fiorese, C. J., & Haynes, C. M. (2017). Integrating the UPR(mt) into the mitochondrial maintenance network. *Crit Rev Biochem Mol Biol, 52*(3), 304-313. doi: 10.1080/10409238.2017.1291577

Fiorese, C. J., Schulz, A. M., Lin, Y. F., Rosin, N., Pellegrino, M. W., & Haynes, C. M. (2016). The Transcription Factor ATF5 Mediates a Mammalian Mitochondrial UPR. *Curr Biol, 26*(15), 2037-2043. doi: 10.1016/j.cub.2016.06.002

Fisher, F. M., Chui, P. C., Antonellis, P. J., Bina, H. A., Kharitonenkov, A., Flier, J. S., & Maratos-Flier, E. (2010). Obesity is a fibroblast growth factor 21 (FGF21)-resistant state. *Diabetes, 59*(11), 2781-2789. doi: 10.2337/db10-0193

Fisher, F. M., Kleiner, S., Douris, N., Fox, E. C., Mepani, R. J., Verdeguer, F., . . . Spiegelman, B. M. (2012). FGF21 regulates PGC-1alpha and browning of white adipose tissues in adaptive thermogenesis. *Genes Dev, 26*(3), 271-281. doi: 10.1101/gad.177857.111

Fisher, F. M., & Maratos-Flier, E. (2016). Understanding the Physiology of FGF21. *Annu Rev Physiol, 78*, 223-241. doi: 10.1146/annurev-physiol-021115-105339

Fon Tacer, K., Bookout, A. L., Ding, X., Kurosu, H., John, G. B., Wang, L., . . . Kliewer, S. A. (2010). Research resource: Comprehensive expression atlas of the fibroblast growth factor system in adult mouse. *Mol Endocrinol, 24*(10), 2050-2064. doi: 10.1210/me.2010-0142

Freeman, H. C., Hugill, A., Dear, N. T., Ashcroft, F. M., & Cox, R. D. (2006). Deletion of nicotinamide nucleotide transhydrogenase: a new quantitive trait locus accounting for glucose intolerance in C57BL/6J mice. *Diabetes, 55*(7), 2153-2156. doi: 10.2337/db06-0358

Fujita, Y., Ito, M., Kojima, T., Yatsuga, S., Koga, Y., & Tanaka, M. (2015). GDF15 is a novel biomarker to evaluate efficacy of pyruvate therapy for mitochondrial diseases. *Mitochondrion, 20*, 34-42. doi: 10.1016/j.mito.2014.10.006

Fujita, Y., Taniguchi, Y., Shinkai, S., Tanaka, M., & Ito, M. (2016). Secreted growth differentiation factor 15 as a potential biomarker for mitochondrial dysfunctions in aging and age-related disorders. *Geriatr Gerontol Int, 16 Suppl 1*, 17-29. doi: 10.1111/ggi.12724

Funfschilling, U., Supplie, L. M., Mahad, D., Boretius, S., Saab, A. S., Edgar, J., . . . Nave, K. A. (2012). Glycolytic oligodendrocytes maintain myelin and long-term axonal integrity. *Nature, 485*(7399), 517-521. doi: 10.1038/nature11007

Gispert, S., Parganlija, D., Klinkenberg, M., Drose, S., Wittig, I., Mittelbronn, M., . . . Auburger, G. (2013). Loss of mitochondrial peptidase Clpp leads to infertility, hearing loss plus growth retardation via accumulation of CLPX, mtDNA and inflammatory factors. *Hum Mol Genet, 22*(24), 4871-4887. doi: 10.1093/hmg/ddt338

Gong, Q., Hu, Z., Zhang, F., Cui, A., Chen, X., Jiang, H., . . . Li, Y. (2016). Fibroblast growth factor 21 improves hepatic insulin sensitivity by inhibiting mammalian target of rapamycin complex 1 in mice. *Hepatology, 64*(2), 425-438. doi: 10.1002/hep.28523

Gotz, A., Tyynismaa, H., Euro, L., Ellonen, P., Hyotylainen, T., Ojala, T., . . . Suomalainen, A. (2011). Exome sequencing identifies mitochondrial alanyl-tRNA synthetase mutations in infantile mitochondrial cardiomyopathy. *Am J Hum Genet, 88*(5), 635-642. doi: S0002-9297(11)00147-9 [pii]

10.1016/j.ajhg.2011.04.006

Gray, M.W. (1989). The evolutionary origins of organelles. *Trends Genet., 5*(9Number), 294-299.

Gray, M.W., Burger, G., & Lang, B.F. (1999). Mitochondrial evolution. *Science, 283*(Number), 1476-1481.

Grynberg, A., & Demaison, L. (1996). Fatty acid oxidation in the heart. *J Cardiovasc Pharmacol, 28 Suppl 1*, S11-17.

Guimaraes, J. C., & Zavolan, M. (2016). Patterns of ribosomal protein expression specify normal and malignant human cells. *Genome Biol, 17*(1), 236. doi: 10.1186/s13059-016-1104-z

Guridi, M., Tintignac, L. A., Lin, S., Kupr, B., Castets, P., & Ruegg, M. A. (2015). Activation of mTORC1 in skeletal muscle regulates whole-body metabolism through FGF21. *Sci Signal, 8*(402), ra113. doi: 10.1126/scisignal.aab3715

Gustafsson, C. M., Falkenberg, M., & Larsson, N. G. (2016). Maintenance and Expression of Mammalian Mitochondrial DNA. *Annu Rev Biochem, 85*, 133-160. doi: 10.1146/annurev-biochem-060815-014402

Hallberg, B. M., & Larsson, N. G. (2014). Making proteins in the powerhouse. *Cell Metab, 20*(2), 226-240. doi: 10.1016/j.cmet.2014.07.001

Han, A. P., Yu, C., Lu, L., Fujiwara, Y., Browne, C., Chin, G., . . . Chen, J. J. (2001). Heme-regulated eIF2alpha kinase (HRI) is required for translational regulation and survival of erythroid precursors in iron deficiency. *EMBO J, 20*(23), 6909-6918. doi: 10.1093/emboj/20.23.6909

Harding, H. P., Zhang, Y., & Ron, D. (1999). Protein translation and folding are coupled by an endoplasmic-reticulum-resident kinase. *Nature, 397*(6716), 271-274. doi: 10.1038/16729

Hatefi, Y., Haavik, A. G., Fowler, L. R., & Griffiths, D. E. (1962). Studies on the electron transfer system. XLII. Reconstitution of the electron transfer system. *J Biol Chem, 237*, 2661-2669.

Hochli, M., & Hackenbrock, C. R. (1977). Thermotropic lateral translational motion of intramembrane particles in the inner mitochondrial membrane and its inhibition by artificial peripheral proteins. *J Cell Biol, 72*(2), 278-291.

Hondares, E., Iglesias, R., Giralt, A., Gonzalez, F. J., Giralt, M., Mampel, T., & Villarroya, F. (2011). Thermogenic activation induces FGF21 expression and release in brown adipose tissue. *J Biol Chem, 286*(15), 12983-12990. doi: 10.1074/jbc.M110.215889

Hood, D. A., Tryon, L. D., Carter, H. N., Kim, Y., & Chen, C. C. (2016). Unravelling the mechanisms regulating muscle mitochondrial biogenesis. *Biochem J, 473*(15), 2295-2314. doi: 10.1042/BCJ20160009

Horwich, A. L., Weber-Ban, E. U., & Finley, D. (1999). Chaperone rings in protein folding and degradation. *Proc Natl Acad Sci U S A, 96*(20), 11033-11040.

Hotta, Y., Nakamura, H., Konishi, M., Murata, Y., Takagi, H., Matsumura, S., . . . Itoh, N. (2009). Fibroblast growth factor 21 regulates lipolysis in white adipose tissue but is not required for ketogenesis and triglyceride clearance in liver. *Endocrinology, 150*(10), 4625-4633. doi: 10.1210/en.2009-0119

Houtkooper, R. H., Mouchiroud, L., Ryu, D., Moullan, N., Katsyuba, E., Knott, G., . . . Auwerx, J. (2013). Mitonuclear protein imbalance as a conserved longevity mechanism. *Nature, 497*(7450), 451-457. doi: 10.1038/nature12188

Inagaki, T., Dutchak, P., Zhao, G., Ding, X., Gautron, L., Parameswara, V., . . . Kliewer, S. A. (2007). Endocrine regulation of the fasting response by PPARalpha-mediated induction of fibroblast growth factor 21. *Cell Metab, 5*(6), 415-425. doi: 10.1016/j.cmet.2007.05.003

Inagaki, T., Lin, V. Y., Goetz, R., Mohammadi, M., Mangelsdorf, D. J., & Kliewer, S. A. (2008). Inhibition of growth hormone signaling by the fasting-induced hormone FGF21. *Cell Metab, 8*(1), 77-83. doi: 10.1016/j.cmet.2008.05.006

Jenkinson, E. M., Rehman, A. U., Walsh, T., Clayton-Smith, J., Lee, K., Morell, R. J., . . . Newman, W. G. (2013). Perrault syndrome is caused by recessive mutations in CLPP, encoding a mitochondrial ATP-dependent chambered protease. *Am J Hum Genet, 92*(4), 605-613. doi: 10.1016/j.ajhg.2013.02.013

Johnen, H., Lin, S., Kuffner, T., Brown, D. A., Tsai, V. W., Bauskin, A. R., . . . Breit, S. N. (2007). Tumor-induced anorexia and weight loss are mediated by the TGF-beta superfamily cytokine MIC-1. *Nat Med, 13*(11), 1333-1340. doi: 10.1038/nm1677

Kaguni, L. S. (2004). DNA polymerase gamma, the mitochondrial replicase. *Annu Rev Biochem, 73*, 293-320.

Kalko, S. G., Paco, S., Jou, C., Rodriguez, M. A., Meznaric, M., Rogac, M., . . . Jimenez-Mallebrera, C. (2014). Transcriptomic profiling of TK2 deficient human skeletal muscle suggests a role for the p53 signalling pathway and identifies growth and differentiation factor-15 as a potential novel biomarker for mitochondrial myopathies. *BMC Genomics, 15*, 91. doi: 10.1186/1471-2164-15-91

Kanki, T., & Klionsky, D. J. (2009). Atg32 is a tag for mitochondria degradation in yeast. *Autophagy, 5*(8), 1201-1202.

Karuppagounder, S. S., Alim, I., Khim, S. J., Bourassa, M. W., Sleiman, S. F., John, R., . . . Ratan, R. R. (2016). Therapeutic targeting of oxygen-sensing prolyl hydroxylases abrogates ATF4-dependent neuronal death and improves outcomes after brain hemorrhage in several rodent models. *Sci Transl Med, 8*(328), 328ra329. doi: 10.1126/scitranslmed.aac6008

Keipert, S., Kutschke, M., Lamp, D., Brachthauser, L., Neff, F., Meyer, C. W., . . . Jastroch, M. (2015). Genetic disruption of uncoupling protein 1 in mice renders brown adipose tissue a significant source of FGF21 secretion. *Mol Metab, 4*(7), 537-542. doi: 10.1016/j.molmet.2015.04.006

Keipert, S., Kutschke, M., Ost, M., Schwarzmayr, T., van Schothorst, E. M., Lamp, D., . . . Jastroch, M. (2017). Long-Term Cold Adaptation Does Not Require FGF21 or UCP1. *Cell Metab, 26*(2), 437-446 e435. doi: 10.1016/j.cmet.2017.07.016

Keipert, S., Ost, M., Johann, K., Imber, F., Jastroch, M., van Schothorst, E. M., . . . Klaus, S. (2014). Skeletal muscle mitochondrial uncoupling drives endocrine cross-talk through the induction of FGF21 as a myokine. *Am J Physiol Endocrinol Metab, 306*(5), E469-482. doi: 10.1152/ajpendo.00330.2013

Kempf, T., Eden, M., Strelau, J., Naguib, M., Willenbockel, C., Tongers, J., . . . Wollert, K. C. (2006). The transforming growth factor-beta superfamily member growth-differentiation factor-15 protects the heart from ischemia/reperfusion injury. *Circ Res, 98*(3), 351-360. doi: 10.1161/01.RES.0000202805.73038.48

Khan, N. A., Nikkanen, J., Yatsuga, S., Jackson, C., Wang, L., Pradhan, S., . . . Suomalainen, A. (2017). mTORC1 Regulates Mitochondrial Integrated Stress Response and Mitochondrial Myopathy Progression. *Cell Metab, 26*(2), 419-428 e415. doi: 10.1016/j.cmet.2017.07.007

Kilkenny, D. M., & Rocheleau, J. V. (2016). The FGF21 Receptor Signaling Complex: Klothobeta, FGFR1c, and Other Regulatory Interactions. *Vitam Horm, 101*, 17-58. doi: 10.1016/bs.vh.2016.02.008

Kim, K. H., Jeong, Y. T., Oh, H., Kim, S. H., Cho, J. M., Kim, Y. N., . . . Lee, M. S. (2013). Autophagy deficiency leads to protection from obesity and insulin resistance by inducing Fgf21 as a mitokine. *Nat Med, 19*(1), 83-92. doi: 10.1038/nm.3014

Komar, A. A., & Hatzoglou, M. (2011). Cellular IRES-mediated translation: the war of ITAFs in pathophysiological states. *Cell Cycle, 10*(2), 229-240. doi: 10.4161/cc.10.2.14472

Konig, T., Troder, S. E., Bakka, K., Korwitz, A., Richter-Dennerlein, R., Lampe, P. A., . . . Langer, T. (2016). The m-AAA Protease Associated with Neurodegeneration Limits MCU Activity in Mitochondria. *Mol Cell, 64*(1), 148-162. doi: 10.1016/j.molcel.2016.08.020

Koppen, M., Metodiev, M. D., Casari, G., Rugarli, E. I., & Langer, T. (2007). Variable and tissue-specific subunit composition of mitochondrial m-AAA protease complexes linked to hereditary spastic paraplegia. *Mol Cell Biol, 27*(2), 758-767. doi: 10.1128/MCB.01470-06

Krieg, A. J., Rankin, E. B., Chan, D., Razorenova, O., Fernandez, S., & Giaccia, A. J. (2010). Regulation of the histone demethylase JMJD1A by hypoxia-inducible factor 1 alpha enhances hypoxic gene expression and tumor growth. *Mol Cell Biol, 30*(1), 344-353. doi: 10.1128/MCB.00444-09

Kuhl, I., Miranda, M., Atanassov, I., Kuznetsova, I., Hinze, Y., Mourier, A., . . . Larsson, N. G. (2017). Transcriptomic and proteomic landscape of mitochondrial dysfunction reveals secondary coenzyme Q deficiency in mammals. *Elife, 6*. doi: 10.7554/eLife.30952

Kukat, A., Dogan, S. A., Edgar, D., Mourier, A., Jacoby, C., Maiti, P., . . . Trifunovic, A. (2014). Loss of UCP2 Attenuates Mitochondrial Dysfunction without Altering ROS Production and Uncoupling Activity. *PLoS Genet, 10*(6). doi: 10.1371/journal.pgen.1004385

Kurosu, H., Choi, M., Ogawa, Y., Dickson, A. S., Goetz, R., Eliseenkova, A. V., . . . Kuro-o, M. (2007). Tissue-specific expression of betaKlotho and fibroblast growth factor (FGF) receptor isoforms determines metabolic activity of FGF19 and FGF21. *J Biol Chem, 282*(37), 26687-26695. doi: 10.1074/jbc.M704165200

Langer, T., Kaser, M., Klanner, C., & Leonhard, K. (2001). AAA proteases of mitochondria: quality control of membrane proteins and regulatory functions during mitochondrial biogenesis. *Biochem Soc Trans, 29*(Pt 4), 431-436.

Lee, M. E., Baker, T. A., & Sauer, R. T. (2010). Control of substrate gating and translocation into ClpP by channel residues and ClpX binding. *J Mol Biol, 399*(5), 707-718. doi: 10.1016/j.jmb.2010.04.027

Lemaire, P. A., Anderson, E., Lary, J., & Cole, J. L. (2008). Mechanism of PKR Activation by dsRNA. *J Mol Biol, 381*(2), 351-360. doi: 10.1016/j.jmb.2008.05.056

Lightowlers, R. N., Chinnery, P. F., Turnbull, D. M., & Howell, N. (1997). Mammalian mitochondrial genetics: heredity, heteroplasmy and disease. *Trends Genet, 13*(11Number), 450-455.

Lin, S. C., & Hardie, D. G. (2017). AMPK: Sensing Glucose as well as Cellular Energy Status. *Cell Metab*. doi: 10.1016/j.cmet.2017.10.009

Liu, F., Yang, X., Geng, M., & Huang, M. (2018). Targeting ERK, an Achilles' Heel of the MAPK pathway, in cancer therapy. *Acta Pharm Sin B, 8*(4), 552-562. doi: 10.1016/j.apsb.2018.01.008

Liu, S. Q., Roberts, D., Kharitonenkov, A., Zhang, B., Hanson, S. M., Li, Y. C., . . . Wu, Y. H. (2013). Endocrine protection of ischemic myocardium by FGF21 from the liver and adipose tissue. *Sci Rep, 3*, 2767. doi: 10.1038/srep02767

Long, J. Z., Svensson, K. J., Bateman, L. A., Lin, H., Kamenecka, T., Lokurkar, I. A., . . . Spiegelman, B. M. (2016). The Secreted Enzyme PM20D1 Regulates Lipidated Amino Acid Uncouplers of Mitochondria. *Cell, 166*(2), 424-435. doi: 10.1016/j.cell.2016.05.071

Luce, K., & Osiewacz, H. D. (2009). Increasing organismal healthspan by enhancing mitochondrial protein quality control. *Nat Cell Biol, 11*(7), 852-858. doi: 10.1038/ncb1893

Lyons, G. E., Mühlebach, S., Moser, A., Masood, R., Paterson, B. M., Buckingham, M. E., & Perriard, J.- C. (1991). Developmental regulation of creatine kinase gene expression by myogenic factors in embryonic mouse and chick skeletal muscle. *Development, 113*(3Number), 1017-1029.

Ma, L., & Spremulli, L.L. (1995). Cloning and sequence analysis of the human mitochondrial translational initiation factor 2 cDNA. *J Biol Chem, 270*(4Number), 1859-1865.

Macia, L., Tsai, V. W., Nguyen, A. D., Johnen, H., Kuffner, T., Shi, Y. C., . . . Sainsbury, A. (2012). Macrophage inhibitory cytokine 1 (MIC-1/GDF15) decreases food intake, body weight and improves glucose tolerance in mice on normal & obesogenic diets. *PLoS One, 7*(4), e34868. doi: 10.1371/journal.pone.0034868

Maerkens, A., Olive, M., Schreiner, A., Feldkirchner, S., Schessl, J., Uszkoreit, J., . . . Kley, R. A. (2016). New insights into the protein aggregation pathology in myotilinopathy by combined proteomic and immunolocalization analyses. *Acta Neuropathol Commun, 4*, 8. doi: 10.1186/s40478-016-0280-0

Mahmoud, S. A., & Poizat, C. (2013). Epigenetics and chromatin remodeling in adult cardiomyopathy. *J Pathol, 231*(2), 147-157. doi: 10.1002/path.4234

Markan, K. R., & Potthoff, M. J. (2016). Metabolic fibroblast growth factors (FGFs): Mediators of energy homeostasis. *Semin Cell Dev Biol, 53*, 85-93. doi: 10.1016/j.semcdb.2015.09.021

Martonosi, A. N. (2000). Animal electricity, Ca2+ and muscle contraction. A brief history of muscle research. *Acta Biochim Pol, 47*(3), 493-516.

Matikainen, N., Taskinen, M. R., Stennabb, S., Lundbom, N., Hakkarainen, A., Vaaralahti, K., & Raivio, T. (2012). Decrease in circulating fibroblast growth factor 21 after an oral fat load is related to postprandial triglyceride-rich lipoproteins and liver fat. *Eur J Endocrinol, 166*(3), 487-492. doi: 10.1530/EJE-11-0783

Matsushima, Y., Goto, Y., & Kaguni, L. S. (2010). Mitochondrial Lon protease regulates mitochondrial DNA copy number and transcription by selective degradation of

mitochondrial transcription factor A (TFAM). *Proc Natl Acad Sci U S A, 107*(43), 18410-18415. doi: 1008924107 [pii]
10.1073/pnas.1008924107
Matsushima, Y., & Kaguni, L. S. (2012). Matrix proteases in mitochondrial DNA function. *Biochim Biophys Acta, 1819*(9-10), 1080-1087. doi: 10.1016/j.bbagrm.2011.11.008
Mazumder, B., Sampath, P., Seshadri, V., Maitra, R. K., DiCorleto, P. E., & Fox, P. L. (2003). Regulated release of L13a from the 60S ribosomal subunit as a mechanism of transcript-specific translational control. *Cell, 115*(2), 187-198.
Melber, A., & Haynes, C. M. (2018). UPR(mt) regulation and output: a stress response mediated by mitochondrial-nuclear communication. *Cell Res, 28*(3), 281-295. doi: 10.1038/cr.2018.16
Minard, A. Y., Tan, S. X., Yang, P., Fazakerley, D. J., Domanova, W., Parker, B. L., . . . James, D. E. (2016). mTORC1 Is a Major Regulatory Node in the FGF21 Signaling Network in Adipocytes. *Cell Rep, 17*(1), 29-36. doi: 10.1016/j.celrep.2016.08.086
Mitchell, P. (1961). Coupling of phosphorylation to electron and hydrogen transfer by a chemi-osmotic type of mechanism. *Nature, 191*(Number), 144-148.
Miyake, M., Nomura, A., Ogura, A., Takehana, K., Kitahara, Y., Takahara, K., . . . Oyadomari, S. (2016). Skeletal muscle-specific eukaryotic translation initiation factor 2alpha phosphorylation controls amino acid metabolism and fibroblast growth factor 21-mediated non-cell-autonomous energy metabolism. *FASEB J, 30*(2), 798-812. doi: 10.1096/fj.15-275990
Murphy, M. P. (2015). Redox Modulation by Reversal of the Mitochondrial Nicotinamide Nucleotide Transhydrogenase. *Cell Metab, 22*(3), 363-365. doi: 10.1016/j.cmet.2015.08.012
Nagao, A., Suzuki, T., & Suzuki, T. (2007). Aminoacyl-tRNA surveillance by EF-Tu in mammalian mitochondria. *Nucleic Acids Symp Ser (Oxf)*(51), 41-42. doi: 10.1093/nass/nrm021
Narendra, D., Tanaka, A., Suen, D. F., & Youle, R. J. (2008). Parkin is recruited selectively to impaired mitochondria and promotes their autophagy. *J Cell Biol, 183*(5), 795-803. doi: 10.1083/jcb.200809125
Nargund, A. M., Pellegrino, M. W., Fiorese, C. J., Baker, B. M., & Haynes, C. M. (2012). Mitochondrial import efficiency of ATFS-1 regulates mitochondrial UPR activation. *Science, 337*(6094), 587-590. doi: 10.1126/science.1223560
Nickel, A. G., von Hardenberg, A., Hohl, M., Loffler, J. R., Kohlhaas, M., Becker, J., . . . Maack, C. (2015). Reversal of Mitochondrial Transhydrogenase Causes Oxidative Stress in Heart Failure. *Cell Metab, 22*(3), 472-484. doi: 10.1016/j.cmet.2015.07.008
Nikkanen, J., Forsstrom, S., Euro, L., Paetau, I., Kohnz, R. A., Wang, L., . . . Suomalainen, A. (2016). Mitochondrial DNA Replication Defects Disturb Cellular dNTP Pools and Remodel One-Carbon Metabolism. *Cell Metab, 23*(4), 635-648. doi: 10.1016/j.cmet.2016.01.019
Novoa, I., Zeng, H., Harding, H. P., & Ron, D. (2001). Feedback inhibition of the unfolded protein response by GADD34-mediated dephosphorylation of eIF2alpha. *J Cell Biol, 153*(5), 1011-1022.
O'Brien, T. W. (2003). Properties of human mitochondrial ribosomes. *IUBMB Life, 55*(9), 505-513. doi: 10.1080/15216540310001626610
O'Rourke, B. (2010). From bioblasts to mitochondria: ever expanding roles of mitochondria in cell physiology. *Front Physiol, 1*, 7. doi: 10.3389/fphys.2010.00007
Pakos-Zebrucka, K., Koryga, I., Mnich, K., Ljujic, M., Samali, A., & Gorman, A. M. (2016). The integrated stress response. *EMBO Rep, 17*(10), 1374-1395. doi: 10.15252/embr.201642195

Peralta, S., Wang, X., & Moraes, C. T. (2012). Mitochondrial transcription: lessons from mouse models. *Biochim Biophys Acta, 1819*(9-10), 961-969. doi: 10.1016/j.bbagrm.2011.11.001

Pierce, S. B., Chisholm, K. M., Lynch, E. D., Lee, M. K., Walsh, T., Opitz, J. M., . . . King, M. C. (2011). Mutations in mitochondrial histidyl tRNA synthetase HARS2 cause ovarian dysgenesis and sensorineural hearing loss of Perrault syndrome. *Proc Natl Acad Sci U S A, 108*(16), 6543-6548. doi: 1103471108 [pii]
10.1073/pnas.1103471108

Pierce, S. B., Gersak, K., Michaelson-Cohen, R., Walsh, T., Lee, M. K., Malach, D., . . . Levy-Lahad, E. (2013). Mutations in LARS2, encoding mitochondrial leucyl-tRNA synthetase, lead to premature ovarian failure and hearing loss in Perrault syndrome. *Am J Hum Genet, 92*(4), 614-620. doi: 10.1016/j.ajhg.2013.03.007

Planavila, A., Fernandez-Sola, J., & Villarroya, F. (2017). Cardiokines as Modulators of Stress-Induced Cardiac Disorders. *Adv Protein Chem Struct Biol, 108*, 227-256. doi: 10.1016/bs.apcsb.2017.01.002

Planavila, A., Redondo, I., Hondares, E., Vinciguerra, M., Munts, C., Iglesias, R., . . . Villarroya, F. (2013). Fibroblast growth factor 21 protects against cardiac hypertrophy in mice. *Nat Commun, 4*, 2019. doi: 10.1038/ncomms3019

Planavila, A., Redondo-Angulo, I., Ribas, F., Garrabou, G., Casademont, J., Giralt, M., & Villarroya, F. (2015). Fibroblast growth factor 21 protects the heart from oxidative stress. *Cardiovasc Res, 106*(1), 19-31. doi: 10.1093/cvr/cvu263

Plitzko, B., Havemeyer, A., Bork, B., Bittner, F., Mendel, R., & Clement, B. (2016). Defining the Role of the NADH-Cytochrome-b5 Reductase 3 in the Mitochondrial Amidoxime Reducing Component Enzyme System. *Drug Metab Dispos, 44*(10), 1617-1621. doi: 10.1124/dmd.116.071845

Poulton, J. (1995). Transmission of mtDNA: Cracks in the bottleneck. *Am J Hum Genet, 57*(2Number), 224-226.

Quiros, P. M., Prado, M. A., Zamboni, N., D'Amico, D., Williams, R. W., Finley, D., . . . Auwerx, J. (2017). Multi-omics analysis identifies ATF4 as a key regulator of the mitochondrial stress response in mammals. *J Cell Biol, 216*(7), 2027-2045. doi: 10.1083/jcb.201702058

Rabanal-Ruiz, Y., Otten, E. G., & Korolchuk, V. I. (2017). mTORC1 as the main gateway to autophagy. *Essays Biochem, 61*(6), 565-584. doi: 10.1042/EBC20170027

Rainbolt, T. K., Saunders, J. M., & Wiseman, R. L. (2015). YME1L degradation reduces mitochondrial proteolytic capacity during oxidative stress. *EMBO Rep, 16*(1), 97-106. doi: 10.15252/embr.201438976

Rainey, R. N., Glavin, J. D., Chen, H. W., French, S. W., Teitell, M. A., & Koehler, C. M. (2006). A new function in translocation for the mitochondrial i-AAA protease Yme1: import of polynucleotide phosphorylase into the intermembrane space. *Mol Cell Biol, 26*(22), 8488-8497. doi: 10.1128/MCB.01006-06

Reinecke, F., Smeitink, J. A., & van der Westhuizen, F. H. (2009). OXPHOS gene expression and control in mitochondrial disorders. *Biochim Biophys Acta, 1792*(12), 1113-1121. doi: 10.1016/j.bbadis.2009.04.003

Ricquier, D. (2005). Respiration uncoupling and metabolism in the control of energy expenditure. *Proc Nutr Soc, 64*(1), 47-52.

Ricquier, D. (2017). UCP1, the mitochondrial uncoupling protein of brown adipocyte: A personal contribution and a historical perspective. *Biochimie, 134*, 3-8. doi: 10.1016/j.biochi.2016.10.018

Riley, L. G., Cooper, S., Hickey, P., Rudinger-Thirion, J., McKenzie, M., Compton, A., . . . Christodoulou, J. Mutation of the mitochondrial tyrosyl-tRNA synthetase gene,

YARS2, causes myopathy, lactic acidosis, and sideroblastic anemia--MLASA syndrome. *Am J Hum Genet, 87*(1), 52-59. doi: S0002-9297(10)00304-6 [pii]
10.1016/j.ajhg.2010.06.001

Rivera, H., Martin-Hernandez, E., Delmiro, A., Garcia-Silva, M. T., Quijada-Fraile, P., Muley, R., . . . Martinez-Azorin, F. (2013). A new mutation in the gene encoding mitochondrial seryl-tRNA synthetase as a cause of HUPRA syndrome. *BMC Nephrol, 14*, 195. doi: 10.1186/1471-2369-14-195

Rose, G., Santoro, A., & Salvioli, S. (2017). Mitochondria and mitochondria-induced signalling molecules as longevity determinants. *Mech Ageing Dev, 165*(Pt B), 115-128. doi: 10.1016/j.mad.2016.12.002

Rotwein, P. (2017). Diversification of the insulin-like growth factor 1 gene in mammals. *PLoS One, 12*(12), e0189642. doi: 10.1371/journal.pone.0189642

Runkel, E. D., Liu, S., Baumeister, R., & Schulze, E. (2013). Surveillance-activated defenses block the ROS-induced mitochondrial unfolded protein response. *PLoS Genet, 9*(3), e1003346. doi: 10.1371/journal.pgen.1003346

Saito, T., Uchiumi, T., Yagi, M., Amamoto, R., Setoyama, D., Matsushima, Y., & Kang, D. (2017). Cardiomyocyte-specific loss of mitochondrial p32/C1qbp causes cardiomyopathy and activates stress responses. *Cardiovasc Res, 113*(10), 1173-1185. doi: 10.1093/cvr/cvx095

Salminen, A., Kaarniranta, K., & Kauppinen, A. (2017). Integrated stress response stimulates FGF21 expression: Systemic enhancer of longevity. *Cell Signal, 40*, 10-21. doi: 10.1016/j.cellsig.2017.08.009

Samms, R. J., Murphy, M., Fowler, M. J., Cooper, S., Emmerson, P., Coskun, T., . . . Tsintzas, K. (2015). Dual effects of fibroblast growth factor 21 on hepatic energy metabolism. *J Endocrinol, 227*(1), 37-47. doi: 10.1530/JOE-15-0334

Santos-Cortez, R. L., Lee, K., Azeem, Z., Antonellis, P. J., Pollock, L. M., Khan, S., . . . Leal, S. M. (2013). Mutations in KARS, encoding lysyl-tRNA synthetase, cause autosomal-recessive nonsyndromic hearing impairment DFNB89. *Am J Hum Genet, 93*(1), 132-140. doi: 10.1016/j.ajhg.2013.05.018

Sasarman, F., Nishimura, T., Thiffault, I., & Shoubridge, E. A. (2012). A novel mutation in YARS2 causes myopathy with lactic acidosis and sideroblastic anemia. *Hum Mutat, 33*(8), 1201-1206. doi: 10.1002/humu.22098

Schaap, F. G., Kremer, A. E., Lamers, W. H., Jansen, P. L., & Gaemers, I. C. (2013). Fibroblast growth factor 21 is induced by endoplasmic reticulum stress. *Biochimie, 95*(4), 692-699. doi: 10.1016/j.biochi.2012.10.019

Schagger, H., & Pfeiffer, K. (2000). Supercomplexes in the respiratory chains of yeast and mammalian mitochondria. *EMBO J, 19*(8), 1777-1783. doi: 10.1093/emboj/19.8.1777

Scheper, G. C., van der Klok, T., van Andel, R. J., van Berkel, C. G., Sissler, M., Smet, J., . . . van der Knaap, M. S. (2007). Mitochondrial aspartyl-tRNA synthetase deficiency causes leukoencephalopathy with brain stem and spinal cord involvement and lactate elevation. *Nat Genet, 39*(4), 534-539. doi: 10.1038/ng2013

Schwartz, M., & Vissing, J. (2002). Paternal inheritance of mitochondrial DNA. *N Engl J Med, 347*(8), 576-580.

Seburn, K. L., Nangle, L. A., Cox, G. A., Schimmel, P., & Burgess, R. W. (2006). An active dominant mutation of glycyl-tRNA synthetase causes neuropathy in a Charcot-Marie-Tooth 2D mouse model. *Neuron, 51*(6), 715-726. doi: 10.1016/j.neuron.2006.08.027

Seiferling, D., Szczepanowska, K., Becker, C., Senft, K., Hermans, S., Maiti, P., . . . Trifunovic, A. (2016). Loss of CLPP alleviates mitochondrial cardiomyopathy without affecting the mammalian UPRmt. *EMBO Rep, 17*(7), 953-964. doi: 10.15252/embr.201642077

Shatla, H. M., Tomoum, H. Y., Elsayed, S. M., Elagouza, I. A., Shatla, R. H., Mohsen, M. M., & Hamed, A. N. (2014). Role of plasma amino acids and urinary organic acids in diagnosis of mitochondrial diseases in children. *Pediatr Neurol, 51*(6), 820-825. doi: 10.1016/j.pediatrneurol.2014.08.009

Shore, D. E., Carr, C. E., & Ruvkun, G. (2012). Induction of cytoprotective pathways is central to the extension of lifespan conferred by multiple longevity pathways. *PLoS Genet, 8*(7), e1002792. doi: 10.1371/journal.pgen.1002792

Silva, J. P., Kohler, M., Graff, C., Oldfors, A., Magnuson, M. A., Berggren, P. O., & Larsson, N. G. (2000). Impaired insulin secretion and beta-cell loss in tissue-specific knockout mice with mitochondrial diabetes. *Nat. Genet., 26*(3Number), 336-340.

Smits, P., Smeitink, J., & van den Heuvel, L. (2010). Mitochondrial translation and beyond: processes implicated in combined oxidative phosphorylation deficiencies. *J Biomed Biotechnol, 2010*, 737385. doi: 10.1155/2010/737385

Spiegelman, B. M. (2007). Transcriptional control of energy homeostasis through the PGC1 coactivators. *Novartis Found Symp, 286*, 3-6; discusssion 6-12, 162-163, 196-203.

Steenweg, M. E., Ghezzi, D., Haack, T., Abbink, T. E., Martinelli, D., van Berkel, C. G., . . . Zeviani, M. (2012). Leukoencephalopathy with thalamus and brainstem involvement and high lactate 'LTBL' caused by EARS2 mutations. *Brain, 135*(Pt 5), 1387-1394. doi: aws070 [pii]
10.1093/brain/aws070

Suzuki, C.K., Suda, K., Wang, N., & Schatz, G. (1994). Requirement for the yeast gene LON in intramitochondrial proteolysis and maintenance of respiration. *Science, 264*(Number), 273-276.

Suzuki, M., Uehara, Y., Motomura-Matsuzaka, K., Oki, J., Koyama, Y., Kimura, M., . . . Imamura, T. (2008). betaKlotho is required for fibroblast growth factor (FGF) 21 signaling through FGF receptor (FGFR) 1c and FGFR3c. *Mol Endocrinol, 22*(4), 1006-1014. doi: 10.1210/me.2007-0313

Szczepanowska, K., Maiti, P., Kukat, A., Hofsetz, E., Nolte, H., Senft, K., . . . Trifunovic, A. (2016). CLPP coordinates mitoribosomal assembly through the regulation of ERAL1 levels. *EMBO J, 35*(23), 2566-2583. doi: 10.15252/embj.201694253

Taanman, J. W. (1999). The mitochondrial genome: structure, transcription, translation and replication. *Biochim Biophys Acta, 1410*(2), 103-123.

Takagi, M., Absalon, M. J., McLure, K. G., & Kastan, M. B. (2005). Regulation of p53 translation and induction after DNA damage by ribosomal protein L26 and nucleolin. *Cell, 123*(1), 49-63. doi: 10.1016/j.cell.2005.07.034

Tanajak, P., Chattipakorn, S. C., & Chattipakorn, N. (2015). Effects of fibroblast growth factor 21 on the heart. *J Endocrinol, 227*(2), R13-30. doi: 10.1530/JOE-15-0289

Tanaka, M., & Kido, Y. (2008). Serotonergic regulation of galanin-induced selective macronutrient intake in self-selecting rats. *J Med Invest, 55*(3-4), 196-203.

Tatsuta, T., & Langer, T. (2009). AAA proteases in mitochondria: diverse functions of membrane-bound proteolytic machines. *Res Microbiol, 160*(9), 711-717. doi: S0923-2508(09)00148-X [pii]
10.1016/j.resmic.2009.09.005

Teske, B. F., Fusakio, M. E., Zhou, D., Shan, J., McClintick, J. N., Kilberg, M. S., & Wek, R. C. (2013). CHOP induces activating transcription factor 5 (ATF5) to trigger apoptosis in response to perturbations in protein homeostasis. *Mol Biol Cell, 24*(15), 2477-2490. doi: 10.1091/mbc.E13-01-0067

Tezze, C., Romanello, V., Desbats, M. A., Fadini, G. P., Albiero, M., Favaro, G., . . . Sandri, M. (2017). Age-Associated Loss of OPA1 in Muscle Impacts Muscle Mass, Metabolic Homeostasis, Systemic Inflammation, and Epithelial Senescence. *Cell Metab, 25*(6), 1374-1389 e1376. doi: 10.1016/j.cmet.2017.04.021

Touvier, T., De Palma, C., Rigamonti, E., Scagliola, A., Incerti, E., Mazelin, L., . . . Brunelli, S. (2015). Muscle-specific Drp1 overexpression impairs skeletal muscle growth via translational attenuation. *Cell Death Dis, 6*, e1663. doi: 10.1038/cddis.2014.595

Trifunovic, A., Wredenberg, A., Falkenberg, M., Spelbrink, J.N., Rovio, A.T., Bruder, C.E., . . . Larsson, N.G. (2004). Premature ageing in mice expressing defective mitochondrial DNA polymerase. *Nature, 429*(Number), 417-423.

Tsukamoto, K., Mani, D. R., Shi, J., Zhang, S., Haagensen, D. E., Otsuka, F., . . . Krieger, M. (2013). Identification of apolipoprotein D as a cardioprotective gene using a mouse model of lethal atherosclerotic coronary artery disease. *Proc Natl Acad Sci U S A, 110*(42), 17023-17028. doi: 10.1073/pnas.1315986110

Tyynismaa, H., Carroll, C. J., Raimundo, N., Ahola-Erkkila, S., Wenz, T., Ruhanen, H., . . . Suomalainen, A. (2010). Mitochondrial myopathy induces a starvation-like response. *Hum Mol Genet, 19*(20), 3948-3958. doi: 10.1093/hmg/ddq310

Ulgherait, M., Rana, A., Rera, M., Graniel, J., & Walker, D. W. (2014). AMPK modulates tissue and organismal aging in a non-cell-autonomous manner. *Cell Rep, 8*(6), 1767-1780. doi: 10.1016/j.celrep.2014.08.006

van Berge, L., Dooves, S., van Berkel, C. G., Polder, E., van der Knaap, M. S., & Scheper, G. C. (2012). Leukoencephalopathy with brain stem and spinal cord involvement and lactate elevation is associated with cell-type-dependent splicing of mtAspRS mRNA. *Biochem J, 441*(3), 955-962. doi: 10.1042/BJ20110795

van Berge, L., Hamilton, E. M., Linnankivi, T., Uziel, G., Steenweg, M. E., Isohanni, P., . . . Group, Lbsl Research. (2014). Leukoencephalopathy with brainstem and spinal cord involvement and lactate elevation: clinical and genetic characterization and target for therapy. *Brain, 137*(Pt 4), 1019-1029. doi: 10.1093/brain/awu026

Vandanmagsar, B., Warfel, J. D., Wicks, S. E., Ghosh, S., Salbaum, J. M., Burk, D., . . . Mynatt, R. L. (2016). Impaired Mitochondrial Fat Oxidation Induces FGF21 in Muscle. *Cell Rep, 15*(8), 1686-1699. doi: 10.1016/j.celrep.2016.04.057

Vernia, S., Cavanagh-Kyros, J., Garcia-Haro, L., Sabio, G., Barrett, T., Jung, D. Y., . . . Davis, R. J. (2014). The PPARalpha-FGF21 hormone axis contributes to metabolic regulation by the hepatic JNK signaling pathway. *Cell Metab, 20*(3), 512-525. doi: 10.1016/j.cmet.2014.06.010

Vernochet, C., Mourier, A., Bezy, O., Macotela, Y., Boucher, J., Rardin, M. J., . . . Kahn, C. R. (2012). Adipose-specific deletion of TFAM increases mitochondrial oxidation and protects mice against obesity and insulin resistance. *Cell Metab, 16*(6), 765-776. doi: 10.1016/j.cmet.2012.10.016

Wall, C. E., Whyte, J., Suh, J. M., Fan, W., Collins, B., Liddle, C., . . . Evans, R. M. (2015). High-fat diet and FGF21 cooperatively promote aerobic thermogenesis in mtDNA mutator mice. *Proc Natl Acad Sci U S A, 112*(28), 8714-8719. doi: 10.1073/pnas.1509930112

Wallace, D. C. (2007). Why do we still have a maternally inherited mitochondrial DNA? Insights from evolutionary medicine. *Annu Rev Biochem, 76*, 781-821. doi: 10.1146/annurev.biochem.76.081205.150955

Wallace, D. C. (2009). Mitochondria, bioenergetics, and the epigenome in eukaryotic and human evolution. *Cold Spring Harb Symp Quant Biol, 74*, 383-393. doi: 10.1101/sqb.2009.74.031

Wallace, D.C. (1992). Mitochondrial genetics: a paradigm for aging and degenerative diseases? *Science, 256*(Number), 628-632.

Wallace, D.C. (1993). Mitochondrial diseases: genotype versus phenotype. *Trends Genet., 9*(4Number), 128-133.

Wang, C., Huang, Z., Du, Y., Cheng, Y., Chen, S., & Guo, F. (2010). ATF4 regulates lipid metabolism and thermogenesis. *Cell Res, 20*(2), 174-184. doi: 10.1038/cr.2010.4

Wang, H., Zhang, Q., Wen, Q., Zheng, Y., Lazarovici, P., Jiang, H., . . . Zheng, W. (2012). Proline-rich Akt substrate of 40kDa (PRAS40): a novel downstream target of PI3k/Akt signaling pathway. *Cell Signal, 24*(1), 17-24. doi: 10.1016/j.cellsig.2011.08.010

Wei, Z. B., Miao, X. Y., Yang, M. Q., & Luo, X. G. (2008). [Advances in the expression and regulation of MnSOD gene]. *Yi Chuan, 30*(7), 831-837.

Wells, T., Davies, J. R., Guschina, I. A., Ball, D. J., Davies, J. S., Davies, V. J., . . . Votruba, M. (2012). Opa3, a novel regulator of mitochondrial function, controls thermogenesis and abdominal fat mass in a mouse model for Costeff syndrome. *Hum Mol Genet, 21*(22), 4836-4844. doi: 10.1093/hmg/dds315

Wesolowska, M. T., Richter-Dennerlein, R., Lightowlers, R. N., & Chrzanowska-Lightowlers, Z. M. (2014). Overcoming stalled translation in human mitochondria. *Front Microbiol, 5*, 374. doi: 10.3389/fmicb.2014.00374

Wollert, K. C., & Kempf, T. (2012). Growth differentiation factor 15 in heart failure: an update. *Curr Heart Fail Rep, 9*(4), 337-345. doi: 10.1007/s11897-012-0113-9

Wredenberg, A., Freyer, C., Sandstrom, M. E., Katz, A., Wibom, R., Westerblad, H., & Larsson, N. G. (2006). Respiratory chain dysfunction in skeletal muscle does not cause insulin resistance. *Biochem Biophys Res Commun, 350*(1), 202-207. doi: 10.1016/j.bbrc.2006.09.029

Xu, Z., Sun, J., Tong, Q., Lin, Q., Qian, L., Park, Y., & Zheng, Y. (2016). The Role of ERK1/2 in the Development of Diabetic Cardiomyopathy. *Int J Mol Sci, 17*(12). doi: 10.3390/ijms17122001

Ye, J., Kumanova, M., Hart, L. S., Sloane, K., Zhang, H., De Panis, D. N., . . . Koumenis, C. (2010). The GCN2-ATF4 pathway is critical for tumour cell survival and proliferation in response to nutrient deprivation. *EMBO J, 29*(12), 2082-2096. doi: 10.1038/emboj.2010.81

Yin, F., Sancheti, H., & Cadenas, E. (2012). Silencing of nicotinamide nucleotide transhydrogenase impairs cellular redox homeostasis and energy metabolism in PC12 cells. *Biochim Biophys Acta, 1817*(3), 401-409. doi: 10.1016/j.bbabio.2011.12.004

Yoneda, T., Benedetti, C., Urano, F., Clark, S. G., Harding, H. P., & Ron, D. (2004). Compartment-specific perturbation of protein handling activates genes encoding mitochondrial chaperones. *J Cell Sci, 117*(Pt 18), 4055-4066. doi: 10.1242/jcs.01275
jcs.01275 [pii]

Yu, A. Y., & Houry, W. A. (2007). ClpP: a distinctive family of cylindrical energy-dependent serine proteases. *FEBS Lett, 581*(19), 3749-3757. doi: 10.1016/j.febslet.2007.04.076

Yun, J., & Finkel, T. (2014). Mitohormesis. *Cell Metab, 19*(5), 757-766. doi: 10.1016/j.cmet.2014.01.011

Zhang, C., Huang, Z., Gu, J., Yan, X., Lu, X., Zhou, S., . . . Li, X. (2015). Fibroblast growth factor 21 protects the heart from apoptosis in a diabetic mouse model via extracellular signal-regulated kinase 1/2-dependent signalling pathway. *Diabetologia, 58*(8), 1937-1948. doi: 10.1007/s00125-015-3630-8

Zhang, X., Ibrahimi, O. A., Olsen, S. K., Umemori, H., Mohammadi, M., & Ornitz, D. M. (2006). Receptor specificity of the fibroblast growth factor family. The complete mammalian FGF family. *J Biol Chem, 281*(23), 15694-15700. doi: 10.1074/jbc.M601252200

Zhang, Y., Xie, Y., Berglund, E. D., Coate, K. C., He, T. T., Katafuchi, T., . . . Mangelsdorf, D. J. (2012). The starvation hormone, fibroblast growth factor-21, extends lifespan in mice. *Elife, 1*, e00065. doi: 10.7554/eLife.00065

Zhao, Q., Wang, J., Levichkin, I. V., Stasinopoulos, S., Ryan, M. T., & Hoogenraad, N. J. (2002). A mitochondrial specific stress response in mammalian cells. *EMBO J, 21*(17), 4411-4419.

Zhu, Y., Pereira, R. O., O'Neill, B. T., Riehle, C., Ilkun, O., Wende, A. R., . . . Abel, E. D. (2013). Cardiac PI3K-Akt impairs insulin-stimulated glucose uptake independent of mTORC1 and GLUT4 translocation. *Mol Endocrinol, 27*(1), 172-184. doi: 10.1210/me.2012-1210

# Acknowledgement

This amaaaaazing piece of work would not be possible without support of many great people I encountered in the last 5 years, as well the ones from the last 29 years.

First, I want to thank to my science and non-science mentor, Sandra (Prof. Dr. Aleksandra Trifunovic). This, of course, would not be possible without You, but that is something everyone says to their PIs. So I really want to emphasize that You are not only a PI, but also a "life mentor" (sounds cheesy, I know), with a deep understanding of your students from 'Generation Y'.
Hvala mnogo na svemu!

Prof. Dr. Rudolf Wiesner, thank You for being a member of my thesis committee and moreover, I enjoyed nice talks with You during different mito-meetings.

Prof. Dr. Jan Riemer, thank You for being the chair of my thesis committee!

Also, thanks Marie Curie Network for the financial support during first 3 years and many opportunities to grow as a young scientist.

I want to thank the whole lab, which has changed so many times during these 5 years, but no matter what, the support was also there. Thank you, Lab (past and present)!
I would like to thank to Alex Kukat for being the 'co-pilot' in the whole experience, for many coffee-breaks and Thursday's lasagnas (which, by the way, we haven't done in a long time?!), walks and moreover, the friendship. <3
Even if they are not here, I wanna thank to Dominic, with whom I shared the best moments in the lab, also Victor, Anil and Steffen, as my first gang and mensa crew. They made me feel very welcome! Additonally, Estela, for being my 'spanish sister' and we could share enthusiasm for photography. And Tina, for being always around there and having patience for all my amateur questions!
Karolina, thank you, because you're just the best. Thanks for the high-end scientific support 24/7! If World Wide Web crashes one day, it won't matter if we still have you! Thanks for attending all my parties and being the coolest!

Thank you, Katha and Linda, for being the best support, and making everything go smoothly! Also, Marija, it is so nice to hear your laughter again in the lab! Thanks for nice talks and support as an “older sister” (bff).
Thank you, Sophie, for being such a good colleague and I am happy we shared our China experience together! Thank you, Hien, for being the mood-lifter, it’s nice to sit back to back to you. Thank you, Eddy, for the nice talks and travel tips! Thank you, Anastasia, Trinu, Sarah, Matthijs and all the past and present members for being great colleagues and good support!

Special thanks go out to my family, for the support and freedom they gave me. Thank you, Ilija, thank you, Olgica!
And last, but not the least, to my family of friends – Jelena (Kuzmonaut), for being simply the best and giving me the highest level of support during these last 5 years; Johanna, for making the Cologne experience feel like home; Tomas and Michi, for making me forget, when necessary; Svetlana, for the artistic stimulation (which is pretty much needed for the scientific career); Elisa, for being my Yugo family abroad; Ivona, for being my family at home; Doris, for being my ‘bro’ from the early beginnings; Stanka, for making me laugh so hard about everything; Daniel, for being my support through many years; my Mülheim gang, Tim and Tom, for making me bike 10 kms to get to you; my family from Berlin – Madza and Dragana and my Copenhagen sister, Popova – you’re just the coolest.
And actually, thank you Cologne, because I thought you and I were not a match, but now you feel like home.

# Erklärung

Ich versichere, dass ich die von mir vorgelegte Dissertation selbständig angefertigt, die benutzten Quellen und Hilfsmittel vollständig angegeben und die Stellen der Arbeit - einschließlich Tabellen, Karten und Abbildungen -, die anderen Werken im Wortlaut oder dem Sinn nach entnommen sind, in jedem Einzelfall als Entlehnung kenntlich gemacht habe; dass diese Dissertation noch keiner anderen Fakultät oder Universität zur Prüfung vorgelegen hat; dass sie - abgesehen von unten angegebenen Teilpublikationen - noch nicht veröffentlicht worden ist sowie, dass ich eine solche Veröffentlichung vor Abschluss des Promotionsverfahrens nicht vornehmen werde.

Die Bestimmungen der Promotionsordnung sind mir bekannt. Die von mir vorgelegte Dissertation ist von Prof. Dr. Aleksandra Trifunovic betreut worden.

Köln, November 2018.

---

Marijana Aradjanski

# Curriculum Vitae


| | |
|---|---|
| Name: | Marijana Aradjanski |
| Date of birth: | March 30, 1989 |
| Place of birth: | Kikinda, Republic of Serbia |
| Nationality: | Serbian |
| Passport nr.: | 007478332 |
| Address: | Vogelsangerstr. 171a50823 Cologne, Germany |
| Telephone: | +49 173 6492967 |
| E-mail: | Marijana049@gmail.com |


## EDUCATION

| | |
|---|---|
| Oct 2013–present | Doctoral studies at University of Cologne, Cluster of Excellencein Cellular Stress Responses in Aging-associated Diseases |
| 2012–2013 | Master studies of Human Molecular Biology, IMGGE, Belgrade |
| 2008–2012 | Studies at University of Belgrade, Faculty of Biology,Department of Molecular Biology and Physiology |
| 2004–2008 | Grammar School “Dusan Vasiljev”, Kikinda, SerbiaDepartment of Natural Sciences |
| 1998–2002 | Elementary Music School “Slobodan Malbaski”, Kikinda, SerbiaPiano Department |

## INTERNSHIPS

| | |
|---|---|
| Nov 2014–Jan 2015 | Center for Healthy Ageing, Copenhagen, DenmarkResearch area: DNA damage response, Cell Culture, Seahorse experiments |
| Sept 2012–Sept 2013 | Institute of Molecular Genetics and Genetic Engineering, BelgradeResearch Area: 3 prime end of prothrombin gene; SNP studiesTechniques: PCR, real-time PCR, Automatic Sequencing, Agarose Gel Electrophoresis, Polyacrilamide Gel Electrophoresis, SDS-PAGE, Western Blot, Cell Cultures |

## ACHIEVEMENTS

2013–2016 Marie Curie Fellowship, ITN, MARRIAGE program

2011–2013 Stipendium of Kikinda (given to best regional students)

2008–2013 Stipendium of Republic of Serbia (given to best University students)

2008–2009 Rotary Club Stipendium (given to best pre-University students in Serbia)

## INTERNATIONAL MEETINGS

2017 – short talk at Cold Spring Harbor conference "Mitochondria", Suzhou, China

2015 – short talk at Copenhagen University meeting "Mitochondrial Physiology"

## PUBLICATIONS

DARS2 protects against neuroinflammation and apoptotic neuronal loss, but is dispensable for myelinproducing cells.**Aradjanski M**, Dogan SA, Lotter S, Wang S, Hermans S,, Wibom R, Rugarli E, Trifunovic AHum Mol Genet. 2017 Nov 1;26(21):4181-4189. doi: 10.1093/hmg/ddx307.

The 3' end prothrombin gene variants in serbian patients with idiopathic thrombophilia.**Aradjanski M**, Djordjevic V, Pruner I, Tomic B, Gvozdenov M, Kovac M, Radojkovic D.Balkan J Med Genet. 2015 Apr 10;17(2):43-8. doi: 10.2478/bjmg-2014-0073. eCollection 2014 Dec.

Prothrombin 3'end gene variants in isolated pulmonary embolism--the first report ofFIIc.*64_*66del and FIIc.*303T>C variants. Gvozdenov M, Pruner I, Tomic B, **Aradjanski M**, Antonijevic N, Radojkovic D, Djordjevic V. Acta Cardiol. 2015 Apr;70(2):177-82.

Can We Accurately Model Mitochondrial Dysfunction in Neurodegeneration? **Aradjanski M** and Trifunovic "A Mitochondrial Dysfunction in Neurodegenerative Disorders" pp 303-328 |

*Human Molecular Genetics*, 2017, Vol. 26, No. 21 4181–4189

**doi: 10.1093/hmg/ddx307**
Advance Access Publication Date: 3 August 2017
Original Article

ORIGINAL ARTICLE

# DARS2 protects against neuroinflammation and apoptotic neuronal loss, but is dispensable for myelin producing cells

Marijana Aradjanski[1,2], Sukru Anil Dogan[1,2], Stephan Lotter[1], Shuaiyu Wang[2,3], Steffen Hermans[1,2], Rolf Wibom[4], Elena Rugarli[2,3,5] and Aleksandra Trifunovic[1,2,5,*]

[1]Institute for Mitochondrial Diseases and Aging, Medical Faculty, University of Cologne, 50931 Cologne, Germany, [2]Cologne Excellence Cluster on Cellular Stress Responses in Aging-Associated Diseases (CECAD), University of Cologne, 50931 Cologne, Germany, [3]Institute for Genetics, University of Cologne, 50674 Cologne, Germany, [4]Department of Medical Biochemistry and Biophysics, Karolinska Institute, 17177 Stockholm, Sweden and [5]Center for Molecular Medicine (CMMC), University of Cologne, 50931 Cologne, Germany

*To whom correspondence should be addressed. Tel:+49 221 478-84291; Email: aleksandra.trifunovic@uk-koeln.de



## Abstract

Although mitochondria are ubiquitous, each mitochondrial disease has surprisingly distinctly different pattern of tissue and organ involvement. Congruently, mutations in genes encoding for different mitochondrial tRNA synthetases result in the development of a very flamboyant group of diseases. Mutations in some of these genes, including aspartyl-tRNA synthetase (*DARS2*), lead to the onset of a white matter disease—leukoencephalopathy with brainstem and spinal cord involvement, and lactate elevation (LBSL) characterized by progressive spastic ataxia and characteristic leukoencephalopathy signature with multiple long-tract involvements. Puzzled by the white matter disease phenotypes caused by DARS2 deficiency when numerous other mutations in the genes encoding proteins involved in mitochondrial translation have a detrimental effect predominantly on neurons, we generated transgenic mice in which DARS2 was specifically depleted in forebrain-hippocampal neurons or myelin-producing cells. Our results now provide the first evidence that loss of DARS2 in adult neurons leads to strong mitochondrial dysfunction and progressive loss of cells. In contrast, myelin-producing cells seem to be resistant to cell death induced by DARS2 depletion despite robust respiratory chain deficiency arguing that LBSL might originate from the primary neuronal and axonal defect. Remarkably, our results also suggest a role for early neuroinflammation in the disease progression, highlighting the possibility for therapeutic interventions of this process.

## Introduction

Although mitochondrial diseases are often multisystemic, brain and muscle are the most commonly affected tissues. Central nervous system (CNS) involvement in mitochondrial disorders is clinically heterogeneous, manifesting as epilepsy, stroke-like episodes, migraine, ataxia, spasticity, extrapyramidal or hypophysial abnormalities, bulbar dysfunction, psychiatric abnormalities or neuropsychological deficits. Leucoencephalopathy has also been added to this long list of symptoms (1). Leucoencephalopathy with brain stem and spinal cord involvement and high brain lactate (LBSL) is a childhood or juvenile-onset disorder clinically characterized by

**Received:** April 28, 2017. **Revised:** July 25, 2017. **Accepted:** July 26, 2017

slowly progressive cerebellar ataxia and spasticity with dorsal column dysfunction (2). LBSL is defined by a characteristic magnetic resonance imaging showing signal abnormalities in the cerebral white matter, specific brain stem and spinal cord tracts. Additionally, there are spectroscopic findings of increased lactate in the abnormal white matter in almost all affected individuals (1–3).

LBSL is caused by recessive mutations in the *DARS2* gene, which encodes the mitochondrial aspartyl-tRNA synthetase (1). DARS2 belongs to the group of mitochondrial tRNA synthases (mtARSs), which differ from their cytoplasmic counterparts (4). These enzymes are responsible for the first step in mitochondrial protein synthesis that involves covalently attaching an amino acid to its cognate tRNA in a process referred to as tRNA charging or loading (4). How mutations in this ubiquitously expressed gene cause a disorder in which tracts of the central and peripheral nervous systems (PNS) are selectively affected is unexplained. An increased number of patients with DARS2 mutations indicates that the phenotypic spectrum in LBSL is much wider than originally assumed. Adult-onset oligosymptomatic cases were described as well as patients with infantile onset, rapid neurological deterioration and early demise (5). Almost all patients are compound heterozygous for different *DARS2* mutations of which one is almost invariably a splice site mutation in intron 2, upstream of exon 3 (1). As a consequence, exon 3 is not included in the messenger RNA, leading to a frameshift, premature stop and absence of a functional protein (6). Other mutations in DARS2 include deletions, non-sense, missense and splice site mutations, for which very little, if any, molecular data are available. More recently, another white matter disease characterized by hypomyelination (HBSL—hypomyelination with brain stem and spinal cord involvement) has been associated with the mutations in *DARS2* gene (7). Intriguingly, a majority of other mitochondrial diseases caused by mutations that disrupt mitochondrial protein synthesis usually lead to syndromes with devastating consequences in neurons, while *DARS2* mutations leading to LBSL or HBSL suggest a primary defect in white matter (1,7). To shed more light on this important question, we generated transgenic mice in which DARS2 was specifically depleted in forebrain-hippocampal neurons or myelin-producing cells.

Our analysis revealed that loss of DARS2 in adult neurons leads to strong mitochondrial dysfunction accompanied by an early inflammation response and progressive loss of cells. Remarkably, DARS2 deficiency in adult myelin-producing cells, despite clear signs of high level of mitochondrial dysfunction, had no effect on survival, inflammatory response or myelination.

## Results and Discussion

We recently demonstrated that DARS2 is an essential protein needed for early mammalian development, as depletion of DARS2 in the whole body leads to lethality around the time of organogenesis (8). To analyse the role of DARS2 in diverse neural cell types, we generated two different models where conditional *Dars2* mice ($Dars2^{fl/fl}$) were bred with mice that postnatally express the Cre recombinase specifically in neurons or in myelin producing cells. Neuron-specific DARS2-deficient mice were obtained by mating $Dars2^{fl/fl}$ to mice expressing *Cre* recombinase under the calcium/calmodulin-dependent kinase II alpha promoter (*CaMKIIα-Cre*) resulting in $Dars2^{fl/fl}$; *CaMKIIα-Cre* mice (referred to as $Dars2^{NEKO}$ mice). In this model, *Cre* recombinase is active in forebrain, hippocampus and striatum neurons from postnatal Day 14, with maximal recombination at postnatal Day 29 (9). To deplete DARS2 in myelin-producing cells, we used mice that express *Cre* recombinase under the control of the tamoxifen-inducible proteolipid 1 promoter (*Plp1-CreERT*), which allows temporal control of the recombination (10). The resulting $Dars2^{fl/fl}$; *Plp-CreERT* animals (referred to as $Dars2^{MYKO}$ mice) were injected intraperitoneally with tamoxifen for five consecutive days at 4 weeks of age. Recently, we demonstrated high sensitivity and specificity of the Cre expression in oligodendrocytes using this protocol, after crossing *Plp1-CreERT* mice with a reporter transgenic line expressing a floxed, mitochondrially targeted YFP ($ROSA26^{+/SmY}$) (11). Using this specific timing for the activation of Cre-mediated recombination in PLP positive cells, we ensured that DARS2 depletion occurs at about the same time in both models.

### Progressive degeneration of cortex and hippocampus owing to massive cell loss observed in $DARS2^{NEKO}$ mice

Initially, we followed the development of phenotypes by monitoring the growth curves in both transgenic lines. We did not observe any change in the growth curves of $Dars2^{MYKO}$ mice, while $Dars2^{NEKO}$ animals had a lower weight gain already at the time of weaning, and this became more prominent around 15 weeks of age (Supplementary Material, Fig. S1A). The gross morphology and weight of $Dars2^{NEKO}$ brains did not change until around 24-26 weeks of age when obvious loss of brain mass occurred, with a strong atrophy of the forebrain (Fig. 1A). Early on, most mice showed no obvious behavioral abnormalities, but around 27-28 weeks of age some mice started scratching their necks and faces, resulting in self-inflicted wounds, at which point mice had to be sacrificed (Supplementary Material, Fig. S1B). In the rest of $Dars2^{NEKO}$ cohort, progressive nature of the phenotype led to a shorter lifespan of up to 32-34 weeks of age. In contrast, neither changes in gross appearance, body weight nor behavior in $Dars2^{MYKO}$ mice were observed (up until 80 weeks of age when the mice were terminated).

In agreement with previous results, no clear change in structure, morphology and size of $Dars2^{NEKO}$ cortex and hippocampus was observed at 20 weeks of age. However, a significant decrease of the cortical thickness was detected at 28 weeks of age, accompanied by an apparent decrease in mean hippocampal area (Fig. 1B and C). Curiously, the number of cells within cortical and hippocampal area seemed increased (Fig. 1B), suggesting that a progressive atrophy is accompanied by cellular infiltration, most likely caused by an immune response. Conversely, a number of neurons within the stratum granulosum of the dentate gyrus (DG) or parts of the stratum pyramidale of the cornu ammonis (primarily CA1 and CA2) was prominently reduced in 28-week-old $Dars2^{NEKO}$ mice (Supplementary Material, Fig. S1C and D). An increasing level of pyknotic cells with clear signs of chromatin condensation suggested an irreversible state of heading into cell death (Supplementary Material, Fig. S1C and E). Vacuolar lesions in the same brain regions of the 28-week-old $Dars2^{NEKO}$ mice further implied cell loss (Supplementary Material, Fig. S1C–E). Transmission electron microscopy of the hippocampus area in the 28-week-old $Dars2^{NEKO}$ brain revealed less dense mitochondria that presented an apparent loss of lamellar-shaped cristae as a clear sign of mitochondrial dysfunction in these cells (Fig. 1D).

Next, we used the TUNEL assay to detect nuclear DNA fragmentation, a hallmark of cells undergoing apoptosis. A massive increase in apoptosis occurred at 20 weeks of age (Fig. 2A and B; Supplementary Material, Fig. S2), although at this time no apparent morphological changes were detected in the same brain regions (Fig. 1B). Remarkably, apoptotic cells in distinct brain regions seem to appear at different dynamics; neurons in the

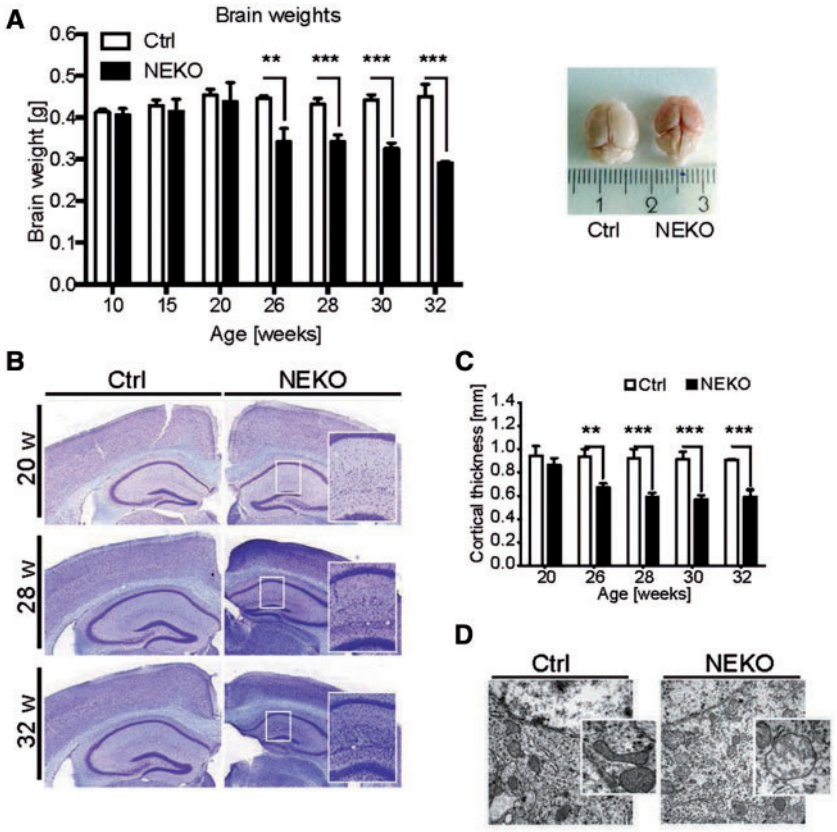


**Figure 1.** Analyses of cortex and hippocampus degeneration in control (Ctrl) and *Dars2*$^{NEKO}$ (NEKO) mice. (**A**) Brain weights of Ctrl and NEKO mice at the indicated age; representative photographs of isolated brains from both knockout and control mice at the indicated age. Bars present mean levels±SD. Statistical difference was calculated by Student's *t*-test; $^{**}P<0.005$, $^{***}P<0.001$ ($n=3-5$). (**B**) Representative Nissl staining (Scale bars: 500 μm) of hippocampal regions of Ctrl and NEKO mice at indicated age. Close-ups are for the indicated areas. (**C**) Quantification of brain cortical thickness [mm] at the indicated age in Ctrl and NEKO mice; bars represent mean levels ±SD. Statistical difference was calculated by Student's *t*-test; $^{**}P<0.005$, $^{***}P<0.001$ ($n=3$–5). (**D**) Representative transmission electron micrographs (Scale bar: 0.5 μm) of Ctrl and NEKO 29-week-old mice.

second and third cortical layer of retrosplenial area (RS) undergo considerable apoptosis only around 20 weeks of age, while in the rest of the cortex massive apoptotic cell death is observed until 26 weeks of age (Fig. 2A and B; Supplementary Material, Fig. S2). At 28 weeks of age, almost no TUNEL-positive nuclei could be observed, suggesting that the majority of them had already been lost (Fig. 2A and B; Supplementary Material, Fig. S2).

In general, cortical neurons seem to be more vulnerable to the loss of DARS2 and mitochondrial translation than hippocampal neurons (Fig. 2A and 2C). The hippocampal CA1 region displayed a high occurrence of progressive apoptotic cells with increased age, while in the DG region, despite having a large number of COX deficient cells, only a few neurons seemed to undergo apoptosis. The variances in the cell death dynamics might be a result of differences in neuronal types and physiology, and therefore their reliance on mitochondrial respiratory function. Indeed, selective neuronal vulnerability to oxidative stress (12), Parkinson's disease (13) or Alzheimer's disease (14) was previously described suggesting distinctive metabolic profiles in different brain regions.

## Strong mitochondrial deficiency and neuroinflammation precede loss of DARS2-deficient neurons

Severe respiratory chain deficiency was observed already at 15 weeks of age, and reached its peak in 20 weeks old *Dars2*$^{NEKO}$ brains (Fig. 3A). The number of COX deficient cells markedly decreased from 24 weeks on, likely owing to the massive apoptosis of DARS2-deficient cells (Fig. 2A). As a result, 28-week-old brains had almost no COX(−)SDH(+) (Complex IV deficient/Complex II positive cells), but a severely reduced cortex. It also became apparent that, instead of cell bodies, *Dars2*$^{NEKO}$ mice had holes throughout the hippocampus and cortex area (Fig. 3A). Analysis of mitochondrial respiratory chain (MRC) enzyme activities in neocortical samples demonstrated decreased activities of complexes containing critical mitochondrial DNA (mtDNA)-encoded subunits, in 28-week-old *Dars2*$^{NEKO}$ mice (Fig. 3B). The observed alterations in the MRC levels and enzyme activities matched the reduction in the amount of fully assembled complex I (C I) and IV (C IV—COX) in *Dars2*$^{NEKO}$ mice (Fig. 3C). The F1 subcomplex of complex V (C V) was also detected in *Dars2*$^{NEKO}$ mitochondria, implying a defect in mitochondrial protein synthesis, as previously reported (8,15,16). Remarkably, at 28 weeks of age, mitochondrial *de novo* protein synthesis in *Dars2*$^{NEKO}$ cortex appeared better than at 22 weeks of age (Fig. 3D). This is likely owing to vast loss of DARS2-deficient cells at 28 weeks, hence the majority of mitochondria in these samples stems from other cell types, unaffected by Cre-mediated deletion of *Dars2*.

The essential role of the OXPHOS function in neurons has been previously demonstrated in other mouse models. Tissue-specific depletion of *Tfam* in forebrain and hippocampus neurons (*Tfam*$^{L/L}$; *CamKIIα-Cre*) guided the reduction of mtDNA levels and

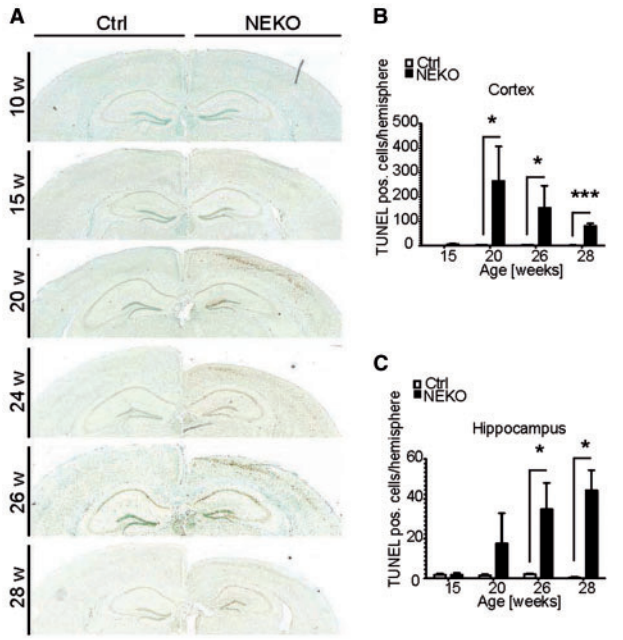


**Figure 2.** Apoptotic cell death in cortical and hippocampal regions in control (Ctrl) and *Dars2*$^{NEKO}$ (NEKO) mice. (**A**) Representative TUNEL staining of brain hemispheres (cortex and hippocampus regions) in Ctrl and NEKO mice at the indicated age. (**B**, **C**) Quantification of TUNEL positive cells per hemisphere in the region of cortex (B) and hippocampus (C) at the indicated age in Ctrl and NEKO mice. Bars present mean levels ±SD. Statistical difference was calculated by Student's *t*-test; *$P<0.05$, ***$P<0.001$ ($n=3$).

strong respiratory chain deficiency from four months of age, resulting in a severe, progressive neurodegeneration and massive apoptosis (17). A complete loss of the complex I (C I) NDUFS4 subunit (*Ndufs4*$^{-/-}$) resulted primarily in a CNS defect and rapid development of a Leigh-like phenotype characterized by ataxia, blindness, retarded growth rate, lethargy and increased serum lactate, leading to premature death at about 7 weeks of age (18). Similarly, depletion of *Cox10* in neurons (*Cox10*$^{L/L}$; *CaMKIIα-Cre*) rendered them respiratory-deficient already at 2 months of age in both the cortex and hippocampus areas, while the neurodegenerative phenotype progressed slowly until the ages of 8 and 12 months when the mice die (19,20). Typically, there is a time lag between the occurrence of OXPHOS deficiency and onset of neurodegeneration (17,20), during which neurons seems to compensate for the disruption of oxidative phosphorylation. Increased glycolysis and support from other cell types have been proposed to account for this (21). However, here we show that DARS2 depletion in neurons leads to a respiratory chain deficiency around 15 weeks of age that quickly culminates in the occurrence of massive cell death at 20 weeks, resulting in a severe brain atrophy (30% loss) within the next four weeks. Therefore, if existing, compensatory ATP supplementation by other cell types seems to be insufficient to maintain neuronal function for prolonged time periods in *Dars2*$^{NEKO}$ mice.

In agreement with a strong OXPHOS defect and disturbed mitochondrial protein synthesis, increased levels of mitochondrial HSP70 chaperone and LONP1 protease were detected, suggesting higher activation of mitochondrial stress responses, possibly mitochondrial unfolded protein response (UPRmt), in 20-week-old *Dars2*$^{NEKO}$ animals (Supplementary Material, Fig. S3A). Increased mitochondrial biogenesis might also contribute to the observed change, as suggested by higher SDH levels (Fig. 3C). Remarkably, the increase was statistically significant only in the hippocampus, possibly owing to a higher number of cells other than neurons in the isolated cortex samples (Supplementary Material, Fig. S3B and C).

Neuronal degeneration frequently leads to a local change in physiological conditions that in turn promotes an inflammatory response and activation of microglia, which are the resident immune cells of the nervous system. Indeed, we detected high levels of activated microglia in the cortical and hippocampal regions of *Dars2*$^{NEKO}$ mice, starting from 15 weeks of age (Fig. 4A). The number of infiltrated microglia in the hippocampal CA1 and DG regions dramatically increased with age, with an almost complete loss of recognizable structure at 32 weeks (Fig. 4A and Supplementary Material, Fig. S4A). On the contrary, the level of activated microglia in the cortex (SC and RS) peaked at 20 weeks (Fig. 4A and Supplementary Material, Fig. S4A), coinciding with the highest levels of OXPHOS deficiency observed in these *Dars2*$^{NEKO}$ brains. The decline of reactive microgliosis over time coincides with a more robust, apoptotic neuronal loss in the cortex layers than observed in the hippocampus (Fig. 4A and 2A). Reactive astrocytes were increasingly detected from 15 weeks of age in both, cortex and hippocampal region of *Dars2*$^{NEKO}$ mice, further emphasizing the presence of a neuroinflammatory response (Fig. 4B and Supplementary Material, Fig. S4B). The highest level of GFAP positive cells was observed around 20 weeks, and was persistently present until the end of the lifespan at around 32 weeks (Fig. 4B and Supplementary Material, Fig. S4B).

Certainly, neuroinflammation is increasingly recognized as a contribution to processes underlying neurodegeneration. Primarily activated in response to diseases, toxins or mechanical injury, neuroinflammation is strongly associated with demyelinating diseases (22). It is now clear that the microgliosis and astrogliosis primarily intended to clear up debris and support neurons in distress, when chronically activated, can convert from a beneficial program into a cytotoxic insult promoting neuronal death (22). This might be one of the mechanisms to explain the abrupt worsening of the *Dars2*$^{NEKO}$ phenotype after 20 weeks of age when we could observe massive micro- and astrogliosis.

Remarkably, activated microglia were detected in both the cortex and hippocampus already at 15 weeks of age before any cell death could be observed, suggesting that respiratory-deficient cells emit specific signals leading to activation of neuroinflammatory processes. We previously showed that DARS2 depletion in heart and skeletal muscle leads to accumulation of unfolded/misfolded proteins that serve as the first signal causing activation of stress signals and systemic changes in metabolism (8). It is tempting to speculate that the buildup of unfolded and/or unassembled respiratory chain subunits owing to the DARS2 depletion, and therefore imbalanced mitochondrial *de novo* protein synthesis acts as an early signal for the cell autonomous activation of stress responses, which might also trigger neuroinflammatory response. This would be in agreement with previous studies where the activation of microglia coincided with the accumulation of misfolded proteins in Alzheimer's disease, amyloid lateral sclerosis or Huntington's disease (23).

## DARS2 depletion in myelin-producing cells does not affect the number of oligodendrocytes nor myelin production, despite strong OXPHOS deficiency

In agreement with our initial observation, DARS2 depletion in adult myelin producing cells (*Dars2*$^{MYKO}$ mice) did not affect cell

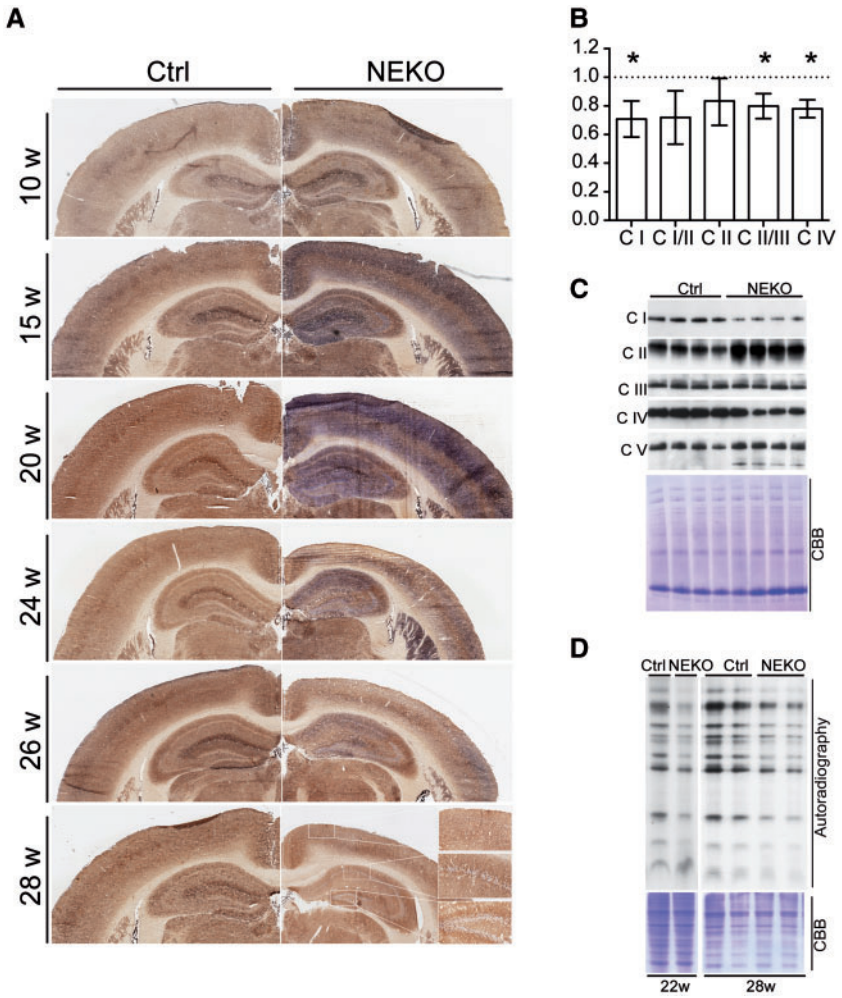


**Figure 3.** Characterization of mitochondrial function in control (Ctrl) and *Dars2*$^{NEKO}$ (NEKO) mice. (**A**) COX-SDH staining of brain hemispheres (cortex and hippocampus region) in Ctrl and NEKO mice at the indicated age. (**B**) Relative MRC complex activities in isolated cortex mitochondria of Ctrl and NEKO mice at 28 weeks of age. Bars present mean levels ±SD. Statistical difference was calculated by Student's *t*-test; *$P<0.05$ ($n=3$). (**C**) Western blots for OXPHOS complexes (with indicated position of specific complexes) and representative Coomassie Brilliant Blue (CBB) stained BN-PAGE gel in cortex mitochondria from 28-week-old Ctrl and NEKO mice. (**D**) Representative gel of *in organello* translation of 22- and 28-week-old Ctrl and NEKO mice cortex mitochondria. CBB stained gel used as loading control.

survival and therefore cell numbers at either 18 or 28 weeks (Supplementary Material, Fig. S5A). Moreover, the level of myelin basic protein, which is one of the most abundant proteins in myelin sheaths, was unchanged in *Dars2*$^{MYKO}$ mice (Supplementary Material, Fig. S5B). We also analyzed myelination in the PNS and found no difference in the thickness of myelin sheaths or appearance of Schwann cells (myelin producing cells in PNS) on both sciatic nerve and spinal cord (Supplementary Material, Fig. S5C).

Puzzled by the initial results, we wondered if DARS2 depletion causes respiratory chain deficiency in myelin producing cells as observed in neurons. Therefore, we analyzed OXPHOS function, again turning to COX-SDH staining. A large number of COX-deficient cells were detected in the striatum of *Dars2*$^{MYKO}$ mice, indicating the presence of strong OXPHOS deficiency (Fig. 5A). In the corpus callosum, the largest white matter structure in the brain, we detected COX-deficient oligodendrocytes in *Dars2*$^{MYKO}$ mice, and in agreement with results on PNS, no changes in the myelination (Fig. 5C). Furthermore, a very prominent stream of OXPHOS deficient axons could be detected in 15-week-old *Dars2*$^{NEKO}$ mice (Fig. 5B), which, remarkably, also did not affect the myelination of the corpus callosum (Fig. 5C and D).

DARS2 deficiency in forebrain and hippocampal neurons induced strong OXPHOS deficiency and neuroinflammatory response (Fig. 4 and Supplementary Material, Fig. S4). Despite clear evidence of strong OXPHOS deficiency in oligodendrocytes, no signs of neuroinflammatory response were detected in *Dars2*$^{MYKO}$ mice (Supplementary Material, Fig. S6).

Finally, using simple composite phenotype scoring system we tested to what extent DARS2 depletion affects motor skills in our two models (24). In accordance with previous results, *Dars2*$^{MYKO}$ mice did not show any signs of motor dysfunction (Fig. 5E). In contrast, DARS2 deficiency in neurons led to progressive loss of motor skills characterized by tremor, ataxia and age-dependent kyphosis (Fig. 5E).

Our results demonstrate that DARS2 deficiency in forebrain and hippocampal neurons leads to devastating cell death and severe neurodegeneration preceded by an early neuroinflammatory response (Supplementary Material, Fig. S7). The loss of DARS2 in oligodendrocytes, despite leading to strong respiratory deficiency, does not trigger any of these responses on either a

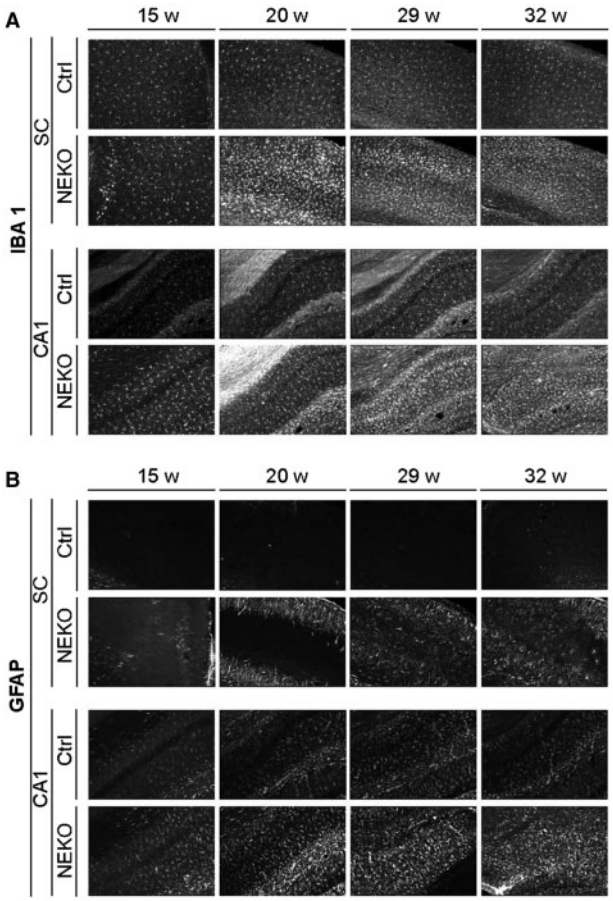


**Figure 4.** Neuroinflammatory processes in cortical and hippocampal areas of control (Ctrl) and *Dars2*$^{NEKO}$ (NEKO) mice. (**A** and **B**) Representative immunofluorescence merged Z-stack images of IBA1 positive microglia (A) and GFAP positive astrocytes (B) in somatosensory cortex (SC) and the hippocampal CA1 region in Ctrl and NEKO mice of the indicated age.

cellular or physiological level (Supplementary Material, Fig. S7). Remarkably, a recent study showed that the most common DARS2 patient mutation, located in a splice-site of intron 2, has the strongest effect causing exon 3 exclusion in neuronal cell lines (6). Therefore, it is tempting to conclude that LBSL in *DARS2* patients is a consequence of a primary neuronal deficiency, as neurons seems to be more affected with the splice-site mutation and here we show that they are also much more sensitive to a *Dars2* depletion than myelin producing cells. However, one has to keep in mind that our models induce the post-natal ablation of *DARS2*, whereas LBSL is typically owing to a hypomorphic allele which partially impairs the function of DARS2 throughout the embryonic and brain development. Therefore, a detrimental role of the mutation during oligodendrocyte-mediated myelinization of the developing brain cannot be excluded in the pathogenesis of the disease.

This is in agreement with a study showing that the most common DARS2 patient mutation located in a splice-site of intron 2, has the strongest effect causing exon 3 exclusion in neuronal cell lines (6).

Why would these two cell types react so differently to the loss of respiratory chain function? A different metabolic profile of adult oligodendrocytes and Schwann cells, enabling them to survive primarily using glycolysis for energy production when mitochondrial respiration is impaired, might be the main reason. In support of this hypothesis, Schwann-cell-specific depletion of Tfam (*Tfam*$^{L/L}$, *P*$_0$*-Cre*), the mitochondrial transcription factor A gene, which is essential for mtDNA transcription and maintenance, did not affect cell proliferation or survival, despite severe mtDNA depletion and respiratory chain abnormalities (25). Oligodendrocyte-specific deletion of *Cox10* (*Cox10*$^{L/L}$*; Cnp1-Cre*), an essential assembly factor for complex IV, also did not lead to axonal degeneration, demyelination or cell death (26). In fact, recent data suggest that oligodendrocytes' mitochondria may be essential for specialized functions relevant for myelin maintenance, such as lipid synthesis or fatty acid oxidation, rather than for ATP production (27). In agreement with this idea, a complete ablation of the m-AAA protease using the same promoter and Cre-induction paradigm as in this study (*Afg3l1*$^{-/-}$*; Afg3l2*$^{L/L}$*; Plp1-Cre*) resulted in progressive motor dysfunction and demyelination, owing to rapid oligodendrocyte cell death (11). In light of our results, this suggests that the imbalance of m-AAA protease substrates, other than the ones related to respiratory chain function, is detrimental for the myelin-producing cells of the central and PNS (11).

In summary, we provide strong *in vivo* evidence in support of the hypothesis that *Dars2* dysfunction, causing LBSL through disturbances in the white matter of both central and PNS, arises from a primary neuronal or axonal deficiency and not from a defect of myelin-producing cells. Remarkably, our results also highlighted neuroinflammatory processes, which coincide with respiratory chain deficiency and precede neuronal cell loss as possible yet unexplored targets of therapeutic interventions in LBSL and potentially other mitochondrial diseases.

## Experimental Procedures

### Generation of *Dars2* mice

Forebrain-specific DARS2-deficient mice (NEKO) were generated by mating Dars2$^{loxP/loxP}$ animals with transgenic mice expressing Cre recombinase under the control of CaMKII$\alpha$ promoter (9). MPC-specific DARS2-deficient mice (MYKO) were created also by using Dars2$^{loxP/loxP}$ animals, mated with mice containing Plp1 driven CreER recombinase (10), whereas the activation of recombination was done by application of tamoxifen. Tamoxifen (T5648, Sigma) was dissolved in a corn oil/ethanol (9:1) mixture at a final concentration of 10 mg/ml. A total of 1 mg tamoxifen was administrated by intraperitoneal injection once a day for five consecutive days to 4 weeks old mice. All genotypes were acquired by PCR. Animal protocols were in accordance with guidelines for humane treatment of animals and were reviewed by the Animal Ethics Committee of the Nord-Rheine Westphalia, Germany.

### Histological analysis

Mice were anesthetized with the combination of ketamine/xylazine, given intraperitoneally. Perfusion was performed intracardially with phosphate buffered saline (PBS) followed by 4% paraformaldehyde (PFA) in 0.1 M PBS (pH 7.4). Isolated brains were post-fixed in 4% PFA at 4 °C (for transmission electron microscopy analysis, post-fixed in 2% glutaraldehyde at 4 °C) overnight and then stored at 4 °C in 0.05% sodium azide-PBS ($NaN_3$-PBS) until further analysis. After perfusion, coronal sections were cut on Leica VT1200S with a thickness of 30–40 µm. Free floating sections were kept at 4 °C in 0.05% $NaN_3$-PBS.

For cryostat sections, freshly isolated brains were directly embedded in Tissue-Tek (Sakura) and frozen using dry ice.

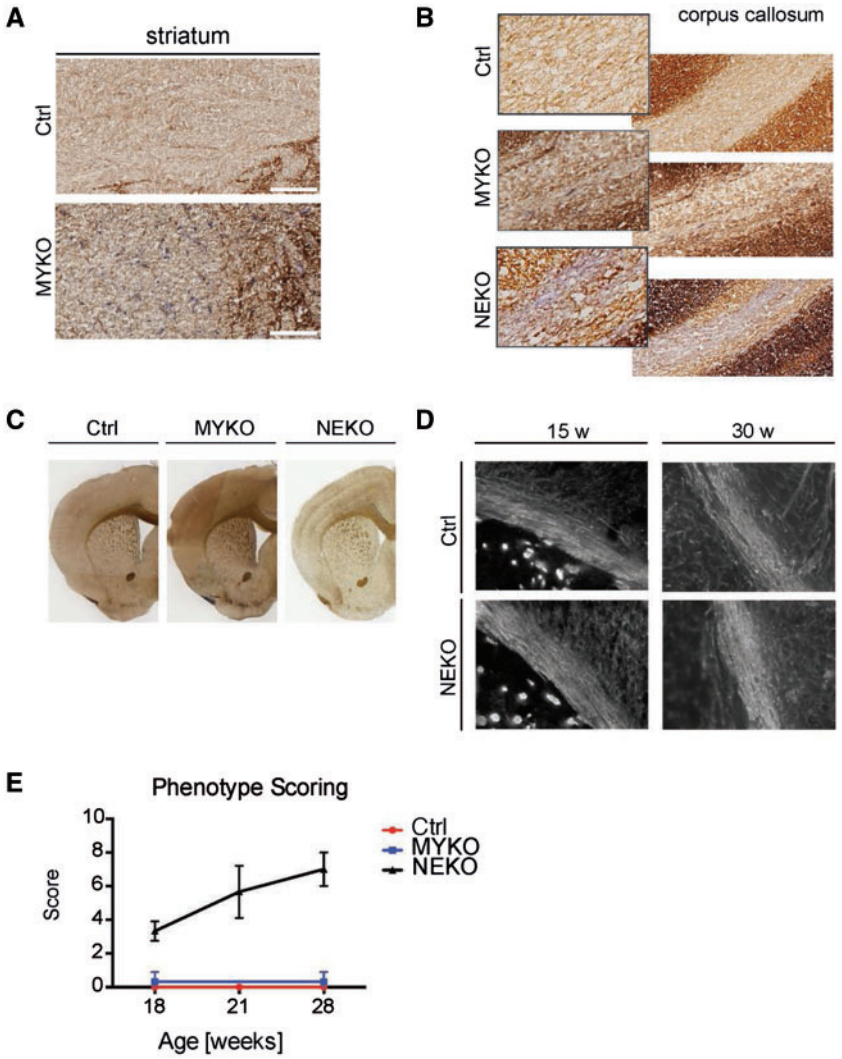


**Figure 5.** Characterization of mitochondrial function in control (Ctrl) and *Dars2* $^{MYKO}$ (MYKO) mice. (**A**) Representative COX-SDH staining of brain striatum in Ctrl and MYKO mice at 18 weeks of age (Scale bars, 100 μm). (**B**) Representative COX-SDH staining of corpus callosum with the close-ups in NEKO and MYKO mice at 18 weeks of age. (**C**) Representative images of Gallyas' myelin staining of the brain in 28-week-old Ctrl, MYKO and NEKO mice. (**D**) Representative immunofluorescence merged Z-stack images of MBP positive cells in corpus callosum of Ctrl and NEKO mice at the indicated age. (**E**) Simple composite phenotype scoring system of NEKO and MYKO mice compared with Ctrl at the indicated age. Bars represent mean±SD.

Coronal sections were cut on a Leica CM1850 cryostat with a thickness of 7 μm. Sections were directly mounted onto microscope slides and stored at −20 °C. Gallyas' staining was performed as previously described (28).

Nissl staining was performed on vibratome sections, which were mounted on microscope slides using cromalin solution. The sections were incubated for 45 s in Nissl solution and washing step was followed by dehydration with different ethanol concentrations.

H&E staining was performed on cryosections using Mayer's Hematoxylin solution (Sigma), and sections were mounted with Entellan (Millipore).

TUNEL staining was performed on vibratome sections via the ApopTag Plus Peroxidase *In situ* Apoptosis Detection Kit (Millipore) according to the manufacturer's protocol.

COX/SDH staining was performed on cryosections, with 40 min of incubation in Cytochrome C solution (0.8 ml 3, 3 diaminobenzidine tetrahydrochloride, 0.2 ml 500 μM cytochrome c, a few grains of catalase), and 40 min Succinate solution (0.8 ml 1.875 mM nitroblue tetrazolium, 0.1 ml 1.3 M sodium succinate, 0.1 ml 2 mM phenazine methosulphate, 0.01 ml 100 mM sodium azide) at 37 °C in a humid chamber. Sections were washed in PBS, dehydrated with increasing ethanol concentrations (75% for 2 min, 95% for 2 min, 100% for 10 min), air dried, and mounted in D.P.X. Light microscopy images were acquired using Leica SCN400 slidescanner. Cortical thickness and hippocampal areas were measured in coronal brain sections of the same rostro-caudal position in all animals. To quantify the number of neurons in the hippocampal DG and CA1 regions, neurons were counted in equally sized areas in the respective regions ($n = 4$ per mouse).

## Immunostaining

Free-floating sections were washed extensively and pretreated for 30 min in 2% Triton X-100/PBS. Sections were permeabilized and blocked in 0.4% Triton X-100, 10% goat serum in PBS for 1 h

at room temperature. Primary antibodies (APC 1:400, OP80, Calbiochem), MBP (1:1000, SMI94, Covance), (GFAP 1:2000, NeoMarkers), IBA1 (1:3000, WAKO Life Sciences) were incubated overnight in 0.4% Triton X-100, 5% goat serum in PBS at 4 °C. After washing with PBS, secondary antibodies anti-mouse Alexa Fluor 488 (1:2000, Invitrogen), anti-rabbit Alexa Fluor 546 (1:2000, Invitrogen) were applied in 5% goat serum in PBS for 2 h. Finally, the sections were washed in PBS and mounted using FluorSave Reagent (Calbiochem).

Light microscopy images were acquired by Leica SCN400 slide scanner (Leica Microsystems). Evaluation and processing was done with SlidePath Gateway Client software (version 2.0). Fluorescent images were acquired by an Axio-Imager M2 microscope, equipped with Apotome 2 (Zeiss). Images were processed with AxioVision software (version 4.8.2).

### Transmission electron microscopy

Coronal semi-thin sections (1 μm) were cut from hippocampus. After treatment with osmium tetroxide, the tissue was embedded in Epon (Fluka). For ultrastructural analyses, the tissue of interest was selected for electron microscopy after examination of semi-thin sections by light microscopy. Ultrathin sections (70 nm) were cut, collected on 200 mesh copper grids (Electron Microscopy Sciences), and stained with uranium acetate (Plano GMBH) and lead citrate (Electron Microscopy Sciences).

### Western blot analysis

Protein lysates were obtained from either homogenized tissue or isolated mitochondria, and subsequently subjected to western blot analysis as described previously (29). MEFs were lysed with the RIPA buffer followed by sonication and lysate clearance. Western blot analysis was performed using the following primary antibodies at indicated concentrations: mtHSP70 and LONP1 (1:1000, Abcam), Actin (1:5000, Santa Cruz), NDUFA9, SDHA, UQCRC1, MTCO1 (1:1000, Invitrogen), ATP5A1 (1:1000, MitoSciences). All secondary antibodies were purchased from Sigma Aldrich and used in 1:2000 dilution. Western blot quantification was performed using the ImageJ software.

### Blue native polyacrylamide gel electrophoresis (BN-PAGE)

BN-PAGE was carried out using the NativePAGE Novex Bis-Tris Mini Gel system (Invitrogen) according to the manufacturer's specifications. Proteins were transferred onto a PVDF (polyvinylidene fluoride) membrane, and immunodetection of mitochondrial OXPHOS complexes was performed (CI: NDUFA9; CII: SDHA; CIII: UQCRC1; CIV: MTCO1; CV: ATP5A1).

### Analyses of *de novo* translation in isolated mitochondria

*In organello* translation was performed as previously described in mitochondria from heart and liver (8). In organello proteins synthesis was performed for 1 h in presence of $^{35}$S-met at 37 °C. Mitochondria were lysed by incubation in SDS-PAGE loading buffer. Translation products were separated by SDS-PAGE, the gel was stained with Coomassie Brilliant Blue R-250; incubated in Amplify solution (GE Healthcare) and newly synthesized polypeptides were detected by autoradiography.

### Respiratory chain enzyme activities

The measurements of respiratory chain enzyme complex activities and citrate synthase activity were performed as previously described (30).

### Phenotype scoring system

The protocol for simple composite scoring system was done according to previously described protocol (24).

### Statistical analysis

Two-tailed unpaired Student's *t* test was used to determine statistical significance. Error bars represent standard deviation (SD). Unless otherwise indicated, all experiments were performed on three biological replicates.

## Supplementary Material

Supplementary Material is available at *HMG* online.

## Acknowledgements

The work was supported by grants of the European Research Council (ERC- StG-2012-310700) and German Research Council (DFG - TR1018/3-1). M.A. received scholarships from Marie Curie ITN - Marriage. The authors wish to thank Alexandra Kukat for critically reading the manuscript and Katherine Dodel for language proofing.

*Conflict of Interest statement*. None declared.

## Funding

This work was supported by grants from Fritz Thyssen Foundation (Az. 10.11.1.221) and German Research Council (DFG - TR 1018/3-1). M.A. obtained an Early Stage Researcher Fellowship through Marie Curie ITN "Marie Curie Aging Network" (316964).

## References

1. Scheper, G.C., van der Klok, T., van Andel, R.J., van Berkel, C.G., Sissler, M., Smet, J., Muravina, T.I., Serkov, S.V., Uziel, G., Bugiani, M. *et al.* (2007) Mitochondrial aspartyl-tRNA synthetase deficiency causes leukoencephalopathy with brain stem and spinal cord involvement and lactate elevation. *Nat. Genet.*, **39**, 534–539.
2. van der Knaap, M.S., van der Voorn, P., Barkhof, F., Van Coster, R., Krageloh-Mann, I., Feigenbaum, A., Blaser, S., Vles, J.S., Rieckmann, P. and Pouwels, P.J. (2003) A new leukoencephalopathy with brainstem and spinal cord involvement and high lactate. *Ann. Neurol.*, **53**, 252–258.
3. Linnankivi, T., Lundbom, N., Autti, T., Hakkinen, A.M., Koillinen, H., Kuusi, T., Lonnqvist, T., Sainio, K., Valanne, L., Aarimaa, T. *et al.* (2004) Five new cases of a recently described leukoencephalopathy with high brain lactate. *Neurology*, **63**, 688–692.
4. Konovalova, S. and Tyynismaa, H. (2013) Mitochondrial aminoacyl-tRNA synthetases in human disease. *Mol. Genet. Metab.*, **108**, 206–211.
5. Steenweg, M.E., van Berge, L., van Berkel, C.G., de Coo, I.F., Temple, I.K., Brockmann, K., Mendonca, C.I., Vojta, S., Kolk,

A., Peck, D. *et al.* (2012) Early-onset LBSL: how severe does it get?. *Neuropediatrics*, **43**, 332–338.
6. van Berge, L., Dooves, S., van Berkel, C.G., Polder, E., van der Knaap, M.S. and Scheper, G.C. (2012) Leukoencephalopathy with brain stem and spinal cord involvement and lactate elevation is associated with cell-type-dependent splicing of mtAspRS mRNA. *Biochem. J.*, **441**, 955–962.
7. Taft, R.J., Vanderver, A., Leventer, R.J., Damiani, S.A., Simons, C., Grimmond, S.M., Miller, D., Schmidt, J., Lockhart, P.J., Pope, K. *et al.* (2013) Mutations in DARS cause hypomyelination with brain stem and spinal cord involvement and leg spasticity. *Am. J. Hum. Genet.*, **92**, 774–780.
8. Dogan, S.A., Pujol, C., Maiti, P., Kukat, A., Wang, S., Hermans, S., Senft, K., Wibom, R., Rugarli, E.I. and Trifunovic, A. (2014) Tissue-specific loss of DARS2 activates stress responses independently of respiratory chain deficiency in the heart. *Cell Metab.*, **19**, 458–469.
9. Xu, B., Gottschalk, W., Chow, A., Wilson, R.I., Schnell, E., Zang, K., Wang, D., Nicoll, R.A., Lu, B. and Reichardt, L.F. (2000) The role of brain-derived neurotrophic factor receptors in the mature hippocampus: modulation of long-term potentiation through a presynaptic mechanism involving TrkB. *J. Neurosci.*, **20**, 6888–6897.
10. Doerflinger, N.H., Macklin, W.B. and Popko, B. (2003) Inducible site-specific recombination in myelinating cells. *Genesis*, **35**, 63–72.
11. Wang, S., Jacquemyn, J., Murru, S., Martinelli, P., Barth, E., Langer, T., Niessen, C.M. and Rugarli, E.I. (2016) The mitochondrial m-AAA protease prevents demyelination and hair greying. *PLoS Genet.*, **12**, e1006463.
12. Wang, X. and Michaelis, E.K. (2010) Selective neuronal vulnerability to oxidative stress in the brain. *Front Aging Neurosci.*, **2**, 12.
13. Surmeier, D.J., Obeso, J.A. and Halliday, G.M. (2017) Selective neuronal vulnerability in Parkinson disease. *Nat. Rev. Neurosci.*, **18**, 101–113.
14. Ray, M. and Zhang, W. (2010) Analysis of Alzheimer's disease severity across brain regions by topological analysis of gene co-expression networks. *BMC Syst. Biol.*, **4**, 136.
15. Park, C.B., Asin-Cayuela, J., Camara, Y., Shi, Y., Pellegrini, M., Gaspari, M., Wibom, R., Hultenby, K., Erdjument-Bromage, H., Tempst, P. *et al.* (2007) MTERF3 is a negative regulator of mammalian mtDNA transcription. *Cell*, **130**, 273–285.
16. Camara, Y., Asin-Cayuela, J., Park, C.B., Metodiev, M.D., Shi, Y., Ruzzenente, B., Kukat, C., Habermann, B., Wibom, R., Hultenby, K. *et al.* (2011) MTERF4 regulates translation by targeting the methyltransferase NSUN4 to the mammalian mitochondrial ribosome. *Cell Metab.*, **13**, 527–539.
17. Sorensen, L., Ekstrand, M., Silva, J.P., Lindqvist, E., Xu, B., Rustin, P., Olson, L. and Larsson, N.G. (2001) Late-onset corticohippocampal neurodepletion attributable to catastrophic failure of oxidative phosphorylation in MILON mice. *J. Neurosci.*, **21**, 8082–8090.
18. Kruse, S.E., Watt, W.C., Marcinek, D.J., Kapur, R.P., Schenkman, K.A. and Palmiter, R.D. (2008) Mice with mitochondrial complex I deficiency develop a fatal encephalomyopathy. *Cell Metab.*, **7**, 312–320.
19. Diaz, F., Garcia, S., Padgett, K.R. and Moraes, C.T. (2012) A defect in the mitochondrial complex III, but not complex IV, triggers early ROS-dependent damage in defined brain regions. *Hum. Mol. Genet.*, **21**, 5066–5077.
20. Fukui, H., Diaz, F., Garcia, S. and Moraes, C.T. (2007) Cytochrome c oxidase deficiency in neurons decreases both oxidative stress and amyloid formation in a mouse model of Alzheimer's disease. *Proc. Natl. Acad. Sci. U.S.A.*, **104**, 14163–14168.
21. Koopman, W.J., Distelmaier, F., Smeitink, J.A. and Willems, P.H. (2013) OXPHOS mutations and neurodegeneration. *EMBO J.*, **32**, 9–29.
22. Skaper, S.D. (2007) The brain as a target for inflammatory processes and neuroprotective strategies. *Ann. N. Y. Acad. Sci.*, **1122**, 23–34.
23. Gentleman, S.M. (2013) Review: microglia in protein aggregation disorders: friend or foe? *Neuropathol. Appl. Neurobiol.*, **39**, 45–50.
24. Guyenet, S.J., Furrer, S.A., Damian, V.M., Baughan, T.D., La Spada, A.R. and Garden, G.A. (2010) A simple composite phenotype scoring system for evaluating mouse models of cerebellar ataxia. *J. Vis. Exp.*, **39**, 1787.
25. Viader, A., Golden, J.P., Baloh, R.H., Schmidt, R.E., Hunter, D.A. and Milbrandt, J. (2011) Schwann cell mitochondrial metabolism supports long-term axonal survival and peripheral nerve function. *J. Neurosci.*, **31**, 10128–10140.
26. Funfschilling, U., Supplie, L.M., Mahad, D., Boretius, S., Saab, A.S., Edgar, J., Brinkmann, B.G., Kassmann, C.M., Tzvetanova, I.D., Mobius, W. *et al.* (2012) Glycolytic oligodendrocytes maintain myelin and long-term axonal integrity. *Nature*, **485**, 517–521.
27. Rinholm, J.E., Vervaeke, K., Tadross, M.R., Tkachuk, A.N., Kopek, B.G., Brown, T.A., Bergersen, L.H. and Clayton, D.A. (2016) Movement and structure of mitochondria in oligodendrocytes and their myelin sheaths. *Glia*, **64**, 810–825.
28. Pistorio, A.L., Hendry, S.H. and Wang, X. (2006) A modified technique for high-resolution staining of myelin. *J. Neurosci. Methods*, **153**, 135–146.
29. Hance, N., Ekstrand, M.I. and Trifunovic, A. (2005) Mitochondrial DNA polymerase gamma is essential for mammalian embryogenesis. *Hum. Mol. Genet.*, **14**, 1775–1783.
30. Wibom, R., Hagenfeldt, L. and von Döbeln, U. (2002) Measurement of ATP production and respiratory chain enzyme activities in mitochondria isolated from small muscle biopsy samples. *Anal. Biochem.*, **311**, 139–151.

*Human Molecular Genetics*, 2017, Vol. 26, No. 21 4181–4189

**doi: 10.1093/hmg/ddx307**
Advance Access Publication Date: 3 August 2017
Original Article

ORIGINAL ARTICLE

# DARS2 protects against neuroinflammation and apoptotic neuronal loss, but is dispensable for myelin producing cells

Marijana Aradjanski[1,2], Sukru Anil Dogan[1,2], Stephan Lotter[1], Shuaiyu Wang[2,3], Steffen Hermans[1,2], Rolf Wibom[4], Elena Rugarli[2,3,5] and Aleksandra Trifunovic[1,2,5,*]

[1]Institute for Mitochondrial Diseases and Aging, Medical Faculty, University of Cologne, 50931 Cologne, Germany, [2]Cologne Excellence Cluster on Cellular Stress Responses in Aging-Associated Diseases (CECAD), University of Cologne, 50931 Cologne, Germany, [3]Institute for Genetics, University of Cologne, 50674 Cologne, Germany, [4]Department of Medical Biochemistry and Biophysics, Karolinska Institute, 17177 Stockholm, Sweden and [5]Center for Molecular Medicine (CMMC), University of Cologne, 50931 Cologne, Germany

*To whom correspondence should be addressed. Tel:+49 221 478-84291; Email: aleksandra.trifunovic@uk-koeln.de



## Abstract

Although mitochondria are ubiquitous, each mitochondrial disease has surprisingly distinctly different pattern of tissue and organ involvement. Congruently, mutations in genes encoding for different mitochondrial tRNA synthetases result in the development of a very flamboyant group of diseases. Mutations in some of these genes, including aspartyl-tRNA synthetase (*DARS2*), lead to the onset of a white matter disease—leukoencephalopathy with brainstem and spinal cord involvement, and lactate elevation (LBSL) characterized by progressive spastic ataxia and characteristic leukoencephalopathy signature with multiple long-tract involvements. Puzzled by the white matter disease phenotypes caused by DARS2 deficiency when numerous other mutations in the genes encoding proteins involved in mitochondrial translation have a detrimental effect predominantly on neurons, we generated transgenic mice in which DARS2 was specifically depleted in forebrain-hippocampal neurons or myelin-producing cells. Our results now provide the first evidence that loss of DARS2 in adult neurons leads to strong mitochondrial dysfunction and progressive loss of cells. In contrast, myelin-producing cells seem to be resistant to cell death induced by DARS2 depletion despite robust respiratory chain deficiency arguing that LBSL might originate from the primary neuronal and axonal defect. Remarkably, our results also suggest a role for early neuroinflammation in the disease progression, highlighting the possibility for therapeutic interventions of this process.

## Introduction

Although mitochondrial diseases are often multisystemic, brain and muscle are the most commonly affected tissues. Central nervous system (CNS) involvement in mitochondrial disorders is clinically heterogeneous, manifesting as epilepsy, stroke-like episodes, migraine, ataxia, spasticity, extrapyramidal or hypophysial abnormalities, bulbar dysfunction, psychiatric abnormalities or neuropsychological deficits. Leucoencephalopathy has also been added to this long list of symptoms (1). Leucoencephalopathy with brain stem and spinal cord involvement and high brain lactate (LBSL) is a childhood or juvenile-onset disorder clinically characterized by

**Received:** April 28, 2017. **Revised:** July 25, 2017. **Accepted:** July 26, 2017

slowly progressive cerebellar ataxia and spasticity with dorsal column dysfunction (2). LBSL is defined by a characteristic magnetic resonance imaging showing signal abnormalities in the cerebral white matter, specific brain stem and spinal cord tracts. Additionally, there are spectroscopic findings of increased lactate in the abnormal white matter in almost all affected individuals (1–3).

LBSL is caused by recessive mutations in the *DARS2* gene, which encodes the mitochondrial aspartyl-tRNA synthetase (1). DARS2 belongs to the group of mitochondrial tRNA synthases (mtARSs), which differ from their cytoplasmic counterparts (4). These enzymes are responsible for the first step in mitochondrial protein synthesis that involves covalently attaching an amino acid to its cognate tRNA in a process referred to as tRNA charging or loading (4). How mutations in this ubiquitously expressed gene cause a disorder in which tracts of the central and peripheral nervous systems (PNS) are selectively affected is unexplained. An increased number of patients with DARS2 mutations indicates that the phenotypic spectrum in LBSL is much wider than originally assumed. Adult-onset oligosymptomatic cases were described as well as patients with infantile onset, rapid neurological deterioration and early demise (5). Almost all patients are compound heterozygous for different *DARS2* mutations of which one is almost invariably a splice site mutation in intron 2, upstream of exon 3 (1). As a consequence, exon 3 is not included in the messenger RNA, leading to a frameshift, premature stop and absence of a functional protein (6). Other mutations in DARS2 include deletions, non-sense, missense and splice site mutations, for which very little, if any, molecular data are available. More recently, another white matter disease characterized by hypomyelination (HBSL—hypomyelination with brain stem and spinal cord involvement) has been associated with the mutations in *DARS2* gene (7). Intriguingly, a majority of other mitochondrial diseases caused by mutations that disrupt mitochondrial protein synthesis usually lead to syndromes with devastating consequences in neurons, while *DARS2* mutations leading to LBSL or HBSL suggest a primary defect in white matter (1,7). To shed more light on this important question, we generated transgenic mice in which DARS2 was specifically depleted in forebrain-hippocampal neurons or myelin-producing cells.

Our analysis revealed that loss of DARS2 in adult neurons leads to strong mitochondrial dysfunction accompanied by an early inflammation response and progressive loss of cells. Remarkably, DARS2 deficiency in adult myelin-producing cells, despite clear signs of high level of mitochondrial dysfunction, had no effect on survival, inflammatory response or myelination.

## Results and Discussion

We recently demonstrated that DARS2 is an essential protein needed for early mammalian development, as depletion of DARS2 in the whole body leads to lethality around the time of organogenesis (8). To analyse the role of DARS2 in diverse neural cell types, we generated two different models where conditional *Dars2* mice ($Dars2^{fl/fl}$) were bred with mice that postnatally express the Cre recombinase specifically in neurons or in myelin producing cells. Neuron-specific DARS2-deficient mice were obtained by mating $Dars2^{fl/fl}$ to mice expressing *Cre* recombinase under the calcium/calmodulin-dependent kinase II alpha promoter (*CaMKIIα-Cre*) resulting in $Dars2^{fl/fl}$; *CaMKIIα-Cre* mice (referred to as $Dars2^{NEKO}$ mice). In this model, *Cre* recombinase is active in forebrain, hippocampus and striatum neurons from postnatal Day 14, with maximal recombination at postnatal Day 29 (9). To deplete DARS2 in myelin-producing cells, we used mice that express *Cre* recombinase under the control of the tamoxifen-inducible proteolipid 1 promoter (*Plp1-CreERT*), which allows temporal control of the recombination (10). The resulting $Dars2^{fl/fl}$; *Plp-CreERT* animals (referred to as $Dars2^{MYKO}$ mice) were injected intraperitoneally with tamoxifen for five consecutive days at 4 weeks of age. Recently, we demonstrated high sensitivity and specificity of the Cre expression in oligodendrocytes using this protocol, after crossing *Plp1-CreERT* mice with a reporter transgenic line expressing a floxed, mitochondrially targeted YFP ($ROSA26^{+/SmY}$) (11). Using this specific timing for the activation of Cre-mediated recombination in PLP positive cells, we ensured that DARS2 depletion occurs at about the same time in both models.

### Progressive degeneration of cortex and hippocampus owing to massive cell loss observed in $DARS2^{NEKO}$ mice

Initially, we followed the development of phenotypes by monitoring the growth curves in both transgenic lines. We did not observe any change in the growth curves of $Dars2^{MYKO}$ mice, while $Dars2^{NEKO}$ animals had a lower weight gain already at the time of weaning, and this became more prominent around 15 weeks of age (Supplementary Material, Fig. S1A). The gross morphology and weight of $Dars2^{NEKO}$ brains did not change until around 24-26 weeks of age when obvious loss of brain mass occurred, with a strong atrophy of the forebrain (Fig. 1A). Early on, most mice showed no obvious behavioral abnormalities, but around 27-28 weeks of age some mice started scratching their necks and faces, resulting in self-inflicted wounds, at which point mice had to be sacrificed (Supplementary Material, Fig. S1B). In the rest of $Dars2^{NEKO}$ cohort, progressive nature of the phenotype led to a shorter lifespan of up to 32-34 weeks of age. In contrast, neither changes in gross appearance, body weight nor behavior in $Dars2^{MYKO}$ mice were observed (up until 80 weeks of age when the mice were terminated).

In agreement with previous results, no clear change in structure, morphology and size of $Dars2^{NEKO}$ cortex and hippocampus was observed at 20 weeks of age. However, a significant decrease of the cortical thickness was detected at 28 weeks of age, accompanied by an apparent decrease in mean hippocampal area (Fig. 1B and C). Curiously, the number of cells within cortical and hippocampal area seemed increased (Fig. 1B), suggesting that a progressive atrophy is accompanied by cellular infiltration, most likely caused by an immune response. Conversely, a number of neurons within the stratum granulosum of the dentate gyrus (DG) or parts of the stratum pyramidale of the cornu ammonis (primarily CA1 and CA2) was prominently reduced in 28-week-old $Dars2^{NEKO}$ mice (Supplementary Material, Fig. S1C and D). An increasing level of pyknotic cells with clear signs of chromatin condensation suggested an irreversible state of heading into cell death (Supplementary Material, Fig. S1C and E). Vacuolar lesions in the same brain regions of the 28-week-old $Dars2^{NEKO}$ mice further implied cell loss (Supplementary Material, Fig. S1C–E). Transmission electron microscopy of the hippocampus area in the 28-week-old $Dars2^{NEKO}$ brain revealed less dense mitochondria that presented an apparent loss of lamellar-shaped cristae as a clear sign of mitochondrial dysfunction in these cells (Fig. 1D).

Next, we used the TUNEL assay to detect nuclear DNA fragmentation, a hallmark of cells undergoing apoptosis. A massive increase in apoptosis occurred at 20 weeks of age (Fig. 2A and B; Supplementary Material, Fig. S2), although at this time no apparent morphological changes were detected in the same brain regions (Fig. 1B). Remarkably, apoptotic cells in distinct brain regions seem to appear at different dynamics; neurons in the

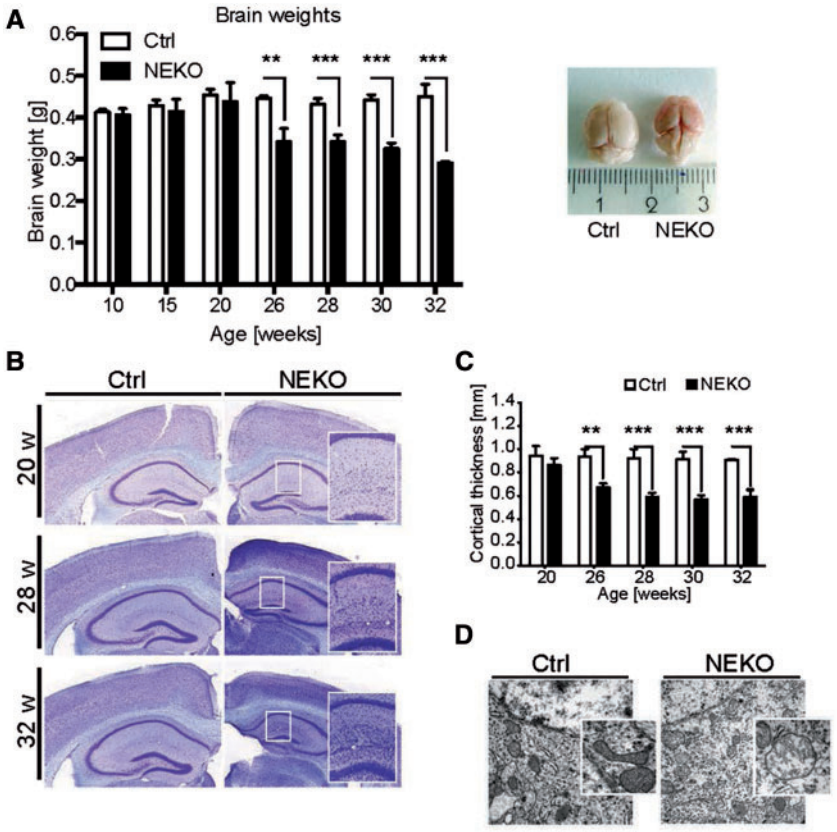


**Figure 1.** Analyses of cortex and hippocampus degeneration in control (Ctrl) and *Dars2*$^{NEKO}$ (NEKO) mice. (**A**) Brain weights of Ctrl and NEKO mice at the indicated age; representative photographs of isolated brains from both knockout and control mice at the indicated age. Bars present mean levels±SD. Statistical difference was calculated by Student's *t*-test; $^{**}P<0.005$, $^{***}P<0.001$ ($n=3-5$). (**B**) Representative Nissl staining (Scale bars: 500 μm) of hippocampal regions of Ctrl and NEKO mice at indicated age. Close-ups are for the indicated areas. (**C**) Quantification of brain cortical thickness [mm] at the indicated age in Ctrl and NEKO mice; bars represent mean levels ±SD. Statistical difference was calculated by Student's *t*-test; $^{**}P<0.005$, $^{***}P<0.001$ ($n=3$–5). (**D**) Representative transmission electron micrographs (Scale bar: 0.5 μm) of Ctrl and NEKO 29-week-old mice.

second and third cortical layer of retrosplenial area (RS) undergo considerable apoptosis only around 20 weeks of age, while in the rest of the cortex massive apoptotic cell death is observed until 26 weeks of age (Fig. 2A and B; Supplementary Material, Fig. S2). At 28 weeks of age, almost no TUNEL-positive nuclei could be observed, suggesting that the majority of them had already been lost (Fig. 2A and B; Supplementary Material, Fig. S2).

In general, cortical neurons seem to be more vulnerable to the loss of DARS2 and mitochondrial translation than hippocampal neurons (Fig. 2A and 2C). The hippocampal CA1 region displayed a high occurrence of progressive apoptotic cells with increased age, while in the DG region, despite having a large number of COX deficient cells, only a few neurons seemed to undergo apoptosis. The variances in the cell death dynamics might be a result of differences in neuronal types and physiology, and therefore their reliance on mitochondrial respiratory function. Indeed, selective neuronal vulnerability to oxidative stress (12), Parkinson's disease (13) or Alzheimer's disease (14) was previously described suggesting distinctive metabolic profiles in different brain regions.

## Strong mitochondrial deficiency and neuroinflammation precede loss of DARS2-deficient neurons

Severe respiratory chain deficiency was observed already at 15 weeks of age, and reached its peak in 20 weeks old *Dars2*$^{NEKO}$ brains (Fig. 3A). The number of COX deficient cells markedly decreased from 24 weeks on, likely owing to the massive apoptosis of DARS2-deficient cells (Fig. 2A). As a result, 28-week-old brains had almost no COX(−)SDH(+) (Complex IV deficient/Complex II positive cells), but a severely reduced cortex. It also became apparent that, instead of cell bodies, *Dars2*$^{NEKO}$ mice had holes throughout the hippocampus and cortex area (Fig. 3A). Analysis of mitochondrial respiratory chain (MRC) enzyme activities in neocortical samples demonstrated decreased activities of complexes containing critical mitochondrial DNA (mtDNA)-encoded subunits, in 28-week-old *Dars2*$^{NEKO}$ mice (Fig. 3B). The observed alterations in the MRC levels and enzyme activities matched the reduction in the amount of fully assembled complex I (C I) and IV (C IV—COX) in *Dars2*$^{NEKO}$ mice (Fig. 3C). The F1 subcomplex of complex V (C V) was also detected in *Dars2*$^{NEKO}$ mitochondria, implying a defect in mitochondrial protein synthesis, as previously reported (8,15,16). Remarkably, at 28 weeks of age, mitochondrial *de novo* protein synthesis in *Dars2*$^{NEKO}$ cortex appeared better than at 22 weeks of age (Fig. 3D). This is likely owing to vast loss of DARS2-deficient cells at 28 weeks, hence the majority of mitochondria in these samples stems from other cell types, unaffected by Cre-mediated deletion of *Dars2*.

The essential role of the OXPHOS function in neurons has been previously demonstrated in other mouse models. Tissue-specific depletion of *Tfam* in forebrain and hippocampus neurons (*Tfam*$^{L/L}$; *CamKIIα-Cre*) guided the reduction of mtDNA levels and

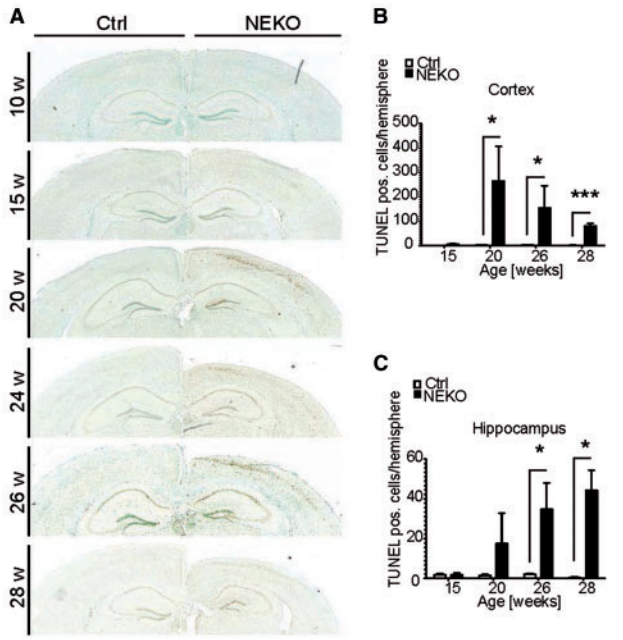


**Figure 2.** Apoptotic cell death in cortical and hippocampal regions in control (Ctrl) and *Dars2*$^{NEKO}$ (NEKO) mice. (**A**) Representative TUNEL staining of brain hemispheres (cortex and hippocampus regions) in Ctrl and NEKO mice at the indicated age. (**B**, **C**) Quantification of TUNEL positive cells per hemisphere in the region of cortex (B) and hippocampus (C) at the indicated age in Ctrl and NEKO mice. Bars present mean levels ±SD. Statistical difference was calculated by Student's *t*-test; *$P<0.05$, ***$P<0.001$ ($n=3$).

strong respiratory chain deficiency from four months of age, resulting in a severe, progressive neurodegeneration and massive apoptosis (17). A complete loss of the complex I (C I) NDUFS4 subunit (*Ndufs4*$^{-/-}$) resulted primarily in a CNS defect and rapid development of a Leigh-like phenotype characterized by ataxia, blindness, retarded growth rate, lethargy and increased serum lactate, leading to premature death at about 7 weeks of age (18). Similarly, depletion of *Cox10* in neurons (*Cox10*$^{L/L}$; *CaMKIIα-Cre*) rendered them respiratory-deficient already at 2 months of age in both the cortex and hippocampus areas, while the neurodegenerative phenotype progressed slowly until the ages of 8 and 12 months when the mice die (19,20). Typically, there is a time lag between the occurrence of OXPHOS deficiency and onset of neurodegeneration (17,20), during which neurons seems to compensate for the disruption of oxidative phosphorylation. Increased glycolysis and support from other cell types have been proposed to account for this (21). However, here we show that DARS2 depletion in neurons leads to a respiratory chain deficiency around 15 weeks of age that quickly culminates in the occurrence of massive cell death at 20 weeks, resulting in a severe brain atrophy (30% loss) within the next four weeks. Therefore, if existing, compensatory ATP supplementation by other cell types seems to be insufficient to maintain neuronal function for prolonged time periods in *Dars2*$^{NEKO}$ mice.

In agreement with a strong OXPHOS defect and disturbed mitochondrial protein synthesis, increased levels of mitochondrial HSP70 chaperone and LONP1 protease were detected, suggesting higher activation of mitochondrial stress responses, possibly mitochondrial unfolded protein response (UPRmt), in 20-week-old *Dars2*$^{NEKO}$ animals (Supplementary Material, Fig. S3A). Increased mitochondrial biogenesis might also contribute to the observed change, as suggested by higher SDH levels (Fig. 3C). Remarkably, the increase was statistically significant only in the hippocampus, possibly owing to a higher number of cells other than neurons in the isolated cortex samples (Supplementary Material, Fig. S3B and C).

Neuronal degeneration frequently leads to a local change in physiological conditions that in turn promotes an inflammatory response and activation of microglia, which are the resident immune cells of the nervous system. Indeed, we detected high levels of activated microglia in the cortical and hippocampal regions of *Dars2*$^{NEKO}$ mice, starting from 15 weeks of age (Fig. 4A). The number of infiltrated microglia in the hippocampal CA1 and DG regions dramatically increased with age, with an almost complete loss of recognizable structure at 32 weeks (Fig. 4A and Supplementary Material, Fig. S4A). On the contrary, the level of activated microglia in the cortex (SC and RS) peaked at 20 weeks (Fig. 4A and Supplementary Material, Fig. S4A), coinciding with the highest levels of OXPHOS deficiency observed in these *Dars2*$^{NEKO}$ brains. The decline of reactive microgliosis over time coincides with a more robust, apoptotic neuronal loss in the cortex layers than observed in the hippocampus (Fig. 4A and 2A). Reactive astrocytes were increasingly detected from 15 weeks of age in both, cortex and hippocampal region of *Dars2*$^{NEKO}$ mice, further emphasizing the presence of a neuroinflammatory response (Fig. 4B and Supplementary Material, Fig. S4B). The highest level of GFAP positive cells was observed around 20 weeks, and was persistently present until the end of the lifespan at around 32 weeks (Fig. 4B and Supplementary Material, Fig. S4B).

Certainly, neuroinflammation is increasingly recognized as a contribution to processes underlying neurodegeneration. Primarily activated in response to diseases, toxins or mechanical injury, neuroinflammation is strongly associated with demyelinating diseases (22). It is now clear that the microgliosis and astrogliosis primarily intended to clear up debris and support neurons in distress, when chronically activated, can convert from a beneficial program into a cytotoxic insult promoting neuronal death (22). This might be one of the mechanisms to explain the abrupt worsening of the *Dars2*$^{NEKO}$ phenotype after 20 weeks of age when we could observe massive micro- and astrogliosis.

Remarkably, activated microglia were detected in both the cortex and hippocampus already at 15 weeks of age before any cell death could be observed, suggesting that respiratory-deficient cells emit specific signals leading to activation of neuroinflammatory processes. We previously showed that DARS2 depletion in heart and skeletal muscle leads to accumulation of unfolded/misfolded proteins that serve as the first signal causing activation of stress signals and systemic changes in metabolism (8). It is tempting to speculate that the buildup of unfolded and/or unassembled respiratory chain subunits owing to the DARS2 depletion, and therefore imbalanced mitochondrial *de novo* protein synthesis acts as an early signal for the cell autonomous activation of stress responses, which might also trigger neuroinflammatory response. This would be in agreement with previous studies where the activation of microglia coincided with the accumulation of misfolded proteins in Alzheimer's disease, amyloid lateral sclerosis or Huntington's disease (23).

## DARS2 depletion in myelin-producing cells does not affect the number of oligodendrocytes nor myelin production, despite strong OXPHOS deficiency

In agreement with our initial observation, DARS2 depletion in adult myelin producing cells (*Dars2*$^{MYKO}$ mice) did not affect cell

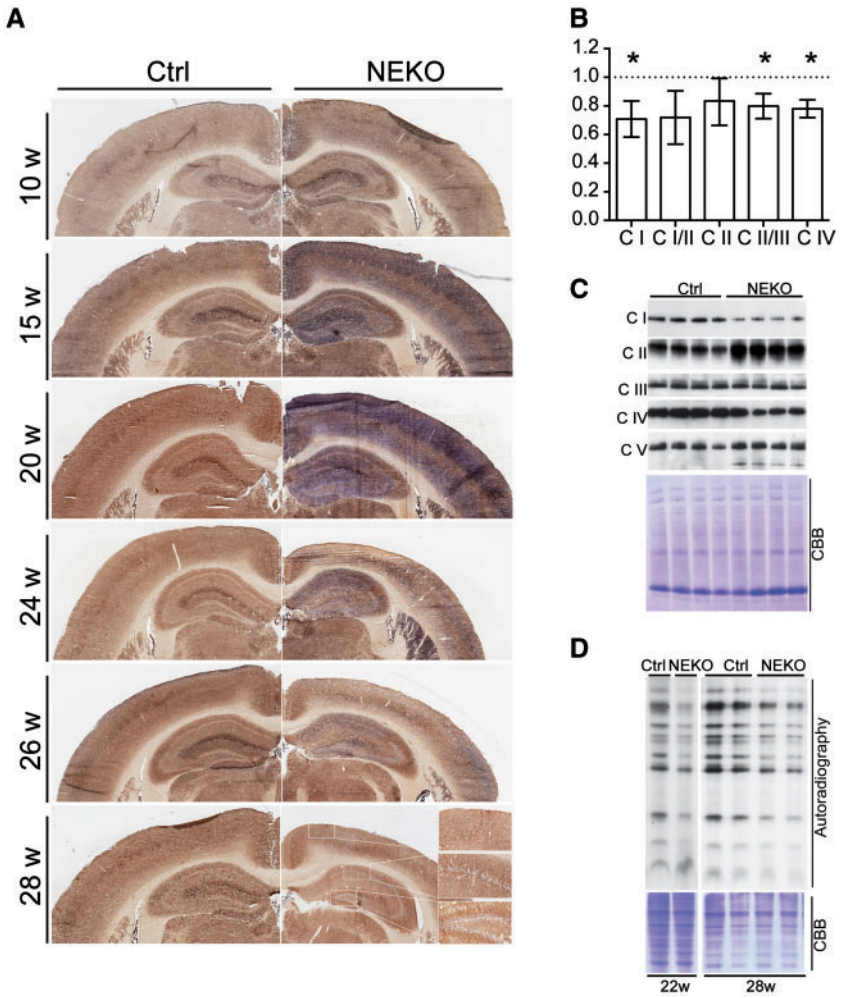


**Figure 3.** Characterization of mitochondrial function in control (Ctrl) and *Dars2*$^{NEKO}$ (NEKO) mice. (**A**) COX-SDH staining of brain hemispheres (cortex and hippocampus region) in Ctrl and NEKO mice at the indicated age. (**B**) Relative MRC complex activities in isolated cortex mitochondria of Ctrl and NEKO mice at 28 weeks of age. Bars present mean levels ±SD. Statistical difference was calculated by Student's *t*-test; *$P<0.05$ ($n=3$). (**C**) Western blots for OXPHOS complexes (with indicated position of specific complexes) and representative Coomassie Brilliant Blue (CBB) stained BN-PAGE gel in cortex mitochondria from 28-week-old Ctrl and NEKO mice. (**D**) Representative gel of *in organello* translation of 22- and 28-week-old Ctrl and NEKO mice cortex mitochondria. CBB stained gel used as loading control.

survival and therefore cell numbers at either 18 or 28 weeks (Supplementary Material, Fig. S5A). Moreover, the level of myelin basic protein, which is one of the most abundant proteins in myelin sheaths, was unchanged in *Dars2*$^{MYKO}$ mice (Supplementary Material, Fig. S5B). We also analyzed myelination in the PNS and found no difference in the thickness of myelin sheaths or appearance of Schwann cells (myelin producing cells in PNS) on both sciatic nerve and spinal cord (Supplementary Material, Fig. S5C).

Puzzled by the initial results, we wondered if DARS2 depletion causes respiratory chain deficiency in myelin producing cells as observed in neurons. Therefore, we analyzed OXPHOS function, again turning to COX-SDH staining. A large number of COX-deficient cells were detected in the striatum of *Dars2*$^{MYKO}$ mice, indicating the presence of strong OXPHOS deficiency (Fig. 5A). In the corpus callosum, the largest white matter structure in the brain, we detected COX-deficient oligodendrocytes in *Dars2*$^{MYKO}$ mice, and in agreement with results on PNS, no changes in the myelination (Fig. 5C). Furthermore, a very prominent stream of OXPHOS deficient axons could be detected in 15-week-old *Dars2*$^{NEKO}$ mice (Fig. 5B), which, remarkably, also did not affect the myelination of the corpus callosum (Fig. 5C and D).

DARS2 deficiency in forebrain and hippocampal neurons induced strong OXPHOS deficiency and neuroinflammatory response (Fig. 4 and Supplementary Material, Fig. S4). Despite clear evidence of strong OXPHOS deficiency in oligodendrocytes, no signs of neuroinflammatory response were detected in *Dars2*$^{MYKO}$ mice (Supplementary Material, Fig. S6).

Finally, using simple composite phenotype scoring system we tested to what extent DARS2 depletion affects motor skills in our two models (24). In accordance with previous results, *Dars2*$^{MYKO}$ mice did not show any signs of motor dysfunction (Fig. 5E). In contrast, DARS2 deficiency in neurons led to progressive loss of motor skills characterized by tremor, ataxia and age-dependent kyphosis (Fig. 5E).

Our results demonstrate that DARS2 deficiency in forebrain and hippocampal neurons leads to devastating cell death and severe neurodegeneration preceded by an early neuroinflammatory response (Supplementary Material, Fig. S7). The loss of DARS2 in oligodendrocytes, despite leading to strong respiratory deficiency, does not trigger any of these responses on either a

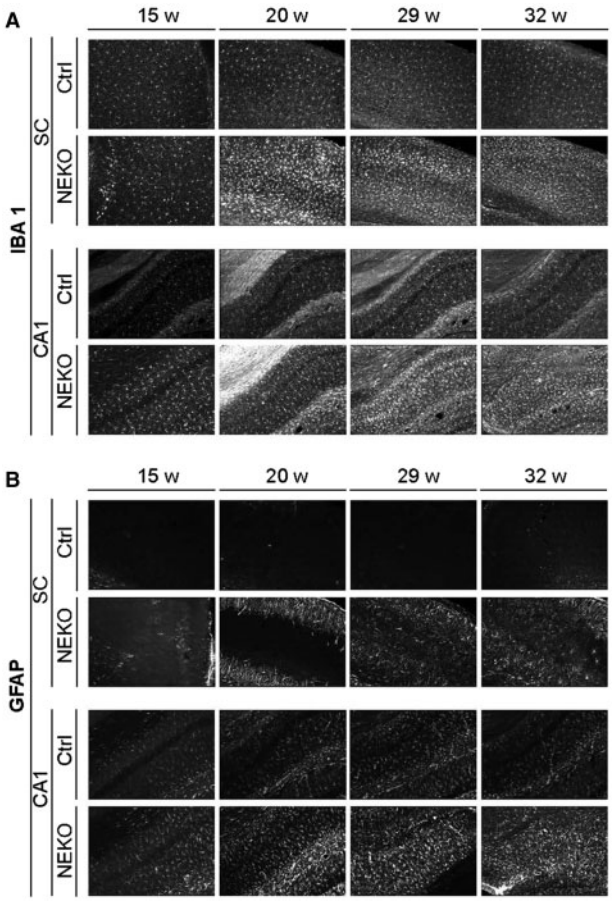


**Figure 4.** Neuroinflammatory processes in cortical and hippocampal areas of control (Ctrl) and *Dars2*$^{NEKO}$ (NEKO) mice. (**A** and **B**) Representative immunofluorescence merged Z-stack images of IBA1 positive microglia (A) and GFAP positive astrocytes (B) in somatosensory cortex (SC) and the hippocampal CA1 region in Ctrl and NEKO mice of the indicated age.

cellular or physiological level (Supplementary Material, Fig. S7). Remarkably, a recent study showed that the most common DARS2 patient mutation, located in a splice-site of intron 2, has the strongest effect causing exon 3 exclusion in neuronal cell lines (6). Therefore, it is tempting to conclude that LBSL in *DARS2* patients is a consequence of a primary neuronal deficiency, as neurons seems to be more affected with the splice-site mutation and here we show that they are also much more sensitive to a *Dars2* depletion than myelin producing cells. However, one has to keep in mind that our models induce the post-natal ablation of *DARS2*, whereas LBSL is typically owing to a hypomorphic allele which partially impairs the function of DARS2 throughout the embryonic and brain development. Therefore, a detrimental role of the mutation during oligodendrocyte-mediated myelinization of the developing brain cannot be excluded in the pathogenesis of the disease.

This is in agreement with a study showing that the most common DARS2 patient mutation located in a splice-site of intron 2, has the strongest effect causing exon 3 exclusion in neuronal cell lines (6).

Why would these two cell types react so differently to the loss of respiratory chain function? A different metabolic profile of adult oligodendrocytes and Schwann cells, enabling them to survive primarily using glycolysis for energy production when mitochondrial respiration is impaired, might be the main reason. In support of this hypothesis, Schwann-cell-specific depletion of Tfam (*Tfam*$^{L/L}$, *P*$_0$*-Cre*), the mitochondrial transcription factor A gene, which is essential for mtDNA transcription and maintenance, did not affect cell proliferation or survival, despite severe mtDNA depletion and respiratory chain abnormalities (25). Oligodendrocyte-specific deletion of *Cox10* (*Cox10*$^{L/L}$*; Cnp1-Cre*), an essential assembly factor for complex IV, also did not lead to axonal degeneration, demyelination or cell death (26). In fact, recent data suggest that oligodendrocytes' mitochondria may be essential for specialized functions relevant for myelin maintenance, such as lipid synthesis or fatty acid oxidation, rather than for ATP production (27). In agreement with this idea, a complete ablation of the m-AAA protease using the same promoter and Cre-induction paradigm as in this study (*Afg3l1*$^{-/-}$*; Afg3l2*$^{L/L}$*; Plp1-Cre*) resulted in progressive motor dysfunction and demyelination, owing to rapid oligodendrocyte cell death (11). In light of our results, this suggests that the imbalance of m-AAA protease substrates, other than the ones related to respiratory chain function, is detrimental for the myelin-producing cells of the central and PNS (11).

In summary, we provide strong *in vivo* evidence in support of the hypothesis that *Dars2* dysfunction, causing LBSL through disturbances in the white matter of both central and PNS, arises from a primary neuronal or axonal deficiency and not from a defect of myelin-producing cells. Remarkably, our results also highlighted neuroinflammatory processes, which coincide with respiratory chain deficiency and precede neuronal cell loss as possible yet unexplored targets of therapeutic interventions in LBSL and potentially other mitochondrial diseases.

## Experimental Procedures

### Generation of *Dars2* mice

Forebrain-specific DARS2-deficient mice (NEKO) were generated by mating Dars2$^{loxP/loxP}$ animals with transgenic mice expressing Cre recombinase under the control of CaMKII$\alpha$ promoter (9). MPC-specific DARS2-deficient mice (MYKO) were created also by using Dars2$^{loxP/loxP}$ animals, mated with mice containing Plp1 driven CreER recombinase (10), whereas the activation of recombination was done by application of tamoxifen. Tamoxifen (T5648, Sigma) was dissolved in a corn oil/ethanol (9:1) mixture at a final concentration of 10 mg/ml. A total of 1 mg tamoxifen was administrated by intraperitoneal injection once a day for five consecutive days to 4 weeks old mice. All genotypes were acquired by PCR. Animal protocols were in accordance with guidelines for humane treatment of animals and were reviewed by the Animal Ethics Committee of the Nord-Rheine Westphalia, Germany.

### Histological analysis

Mice were anesthetized with the combination of ketamine/xylazine, given intraperitoneally. Perfusion was performed intracardially with phosphate buffered saline (PBS) followed by 4% paraformaldehyde (PFA) in 0.1 M PBS (pH 7.4). Isolated brains were post-fixed in 4% PFA at 4 °C (for transmission electron microscopy analysis, post-fixed in 2% glutaraldehyde at 4 °C) overnight and then stored at 4 °C in 0.05% sodium azide-PBS ($NaN_3$-PBS) until further analysis. After perfusion, coronal sections were cut on Leica VT1200S with a thickness of 30–40 µm. Free floating sections were kept at 4 °C in 0.05% $NaN_3$-PBS.

For cryostat sections, freshly isolated brains were directly embedded in Tissue-Tek (Sakura) and frozen using dry ice.

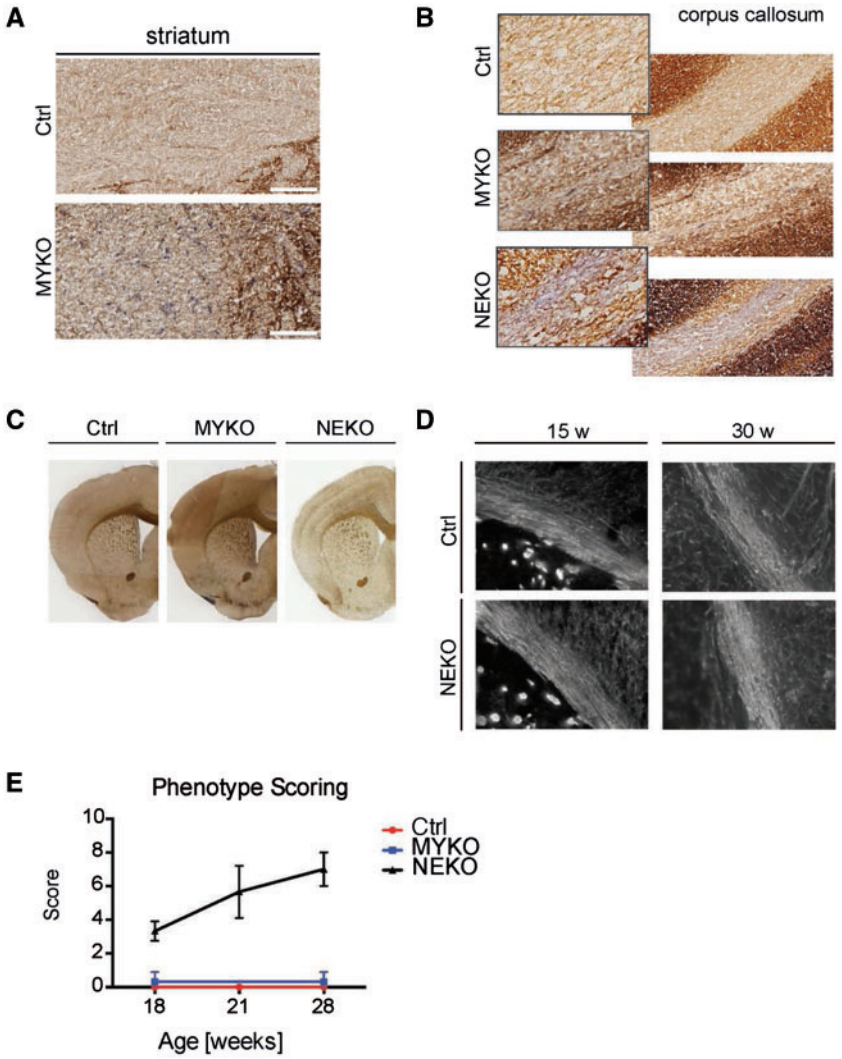


**Figure 5.** Characterization of mitochondrial function in control (Ctrl) and *Dars2* $^{MYKO}$ (MYKO) mice. (**A**) Representative COX-SDH staining of brain striatum in Ctrl and MYKO mice at 18 weeks of age (Scale bars, 100 μm). (**B**) Representative COX-SDH staining of corpus callosum with the close-ups in NEKO and MYKO mice at 18 weeks of age. (**C**) Representative images of Gallyas' myelin staining of the brain in 28-week-old Ctrl, MYKO and NEKO mice. (**D**) Representative immunofluorescence merged Z-stack images of MBP positive cells in corpus callosum of Ctrl and NEKO mice at the indicated age. (**E**) Simple composite phenotype scoring system of NEKO and MYKO mice compared with Ctrl at the indicated age. Bars represent mean±SD.

Coronal sections were cut on a Leica CM1850 cryostat with a thickness of 7 μm. Sections were directly mounted onto microscope slides and stored at −20 °C. Gallyas' staining was performed as previously described (28).

Nissl staining was performed on vibratome sections, which were mounted on microscope slides using cromalin solution. The sections were incubated for 45 s in Nissl solution and washing step was followed by dehydration with different ethanol concentrations.

H&E staining was performed on cryosections using Mayer's Hematoxylin solution (Sigma), and sections were mounted with Entellan (Millipore).

TUNEL staining was performed on vibratome sections via the ApopTag Plus Peroxidase *In situ* Apoptosis Detection Kit (Millipore) according to the manufacturer's protocol.

COX/SDH staining was performed on cryosections, with 40 min of incubation in Cytochrome C solution (0.8 ml 3, 3 diaminobenzidine tetrahydrochloride, 0.2 ml 500 μM cytochrome c, a few grains of catalase), and 40 min Succinate solution (0.8 ml 1.875 mM nitroblue tetrazolium, 0.1 ml 1.3 M sodium succinate, 0.1 ml 2 mM phenazine methosulphate, 0.01 ml 100 mM sodium azide) at 37 °C in a humid chamber. Sections were washed in PBS, dehydrated with increasing ethanol concentrations (75% for 2 min, 95% for 2 min, 100% for 10 min), air dried, and mounted in D.P.X. Light microscopy images were acquired using Leica SCN400 slidescanner. Cortical thickness and hippocampal areas were measured in coronal brain sections of the same rostro-caudal position in all animals. To quantify the number of neurons in the hippocampal DG and CA1 regions, neurons were counted in equally sized areas in the respective regions ($n = 4$ per mouse).

## Immunostaining

Free-floating sections were washed extensively and pretreated for 30 min in 2% Triton X-100/PBS. Sections were permeabilized and blocked in 0.4% Triton X-100, 10% goat serum in PBS for 1 h

at room temperature. Primary antibodies (APC 1:400, OP80, Calbiochem), MBP (1:1000, SMI94, Covance), (GFAP 1:2000, NeoMarkers), IBA1 (1:3000, WAKO Life Sciences) were incubated overnight in 0.4% Triton X-100, 5% goat serum in PBS at 4 °C. After washing with PBS, secondary antibodies anti-mouse Alexa Fluor 488 (1:2000, Invitrogen), anti-rabbit Alexa Fluor 546 (1:2000, Invitrogen) were applied in 5% goat serum in PBS for 2 h. Finally, the sections were washed in PBS and mounted using FluorSave Reagent (Calbiochem).

Light microscopy images were acquired by Leica SCN400 slide scanner (Leica Microsystems). Evaluation and processing was done with SlidePath Gateway Client software (version 2.0). Fluorescent images were acquired by an Axio-Imager M2 microscope, equipped with Apotome 2 (Zeiss). Images were processed with AxioVision software (version 4.8.2).

### Transmission electron microscopy

Coronal semi-thin sections (1 μm) were cut from hippocampus. After treatment with osmium tetroxide, the tissue was embedded in Epon (Fluka). For ultrastructural analyses, the tissue of interest was selected for electron microscopy after examination of semi-thin sections by light microscopy. Ultrathin sections (70 nm) were cut, collected on 200 mesh copper grids (Electron Microscopy Sciences), and stained with uranium acetate (Plano GMBH) and lead citrate (Electron Microscopy Sciences).

### Western blot analysis

Protein lysates were obtained from either homogenized tissue or isolated mitochondria, and subsequently subjected to western blot analysis as described previously (29). MEFs were lysed with the RIPA buffer followed by sonication and lysate clearance. Western blot analysis was performed using the following primary antibodies at indicated concentrations: mtHSP70 and LONP1 (1:1000, Abcam), Actin (1:5000, Santa Cruz), NDUFA9, SDHA, UQCRC1, MTCO1 (1:1000, Invitrogen), ATP5A1 (1:1000, MitoSciences). All secondary antibodies were purchased from Sigma Aldrich and used in 1:2000 dilution. Western blot quantification was performed using the ImageJ software.

### Blue native polyacrylamide gel electrophoresis (BN-PAGE)

BN-PAGE was carried out using the NativePAGE Novex Bis-Tris Mini Gel system (Invitrogen) according to the manufacturer's specifications. Proteins were transferred onto a PVDF (polyvinylidene fluoride) membrane, and immunodetection of mitochondrial OXPHOS complexes was performed (CI: NDUFA9; CII: SDHA; CIII: UQCRC1; CIV: MTCO1; CV: ATP5A1).

### Analyses of *de novo* translation in isolated mitochondria

*In organello* translation was performed as previously described in mitochondria from heart and liver (8). In organello proteins synthesis was performed for 1 h in presence of $^{35}$S-met at 37 °C. Mitochondria were lysed by incubation in SDS-PAGE loading buffer. Translation products were separated by SDS-PAGE, the gel was stained with Coomassie Brilliant Blue R-250; incubated in Amplify solution (GE Healthcare) and newly synthesized polypeptides were detected by autoradiography.

### Respiratory chain enzyme activities

The measurements of respiratory chain enzyme complex activities and citrate synthase activity were performed as previously described (30).

### Phenotype scoring system

The protocol for simple composite scoring system was done according to previously described protocol (24).

### Statistical analysis

Two-tailed unpaired Student's *t* test was used to determine statistical significance. Error bars represent standard deviation (SD). Unless otherwise indicated, all experiments were performed on three biological replicates.

## Supplementary Material

Supplementary Material is available at *HMG* online.

## Acknowledgements

The work was supported by grants of the European Research Council (ERC- StG-2012-310700) and German Research Council (DFG - TR1018/3-1). M.A. received scholarships from Marie Curie ITN - Marriage. The authors wish to thank Alexandra Kukat for critically reading the manuscript and Katherine Dodel for language proofing.

*Conflict of Interest statement*. None declared.

## Funding

This work was supported by grants from Fritz Thyssen Foundation (Az. 10.11.1.221) and German Research Council (DFG - TR 1018/3-1). M.A. obtained an Early Stage Researcher Fellowship through Marie Curie ITN "Marie Curie Aging Network" (316964).

## References

1. Scheper, G.C., van der Klok, T., van Andel, R.J., van Berkel, C.G., Sissler, M., Smet, J., Muravina, T.I., Serkov, S.V., Uziel, G., Bugiani, M. *et al.* (2007) Mitochondrial aspartyl-tRNA synthetase deficiency causes leukoencephalopathy with brain stem and spinal cord involvement and lactate elevation. *Nat. Genet.*, **39**, 534–539.
2. van der Knaap, M.S., van der Voorn, P., Barkhof, F., Van Coster, R., Krageloh-Mann, I., Feigenbaum, A., Blaser, S., Vles, J.S., Rieckmann, P. and Pouwels, P.J. (2003) A new leukoencephalopathy with brainstem and spinal cord involvement and high lactate. *Ann. Neurol.*, **53**, 252–258.
3. Linnankivi, T., Lundbom, N., Autti, T., Hakkinen, A.M., Koillinen, H., Kuusi, T., Lonnqvist, T., Sainio, K., Valanne, L., Aarimaa, T. *et al.* (2004) Five new cases of a recently described leukoencephalopathy with high brain lactate. *Neurology*, **63**, 688–692.
4. Konovalova, S. and Tyynismaa, H. (2013) Mitochondrial aminoacyl-tRNA synthetases in human disease. *Mol. Genet. Metab.*, **108**, 206–211.
5. Steenweg, M.E., van Berge, L., van Berkel, C.G., de Coo, I.F., Temple, I.K., Brockmann, K., Mendonca, C.I., Vojta, S., Kolk,

A., Peck, D. *et al.* (2012) Early-onset LBSL: how severe does it get?. *Neuropediatrics*, **43**, 332–338.
6. van Berge, L., Dooves, S., van Berkel, C.G., Polder, E., van der Knaap, M.S. and Scheper, G.C. (2012) Leukoencephalopathy with brain stem and spinal cord involvement and lactate elevation is associated with cell-type-dependent splicing of mtAspRS mRNA. *Biochem. J.*, **441**, 955–962.
7. Taft, R.J., Vanderver, A., Leventer, R.J., Damiani, S.A., Simons, C., Grimmond, S.M., Miller, D., Schmidt, J., Lockhart, P.J., Pope, K. *et al.* (2013) Mutations in DARS cause hypomyelination with brain stem and spinal cord involvement and leg spasticity. *Am. J. Hum. Genet.*, **92**, 774–780.
8. Dogan, S.A., Pujol, C., Maiti, P., Kukat, A., Wang, S., Hermans, S., Senft, K., Wibom, R., Rugarli, E.I. and Trifunovic, A. (2014) Tissue-specific loss of DARS2 activates stress responses independently of respiratory chain deficiency in the heart. *Cell Metab.*, **19**, 458–469.
9. Xu, B., Gottschalk, W., Chow, A., Wilson, R.I., Schnell, E., Zang, K., Wang, D., Nicoll, R.A., Lu, B. and Reichardt, L.F. (2000) The role of brain-derived neurotrophic factor receptors in the mature hippocampus: modulation of long-term potentiation through a presynaptic mechanism involving TrkB. *J. Neurosci.*, **20**, 6888–6897.
10. Doerflinger, N.H., Macklin, W.B. and Popko, B. (2003) Inducible site-specific recombination in myelinating cells. *Genesis*, **35**, 63–72.
11. Wang, S., Jacquemyn, J., Murru, S., Martinelli, P., Barth, E., Langer, T., Niessen, C.M. and Rugarli, E.I. (2016) The mitochondrial m-AAA protease prevents demyelination and hair greying. *PLoS Genet.*, **12**, e1006463.
12. Wang, X. and Michaelis, E.K. (2010) Selective neuronal vulnerability to oxidative stress in the brain. *Front Aging Neurosci.*, **2**, 12.
13. Surmeier, D.J., Obeso, J.A. and Halliday, G.M. (2017) Selective neuronal vulnerability in Parkinson disease. *Nat. Rev. Neurosci.*, **18**, 101–113.
14. Ray, M. and Zhang, W. (2010) Analysis of Alzheimer's disease severity across brain regions by topological analysis of gene co-expression networks. *BMC Syst. Biol.*, **4**, 136.
15. Park, C.B., Asin-Cayuela, J., Camara, Y., Shi, Y., Pellegrini, M., Gaspari, M., Wibom, R., Hultenby, K., Erdjument-Bromage, H., Tempst, P. *et al.* (2007) MTERF3 is a negative regulator of mammalian mtDNA transcription. *Cell*, **130**, 273–285.
16. Camara, Y., Asin-Cayuela, J., Park, C.B., Metodiev, M.D., Shi, Y., Ruzzenente, B., Kukat, C., Habermann, B., Wibom, R., Hultenby, K. *et al.* (2011) MTERF4 regulates translation by targeting the methyltransferase NSUN4 to the mammalian mitochondrial ribosome. *Cell Metab.*, **13**, 527–539.
17. Sorensen, L., Ekstrand, M., Silva, J.P., Lindqvist, E., Xu, B., Rustin, P., Olson, L. and Larsson, N.G. (2001) Late-onset corticohippocampal neurodepletion attributable to catastrophic failure of oxidative phosphorylation in MILON mice. *J. Neurosci.*, **21**, 8082–8090.
18. Kruse, S.E., Watt, W.C., Marcinek, D.J., Kapur, R.P., Schenkman, K.A. and Palmiter, R.D. (2008) Mice with mitochondrial complex I deficiency develop a fatal encephalomyopathy. *Cell Metab.*, **7**, 312–320.
19. Diaz, F., Garcia, S., Padgett, K.R. and Moraes, C.T. (2012) A defect in the mitochondrial complex III, but not complex IV, triggers early ROS-dependent damage in defined brain regions. *Hum. Mol. Genet.*, **21**, 5066–5077.
20. Fukui, H., Diaz, F., Garcia, S. and Moraes, C.T. (2007) Cytochrome c oxidase deficiency in neurons decreases both oxidative stress and amyloid formation in a mouse model of Alzheimer's disease. *Proc. Natl. Acad. Sci. U.S.A.*, **104**, 14163–14168.
21. Koopman, W.J., Distelmaier, F., Smeitink, J.A. and Willems, P.H. (2013) OXPHOS mutations and neurodegeneration. *EMBO J.*, **32**, 9–29.
22. Skaper, S.D. (2007) The brain as a target for inflammatory processes and neuroprotective strategies. *Ann. N. Y. Acad. Sci.*, **1122**, 23–34.
23. Gentleman, S.M. (2013) Review: microglia in protein aggregation disorders: friend or foe? *Neuropathol. Appl. Neurobiol.*, **39**, 45–50.
24. Guyenet, S.J., Furrer, S.A., Damian, V.M., Baughan, T.D., La Spada, A.R. and Garden, G.A. (2010) A simple composite phenotype scoring system for evaluating mouse models of cerebellar ataxia. *J. Vis. Exp.*, **39**, 1787.
25. Viader, A., Golden, J.P., Baloh, R.H., Schmidt, R.E., Hunter, D.A. and Milbrandt, J. (2011) Schwann cell mitochondrial metabolism supports long-term axonal survival and peripheral nerve function. *J. Neurosci.*, **31**, 10128–10140.
26. Funfschilling, U., Supplie, L.M., Mahad, D., Boretius, S., Saab, A.S., Edgar, J., Brinkmann, B.G., Kassmann, C.M., Tzvetanova, I.D., Mobius, W. *et al.* (2012) Glycolytic oligodendrocytes maintain myelin and long-term axonal integrity. *Nature*, **485**, 517–521.
27. Rinholm, J.E., Vervaeke, K., Tadross, M.R., Tkachuk, A.N., Kopek, B.G., Brown, T.A., Bergersen, L.H. and Clayton, D.A. (2016) Movement and structure of mitochondria in oligodendrocytes and their myelin sheaths. *Glia*, **64**, 810–825.
28. Pistorio, A.L., Hendry, S.H. and Wang, X. (2006) A modified technique for high-resolution staining of myelin. *J. Neurosci. Methods*, **153**, 135–146.
29. Hance, N., Ekstrand, M.I. and Trifunovic, A. (2005) Mitochondrial DNA polymerase gamma is essential for mammalian embryogenesis. *Hum. Mol. Genet.*, **14**, 1775–1783.
30. Wibom, R., Hagenfeldt, L. and von Döbeln, U. (2002) Measurement of ATP production and respiratory chain enzyme activities in mitochondria isolated from small muscle biopsy samples. *Anal. Biochem.*, **311**, 139–151.